JOINT TRANSPORTATION RESEARCH PROGRAM

INDIANA DEPARTMENT OF TRANSPORTATION
AND PURDUE UNIVERSITY

HIGH PERFORMANCE CONCRETE (HPC) BRIDGE PROJECT FOR SR 43

Jon A. Jonsson
Graduate Research Assistant
School of Civil Engineering, Purdue University

Jan Olek
Professor of Civil Engineering
School of Civil Engineering, Purdue University
Corresponding Author

Julio A. Ramirez
Professor of Civil Engineering
School of Civil Engineering, Purdue University

Charles F. Scholer
Professor of Civil Engineering
School of Civil Engineering, Purdue University

Robert J. Peterman
Martin K. Eby Distinguished Professor in Engineering
College of Engineering, Kansas State University
Formerly a post-doctoral research associate at Purdue University

SPR-2200
Report Number: FHWA/IN/JTRP-2012/17
DOI: 10.5703/1288284314979

RECOMMENDED CITATION

Jonsson, J. A., J. Olek, J. A. Ramirez, C. F. Scholer, and R. J. Peterman. *High Performance Concrete (HPC) Bridge Project for SR 43*. Publication FHWA/IN/JTRP-2012/17. Joint Transportation Research Program, Indiana Department of Transportation and Purdue University, West Lafayette, Indiana, 2012. doi: 10.5703/1288284314979.

CORRESPONDING AUTHORS

Professor Jan Olek
School of Civil Engineering
Purdue University
(765) 494-5015
olek@purdue.edu

ACKNOWLEDGMENTS

Appreciation is expressed to the Indiana Department of Transportation (INDOT) and the Federal Highway Administration (FHWA) for providing funding for this research. Specifically, INDOT personnel Youlanda Belew, Tommy Nantung, John Wright and Hasmukh Patel and FHWA personnel Tom Saad were key resource persons within these organizations.

Special thanks are due to Rick Yoder and all the other exceptional people at Rinker Materials, Lafayette, for their many helpful suggestions and unfailing willingness to be of assistance. Their involvement in this work is deeply appreciated. Countless contributions of laboratory managers Mark S. Baker, Janet E. Lovell, Harry S. Tidrick, and Joseph R. Walters are deeply appreciated. Many helpful suggestions and comments by Professors Mete A. Sozen, Terry R. West, Robert J. Frosh, and W. Jason Weiss are acknowledged.

Among the numerous current and former Purdue University students that have displayed their unselfishness time and time again in support of this project, the following are specially acknowledged: Philip J. Bender, Todd M. Chariton, Amir A. Elsharief, Rolando H. Garcia, Ryan Glanz, Luis Graf, Jeremy M. Gries, Jingdong Huang, Anthony J. Lamanna, Rongtang Liu, Aiping Lu, Brian Malone, Farrell Martin, Sarah Moses, Scott A. Newbolds, Jennifer Pierce, Chengqing Qi, Prasadarao Rangaraju, Eric Rolle, Manu Santhanam, Bing Tian, Kristin M. Wegner, and Zhifu Yang.

Finally, the investigators would like to thank Insteel, Florida Wire & Cable, Essroc Cement Corp., Holcim, W.R. Grace & Co.-Conn., Master Builders, and U.S. Aggregates for donating materials used in this study.

JOINT TRANSPORTATION RESEARCH PROGRAM

The Joint Transportation Research Program serves as a vehicle for INDOT collaboration with higher education institutions and industry in Indiana to facilitate innovation that results in continuous improvement in the planning, design, construction, operation, management and economic efficiency of the Indiana transportation infrastructure.
https://engineering.purdue.edu/JTRP/index_html

Published reports of the Joint Transportation Research Program are available at: http://docs.lib.purdue.edu/jtrp/

NOTICE

The contents of this report reflect the views of the authors, who are responsible for the facts and the accuracy of the data presented herein. The contents do not necessarily reflect the official views and policies of the Indiana Department of Transportation or the Federal Highway Administration. The report does not constitute a standard, specification or regulation.

TECHNICAL REPORT STANDARD TITLE PAGE

1. Report No. FHWA/IN/JTRP-2012/17	**2. Government Accession No.**	**3. Recipient's Catalog No.**
4. Title and Subtitle High Performance Concrete (HPC) Bridge Project for SR 43		**5. Report Date** October 2012
		6. Performing Organization Code
7. Author(s) Jon A. Jonsson, Jan Olek , Julio A. Ramirez, Charles F. Scholer, Robert J. Peterman		**8. Performing Organization Report No.** FHWA/IN/JTRP-2012/17
9. Performing Organization Name and Address Joint Transportation Research Program Purdue University 550 Stadium Mall Drive West Lafayette, IN 47907-2051		**10. Work Unit No.**
		11. Contract or Grant No. SPR-2200
12. Sponsoring Agency Name and Address Indiana Department of Transportation State Office Building 100 North Senate Avenue Indianapolis, IN 46204		**13. Type of Report and Period Covered** Final Report
		14. Sponsoring Agency Code

15. Supplementary Notes
Prepared in cooperation with the Indiana Department of Transportation and Federal Highway Administration.

16. Abstract

The objective of this research was to develop and test high performance concrete mixtures, made of locally available materials, having durability characteristics that far exceed those of conventional concrete mixtures. Based on the results from the development of high performance concrete, guidelines for a high performance concrete bridge over Burnett Creek on SR 43, just north of I-65 near West Lafayette, Indiana, will be prepared. In addition, the effects of different curing conditions, with respect to temperature and moisture conditions, were evaluated. The use of 15.2 mm (0.6 in) prestressing strand in girders made of 69 MPa (10 ksi) concrete was also evaluated with respect to pullout resistance and transfer and development lengths.

17. Key Words curing temperature, pullout test, development length, chloride ion penetration, mixture design, structural testing	**18. Distribution Statement** No restrictions. This document is available to the public through the National Technical Information Service, Springfield, VA 22161.

19. Security Classif. (of this report)	**20. Security Classif. (of this page)**	**21. No. of Pages**	**22. Price**
Unclassified	Unclassified	123	

Form DOT F 1700.7 (8-69)

EXECUTIVE SUMMARY

HIGH PERFORMANCE CONCRETE (HPC) BRIDGE PROJECT FOR SR 43

Introduction

Premature deterioration of concrete bridges in the United States has been identified as a major problem with respect to cost of repair and rehabilitation. Most often, chloride ion penetration and subsequent corrosion of the reinforcement is the cause. Many studies have been conducted to develop concrete mixtures that will better protect the reinforcement from corroding. However, due to the variability of concrete materials from one location to another, a universal solution cannot be developed. Unique approaches, each intended for a particular geographical location, are therefore needed to ensure full compatibility between locally available materials.

The objective of this research was to develop and test high performance concrete (HPC) mixtures, made of locally available materials, having durability characteristics that far exceed those of conventional concrete mixtures. Based on the results from the development of HPC, guidelines for a HPC bridge over Burnett Creek on SR 43, just north of I-65 near West Lafayette, Indiana, will be prepared. In addition, the effects of different curing conditions, with respect to temperature and moisture conditions, were evaluated. The use of 15.2 mm (0.6 in.) prestressing strand in girders made of 69 MPa (10 ksi) concrete was also evaluated with respect to pullout resistance and transfer and development lengths.

In order to find solutions to the previously stated problems, the following scope was adopted:

1. Develop a high strength concrete mixture, with a compressive strength in excess of 69 MPa (10 ksi), suitable for bridge applications using locally available materials and construction practices.
2. Investigate and evaluate the effects of two kinds of supplementary cementitious materials (silica fume and ground granulated blast furnace slag) with respect to factors such as chloride ion diffusivity, salt scaling resistance, freezing and thawing resistance, and shrinkage of concrete.
3. Compare the effects of different humidity conditions during curing of compressive strength and durability specimens.
4. Evaluate experimentally whether the existing AASHTO* design requirements for transfer and development lengths are valid for the combination of 15.2 mm (0.6 in.) strand and 69 MPa (10 ksi) concrete.

Findings

The conclusions drawn from this study are divided into two sections, one from the materials part of the study (concrete mixture development and testing discussed in Chapter 4) and the other from the structural part of the study (discussed in Chapter5).

Concrete Mixture Development and Testing

1. In order to reduce possible effects of temperature and account for the change in uniformity of the raw materials used to produce concrete in the field, it is important to conduct trial pours within a few days before the actual pours are to be done.
2. The ACI equation recommended for calculating static modulus of elasticity† can be used to determine the static modulus of concrete with a design strength of 69 MPa (10.0 ksi).
3. The effectiveness of air-entraining admixtures (AEAs) to entrain and maintain a desired air content in fresh concrete should be carefully evaluated prior to their use in field applications. If changes in the air content of freshly mixed concrete are expected, the timing of specimen preparation is important as the compressive strength of the hardened concrete will vary approximately 5% with each 1% change in the air content.
4. Very good freeze-thaw resistance can be achieved for concrete mixes where up to 70% of the cement has been replaced with ground granulated blast furnace slag (GGBFS). Replacing some of the cement with silica fume, or a blend of silica fume and GGBFS, can also result in freeze-thaw durable concrete.
5. Using mineral admixtures, such as a combination silica fume and GGBFS or GGBFS alone, as a replacement for some of the cement may adversely affect the deicing scaling resistance of concrete. The scaling resistance can also be expected to decrease as the proportions of the mineral admixtures increase. Using 3% sodium chloride instead of 4% calcium chloride as a ponding solution will generally accelerate the deterioration. Reducing the period of moist curing and increasing the air curing period was found to improve scaling resistance for the field trial mixture containing both GGBFS and silica fume.
6. Based on the charge passed, in coulombs, during six hours, both silica fume and GGBFS will increase the resistance of concrete to chloride ion penetration. Using a ternary binders system of cement, silica fume, and GGBFS may provide the most favorable results in terms of chloride ion penetration resistance.
7. Shrinkage reducing admixture (SRA) can be used to effectively reduce drying shrinkage. However, before using SRA in concrete intended for freeze-thaw exposure, the compatibility of the SRA and the AEA must be conformed. In this study, the SRA greatly reduced the effectiveness of the AEA.
8. Increasing the moist curing time from 3 to 14 days for regular Indiana Department of Transportation (INDOT) Class C concrete, the time to failure of corrosion specimens was increased by at least 67%.
9. Replacing a portion of the cement with GGBFS and/or silica fume and lowering the water/binder ratio resulted in concrete mixtures that greatly reduced chloride ion ingress when compared with the regular INDOT Class C concrete. This in turn substantially extended the time to failure of the corrosion specimens. After 30 weeks of exposure to 6% NaCl solution, only one of 18 specimens made with GGBFS and/or silica fume modified mixture had failed while all six of the specimens made from the regular INDOT Class C concrete had failed after only 19 weeks.

*AASHTO. *LRFD Bridge Design Specifications*, 1st ed. American Association of State Highway and Transportation Officials, Washington, D.C., 1994.

†ACI Committee 318. *Building Code Requirements for Structural Concrete (ACI 318-02) and Commentary (ACI 318R-02)*. American Concrete Institute, Farmington Hills, Michigan, 2002, p. 89.

10. Inadequate moist curing of 102 mm (4 in.) diameter concrete cylinders may significantly impair the compressive strength development of the concrete. Based on electrical tests, the ability of inadequately moist cured concrete to resist chloride ion ingress is also compromised.

Structural Testing

1. Measurements of concrete surface strains in specimens containing 15.2 mm (0.6 in.) strand and 69 MPa (10 ksi) normal density concrete indicated that the transfer length was less than the code-assumed 50-strand diameter in the absence of longitudinal splitting cracks at the ends.
2. Six load tests on rectangular single-strand beams and two load tests on multiple-strand beams indicated that in the absence of web shear cracking near the ends, the AASHTO and ACI development length of $L_d = \left(f_{ps} - \frac{2}{3} f_{se}\right) d_b$ provided sufficient embedment to develop the full capacity of a single strand in the 69 MPa (10 ksi) concrete mixes used. Rupture of the prestressing strands occurred in each of the eight load tests.
3. The instrumentation used in the multiple-strand development beams, namely vibrating wire gages, internal electrical resistance strain gages, and surface mounted strain gages, gave consistent readings throughout this study. All of the gages survived the casting, de-tensioning, and shipping processes.

Implementation

This study provided INDOT with a set of recommendations regarding the usage of HPC in bridge construction. These recommendations have been used to develop a set of provisional standards (see Appendix G) that have been utilized in the production of the girders and the construction of the deck on the SR 43 bridge over Burnett Creek near west Lafayette, Indiana.

The benefits of this research include:

- Assemblage of detailed data on the influence of various material components, temperature and moisture during curing on the properties of HPC.
- Reassessment of the existing practices regarding the development length and the transfer lengths for structural applications involving HPC.
- This information was utilized in the development of provisional specifications for the construction of the SR 43 bridge. Furthermore, similar provisions are currently being utilized in the construction of several bridges as a part of the reconstruction of I-465 in Indianapolis, Indiana.
- An increased level of awareness among INDOT's engineers and contractors about the important characteristics of HPC and the procedures that need to be followed in order to build a successful project utilizing this material.

CONTENTS

LIST OF TABLES

LIST OF FIGURES

1. INTRODUCTION

Significant developments have been made in the field of concrete technology and engineering during the past 30 years. New chemical admixtures have been developed that reduce the water demand of fresh concrete by 40% or more. With the new admixtures and supplementary cementitious materials such as fly ash, silica fume and ground granulated blast furnace slag (GGBFS), new concrete mixtures with enhanced durability have been developed and used.

With the development of specially engineered concrete in the advent of new and improved mineral admixtures, the term high performance concrete (HPC) has emerged. This term generally refers to concrete that has been designed to have significantly improved durability characteristics, ease of placement, and high strength. Other advantages may include reduced creep and shrinkage, improved aesthetics, and rate of set. Although generally more costly to manufacture, the use of HPC offers long term cost effectiveness through improved service life and reduced maintenance costs when compared with structures constructed using conventional concrete.

Numerous methods are presently used in attempts to evaluate concrete durability. However, concrete deterioration is typically a very slow process and it is therefore difficult and time consuming to conduct tests that replicate actual field conditions. Much emphasis has therefore been placed on accelerated tests that reduce the time needed to obtain results that correlate with actual field conditions. On the other hand, limited attention has been given to possible influence on strength and durability of different curing conditions and the effects of early age temperature development.

In the United States, fly ash has been the most commonly used supplementary cementitious material and as a result, extensive experience and knowledge related to its use in concrete exists. In the present study, the supplementary cementitious materials considered are GGBFS and silica fume. They are expected to provide potential for durability improvements of concrete that is at least equal to that provided by fly ash.

From the structural point of view the use of HPC with enhanced strength offers increased flexural capacity and such concrete has been used in many cases to increase the span length or to reduce the number of girders in bridges (*1*). This results in a lighter superstructure and substructure. Typically, 25 to 30% reduction in concrete volumes, resulting in a decreased dead load up to 25%, are reported in the literature when high-strength concrete is used in place of normal strength concrete. Also, an average increase of 10% in span lengths was reported for cases where concrete strength was increased from 41 to 69 MPa (6 to 10 ksi).

Cast-In-Place (CIP) concrete member cross-sections can be optimized to fully take advantage of increased compressive strengths available with HPC mixes. In the prestressed concrete industry, however, economy is obtained through repetition and use of existing forms. Thus, in order to take advantage of the higher compressive strength in HPC prestressed girders it is usually necessary to also increase the tensile capacity of the girders through additional prestressing steel. For standard prestressing setups in which strand spacing is set at 50 mm (2 in.), the increased tensile capacity can be achieved by using larger-diameter strands.

1.1 Problem Statements

- Premature deterioration of concrete bridges in the United States has been identified as a major problem with respect to cost of repair and rehabilitation. Most often, chloride ion penetration and subsequent corrosion of the reinforcement is the cause. Many studies have been conducted to develop concrete mixtures that will better protect the reinforcement from corroding. However, due to the variability of concrete materials from one location to another, a universal solution cannot be developed. Unique approaches, each intended for a particular geographical location, are therefore needed to ensure full compatibility between locally available materials.
- Several large bridges, with a design life of 100 years, have recently been constructed or are under construction. These bridges include the Great Belt Link in Denmark (*2*), the Northumberland Strait in Canada (*3*), and the Øresund Link between Denmark and Sweden (*4*). Supplementary cementitious materials were selected for all of the aforementioned bridges to enhance durability characteristics of the concrete. For each of the bridges, several unique concrete mixture designs were developed, tested, and used. A HPC mixture with good durability characteristics is needed for bridge construction in the state of Indiana.
- In the design of HPC mixtures, the cement content is often high. A high cement content may lead to excessive rise in temperature of large concrete members during the cement hydration process. It has often been suggested that high curing temperature may adversely affect the later age strength development and possibly also the durability characteristics of the concrete. The adverse effects due to elevated curing temperatures at early ages have been attributed to an increase in porosity of the cement paste [(*5*), p. 360]. How, or if, adverse effects of elevated curing temperature can be reduced or eliminated is still a subject of considerable debate. However, the incorporation of supplementary cementitious materials will, in general, reduce the rate of temperature rise and improve the concrete microstructure.
- Standard curing of concrete test cylinders normally involves moist curing where free moisture is present on the surfaces of the specimens until they are tested. However, even under such favorable curing conditions, the low mixture water content and low porosity of HPC will leave a portion of the cement unhydrated. By continuously supplying free moisture to the specimens, absorption of water is likely to allow the cement hydration to proceed further than will be expected for the field cured structural concrete the specimens represent. Aïtcin [(*6*), p. 397] suggested that sealing the specimens in plastic, therefore eliminating the need for moist curing, will perhaps best simulate the moisture conditions of the structural concrete. A better understanding of this topic is desirable.

- High costs associated with rehabilitation and replacement of deteriorating concrete bridges have created a significant need for exploring the utilization of different methods or materials that hold promise of improved long-term performance. Several studies have been conducted in the past to evaluate the impact of HPC on the design of bridges and other structures. These studies indicate that the use of high-strength concrete results in significant design advantages and economic savings in bridge structures. In order to take full advantage of high-strength concrete in prostheses concrete girders, the use of 15.2 mm (0.6 in.) diameter low-relaxation prestressing strand is required. However, before implementing the use of this type of strand, verification on the transfer and development length requirements are needed.

1.2 Research Objective and Scope

The objective of this research was to develop and test HPC mixtures, made of locally available materials, having durability characteristics that far exceed those of conventional concrete mixtures. Based on the results from the development of HPC, guidelines for a HPC bridge over Burnett Creek on SR 43, just north of I-65 near West Lafayette, Indiana, will be prepared. In addition, the effects of different curing conditions, with respect to temperature and moisture conditions, were evaluated. The use of 15.2 mm (0.6 in.) prestressing strand in girders made of 69 MPa (10 ksi) concrete was also evaluated with respect to pullout resistance and transfer and development lengths.

In order to find solutions to the previously stated problems, the following scope was adopted:

1. Develop a high strength concrete mixture, with a compressive strength in excess of 69 MPa (10 ksi), suitable for bridge applications using locally available materials and construction practices.
2. Investigate and evaluate the effects of two kinds of supplementary cementitious materials (silica fume and ground granulated blast furnace slag) with respect to factors such as chloride ion diffusivity, salt scaling resistance, freezing and thawing resistance, and shrinkage of concrete.
3. Compare the effects of different humidity conditions during curing of compressive strength and durability specimens.
4. Evaluate experimentally whether the existing AASHTO (*7*) design requirements for transfer and development lengths are valid for the combination of 15.2 mm (0.6 in.) strand and 69 MPa (10 ksi) concrete.

1.3 Structure of the Report

This report starts with an introduction in Chapter 1, followed by a comprehensive literature review in Chapter 2. The experimental program along with a description of the materials and experimental methods are presented in Chapter 3. Chapter 4 contains the results and related discussion of the concrete mixture development and testing. Results and discussions related to the structural testing are given in in Chapter 5. Chapter 6 contains the conclusions, while the recommendations are listed in Chapter 7. More detailed descriptions of some of the testing techniques used along with results of individual tests are given in Appendices A to G.

2. LITERATURE REVIEW

In this literature review, an attempt has been made to summarize pertinent information on the development of high strength and HPC for bridge applications and the effect high curing temperatures may have on concrete properties. Although much information exists on how to make high strength and HPC, only limited information is available on how to accurately relate improvements in concrete properties to actual field performance. Test specimens are rarely subjected to the same conditions as the structural element with regard to temperature and moisture.

2.1 Design for Durability

In recent years, there has been a strong movement in North America and Europe to develop and use concrete with enhanced durability characteristics. Improved durability is of particular importance in structures exposed to salts because of the potential of premature corrosion of reinforcement and salt scaling. The exposure of structures to salt can result from the use of deicing salts and/or proximity to a marine environment. Using concrete with high resistance to chloride ion penetration has therefore become a priority.

Structures designed for enhanced durability are typically produced from concrete with high resistance to chloride ion penetration and reinforcement corrosion. This type of concrete almost always contains some amount of supplementary cementitious materials (binders) such as fly ash, ground granulated blast furnace slag (GGBFS), or silica fume.

A section in the literature review related to durability issues is focused on different cementitious materials and how they may affect the durability characteristics of concrete.

2.1.1 Supplementary Cementitious Materials

Although several types of supplementary cementitious materials exist, the focus of this review will be on the two types used in this study, namely GGBFS and silica fume. A brief overview of the history, properties, and usage of granulated blast furnace slag and silica fume in concrete is presented in Sections 2.1.1.1 and 2.1.1.2.

2.1.1.1 Ground Granulated Blast Furnace Slag. Ground granulated blast furnace slag (GGBFS) has been used as partial replacement for Portland cement in concrete for more than 100 years (*8*). As a by-product of the pig iron industry, blast furnace slag is produced in large quantities in many areas around the world. In

the United States, blast furnace slag is most commonly used as base course for roads and other structures. However, in many other countries, most of the available slag is ground to approximately the same fineness as cement and then utilized as a partial replacement for Portland cement in concrete.

Although GGBFS is not widely used in North America, new, more stringent, environmental regulations will make its production and use more feasible as the cost of producing cement is likely to increase. In 1991, the production capacity of GGBFS in North America was estimated to be approximately two million metric tons (*9*). That same year, more than 13 million metric tons of blast furnace slag were sold in the United States. Most of these 13 million tons could have been used for the production of concrete if enough grinding facilities were available.

The composition of slag can vary considerably between production facilities. The presence of the major oxides are typically found to be within the following ranges: magnesium oxide (MgO), 0 to 21%; aluminum oxide (Al_2O_3), 5 to 33%; silicon dioxide (SiO_2), 27 to 42%; and calcium oxide (CaO), 30 to 50% [(*10*), p. 262]. Although the composition of slag is important, the method used in its production is perhaps more important as air-cooled slag has very limited, if any, cementing properties (*11*). However, if the slag is cooled rapidly from its liquid state at 1350–1550°C (2460–2820°F) down to about 800°C (1470°F), crystallization of the material can be avoided and the resulting product often contains over 95% glass which is a latent hydraulic cement [(*10*), p. 262].

For any substantial reaction to occur between GGBFS and water, an activator is required. High alkaline environments have proved to be suitable activators. Fortunately, the pore solution of cement paste is basically composed of alkaline hydroxides and as such, provides for an excellent activator. The use of GGBFS in concrete tends to slow down the rate of hydration at early ages at room temperature. However, elevated temperatures help activate the slag and increase the rate of hydration (*12*). Therefore, GGBFS can be used in steam-cured concrete. In addition, the damaging effects, such as reduced strength and increased permeability, of high early age temperature on concretes containing GGBFS are less pronounced than when GGBFS is not used [(*5*), p. 662].

The reaction of a blend of cement and GGBFS results in a higher percentage of calcium-silicate-hydrate (C–S–H) and less calcium hydroxide than plain cement [(*5*), p. 662]. This alteration in the hydration products is attributable to the higher silicon content of the cement and GGBFS blend when compared with plain cement. The change in the microstructure and the slower rate of hydration when GGBFS is used typically yields denser and less permeable concretes.

In addition to lower permeability, concretes made with GGBFS tend to have better resistance to chloride ion penetration than normal concretes. The freeze-thaw resistance of concrete made with GGBFS is believed to be adequate and not adversely affected when compared with concrete made without GGBFS [(*5*), p. 666]. However, concretes made with GGBFS generally suffer higher degree of deicing salt scaling than do reference concretes made without GGBFS (*13*). Consequently, ACI Committee 318 [(*14*), p. 43] limits the maximum amount of GGBFS to 50% of the total binder content if the concrete will be exposed to deicing chemicals. The total amount of slag and other supplementary cementitious materials is also limited to a maximum of 50% of the total binder content.

2.1.1.2 Silica Fume. Silica fume is a by-product of the silicon metal and ferrosilicon alloy industries. The production of other silicon alloys also yields silica fume [(*6*), p. 140]. The silica fume is collected as fine dust from the exhaust of submerged electric-arc furnaces. After it is collected, it is often densified for easier handling. However, it is also available in undensified form, as a slurry, and as a component of blended cement (*15*).

Silica fume, sometimes referred to as microsilica or condensed silica fume, consists of small spherical particles. The typical silica fume particle has a diameter of about 100 nm ($4{\cdot}10^{-6}$ in.) and consists of roughly 90% SiO_2 [(*10*), p. 284]. The specific gravity of silica fume is around 2.20.

When used with cement, silica fume reacts with calcium hydroxide to produce calcium silicate hydrate (C–S–H). The C–S–H produced from silica fume and calcium hydroxide tends to have a lower calcium-silicate (C–S) ratio than C–S–H produced from the reaction of water and cement alone. A C/S ratio of 1.1 has been suggested for C–S–H produced from silica fume and calcium hydroxide [(*10*), p. 285]. Much of the silica fume reacts rapidly once calcium hydroxide becomes available in the system. When 10% of the cement was replaced with silica fume, Roy (*12*) found that half of the silica fume reacted during the first day and 67% during the first three days. Subsequent reaction of the silica fume was slow and only 75% had reacted after 90 days.

The use of silica fume as a partial cement replacement in concrete first gained acceptance in the Scandinavian countries in the 1970's. After 1979, all cement produced in Iceland contains about 7.5% of interground silica fume to reduce the risk of alkali-silica reaction between the high alkali cement and reactive aggregates (*16*). By the mid 1980's, silica fume had been used on trial basis in bridge decks in the United States (*17*). More recently, silica fume has gained popularity for use in HPC.

Silica fume is generally believed to enhance the concrete's ability to resist the penetration of aggressive ions such as chloride ions. Freezing and thawing resistance of concrete made with silica fume is believed to be comparable to that of concrete made with cement alone. However, in specifications for the Øresund bridge, between Denmark and Sweden, the silica fume content was limited to a maximum of 5% to reduce the risk of deicing salt scaling damage (*18*).

2.1.2 Durability Characteristics

Predicting durability characteristics of concrete is a difficult task. A series of factors can influence how resistant the concrete will be against deterioration. Provided that internal concrete damage, such as alkali-silica reaction or delayed ettringite formation, will not take place, the most important remaining factors are freeze-thaw damage and reinforcement corrosion. Concrete properties governing resistance to chloride ion penetration and freezing and thawing are therefore of utmost importance with regard to improving durability characteristics.

2.1.2.1 Chloride Ion Penetration and Reinforcement Corrosion. in Portland cement concrete, the pH of the pore solution can be expected to range from about 12.5 to 14 depending on the original binder composition. Reinforcing steel, when not in contact with chloride ions, will develop and mainta in a passive oxide layer when exposed to solutions with a pH greater than about 11.5. The passive layer acts as a protective film and prevents corrosion of the reinforcement as long as it remains intact.

There are primarily two factors, carbonation and chloride ions, that negatively affect the stability of the passive layer of steel reinforcement embedded in concrete. When carbon dioxide (CO_2) from the atmosphere diffuses into concrete, it will, in the presence of moisture, cause reactions that eventually decompose the calcium hydroxide (CH) present in the hydrated cement paste. These reactions are known as carbonation process. As the CH carbonates, the pH of the pore solution decreases and eventually reaches a value of 8.3 when all the CH is carbonated [(*5*), p. 498]. At this low value of pH, the protective passive layer becomes unstable and the corrosion process can beg in if adequate amounts of moisture and oxygen are present.

in 1995, Gjørv (*19*) concluded that there was no evidence of a carbonation problem for concretes with or without silica fume when the compressive strength of the concrete was above 50 MPa (7.25 ksi). This is believed to be attributable to the high quality of the concrete microstructure when the compressive strength reaches this limit. Therefore, the following discussion will be confined to factors affecting the penetration of chlorides into concrete.

When the chloride ion concentration in the pore solution reaches a certa in threshold level, the chlorides can damage or even destroy the passive layer at pH levels well above 11.5. The threshold concentration is not a constant value, but appears to be a function of the pH [(*20*), p. 28].

Generally, the penetration of chloride ions into concrete is considered to take place through diffusion. Ionic diffusion takes place when there is a concentration gradient and it is thought to follow Fick's 2nd law:

$$\frac{\partial \mathrm{C}}{\partial \mathrm{t}} = \frac{\partial}{\partial x}\left(D\frac{\partial \mathrm{C}}{\partial \mathrm{x}}\right) \qquad (2.1)$$

If the boundary conditions are assumed constant and independent of time (t), chloride content (C), and the distance (x), the solution of Fick's 2nd law becomes (*21*):

$$C(x,t) = C_i + (C_s - C_i)\cdot erfc\left(\frac{x}{2\sqrt{(t-t_{ex})\cdot D_{eff}}}\right) \qquad (2.2)$$

Where:

$C(x,t)$ = chloride concentration at a given location and time

C_i = initial chloride concentration of the concrete

C_s = surface chloride concentration of the concrete

x = distance from the concrete surface

t = time from concrete placement

t_{ex} = time from concrete placement until chloride exposure

D_{eff} = effective chloride ion diffusion coefficient

$erfc(z)$ = error function complement ($erfc(z) = -erf(z)$)

The units for the chloride concentrations in the above equation are typically in mass/volume of concrete, or as percentages of the cement content (by mass). The effective chloride ion diffusion coefficient is in units of distance squared over time, most commonly m^2/s. The distance and time factors need to be in units corresponding with the units of the diffusion coefficient.

Although ionic diffusion may be the primary mechanism for chloride ions to enter concrete, other possibilities need to be considered as well. Neville [(*5*), p. 566] suggests that chlorides may also enter uncracked concrete by absorption and with chloride contaminated water penetrating the concrete. in fact, Leeming (*22*) considers absorption to be a more important factor regarding deterioration mechanism of marine exposed concrete than diffusion.

Resistance to chloride ion penetration of concretes made with GGBFS has been found to be superior to that of regular concretes. Chloride contents in GGBFS concretes measured after two years of exposure have been found to be about one fifth of those in normal concretes exposed to the same conditions (*23*). Other tests have shown the water permeability to be reduced even more, or up to 100 times when GGBFS is used [(*5*), p. 665].

In 1999, Dehghanian (*24*) reported results of corrosion tests of small steel plates embedded in concretes made with different GGBFS replacement levels and having a water-binder ratio of 0.55. Samples where 30% of the cement was replaced with GGBFS had the lowest corrosion rates after 90 days of exposure to 2 to 5% sodium chloride (NaCl) solutions. Replacement levels of 15 and 25% also gave good results, but replacing 45% of the cement with GGBFS did not appear to provide much benefit when compared with the reference specimens made without GGBFS.

2.1.2.2 Electrical Properties. During the last two decades, determining electrical properties of concrete has gained significant popularity among concrete

researchers and testing agencies. The reason for this popularity can be attributed to a report written by D. Whiting in 1981 for the Federal Highway Administration (FHWA) and subsequent development of a test method (T-277) by the American Association of State Highway and Transportation Officials (AASHTO) in 1983. Both the report and the test method had the same title, "Rapid Determination of the Chloride Permeability of Concrete." In 1991, the American Society of Testing and Materials (ASTM) adopted the test with minor adjustments and issued it as ASTM C1202 (Standard Test Method for Electrical Indication of Concrete's Ability to Resist Chloride Ion Penetration).

During the aforementioned AASHTO and ASTM tests, 51 ± 3 mm ($2 \pm 1/8$ in.) thick concrete discs with a diameter of 102 mm (4 in.) are placed between two chambers which are later filled with 3% sodium chloride (NaCl) and 0.3N sodium hydroxide (NaOH) solutions to form a test cell. During the test, the cells are connected to a direct current circuit with a potential of 60 volts for a period of six hours. The current in the circuit is monitored and the charge passed, in coulombs, through the specimen during the six hours is calculated. The specimens can be either cores or prefabricated cylinders.

Often, results from this electrical test are used to compare and evaluate different concrete mixtures with respect to resistance to chloride ion penetration. In many cases, this will yield information of limited value since the charge passed during the testing period depends on the resistivity of the concrete, but not the effective chloride ion diffusion coefficient. However, Bentur, Diamond, and Berke [(*20*), p. 161] stated that the charge passed is linearly related to the effective diffusion coefficient and gave the relationship:

$$D_{eff} = 0.0103 \cdot 10^{-8} (\text{Charge Passed} - \text{Coulomb})^{0.84} \quad (2.3)$$

Currently, it is not uncommon to specify concrete that must meet one of the categories listed in the ASTM C1202 test method. Common maximum allowable values for the charge passed during the six hour test are either 1000 or 2000 coulombs. Values below 2000 coulombs can be obtained with low water-cement ratio concretes without using a mineral admixture. However, values below 1000 coulombs are not easily attained unless the concrete contains a mineral admixture (*25*).

Several factors can affect the charge passed during the ASTM C1202 test, some of which have been known since before the test was invented. Monfore (*26*) reported results of extensive tests on the electrical resistivity of cement paste and concrete. He found the resistivity to increase considerably with specimen age. This increase was typically around 40% between 7 and 90 days. Another factor that considerably affected the results was the aggregate fraction in the mixture. Increasing the volume of the aggregate from 35 to 61% doubled the resistivity. Although perhaps not of much interest with respect to resistivity of concrete, Monfore also measured the resistivity of several common rock types. The resistivity of limestone was 30,000 ohm-cm and the resistivity of granite was 880,000 ohm-cm. Compared with ordinary cement paste with a resistivity of roughly 1000 ohm-cm at age of 90 days, the resistivity of the rocks is considerably larger and may not affect the concrete resistivity much.

The effectiveness of silica fume, fly ash, and GGBFS, when used as partial cement replacement, in reducing the charge passed during the ASTM C1202 test when compared with plain Portland cement concrete has been demonstrated by many researchers. Since the test is intended to give indication of chloride ion penetration resistance of the concrete, concretes passing lower amount of charge are generally regarded better in terms of their ability to protect embedded reinforcement. However, Shi et al. (*27*) showed that the specific conductivity (the reciprocal of resistivity) of the pore solution of cement paste is dependent on the composition of the binder and is reduced if mineral admixtures are used to replace some of the cement. The reduction in the specific conductivity varied with the type of mineral admixtures used, with a maximum reduction observed for a combination of 15% silica fume and 42.5% GGBFS replacements. For this particular combination, the reduction in the specific conductivity of the pore solution when compared with pore solution from plain cement paste was roughly 92%. This reduction in the specific conductivity amounts to an increase in resistivity by more than an order of magnitude.

High concrete resistivity, including high pore solution resistivity, is likely to impair reinforcement corrosion rates once corrosion has initiated. However, as Shi et al. (*27*) pointed out, the use of silica fume, fly ash, and GGBFS will lead to reduction in the charge passed during the ASTM C1202 test, but their effect on the pore solution resistivity will have limited effect on chloride ion penetration. It should not be overlooked that replacing some of the cement with mineral admixtures generally improves the concrete microstructure and its resistance to chloride ions although the effects are perhaps not as significant as implied by the relatively large differences observed from the ASTM C1202 test results.

2.1.2.3 Freezing and Thawing Under Water. Some controversy appears to exist among concrete researchers in regard to freeze-thaw resistance of HPC and the need for entrained air in such systems. Some researchers claim that HPC does not need to contain entrained air. On a recent project in Austria, a non-air-entrained HPC, with a water-binder ratio of 0.33, was specified for a bridge deck (*28*). Aïtcin [(*6*), p. 480] suggests that there is a critical water-binder ratio between 0.25 and 0.30 at which entrained air is not required. He therefore recommends using entrained air when the water-binder ratio exceeds 0.25.

The validity of the standard ASTM C666 (Standard Test Method for Resistance of Concrete to Freezing and Thawing) test method with respect to evaluating the freeze-thaw resistance of HPC has been criticized. Fagerlund and Nordström (*29*) pointed out that the ASTM C666 method is harmful to HPC not containing entrained air. They attributed this to unnatural, forced absorption of water that takes place during the rapid freezing and thawing in water. The rapid freezing and thawing of this absorbed water will gradually damage the surface of the concrete and therefore reduce the dynamic modulus of elasticity, the typical freeze-thaw quality measure of concrete.

2.1.2.4 Deicing Salt Scaling. The mechanism of deicing salt scaling resistance of concrete is not well understood. It is believed that factors such as air content, cement type, binder composition, and even hardness of water, among others, affect the scaling resistance of concrete. Of two Swedish cements, the one with lower alkali and tricalcium aluminate (C_3A) contents resulted in higher concrete deicing scaling resistance (*30*). In a recent European round robin test, a considerable variation was observed in the amount of scaling residue collected between testing agencies although they all received specimens from the same batch of concrete (*31*). A possible explanation for the variations of results from the different European testing agencies might be the water quality as the hardness of the water used in the solution appears to greatly affect the amount of scaled (*32*).

In 1997, Petersson described how scaling tests are performed in Sweden. According to the Swedish standard, SS137244, saw cut surfaces are obtained by cutting 50 mm (2 in.) thick slices from 150 mm (6 in.) cubes. The cuts are placed perpendicular to the original top surfaces of the cubes. The cubes are moist cured for 7 days before being allowed to dry at 50% RH for 21 days. During the last week of the drying period, a rubber membrane is glued to all sides of the specimens, except the test surface, which is also the saw cut surface. After 56 freeze-thaw cycles in the presence of 3% NaCl solution, the amount of scaling residues collected from concrete intended for bridges may not exceed 0.5 kg/m^2 (0.92 lb/yd^2). The amount of scaling residues collected from specimens representing concrete in the actual bridges may not exceed 1.0 kg/m^2 (1.84 lb/yd^2) after 56 cycles. In 1990, the mean amount of scaling residue collected from specimens prepared during bridge construction in Sweden was 0.09 kg/m^2 (0.17 lb/yd^2) (*30*).

Concretes made with GGBFS generally suffer higher degree of deicing salt scaling than do reference concretes made without GGBFS [Stark and Ludwig, 1997b]. Bilodeau and Malhotra (*33*) reported data from a Canadian study where GGBFS was used as 25 and 50% replacement for cement. The GGBFS concretes showed a considerably higher degree of scaling than did the reference concretes. The amount of scaling residues collected from the reference specimens ranged from roughly 0.2 to 0.6 kg/m^2 (0.37 to 1.1 lb/yd^2) after 50 freeze-thaw cycles. For specimens where GGBFS was used, the amount of scaling residues ranged from 1.6 to 2.5 kg/m^2 (2.9 to 4.6 lb/yd^2). The difference in scaling between the two replacement levels was not significant, although it was slightly higher when 50% of the cement was replaced with slag. A constant water-binder ratio of 0.55 was used for all the concretes and the ponding solution contained 5% sodium chloride.

Deicing salt scaling resistance of concretes made with silica fume has been found satisfactory when compared with concretes made without silica fume. Jacobsen and Sellevold (*34*) tested the deicing scaling resistance of concretes with and without silica fume. They found silica fume to increase the scaling resistance of both normal strength and high strength concretes with water-binder ratios of 0.45 and 0.30, respectively. The concretes did not contain entrained air.

In specifications for the Øresund bridge, between Denmark and Sweden, the length of deicing salt scaling test was increased from 56 to 112 cycles to reveal possible long term negative effects of silica fume on the scaling resistance of the concrete (*18*). The silica fume replacement level was limited to a maximum of 5% and the water-binder ratio to 0.40. Air-entrained concrete was specified for all parts of the bridge that will be exposed to freezing and thawing.

2.1.2.5 Shrinkage. Traditionally, concrete shrinkage measurements have been started one day after fabrication of the specimens. The ASTM standard governing shrinkage measurements is C157 (Standard Test Method for Length Change of Hardened Cement Mortar and Concrete). Based on this standard, initial length measurements shall be taken 24 hours after water is added to the cement during the mixing operation. According to Aïtcin [(*6*), p. 401], taking initial readings 24 hours after the addition of water has proved to be sufficient for normal concrete with a water-binder ratio of 0.50 or higher. However, he also notes that at water-binder ratios lower than 0.50, autogenous shrinkage is likely to develop during the first 24 hours. The presence or extent of autogenous shrinkage cannot be monitored by following ASTM C157 and is therefore not reflected in traditional drying shrinkage results.

2.1.2.6 Effects of Different Curing Procedures on Concrete Strength. The importance of adequately moist curing concrete has been recognized for many years. Abrams (*35*) evaluated the effects of water-cement ratio and the extent of moist curing on concrete compressive strength, abrasion, and absorption. The compressive strength tests were made on 152×305 mm (6×12 in.) cylinders and the abrasion tests on 127 mm (5 in.) thick blocks. All specimens were tested at the age of 120 days. The length of the moist curing period was either 0, 3, 7, 21, or 120 days. When the moist curing period was less than 120 days, the samples were stored in air until tested. The compressive strength was found to greatly

increase as the moist curing period was extended from 0 to 120 days. Cylinders that were moist cured for 120 days were 2.5 to 3 times stronger than companion cylinders stored in air for the same period. The effects of moist curing were not as dramatic in terms of the wear resistance as they were on the strength, but, nonetheless, significant. A minimum curing period of one week was recommended. It should be noted here that the dramatic effects of moist curing observed by Abrams around 80 years ago are not likely to be repeated with modern cements. Neville [(*5*), p. 333] states that properties such as cement fineness, alkali content, and the ratio of tricalcium silicate (C_3S) to dicalcium silicate (C_2S) have been altered in order to achieve more rapid strength development than was previously possible. Furthermore, he suggests that strength increase beyond 28 days should no longer be assumed.

The effect of moist curing on long-term strength of silica fume concrete was investigated by Carette and Malhotra (*36*). They compared the compressive and flexural strengths of concrete cured in water to strengths of concrete cured in water for seven days and then in the laboratory air. The replacement level of silica fume was 10%. At the age of 3.5 years, the compressive strength of air cured silica fume concrete with a water-binder ratio of 0.30 had decreased by 8.5% when compared with the 28-day strength. For a water-binder ratio of 0.40, the corresponding reduction was 11.9%. Companion concretes made without silica fume all showed a slight strength increase during the same period. For continuously moist cured concretes made with and without silica fume, a strength increase of about 50 and 23% was observed between 28 days and 3.5 years, respectively. The flexural strength was comparable for both curing methods after 2.5 years. However, the 28-day flexural strength of the air cured concretes, both with and without silica fume, was adversely affected.

2.2 Effects of Curing Temperature on Strength and Other Properties

The effect of concrete curing temperature on compressive strength development has been recognized for many years. In 1915, McDaniel (*37*) reported results from an investigation on concrete compressive strength development for various curing temperatures. Since then, extensive amount of work has been done to show how the curing temperature affects the strength development of concrete.

Possible effects of curing temperature on microstructure and durability characteristics of concrete have received limited attention. This is despite the fact that curing temperatures of HPCs containing high cement contents can reach up to 80 to 90°C (176 to 194°F) at early ages (*38*). At curing temperature above 60 to 70°C (140 to 158°F), the durability characteristics of the concrete can be adversely affected [(*10*), p. 339].

2.2.1 Effects of Curing Temperature on Compressive Strength

The general notion is that the 28-day compressive strength is adversely affected if the concrete is subjected to high curing temperatures. Klieger (*39*) reported results of tests where concrete was mixed, placed, and cured at temperatures ranging from 4 to 49°C (40 to 120°F). The specimens were cured at their initial curing temperatures for 28 days and then at 23°C (73°F) until tested after 90 and 365 days of moist curing. With respect to ultimate compressive strength, he concluded that optimum early age temperature for concrete made with Type I or Type II cement was 13°C (55°F) and 4°C (40°F) for concrete made with Type III cement. After 28 days of curing, the trend was not as clear, but the compressive strength of all mixtures made and cured at 49°C (120°F) was adversely affected and lower than of the reference mixtures made and cured at 23°C (73°F).

Moderate mixing and placing temperature of the concrete may reduce or eliminate negative effects of elevated curing temperature. Compressive strength results for 203×406 mm (8×16 in.) concrete cylinders fabricated at 20°C (68°F) and then cured at temperatures ranging from −7 to 32°C (20 to 90°F) after six hours of initial curing at 20°C (68°F) were reported by McDaniel (*37*). He found the compressive strength after 28 days of moist curing to increase with increased curing temperatures. The average 28-day compressive strength of specimens cured at 32°C (90°F), the highest curing temperature used in the study, was 10.5 MPa (1530 psi).

In 1951, Saul (*40*) showed that 28-day compressive strength of steam cured concrete depends on the temperature history at early ages, in particular the rate of temperature increase. He found that if the time from mixing until the concrete temperature reached 95°C (203°F) was at least six hours, the strengths at 28 days of steam cured specimens were not noticeably reduced compared with normally cured specimens. However, if the time until the temperature reached 95°C (203°F) was less than two hours, the strengths at 28 days were reduced by about 25%.

Owens (*41*) varied the peak concrete curing temperature from 20 to 60°C (68 to 140°F), while attempting to reproduce in situ temperature cycles. He found the 28-day strength reduction to increase with increasing cement content and temperature differential. A maximum compressive strength reduction of 28% was measured for concrete containing 400 kg/m^3 (674 lb/yd^3) of cement when the peak curing temperature was allowed to rise from 20 to 60°C (68 to 140°F). Incorporating Class F fly ash appeared to reduce the negative effects of elevated curing temperatures.

In a more recent study, Le Bris et al. (*42*) compared compressive strength of cylinders cured in water at 20°C (68°F) to that of cylinders cured in an oven which was used to simulate field curing of large pylons. The concrete was HPC with 8% silica fume and a compressive strength at 28 days of about 100 MPa

(14.5 ksi). The compressive strength of the oven cured cylinders was 9% lower than that of the regularly cured cylinders. The maximum temperature of the oven cured cylinders reached 85°C (185°F). They concluded that the observed strength reduction was smaller than one would have expected had normal strength concrete been used.

Burg and Ost (*43*) compared compressive strength of cylinders insulated with polystyrene and cores taken from 1220 mm (48 in.) cubes to that of control cylinders. When tested at the age of 91 days, insulated cylinders from four of the five high strength mixes tested and cores from all of the mixes had lower compressive strengths than the control cylinders. The maximum strength reduction for insulated cylinders was about 15% and occurred in a mix that gained maximum temperature faster than any of the other four mixes. The maximum temperature inside the five cubes ranged from 67 to 78°C (136 to 172°F) and occurred from 28 to 54 hours after concrete placement. It should be noted here that the maximum temperatures of the insulated cylinders were generally at least 15°C (27°F) lower than the maximum cube temperatures.

Although the effects of curing temperature on concrete strength vary, considerable reduction in strength has been noted. Committee 318 of the American Concrete Institute (ACI) limits the strength contribution of concrete in compression to 0.85 times the specified compressive strength of the concrete, f'_c [(*14*), p. 115]. This reduction is based on tests of 564 columns conducted at Lehigh University and the University of Illinois from 1927 to 1933 (*44*). Hognestad [(*45*), p. 45] used the 0.85 factor to account for the effects of size, shape, and casting position on the strength of reinforced concrete members. Concrete strength is generally believed to decrease with member size. Price (*46*) showed this reduction to be almost 9% when the cylinder diameter was increased from 152 to 305 mm (6 to 12 in.) and almost 18% when the cylinder diameter was increased from 152 to 914 mm (6 to 36 in.). Whether the strength reduction with increased cylinder size depended on the internal temperature rise, other size effects, or both, is not known. Generally, compression test cylinders do not develop the same internal temperature as large concrete members. It is therefore likely that the compressive strength development of small cylinders is not the same as that of the large concrete members they represent. As a result, the 0.85 reduction factor may, in some cases, be unconservative.

2.2.2 Effects of Curing Temperature on Durability

Owens [1985] measured the water surface absorption of concretes having peak concrete curing temperatures from 20 to 60°C (68 to 140°F) while attempting to reproduce in situ temperature cycles. He found the water surface absorption to increase with increase in peak curing temperature for plain Portland cement concretes. For concretes incorporating Class F fly ash and subjected to the same curing temperatures, the surface water absorption decreased with increase in peak curing temperature.

In an industry sponsored study, Sherman et al. (*25*) found that concretes cured at 63°C (145°F) for 7.5 hours after initial set had considerably lower water absorption than conventionally cured concretes with and without silica fume. They also found the resistance of the heat cured concrete to chloride ion penetration to be equal or better than of conventionally cured concrete. The water-cement ratio of the concretes was varied from 0.32 to 0.46.

The effects of elevated curing temperature on freeze-thaw resistance of concrete appear to vary from study to study. In 1960, Klieger [(*47*), p. 12] concluded that the freeze-thaw resistance of concrete exposed to elevated curing temperature was not adversely affected, provided that some drying of the concrete took place prior to freezing. Johnston (*48*) found that decreasing the temperature of an accelerated curing cycle from 65 to 45°C (149 to 113°F) improved the scaling resistance of concrete. The resistivity of the concrete was also improved, indicating a better resistance to chloride ion penetration. The resistance to freezing and thawing in water did not appear to be affected by the difference in curing temperature. In another study, Khurana and Torresan (*49*) found the freeze-thaw resistance of concrete to improve when the curing temperature was increased from 20 to 60°C (68 to 140°F). The concrete did not contain entrained air.

Jacobsen and Sellevold (*34*) found the scaling resistance of non-air-entrained concrete to be generally reduced when the curing temperature was increased from 20 to 60°C (68 to 140°F). The detrimental effects were greater for concretes with a water-binder ratio of 0.45 than for concretes with a water-binder ratio of 0.30. Replacing 8% of the cement with silica fume proved to be an effective way of increasing the scaling resistance for both water-binder ratios and all curing regimes. The typical curing regime consisted of seven hours at 20°C (68°F), followed with seven days at the desired curing temperature before being returned back to 20°C (68°F).

2.2.3 Effects of Curing Temperature on Concrete Microstructure

The rate at which cement hydrates can be greatly increased at early ages by elevating the curing temperature. The hydration products have low solubility and low diffusibility and, during rapid hydration, may therefore accumulate around the hydrating cement grains and prevent further hydration (*50*). The lack of proper hydration of the cement grains may reduce long-term strength development [(*5*), p. 360].

Kjellsen, Detwiler, and Gjørv (*51*) measured the porosity of plain cement paste with a water-cement ratio of 0.50. By analysing images obtained with a scanning electron microscope in the backscatter mode, they found the porosity of the paste to increase as the curing temperature was increased. For constant mixing

and curing temperatures of 5, 20, and 50°C (41, 68, and 122°F) until the degree of hydration had reached 70%, the measured porosity was 4.27, 10.93, and 15.11%, respectively. They attributed the increase in measured porosity more to the difference in size distribution of the pores, rather than to a difference in total porosity, as the settings of the microscope limited the analysis to pores having a diameter of about 3500 Å and up. It should be noted here that the cement paste cured at 50°C (122°F) was mixed at 35°C (95°F) to avoid premature stiffening and permit adequate compaction of the specimens.

2.3 Methods of Making and Curing Concrete Specimens in the Field

Several methods of curing concrete specimens exist. Most commonly, the specimens are left by the structure for the first day and either exposed to controlled temperature or atmospheric temperature. Neither method is likely to duplicate temperature conditions that exist in the actual structure.

2.3.1 Temperature Matched Curing of Concrete

The principle behind temperature matched curing is to ensure that concrete test specimens have the same temperature development as the concrete member they represent. This is achieved by continuously monitoring the temperature development in a newly cast structure and using that information to adjust the temperature of the concrete specimens as needed. At least two types of temperature matched curing systems have been developed and manufactured for commercial use. In England, concrete cubes, still in their steel molds, were cured in a small enclosure containing water and an electronically controlled immersion heater (*52*). In the United States, a different approach was taken and special reusable insulated molds, with heaters, were used to temperature match cure cylinders [(*53*), pp. 173], (*54,55*). Experimentation with different TMC systems has also been done in Virginia (*56*) and in Szczecin, Poland (*57*).

In 1976, Blakey (*52*) described the use of a temperature matched curing bath during the construction on a multi-story concrete frame structure in England. The temperature of the water bath was maintained at the same temperature as the concrete element. The concrete cubes, cured in their molds in the water, were later tested to determine the time of safe form removal. This curing method accelerated the rate of concrete construction and the contractor therefore justified the use of the temperature matched curing bath.

Whiting et al. [(*53*), pp. 173 and 181] used reusable insulated steel molds, containing internal heaters, to cure 102×203 mm (4×8 in.) concrete cylinders. The cylinders were used to predict strength of rapid hardening pavement repairs. The researchers noted that the temperature matched cured cylinders were invariably warmer than the pavement they represented as well as insulated companion cylinders. This was attributed to extensive insulation, applied heat, and the location of the reference thermocouple. The thermocouple was placed at mid-depth of the slab.

Russell et al. (*54*) also reported on the use of special insulated cylinder molds. The molds were used to temperature match cure cylinders representing prestressed high-strength concrete girders. They found that conventionally field-cured cylinders resulted in underestimation of the compressive strength at early ages and recommended that temperature matched cured cylinders be used for determining the strength of HPC girders at all ages.

2.3.2 Current Practice of Making and Curing Concrete Specimens

The most commonly tested property of structural concrete for purposes of acceptance is compressive strength of cubes or cylinders. In North America, 152×304 mm (6×12 in.) cylinders are generally used although 102×203 mm (4×8 in.) cylinders are gaining acceptance. Most structural concrete elements will have a minimum dimension larger than 152 mm (6 in.). As a result, the temperature of concrete cylinders stored near the structural element they represent will be lower than of the larger element. In addition, compressive strength cylinders are often continuously moist cured until tested although the structural elements they represent may not be subjected to external moisture.

Based on ASTM C31 (Standard Practice for Making and Curing Test Specimens in the Field), standard curing of concrete test cylinders is achieved by moist curing them. This may subject the cylinders to more favorable conditions than the structural concrete is exposed to. When curing cylinders intended for determining time of safe removal of forms, they shall be subjected to the same temperature and moisture conditions as the concrete they represent. When there is a considerable difference in the minimum dimension of the cylinders and the structural members, air-drying may inhibit the cement hydration in the smaller member and result in a strength difference. As a solution to different conditions mentioned above, Aïtcin [(*6*), p. 397] suggested that sealing the specimens in plastic, therefore eliminating the need for moist curing, will perhaps best simulate the moisture conditions of the structural concrete.

Burg and Ost [(*43*), p. 45] reported a maximum temperature increase of 56°C (100°F) for an insulated 1220 mm (48 in.) high strength concrete cube. Corresponding values for control cylinders were not available. A temperature difference between concrete cylinders and larger element will result in a strength differential. At early ages, the strength estimations will generally be conservative, but the same may not be true at later ages.

2.4 Bond Performance of Prestressing Strands

Characteristics of bond between concrete and reinforcing steel have been studied for over 120 years

(*58*). The focus of many bond investigations has been on determining development lengths and comparing the results with existing code provisions and/or suggesting new design formulas. Other investigations have been geared towards developing a general understanding of the nature of bond. The efforts of Abrams (*35,58*) and Stocker and Sozen (*59*) provided a needed basic understanding of bond of reinforcing bars and prestressing strands respectively. Unless otherwise stated, the review of prestressing strands presented in this report is limited to seven-wire strands.

2.4.1 Concrete to Prestressing Strand Bond

Many different factors have been found to affect the quality of bond between prestressing strands and concrete. The most commonly investigated factors include concrete compressive strength, depth of concrete below strand, strand surface condition (as received, rusted, etc.), and concrete workability. A standard experimental technique to evaluate bond characteristics of different strands has not yet been established. As a result the available data are based on many different techniques which make direct comparisons of results often difficult.

There are three commonly used methods of studying the bond performance of prestressing strands. The most convenient way is by testing simple pullout specimens. Pullout specimens are generally fabricated with unprestressed strands and therefore do not simulate actual conditions well. However, the effects of different variables such as strand surface condition and concrete strength can be evaluated qualitatively. Another way of comparing bond performance is by determining the strain distribution along prestressed elements. The distance it takes for the strand to transfer 90 to 100% of the prestress force to the concrete is called transfer length. The third commonly used method is to test prestressed elements in flexure. The objective is to determine the minimum distance needed to fully develop the ultimate stress in the strand. This distance is called development length.

Determining the development length is more complicated than measuring transfer length. A predetermined location must be selected for applying load to the member to be tested. The member is then loaded to failure and the failure mode noted. If the member fails by strand rupture, the development length is equal to or less than the distance it took to fully develop the strand. If the failure is by end slip of the strand, the development length generally exceeds the distance the strand was allowed to develop its full tensile capacity. End slip of the strand can be facilitated by the formation of shear and flexural cracks or a combination thereof. This will reduce the distance available for developing the strand and can lead to an inaccurate determination of bond performance.

According to Russell and Burns (*60*), the equations used in the current ACI Building Code (*61*) are based on tests done by Janney (*62*), and Hanson and Kaar (*63*). Janney (*62*) determined the transfer lengths of clean, rusted, and lubricated wires. He also tested beams, reinforced with prestressing wires and strands, to failure. Both the wires and strands were carefully cleaned with carbon tetrachloride and then wiped with acetone soaked cloth before being used. The concrete was made with a blend of Type I cements and 9.5 mm (0.375 in.) maximum size aggregates. Hanson and Kaar (*63*) focused their work on how embedment length and diameter of strand effect bond performance. Before using the strands, they washed them in carbon tetrachloride to remove surface oil. Of the 47 beams tested, 37 were prestressed with clean strands, 7 with rusted strands, and 3 with clean strands with anchors embedded at the ends. The concrete contained 38 mm (1½ in.) maximum size aggregate and a blend of Type I cements. The use of admixtures was not mentioned.

Kaar, LaFraugh, and Mass (*64*) studied the influence of concrete strength on strand transfer length. Their concrete target strength ranged from 11.4 to 34.5 MPa (1.7 to 5 ksi). The different concrete strengths were achieved by varying the age at transfer, on average, from 1 to 22 days. A single concrete mix, utilizing Type III cement and 19 mm (¾ in.) maximum size aggregates, was used when fabricating all specimens. Both transfer length specimens and compression strength cylinders were covered with plastic at 21°C (70°F) for the first day and then exposed to 50% relative humidity for the remainder of the test program. They concluded that concrete strength at transfer of clean strands with a 12.7 mm (½ in.) diameter or less had little effect on the transfer length.

Kaar and Magura (*65*) studied the effects of strand blanketing on performance of prestressed beams. They concluded that the requirements for bond embedment length set forth in the 1963 ACI Building Code (Section 2611) could not be directly applied to blanketed strand. However, when the requirements were doubled, the flexural capacity of a beam with blanketed strand was comparable to the capacity of a beam without blanketed strand. The concrete was air entrained and contained a blend of Type III cement. The maximum aggregate size was 19 mm (¾ in.). The 9.5 mm (0.375 in.) strand used in the study was cleaned to remove surface oil before it was tensioned.

Hanson (*66*) reported results of tests aimed at showing how surface roughness of prestressing strand influences bond performance. The surface conditions of the strands were clean (as received), partially rusted, rusted, and deformed. Hanson found that using partially rusted, or rusted strand could reduce the transfer length by about 30% compared with clean strand. Similar improvement was obtained with the deformed strand. The concrete used for the tests contained a blend of three Type I cements and 19 mm (0.75 in.) maximum size aggregates. Use of chemical admixtures was not mentioned.

One of the most comprehensive studies aimed at providing a basic understanding of bond of prestressing strands based on pullout specimens was conducted by Stocker and Sozen (*59*). They tested 486 pullout specimens and 5 prestressed beams. Most of the pullout

samples had an embedment length of only 25.4 mm (1 in.). Some of the factors investigated were strand size, concrete strength and consistency, curing conditions, age, and concrete settlement. Although Stocker and Sozen only tested strand from a single manufacturer, they noticed that not all strand is created equal. They observed different bond behavior of strand obtained from different coils. The water to cement ratio of the concrete varied from 0.4 to 1.05. The concrete contained Type III cement and 9.5 mm (0.375 in.) maximum size gravel aggregates. Chemical admixtures were not used when mixing the concrete.

In industry sponsored studies, Anderson and Anderson (*67*) and Brooks, Gerstle, and Logan (*68*) showed how initial strand slip dictates the flexural bond in pretensioned hollow core slabs. Both studies found a good correlation between the depth of the free end slip and flexural capacity. Generally, if the end slip was 2.3 mm (0.09 in.) or less, code provisions for flexural bond were met. However, a development length of more than 1524 mm (60 in.) was required in the Anderson and Anderson study to prevent failure by bond or shear.

According to Buckner (*69*), the Federal Highway Administration (FHWA) set new restrictions regarding the use of seven-wire strands in bridges. The new restrictions were based on a study done at North Carolina State University (NCSU) in 1986 and the fact that tensile capacity of commercially available strands had increased because of larger cross-sectional area and higher tensile strength. The new restrictions eliminated 15.2 mm (0.6 in.) strand from being used, increased development lengths for all strand sizes by 1.6, and doubled development length in certain cases where strands were blanketed. Buckner also noted that the new requirements led many researchers to focus their efforts on bond of pretensioned strand, which in turn resulted in numerous conflicting recommendations. In general though, the recommendations were conservative compared with the existing code provisions set forth by ACI and AASHTO.

Buckner's review (*69*) prompted Logan (*70*) and others to provide comments. In his comments, Logan suggested that the wide variation in measured transfer and development lengths in the studies reviewed by Buckner were attributable to variations in strand characteristics. He reported results of pullout tests, with a 457 mm (18 in.) strand embedment, conducted at his company, Stresscon Corporation, and at Concrete Technology Corporation. Strand from several producers was used in the tests. The average maximum pullout force ranged from 87.2 to 190.3 kN (19.6 to 42.8 kip) for 12.7 mm (½ in.) diameter strand. He also noted that strand produced using sodium stearate wire lubricant was found have better bond performance than strand produced using calcium stearate wire lubricant.

2.4.2 Pullout Tests (Mustafa Method)

In May and June, 1996, Logan (*71*) and others conducted a series of tests at Stresscon Corporation to correlate results of simple pullout tests with transfer and development lengths. The transfer lengths were estimated based on the strand end slip. They obtained and tested 12.7 mm (½ in.) diameter Grade 270 strand from six different producers. The average maximum pullout force of strand embedded 457 mm (18 in.) ranged from 47.6 to 185 kN (10.7to 41.6 kip). Subsequent beam tests showed the ACI equation for development length to be valid for strands having a pullout force in excess of 36 kip. However, the equation proved to be unconservative for strands having a pullout force of less than 53.4 kN (12 kip). None of the strand sources resulted in average pullout force between 53.4 and 160 kN (12 and 36 kip). The pullout values are maximum values, which may not be reached until after substantial slip has occurred. The concrete used for the test contained 391 kg/m^3 (660 lb/yd^3) of Type III cement and crushed gravel with 19 mm (0.75 in.) maximum size aggregates. The only admixture used was a normal range water reducer. The aforementioned pullout test procedure has become known as the Mustafa method, named after Saad Mustafa who conducted pullout tests on similar specimens in the 1970's (*72*). The Mustafa method is described in detail in Appendix A.

2.4.3 The Importance of Transfer and Development Lengths

The "transfer length" is defined as the distance required to transfer the fully effective prestress force in the strand to the concrete. The transfer length is not a quantity specified in either the ACI (*61*) or AASHTO (*7*) codes. However, both codes suggest a transfer length of 50 strand diameters when checking shear provisions. The ACI Commentary to the Building Code (Section 12.9) provides a formula for calculating the transfer length that is based on the expression for development length. According to this formula, the transfer length (L_t) is given by:

$$L_t = \frac{f_{se}}{3} \cdot d_b \tag{2.4}$$

where f_{se} is the effective stress (in ksi) in the strand after all losses, and d_b is the nominal diameter of the strand in inches.

The "development length" is the bond length required to anchor the strand as it resists external loads on the member (*60*). As external loads are applied to a flexural member, the member resists the increased moment demand through increased internal tensile and compressive forces. The increased tension in the strand is achieved through additional anchorage to the surrounding concrete. Thus, the development length is equal to the length required to transfer the effective prestress force (transfer length) plus an additional length required to develop the increase in strand tension produced by the external load demand. This additional length required to develop the maximum stress in the strand is often referred to as the "flexural

bond length." The development length is specified by both the ACI and AASHTO codes as:

$$L_d = \left(f_{ps} - \frac{2}{3} \cdot f_{se}\right) \cdot d_b \qquad (2.5)$$

where f_{ps} is the stress (in ksi) in the prestressed strand at nominal strength of the member, f_{se} and d_b are the same as in Equation 2.4.

The ACI Commentary assumptions (Figure R12.9 in the Commentary) [(*61*), p. 188] for transfer and development of stress in prestressing strand are reproduced in Figure 2.1. In this figure, the stress in the strand is plotted against the distance from the free end of the strand. The transfer length is represented by the first portion of the curve having a larger slope, while the flexural bond length is represented by the second portion of the curve.

Transfer lengths affect structural design considerations in two ways. First, as mentioned in the preceding paragraph, current code provisions for shear design of prestressed members are based on the amount of precompression in the member. Since the effective prestress varies approximately linearly from zero at the end of the member to the fully effective at the end of the transfer zone, significant deviations in the transfer length from the code-suggested 50 strand diameters could mean inadequate performance of the member in shear.

The transfer length can also have a significant impact on the flexural behavior of prestressed members. Russell and Burns (*60*) found that anchorage failures were likely when flexural cracking of a beam propagated through the transfer zone of a pretensioned strand. Beams with de-bonded strand are especially susceptible to this phenomenon. Therefore, the value of the transfer length is important to determine whether flexural cracks will likely propagate into this zone prior to the member reaching nominal capacity.

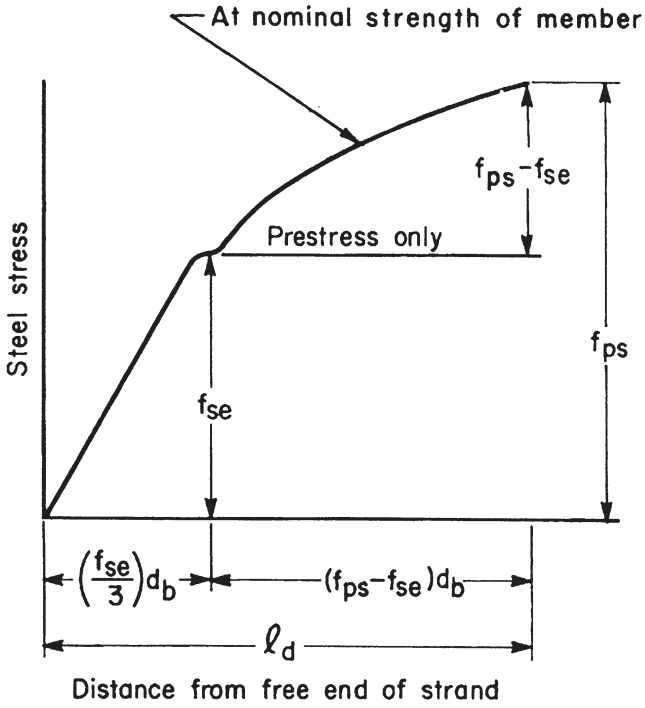

Figure 2.1 ACI Commentary Figure R12.9 depicting transfer and development lengths [(*61*), p. 188].

Development length requirements are typically "checked," rather than designed for. When a prestressed member is designed, required longitudinal reinforcement quantities are based on service-load stresses as well as calculations of nominal capacities. The ACI and AASHTO codes prescribe reinforcement-ratio limits to ensure that ductility is provided through ample yielding of the prestressed reinforcement at ultimate loads. Thus, for flexural considerations, the designer calculates a nominal moment capacity of the prestressed section by estimating a final level of stress that will be achieved by the strand (f_{ps}). Based on the estimate of f_{ps}, the designer calculates a development length (L_d) by Equation 2.5. A check is then made to ensure that the strand will have a large enough embedment length (L_e) in the concrete to obtain the estimated stress at nominal capacity (f_{ps}).

The embedment length is defined as the bonded length of the prestressed strand from the beginning of bond to the critical section. In most design applications, and in the literature, the critical section is interpreted as the point of maximum moment (*60*). ACI Section 12.10.2 [(*61*), p. 189] states that "Critical sections for development of reinforcement in flexural members are at points of maximum stress and at points within the span where adjacent reinforcement terminates, or is bent." Both the ACI and AASHTO codes imply that if the embedment length is greater than the development length ($L_e > L_d$) then the beam will be able to reach the nominal moment capacity and will fail in flexure. Conversely, if the embedment length is less than the development length ($L_e < L_d$) then bond failure will occur prior to the beam reaching its nominal capacity and the design is unsatisfactory. However, research has shown that bond failures may still occur when $L_e > L_d$ if web shear cracking occurs and propagates into the transfer zone. Russell and Burns (*60*) recommended design procedures which take this into consideration when normal weight concrete is used.

3. EXPERIMENTAL PROGRAM

The following discussion on the experimental program of this project is divided into two sections. The materials testing is covered in Section 3.1 and the structural testing in Section 3.2.

3.1 Materials Testing

All concrete materials testing, except for the tests on fresh concrete mentioned in Section 3.1.3, were carried out in the concrete materials laboratories at Purdue University. Concrete made and tested in the field was prepared at Rinker Materials (formerly CSR Hydro Conduit), Lafayette, Indiana. Rinker Materials in

TABLE 3.1
Chemical composition of the cements used for deck concrete

	Cement used for deck laboratory trials	Cement used for deck field trials
Chemical analyses by mass (%)		
Silicon dioxide (SiO_2)	19.36	20.16
Aluminum oxide (Al_2O_3)	5.72	4.87
Ferric oxide (Fe_2O_3)	2.97	2.92
Calcium oxide (CaO)	63.94	64.55
Magnesium oxide (MgO)	1.96	2.43
Sodium oxide (Na_2O)	0.23	0.28
Potassium oxide (K_2O)	0.13	0.09
Sulfur trioxide (SO_3)	2.94	2.55
Titanium dioxide (TiO_2)	0.47	0.46
Phosphorus pentoxide (P_2O_5)	0.09	0.07
Manganic oxide (Mn_2O_3)	0.08	0.05
Strontium oxide (SrO)	0.07	0.06
Chromic oxide (Cr_2O_3)	0.02	0.02
Zinc oxide (ZnO)	0.04	0.03
Loss on ignition (950°C)	2.14	1.45
Total	100.18	99.99
Alkalies as Na2O	0.32	0.34
Calculated potential compounds as per ASTM C 150-00 (%)		
Tricalcium silicate (C3S)	62	65
Dicalcium silicate (C2S)	9	8
Tricalcium aluminate (C3A)	10	8
Tetracalcium aluminoferrite (C4AF)	9	9

NOTES:
1. Oxide analyses by X-ray fluorescence spectrometry. Samples fused at 1000°C with $Li_2B_4O_7$.
2. Values for TiO_2 and P_2O_5 are not added to the Al_2O_3 when the compounds are calculated, in accordance with ASTM C 150-00.
3. X-Ray Fluorescence oxide analysis meets the precision and accuracy requirements for rapid methods per ASTM C 114-00. Most recent re-qualification date is March 15, 2002.
4. The analyses in Table 3.1 were performed at Construction Technology Laboratories, Inc., Chicago, on Nov. 21, 2002.

Lafayette is a manufacturing facility for precast concrete with specialization in the production of prestressed bridge girders.

3.1.1 Concrete Materials

The raw materials used in this study were selected based on the two following criteria: (a) be locally available, and (b) be approved by the Indiana Department of Transportation (INDOT) for use on highway projects.

3.1.1.1 Cement. Two different cements were used in this study. A TypeI cement from Essroc Cement Corp., Logansport, Indiana, was used for all deck concrete and a TypeIII cement from Lone Star Industries, Inc., Greencastle, Indiana, was used for all girder concrete. Results of chemical analyses of the cements used for deck concrete are listed in Table 3.1. The Type I cement used for the laboratory portion of the study was delivered in bags containing 42.6 kg (94 lb) each and stored in a dry room in the laboratory until used. The Type I cement used for the field trials delivered in bulk to silos at the Irving Materials Inc. batch plant in West Lafayette, Indiana. The TypeIII cement was also delivered in bulk to silos at Rinker Materials, Lafayette, Indiana. All TypeIII cement used in the laboratory, as well as TypeI cement used for final mixture proportioning for deck field trials, was transported in sealed buckets from the plants to the laboratory. In addition, two mixtures were prepared with two different Type I cements for comparison purposes. The results from those mixtures are discussed in greater detail in Section 4.2.1.

3.1.1.2 Mineral Admixtures. The silica fume used in both girder and deck concrete was from W.R. Grace and was supplied in bags containing 11.3 kg (25 lb) each. The ground granulated blast furnace slag (GGBFS) used for the deck concrete was a Grade 100, supplied by Holnam Inc. Results of chemical analyses of the silica fume and GGBFS are listed in Table 3.2. Based on the specific gravity of silica fume reported by Neville [(*5*), p. 87], the specific gravity of silica fume was assumed to be 2.2. Similarly, a value of 2.9 was used for the specific gravity of the GGBFS [(*5*), p. 80)].

3.1.1.3 Aggregates. All coarse aggregate used in this study was crushed dolomite from Delphi, Indiana. The maximum aggregate size was 25 mm (1 in.) for the girder concrete and 19 mm (0.75 in.) for most of the deck concrete laboratory mixtures. However, towards the latter part of the study, the maximum aggregate size was

TABLE 3.2
Chemical analyses of the silica fume and ground granulated blast furnace slag (GGBFS)

	Silica fume	GGBFS
Chemical analyses by mass (%)		
Silicon dioxide (SiO_2)	93.07	37.73
Aluminum oxide (Al_2O_3)	0.62	7.75
Ferric oxide (Fe_2O_3)	0.41	0.39
Calcium oxide (CaO)	0.66	39.45
Magnesium oxide (MgO)	1.16	10.77
Sodium oxide (Na_2O)	0.16	0.35
Potassium oxide (K_2O)	0.79	0.29
Sulfur trioxide (SO_3)	<0.01	2.59
Titanium dioxide (TiO_2)	<0.01	0.84
Phosphorus pentoxide (P_2O_5)	0.10	<0.01
Manganic oxide (Mn_2O_3)	0.06	0.50
Strontium oxice (SrO)	<0.01	0.04
Chromic oxide (Cr_2O_3)	0.02	<0.01
Zinc oxide (ZnO)	0.10	<0.01
Loss on ignition (950°C)	2.71	−0.82
Total	99.85	99.89
Alkalies as Na_2O	0.67	0.55

NOTES:

1. Results reported on an oven dry basis.
2. Oxide analyses by X-ray fluorescence spectrometry. Samples fused at 1000°C with $Li_2B_4O_7$.
3. Elemental sulfur and sulfide sulfur may be lost during high temperature fusion.
4. The analyses in Table 3.2 were performed at Construction Technology Laboratories, Inc., Chicago, on Nov. 21, 2002.

increased to 25 mm (1 in.). That maximum aggregate size was also used for the deck field trials. All fine aggregate was natural river sand. The specific gravity of the dolomite was 2.71 and the specific gravity of the sand was 2.68.

3.1.1.4 Chemical Admixtures. A variety of chemical admixtures from both W.R. Grace and Master Builders was used. All girder concrete was made with admixtures from W.R. Grace while admixtures from both manufacturers were used for the deck concrete. When proportioning the concrete, the water present in the admixtures was subtracted from the mixing water in an attempt to obtain a "true" water-binder ratio.

3.1.2 Concrete Mixing and Specimen Preparation in the Laboratory

All concrete made in the laboratory was mixed in a Lancaster counter current pan mixer. Each mixture had a volume of 0.042 m^3 (1.5 ft^3). The mixing was carried out in accordance with ASTM C192 (Standard Practice for Making and Curing Concrete Test Specimens in the Laboratory). The moisture content of both coarse and fine aggregates was measured prior to mixing and the amount of mixture water adjusted to maintain the desired water-cement ratio. The water in the admixtures was also considered when adjusting the amount of the mixture water. The aggregate samples were dried in a

Figure 3.1 Counter current pan concrete mixer used to mix all concrete made in the laboratory.

steel bowl over a hot plate or in an oven. The concrete mixer used to mix all concrete made in the laboratory is shown in Figure 3.1.

At the conclusion of mixing, the slump, density, and air content of fresh concrete were measured. The slump was measured in accordance with ASTM C143 (Standard Test Method for Slump of Hydraulic Cement Concrete), the density in accordance with ASTM C138 (Standard Test Method for Density (Unit Weight), Yield, and Air Content (Gravimetric) of Concrete), and the air content was measured in accordance with ASTM C231 (Standard Test Method for Air Content of Freshly Mixed Concrete by the Pressure Method). Tests on the fresh concrete were normally finished within about 10 minutes from the conclusion of mixing. To monitor changes in the concrete properties of selected mixtures, the tests on the fresh concrete were repeated after 20 to 30 minutes had elapsed from the end of mixing.

Fabrication of compressive strength cylinders and other specimens was generally started immediately at the conclusion of mixing. In the event that a batch was made by one person, the specimen preparation was started at the conclusion of the tests made on the fresh concrete. When making test specimens, the ASTM C192 (Standard Practice for Making and Curing Concrete Test Specimens in the Laboratory) standard was, in general, followed. However, single-use plastic cylinder molds, conforming to ASTM C470 (Standard Specification for Molds for Forming Concrete Test Cylinders Vertically), were used several times, or until a visible deformation had occurred, before they were discarded.

Consolidating all specimens by rodding proved to be labor intensive and time consuming. Shortly after the start of the experimental program and after a suitable vibrator became available, it was decided to consolidate all concrete specimens, except drying shrinkage specimens and samples used for measuring fresh concrete properties, using a 19 mm (3/4 in.) diameter vibrator. All specimens consolidated by vibration were filled in a

single layer, except cylinders, which were filled in two layers. Vibrating the concrete was not believed to negatively affect the variation between specimens from the same batch. Drying shrinkage specimens were consolidated by rodding throughout the study to prevent displacement of the gage studs.

All concrete specimens, except most of the temperature matched cured (TMC) specimens, were stored in their molds on the laboratory floor for the first day. They were covered with plastic to minimize moisture evaporation. After one day (two days for most of the TMC specimens), they were removed from the molds, labeled, and moved to the fog room for further curing.

3.1.3 Concrete Mixing and Specimen Preparation in the Field

Procedures for making and testing fresh girder concrete in the field did not differ greatly from those used in the laboratory. The main difference was the size of the concrete mixer and the mixing time. The mixer used at the precast plant was also a pan mixer, not unlike the one used in the laboratory, with a capacity of 3.1 m^3 (4 yd^3). The size of the batches made in the field ranged from 0.76m^3 to 3.1 m^3 (1 yd^3 to 4 yd^3). The mixing time varied between mixtures and was not monitored. As in the laboratory, moisture contents of both coarse and fine aggregates were measured prior to mixing to maintain the desired water-binder ratio.

Field deck concrete was mixed entirely in the ready mix trucks. The batch plant did not contain a mixer and its sole purpose was to measure the materials and place them in the trucks where they were mixed. When supplementary materials were used, they were loaded into the truck by hand before the truck was loaded with the rest of the materials. The volume of each of the mixtures was 1.5 m^3 (2 yd^3) which was considered the minimum required for adequate proportioning and mixing.

Fresh concrete properties were determined in the same manner as in the laboratory. Concrete specimens were consolidated by internal vibration with a 19 mm (3/4 in.) diameter vibrator. All concrete specimens were left in the field for the first day, then transported to the laboratory, removed from the molds, labeled, and moved to the fog room for further curing. Attempts to control the temperature around the specimens, while at the precast plant, were not made and the specimens were stored outdoors. Care was taken to minimize moisture evaporation by covering all specimens with plastic.

3.1.4 Compressive Strength

Compressive strength test specimens were prepared in accordance with ASTM C39 (Standard Test Method for Compressive Strength of Cylindrical Concrete Specimens). A deviation from the standard procedure was made when testing specimens with compressive strength in excess of 48 MPa (7000 psi) as all specimens were tested using unbonded caps. Neoprene pads with a durometer hardness of 70 were generally used, but pads with a durometer hardness of 60 were used for some specimens expected to have low compressive strength.

The compressive tests of specimens from girder mixtures and laboratory deck mixtures were carried out with an 1100 kN (250 kip) hydraulic testing machine manufactured by Forney Incorporated. Specimens from TMC mixtures and deck field trials were tested with a 2670 kN (600 kip) machine, also manufactured by Forney Incorporated. All compression tests were done on 102×203 mm (4×8 in.) cylinders. At each testing date, two cylinders were tested from each of the mixtures except for mixtures prepared at the precast plant, where three cylinders were tested. The target loading rate was 0.27 MPa (40 psi) per second, or 133 kN (30 kip) per minute.

3.1.5 Static Modulus of Elasticity

Static modulus of elasticity was measured on sets of two 152×305 mm (6×12 in.) cylinders. Each set of cylinders was tested at different ages. A compressometer, as per ASTM C469 (Standard Test Method for Static Modulus of Elasticity and Poisson's Ratio of Concrete in Compression), was used to measure the strains for given loads up to 40% of the ultimate compressive strength. The chord modulus of elasticity was then calculated. The ends of all cylinders were capped using a high strength sulfur compound prior to the first test.

3.1.6 Dynamic Modulus of Elasticity

Dynamic modulus of elasticity was determined on $76 \times 76 \times 381$ mm ($3 \times 3 \times 15$ in.) prisms from selected mixtures. The specimen were cured in the moist room throughout the duration of the testing period and only removed from the moist room when tested. The mass and fundamental transverse, longitudinal, and torsional frequencies of the specimens were measured at each testing date. A waveform spectrum analyzer was used to determine the frequencies. The dynamic modulus of elasticity was calculated using a software from Grindo-Sonic, the manufacturer of the equipment.

3.1.7 Splitting-Tensile Strength

Splitting tensile strength of specimens from the four field trial deck mixtures was performed after 28 and 56 days of moist curing. A set of three 152×305 mm (6×12 in.) cylinders was tested for each test in accordance with ASTM C496 (Standard Test Method for Splitting Tensile Strength of Cylindrical Concrete Specimens). The splitting tensile tests were carried out with a 2670 kN (600 kip) hydraulic testing machine manufactured by Forney Incorporated. The target loading rate was 1.22 MPa (177 psi), or 89 kN (20 kip) per minute. A 3.2-mm (1/8-in.) thick sheet of plywood was obtained from a local furniture manufacturer and cut to provide roughly 25 mm (1 in.) wide bearing strips for testing the cylinders.

3.1.8 Temperature Measurements

A Campbell Scientific CR10X datalogger and control unit was set up with a Campbell Scientific AM416 multiplexer to read and record temperature data. With the multiplexer, two of the six datalogger channels can be used to monitor up to 32 TypeT (Copper-Constantan) thermocouples simultaneously. The system is powered with one 12volt battery and can be operated under all regular field conditions. A personal computer was used to retrieve the data and to write programs to control the unit. A sample program is included in Appendix B and the setup of the temperature monitoring instrument is shown in Figure 3.2.

The sockets seen on the front of the box shown in Figure 3.2 are connected with thermocouple wires to a wiring panel on the multiplexer. The multiplexer and the datalogger are connected with regular copper wires, leaving the reference junctions on the multiplexer. For an accurate determination of the reference temperature, a thermistor was installed on top of the multiplexer and monitored with the datalogger.

The multiplexer was enclosed in an air tight aluminum box with a plastic lid. This was done to protect the sensitive relay mechanism of the multiplexer and to provide a stable environment for the reference junction. A small bag of silica gel desiccant was enclosed in the aluminum box in order to maintain a low relative humidity.

All thermocouples used in this study were fabricated in the laboratory. The wires were cut to desired lengths, the ends stripped, soldered together, and insulated. The thermocouple wire was a Gage 24 with a double Teflon insulation. Two thermocouples with attached male plugs are shown in Figure 3.3. The connectors of the plugs are made of copper and constantan to avoid having an extra reference junction in the thermocouple circuit.

Temperature measurements were done on multiple specimens. Two rapid freeze-thaw specimen and one deicing salt scaling specimen were instrumented with thermocouples in order to monitor the temperatures in their respective testing environments. The temperature developments of the multiple-strand development length beams and accompanying cylinders made with mixtures HPC-1 and HPC-2 were also monitored. The temperature development in the web of both beams and in the flange of one beam was monitored. The thermocouples were attached to wooden rods to allow for quick installation in the field and to provide support for the thermocouples during concrete placement. The thermocouples, installed in the form, used to cast multiple-strand development length specimen HPC-2 are shown in Figure 3.4.

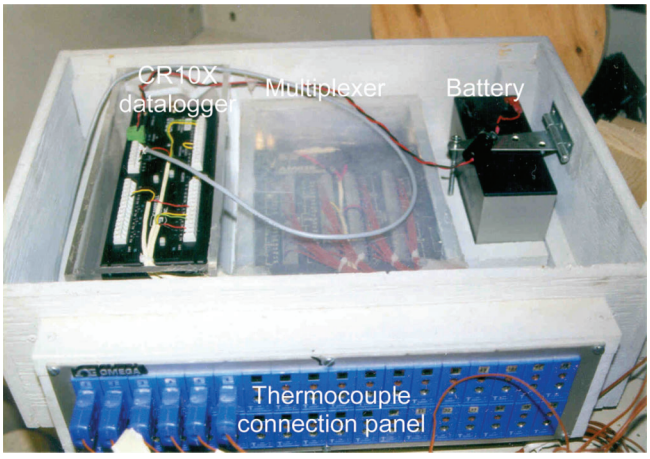

Figure 3.2 Instrument used for temperature monitoring.

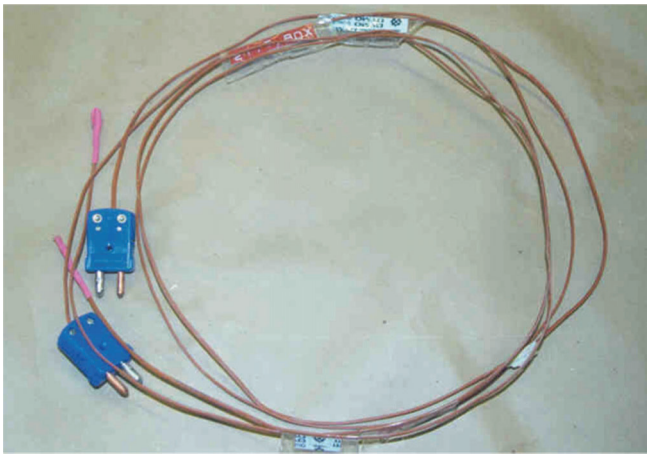

Figure 3.3 Two thermocouples with copper-constantan plugs attached.

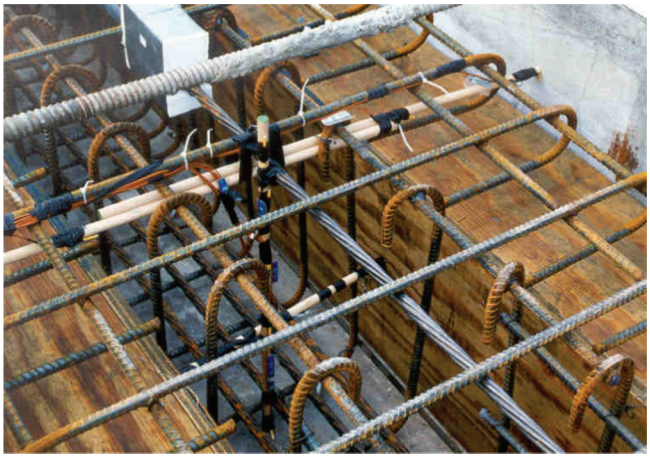

Figure 3.4 Thermocouples installed in the formwork prior to casting of multiple-strand development length specimen HPC-2. The thermocouples were attached to wooden rods to allow for quick installation.

3.1.9 Rapid Freezing and Thawing in Water

The durability of concrete to freezing and thawing was evaluated according to ASTM C666 (Standard Test Method for Resistance of Concrete to Rapid Freezing and Thawing), procedure A, in which

$76 \times 76 \times 381$ mm ($3 \times 3 \times 15$ in.) prisms from selected mixtures were subjected to rapid freezing and thawing in water. The specimens were cured in the moist room for 14 days before the test was started. Frequently, the specimens were stored frozen for several weeks until space became available in the freeze-thaw apparatus. Due to large number of specimens and limited space in the freeze-thaw machine, only one specimen was tested from several of the mixtures.

The mass and fundamental transverse, longitudinal, and torsional frequencies of the specimens were measured prior to freezing and then periodically during the test. A waveform spectrum analyzer was used to determine the frequencies. The change in relative dynamic modulus of elasticity, as per ASTM C666, was used to evaluate the performance of the specimens. Generally, around 30 freeze-thaw cycles passed between measurements.

The freeze-thaw machine used in this study was a Model C6461 from Logan Freeze-Thaw Mfg. Co., Logan, Utah. A total of 18 specimens were tested simultaneously. In the event that not enough specimens were available, dummy specimens were used to maintain the machine at its capacity. The freeze-thaw machine, fully loaded with specimens, is shown in Figure 3.5.

After instrumenting one specimen with thermocouples and monitoring the temperature variations in the freeze-thaw machine for several days, it was discovered that the temperature variations in the instrumented specimen exceeded the range of 4.4 to -17.8°C (40 to 0°F) specified in the ASTM C666 standard. The temperature in the center of the specimen was found to vary between 12 and -23°C (54 and -9°F). In order to maintain as uniform test conditions as possible for all test specimens, the temperature settings of the freeze-thaw machine were not altered after the actual temperature variations were discovered. The temperature variations during 15 hours at different depths along the vertical centerline of one specimen and the air inside the freeze-thaw machine are shown in Figure 3.6.

Figure 3.5 Freeze-thaw machine used for rapid freezing and thawing of specimens under water.

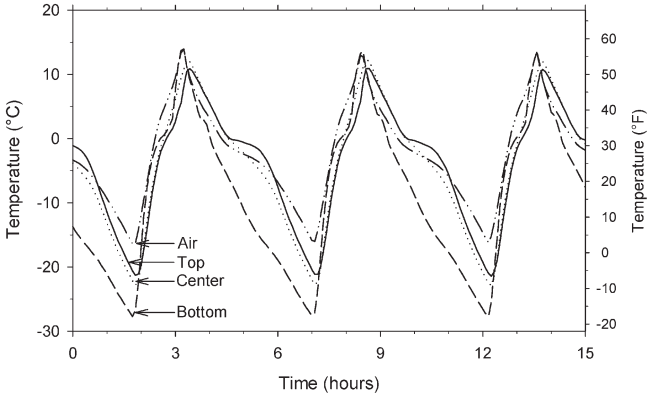

Figure 3.6 Temperature variations during 15 hours at different depths along the vertical centerline of one specimen and the air inside the freeze-thaw machine.

Figure 3.7 A new Omega CN9111A temperature controller installed on an existing freeze-thaw machine. The digital display on the controller is showing 3.3°C.

Before testing of the TMC mixtures, new specimen holders were purchased to accommodate $76 \times 102 \times 381$ mm ($3 \times 4 \times 16$ in.) prisms. Also, before the deck field trial specimens were tested, the control system of the machine was replaced with an Omega CN9111A temperature controller. The Omega controller, installed on the freeze-thaw machine, is shown in Figure 3.7. This controller uses an input from a thermocouple instead of a thermistor as the previous controller did. The temperature variations in the freeze-thaw machine were monitored after the larger size specimen were introduced and again after the new controller was installed. The temperature range was found to be acceptable.

3.1.10 Freezing and Thawing in the Presence of Deicing Salts

The scaling resistance of concrete specimens was tested in accordance with ASTM C672 (Standard Test Method for Scaling Resistance of Concrete Surfaces Exposed to Deicing Chemicals), except that the relative

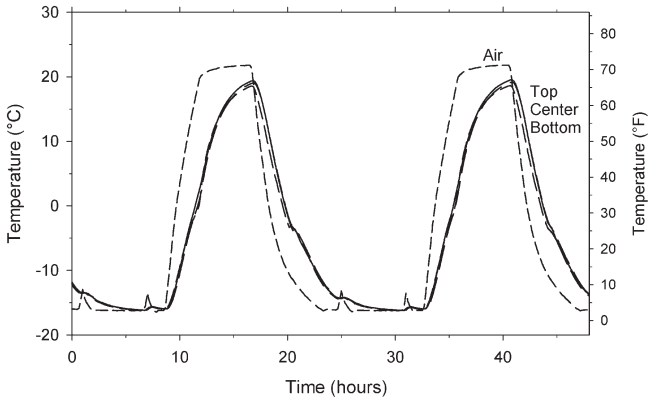

Figure 3.8 Temperature variations in the freeze-thaw room and a scaling specimen during 48 hours. Temperature variations at any given time within the depth of the 76mm (3in.) thick specimen were minimal. The temperature measurements started at midnight.

humidity during thawing was not controlled due to lack of such instrumentation. The tests were carried out in a walk-in freeze-thaw room manufactured by Environmental Growth Chambers, Chagrin Falls, Ohio. Each freeze-thaw cycle lasted 24 hours and the temperature was varied between 22°C (72°F) and −16°C (3°F). The temperature variations in the freeze-thaw room and one scaling sample are shown in Figure 3.8 and the setup of the freeze-thaw room is shown in Figure 3.9. The small peaks in the air temperature were due to timed defrosting cycles of the freezing equipment.

Two $188 \times 254 \times 76$ mm ($7.4 \times 10 \times 3$ in.) specimens were tested from selected laboratory mixtures and four specimens from the deck field mixtures and four of the TMC mixtures. From each set of specimens from the laboratory deck mixtures, one specimen was ponded with 4% $CaCl_2$ solution while the other was ponded with 3% NaCl solution. For the deck field mixtures and TMC mixtures, all specimens were ponded with 3% NaCl solution. A rubber membrane, glued to the sides of the specimens, was used to contain the solutions on the top surfaces of the specimens. After every five

Figure 3.9 A view of the setup in the freeze-thaw room used for testing deicing salt scaling specimens.

Figure 3.10 Four sets of deicing salt scaling specimens prior to freeze-thaw testing.

cycles, scaling residues were collected and the solutions replaced with fresh solutions.

The rubber membrane was initially glued to the sides of the specimens using a Dow silicon sealer to provide a ponding dam. After around 40 cycles, a few of the specimens started losing the solutions through openings between the silicon and the concrete. Apparently, the bond between the silicon and the concrete deteriorated as the concrete became saturated. After this problem surfaced, a roughly 40 mm (1.6 in.) wide layer of a two-part Devcon epoxy (#14260) was applied to the sides of the specimens before the rubber membrane was attached using the silicon. The bond between the epoxy and the concrete was more resilient and further leaks were not observed. A set of four specimens prepared for testing are shown in Figure 3.10.

A slight modification was made to the testing procedure before testing of the TMC and deck field specimens. A plastic food wrap was stretched over the top of the rubber membrane dams. This significantly reduced the evaporation of solution from the specimens and eliminated the need for adding water to maintain the specified solution depth of 6 mm (¼ in.). It is believed that covering the specimens will increase the uniformity of exposure condition, including solution concentration.

3.1.11 Microscopical Determination of Air-Void Parameters in Hardened Concrete

Test specimens for microscopical evaluation were cut from freeze-thaw beams. The cuts were made perpendicular to the finished surface. After being cut, the specimens were polished using a progressively finer silicon carbide or aluminum oxide powders until acceptable surfaces were attained. Polishing with powders between Grit 100 and 600 was done on a polishing wheel while final polishing with Grit 800 and Grit 1000 powders was done by hand on a glass plate.

The microscopical determination of the air-void parameters was performed in accordance with the

modified point-count method of ASTMC457 (Standard Test Method for Microscopical Determination of Parameters of the Air-Void System in Hardened Concrete). A stereoscopic microscope, set at a magnification of 100×, was used and the distance between stops was set at 2.5 mm (0.1 in.)

3.1.12 Accelerated Curing of Deck Field Trial Specimens

One cylinder from each of the deck field trials was cured in saturated limewater at 38°C (100°F) from the age of seven days until prepared for testing at the age of 26 days. After being moist cured in the fog room, the specimens were placed inside a plastic container that was kept in large water heater. Only the water inside the plastic container was saturated with lime. The water heater is shown in Figure 3.11.

The water heater was modified specifically for this test. Before the modifications, the heater contained controls that were difficult to adjust. The heater also required 33.3A at 240 V to operate. After careful analysis of the heater's circuitry, the original control system was removed and a new Omega CN4321 temperature/process controller, using Type T thermocouple input, was installed. At the same time, the power current requirements of the heater was reduced to 8.3 A at 120 V. This modification made the water heater portable around the laboratory as any regular 15 A outlet was sufficient to meet the new current requirements.

3.1.13 Electrical Indication of Chloride Ion Penetration Resistance

Concrete's ability to resist chloride ion penetration was evaluated in accordance with ASTM C1202 (Standard Test Method for Electrical Indication of Concrete's Ability to Resist Chloride Ion Penetration). Two 97 × 203 mm (3.8 × 8 in.) cylindrical specimens were prepared from selected mixtures. At the time of testing, two 51 mm (2 in.) thick discs were obtained from each cylinder after cutting off and discarding the top 13 mm (½ in.) to reduce surface effects. Two specimens were prepared for testing after 28 days of moist curing and other two specimens after 91 days of moist curing.

After the test discs were cut, their surfaces were allowed to dry before the sides were coated with a two-part Devcon epoxy (#14260). The epoxy was allowed to harden before the samples were vacuum saturated. After the vacuum saturation, the specimens were placed between two chambers that were later filled with 3% sodium chloride and 0.3 N sodium hydroxide solutions. During the test, the cells were connected to a direct current circuit with a potential of 60 volts for a period of six hours. The current in the circuit was monitored and the charge passed, in coulombs, through the sample during the six-hour test period was calculated. The instrument used for the testing, shown in Figure 3.12, was Model 164 made by RLC Instrument Co. and was capable of testing four specimens simultaneously.

3.1.14 Corrosion

The effectiveness of each of the four deck field trial mixtures to protect reinforcement against corrosion was evaluated. The variables that were investigated within each mixture were length of moist curing and cover thickness. The length of the moist curing was either 3 or 14 days. All corrosion specimens were moist cured under wet burlap covered with a plastic sheet. Specimen preparation and testing procedures of the corrosion specimens are described in detail in Sections 3.1.14.1 to 3.1.14.5.

3.1.14.1 Steel. All steel bars used in the corrosion specimens were 13 mm (0.5 in.) in diameter and came from the same heat. The bars were cut to length in an industrial shearing machine. Each bar was roughly 355 mm (14 in.) long.

After cutting, the ends of the bars were ground to remove sharp edges. Then, a roughly 76-mm (3-in.)

Figure 3.11 Water heater used for accelerated curing of deck field trial specimens requiring curing in lime water at 38°C (100°F).

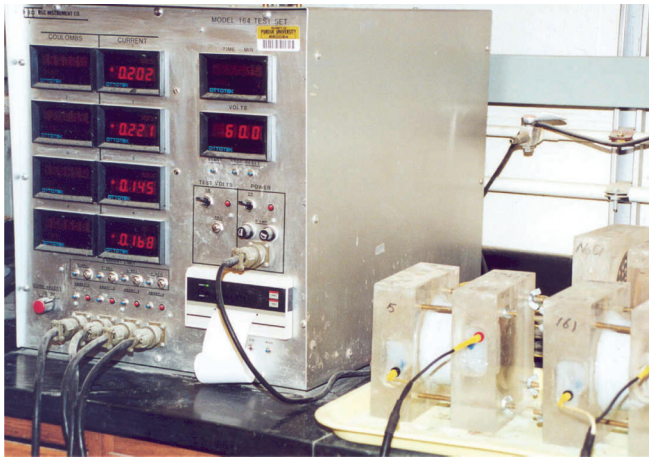

Figure 3.12 Instrument used for determining electrical indication of concrete's ability to resist chloride ion penetration.

long lead wire was soldered to one end of each bar. The soldering was done by first heating the bars to about 70°C (160°F) in an oven and then using a combination of a miniature butane torch and an electrical soldering iron to attach the wires.

A few days before the corrosion specimens were to be cast, the bars were polished with a mechanical wire brush until all surface deposits had been removed. After brushing, the bars were cleaned with hexane and allowed to dry. Care was taken to store the bars in a warm and dry place in a container containing some silica gel to prevent corrosion of the near white metal. Also, an intense effort was made to prevent the bars from coming in contact with oil, including skin oil, or other foreign material after they were cleaned. Cleaned rebar specimens along with fresh silica gel are shown in Figure 3.13.

As the entire lengths of some of the bars, including the protected ends, were to be exposed to chlorides, the ends were covered with epoxy, which in turn was covered with heat shrink tube. It was believed that epoxy would be more effective in preventing corrosion of the covered ends than electroplater's tape would. Due to the longitudinal ribs on the bars, there would be a void between the electroplater's tape and the bars, which would then be likely to promote rapid corrosion of the underlying steel if exposed to chlorides.

Before the epoxy was applied, the wires that had previously been soldered to the bars were extended with wires having their insulation intact to ensure that ends of the bars were fully sealed after the heat shrink tube had been put in place. For specimens used in the ladder type macrocells, the three bars of each cell were connected to a two-wire cable, which was then used to provide connection to the instrumentation used to monitor the corrosion current.

3.1.14.2 Corrosion Specimens. From each of the four field trial mixtures, six beams were made in accordance with a modified ASTM G109 standard (Standard Test Method for Determining the Effects of Chemical Admixtures on the Corrosion of Embedded Steel Reinforcement in Concrete Exposed to Chloride Environments). In addition, a series of five sets of steel bars, identical to those used in the G109 beams, were assembled and placed in a $610 \times 914 \times 152$ mm ($24 \times 36 \times 6$ in.) slab. Three of the beam specimens were moist cured for three days and the other three, along with the slab, were moist cured for 14 days. The modification of the ASTM G109 standard included alteration of the mixture design, steel bar preparation, and salt solution concentration. The concentration of the sodium chloride solution was 6%. Preparation of six beams used for corrosion testing is shown in Figure 3.14.

The design of the series of five sets of steel bars placed in the slab was based on the ASTM G109 configuration and corrosion sensors, designed by Schiessl and Raupach (*73*), where the cover of the anodic steel was varied. For this series, the cover of the anodic bars ranged from 13 mm to 64 mm (½ in. to 2½ in.) while the cathodic bars were kept at a constant distance of 51 mm (2 in.) from their respective anodic bars. The cover of the anodic bars of the standard G109 beams was 25 mm (1 in.).

The five sets of steel bars were supported with two small sheets of Plexiglas with a thickness of 3.175 mm (0.125 in.). A photograph of a series of five sets of steel bars designed to have a variable cover thickness is shown in Figure 3.15.

3.1.14.3 Exposure. As mentioned in the previous section, the concentration of the sodium chloride solution used to pond the specimens was 6%. Exposure to the solution was started when the specimens were 42 days old. After four days of exposure, the solution was removed and the specimens dried under halogen heat lamps. None of the specimens were covered during the ponding, which, due to evaporation, resulted in some increase of the solution

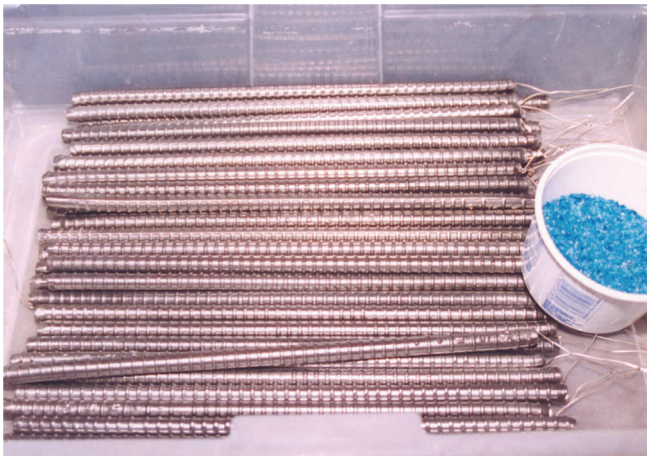

Figure 3.13 Rebar specimen after being wire brushed and cleaned with hexane. After cleaning, the specimens were stored in a plastic container containing silica gel to prevent premature corrosion due to moisture in the atmosphere.

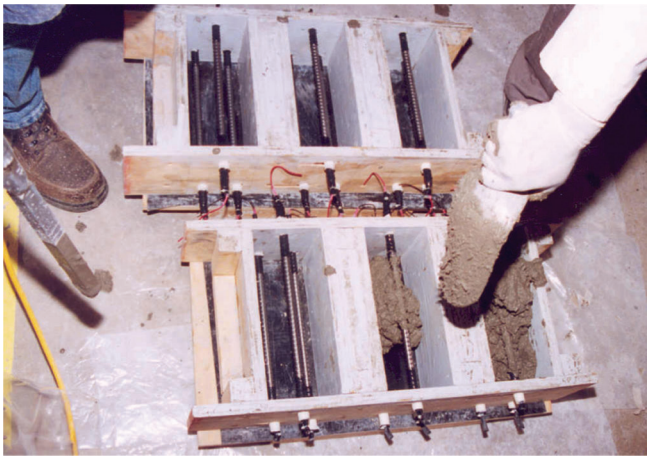

Figure 3.14 Preparation of six beams used for corrosion testing.

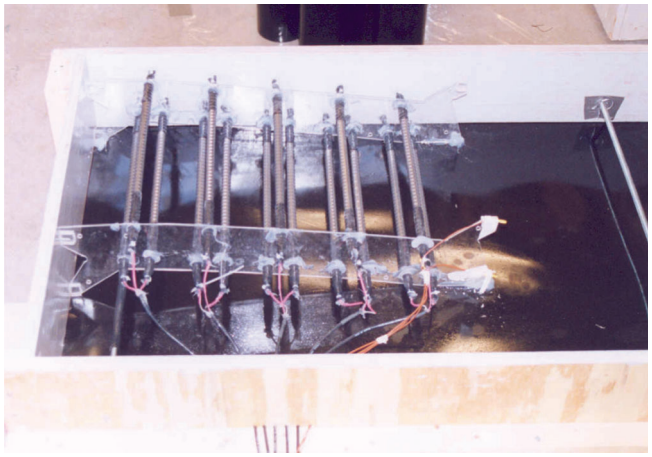

Figure 3.15 A series of five sets of steel bars designed to have a variable cover thickness. This series has been placed in the form just prior to casting of the concrete.

concentration during the ponding period. The increase in solution concentration was not quantified. All corrosion specimens from each mixture were placed in the same stainless steel pan with dimensions of $914 \times 1219 \times 38$ mm ($36 \times 48 \times 1.5$ in.) and dried with four 500 W heat lamps for three days to complete each weekly cycle.

The purpose of using the heat lamps was to create exposure conditions similar to those used by other researchers (*74,75*) to accelerate the deterioration process. The distance between the lamps and the specimens was 965 mm (38 in.). A view of the experimental setup during drying is shown in Figure 3.16.

The temperature development in the slabs was monitored for one week to evaluate the effectiveness of the heat lamps. As shown in Figure 3.17, the heat lamps were effective in raising the temperature of the concrete. In fact, the temperature reached values that were higher than anticipated. However, the temperature differential between different specimens was only about

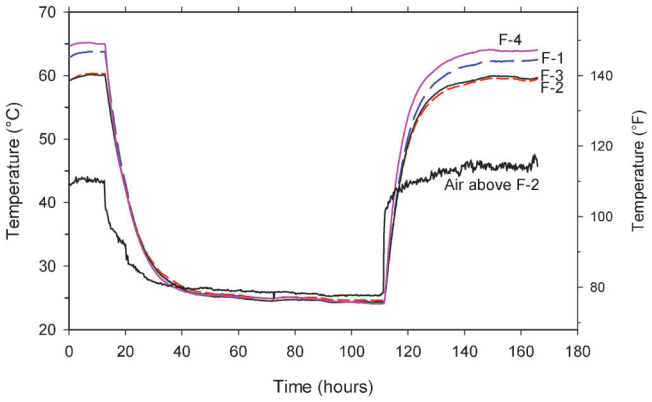

Figure 3.17 Temperature development in the center of the four field trial slabs containing series of five sets of steel bars during one week. The air temperature above slab F-2 was also monitored.

5°C (9°F) during the heating portion of the cycle. In terms of energy use and uniform heating conditions, a heated room or an enclosure might have been more efficient than the heating lamps.

3.1.14.4 Current Flow. A 100-ohm resistor was used to connect the anodic bar of each macrocell to the cathodic bars. The voltage over the resistors was monitored every 10 minutes with a Campbell Scientific CR10X datalogger and control unit. Two AM416 multiplexers were connected to the datalogger to expand four of the six channels to 64. Forty-four of the channels were used for this study while the rest was made available for another study. The multiplexers were placed in an airtight enclosure to provide a stable environment for the switching mechanisms of the relays in the multiplexers. The system, shown in Figure 3.18, was powered with a 12 V power supply. At the end of each weekly exposure cycle, the data was downloaded from the datalogger to a personal computer for analysis.

Figure 3.16 Experimental setup of halogen heat lamps and corrosion specimens during the drying portion of the weekly exposure cycle.

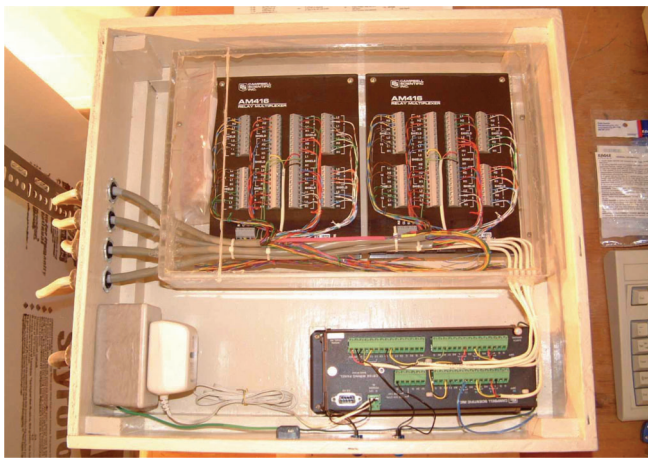

Figure 3.18 Data acquisition system used for monitoring corrosion current of macrocells.

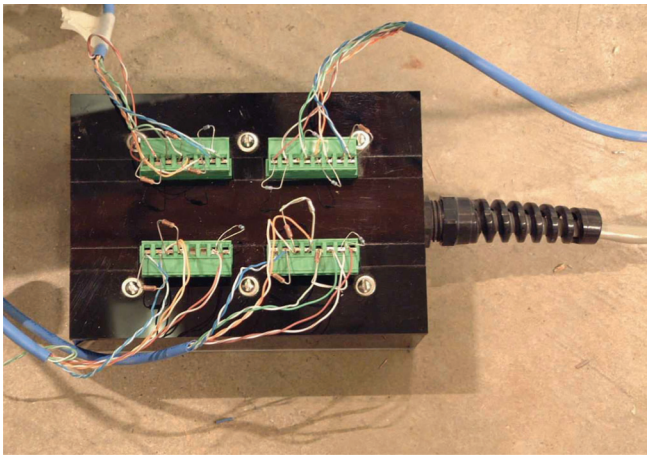

Figure 3.19 One of four connector modules used to connect macrocells to the current flow measurement system.

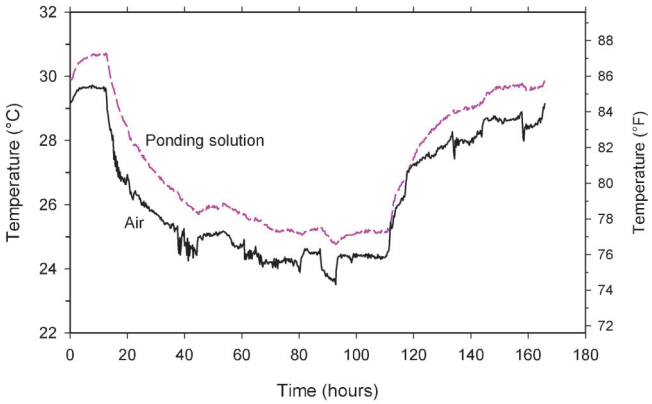

Figure 3.20 Temperature variations of ponding solution on chloride ion penetration slabs and surrounding air during one week of exposure.

For this study, the datalogger was programmed to monitor an input voltage range of ± 7.5 mV. At this range, the rated resolution is 1 μV. The impedance of the datalogger is very high, or 20Gohms.

Indoor telephone cables were used to connect each 16 channels of the multiplexers to separate modules, shown in Figure 3.19, which could be placed in different places at a maximum distance of about 3.6 m (11 ft) from the current flow measurement system. Smaller telephone cables, each having eight wires, were then used to connect the corrosion specimens to the modules. The connection was accomplished with pluggable strip connectors. With the connectors, a set of specimens could be easily disconnected when they had to be moved for coring or other purposes.

3.1.14.5 Half-Cell Potential. At the conclusion of each four day ponding period, the half-cell potentials of each macrocell were measured. An RE-5 copper-sulfate half-cell manufactured by MCMILLER Co., Ringwood, New Jersey, and a Model No. 82326 Craftsman multimeter were used to measure the half-cell potentials. Two readings were taken for each anodic bar. The impedance of the multimeter was 10 Mohms.

3.1.15 Chloride Ion Penetration

The penetration of chloride ions was monitored by collecting and analyzing powder samples from $610 \times 914 \times 152$ mm ($24 \times 36 \times 6$ in.) slabs. These slabs also contained the series of macrosells described in Section 3.1.14.2. The slabs, one from each mixture, were subjected to four days of ponding with a 6% NaCl solution. At the end of four days, the NaCl solution was removed and the specimens dried under heat lamps for three days to complete each weekly cycle.

Another series of smaller slabs was prepared and subjected to exposure conditions described in the AASHTO T259 standard. This was done in an effort to compare the effects of the traditional exposure method and the accelerated exposure method. The same sample collection method and schedule were also followed for the additional slabs. Sides of all chloride ion penetration slabs were sealed with an epoxy sealer to simulate two dimensional field conditions. These slabs were stored in the same room as the corrosion specimens. Due to the use of a large number of heat lamps in this room, the temperature of the solution on the slabs fluctuated from 25 to 31°C (77 to 88°F) as shown in Figure 3.20.

Powder samples used to determine base chloride levels were collected from all of the slabs prior to chloride exposure. These samples were obtained using a rotary hammer drill. Three samples were collected from each of the larger slabs and two samples from each of the smaller slabs. Before being analyzed, the powder samples were fine ground with a mortar and pestle until they passed a 0.3 mm (#50) sieve.

Samples of fine and coarse aggregates were crushed using a jaw crusher to prepare powder samples for chloride ion levels in the aggregates. The aggregate powder samples were also fine ground using a mortar and pestle until they passed a 0.3 mm (#50) sieve. Preparing powder samples from the aggregates was believed particularly important as baseline chloride ion concentrations reported by Samples and Ramirez (1999, p. 169) were as high as 1.28 kg/m^3 (1.67 lb/yd^3). The source of their baseline chloride ion concentrations was not identified.

After being exposed to chlorides for 90 days, a roughly 102 mm (4 in.) long core was extracted from each specimen. The remaining holes were cleaned and filled with mortar. The cores were allowed to dry for about three weeks and then ground to collect powder samples for chloride ion determination.

The grinding of the cores was accomplished with a diamond bit and a grinder. The grinder and associated setup is shown in Figure 3.21. The diamond bit had a diameter of 59 mm (2.3 in.) and was rotated at 400 rounds per minute. The core was clamped in a small vise that was attached to a traveling table. The traveling table had a horizontal velocity of 13 mm (0.5 in.) per

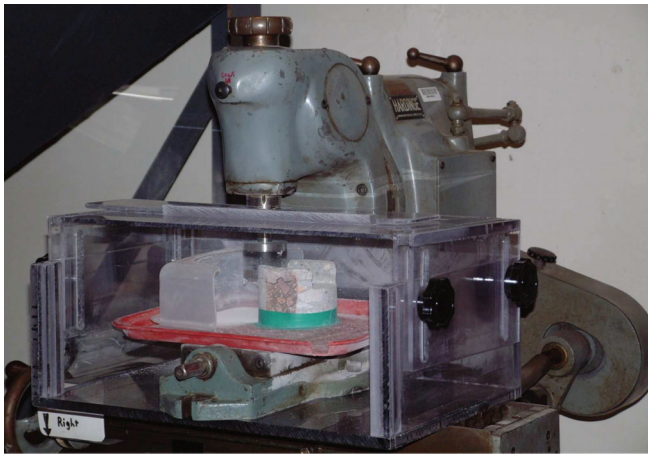

Figure 3.21 Chloride profile grinder and concrete core. Not shown in the picture is a front cover to the Plexiglas enclosure surrounding the core and diamond bit.

Figure 3.22 Preparation of three shrinkage specimens by rodding.

minute when automatically moved by the grinder. Vertical adjustments were made after each passing of the diamond bit. A typical thickness ground in each passing was 1 mm (39/1000 in.). If thicker layers were ground in each passing, there appeared to be a risk of overheating the diamond bit as well as the core. Thinner layers yielded finer powder samples, but at the cost of increased grinding time.

After each sample had been ground from the core, the sample was collected with a brush and placed in a plastic bag. The core, diamond bit, brush, and surroundings were then thoroughly cleaned with a powerful vacuum cleaner to minimize cross contamination of powder samples. Once the core had been ground to the desired depth and all powder samples collected, the powder samples were ground with a mortar and pestle until they passed a 0.3 mm (#50) sieve.

3.1.16 Drying Shrinkage

Four $76 \times 76 \times 279$ mm ($3 \times 3 \times 11$ in.) specimens, with a gage length of 254 mm (10 in.) as per ASTM C157 (Standard Test Method for Length Change of Hardened Hydraulic-Cement and Concrete), were fabricated and tested from selected mixes. During fabrication, the specimens were compacted by rodding rather than vibration to prevent displacement of the gage studs. The specimens were demolded after one day and placed in lime-saturated water bath for further curing. At age of seven days, two of the four specimens were removed from the water bath and placed in a drying room with $50 \pm 5\%$ relative humidity (RH). At age of 28 days, the remaining two specimens were also moved to the same room.

Three shrinkage specimens were prepared from each of the deck field trial mixtures. These specimens were cured in lime-saturated water for 28 days before being moved to the $50 \pm 5\%$ RH room. Unfortunately, the equipment used to maintain the desired humidity and temperature conditions in the room malfunctioned several times during the duration of the drying period. The results from this portion of the shrinkage measurements can therefore not be compared directly to results from other parts of this study. However, the data from the different field trial mixtures can be compared for relative performance as all of the field trial specimens remained under the same conditions throughout the test.

Drying shrinkage measurements were made with a length comparator equipped with a digital micrometer with a resolution of 0.0025 mm (0.0001 in.). At each testing period, both length and mass measurements were made. In addition to the ASTM testing schedule, all specimens were also tested at ages of 3, 7, and 14 days. Preparation of three shrinkage specimens is shown in Figure 3.22.

3.1.17 Experimental Program Involving TMC

A temperature matched curing (TMC) system, shown in Figure 3.23, was used for the four deck field trials. The specimens were cured for 24 hours. The specimens were demolded at the end of the 24-hour curing period and placed in the moist room. The reference temperature for the TMC system was obtained by placing about 0.2 cu ft. of concrete in the plastic bag, inserting the thermocouple inside the concrete, and placing the entire assembly into the void of the polystyrene block shown in Figure 3.24.

An inherent benefit of TMC cylinders, unrelated to strength or durability aspects, in single use plastic forms was the ease of form removal. As the temperature of these specimens was often near 50°C (120°F) when the TMC was concluded, the plastic forms could be removed by simply taking the lid off and holding the form with the specimen upside down. The specimen would then slide out of the form due to the force of gravity alone. However, when warm specimens are demolded, it becomes extremely critical to place them in a moist environment immediately as the loss of moisture is rapid. This moisture loss was found to be

Figure 3.23 Temperature matched curing enclosure with five 102×203mm (4×8in.) cylinder molds and two ducts for facilitating movement of air from two of the fans to the top of the enclosure.

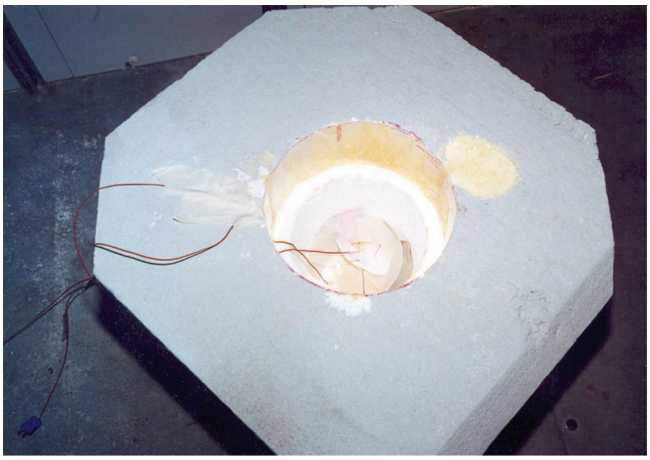

Figure 3.24 Polystyrene block used to contain reference concrete to allow natural temperature rise of the concrete.

as high as 1g (0.04 oz) per minute for 102×203 mm (4×8 in.) concrete cylinders.

The TMC specimens were filled and consolidated along with the control specimens. They were then placed on the aluminum grading, their tops finished and a plastic cap placed on the cylinder mold. The TMC commenced as soon as all the specimens had been prepared.

3.2 Structural Testing

All structural testing, except initial monitoring of strain gages and some transfer length measurements, was carried out in the Karl H. Kettelhut Structural Engineering Laboratory at Purdue University. Initial monitoring of strain gages and some transfer length measurements were done where the specimens were fabricated. All specimens used for structural testing were fabricated at Rinker Materials (formerly CSR Hydro Conduit), Lafayette, Indiana.

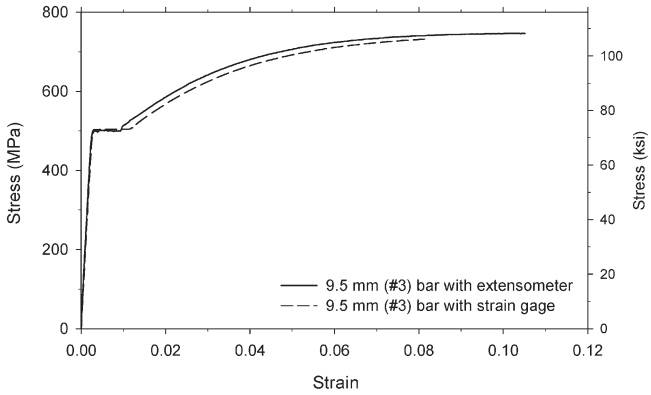

Figure 3.25 Stress-strain relationships for two 9.5 mm (#3) bars representative of those used for the multiple-strand development length specimens.

3.2.1 Steel Reinforcement and Prestressing Strand Properties

Prestressing strand from two manufacturers was used in this study. The pullout specimen, all single-strand development length specimen, and one of the multiple-strand specimens contained 15.2 mm (0.6 in.) strand from Insteel (INS). The other multiple-strand specimen contained 15.2 mm (0.6 in.) strand from Florida Wire and Cable (FWC). Both strands were a Grade 270, with a rated yield strength of 1860 MPa (270 ksi). The ultimate elongation of the Insteel strand, as reported by the manufacturer, was 6.5%. A corresponding value for the Florida Wire and Cable strand was not available, but was believed to be in excess of 5% based on other strand supplied by that manufacturer. The surface of the strand used for the pullout specimen and the single-strand specimens was clean (as received), while the surface of the strands used for the multiple-strand specimens was slightly rusted.

The additional tensile reinforcement used for the multiple-strand development length specimens were two deformed 9.5 mm (#3) bars placed at the level of the prestressing strands. The stress-strain relationship for the additional tensile reinforcement is shown in Figure 3.25.

3.2.2 Evaluation of Concrete to Prestressing Strand Bond Using Pullout Specimen

The first task of this study involved the fabrication and testing of a pullout specimen to determine if the strand used in this study would meet the minimum average pullout capacity recommended by Logan (*71*). After numerous consultations with Don Logan, the transverse reinforcement used in the pullout specimens in this study was modified from that shown in Appendix A to provide a transverse tie next to each strand. The details of the pullout specimen used in this study are shown in Figure 3.26. The reinforcement cage and strand specimens used in the pullout specimen are shown in Figure 3.27 and the completed pullout specimen in Figure 3.28. Each strand specimen was

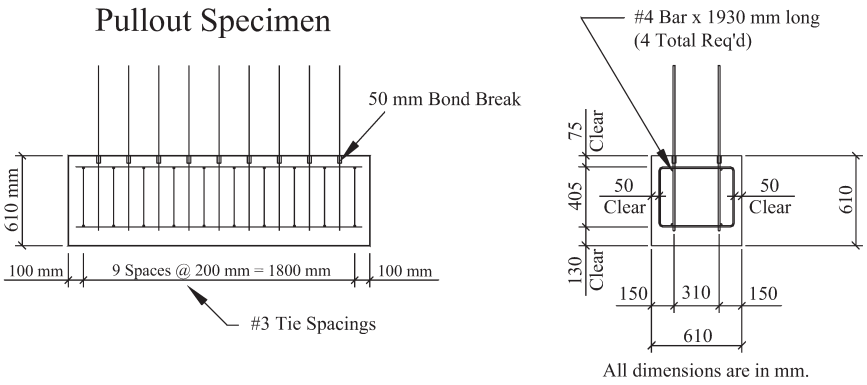

Figure 3.26 Details of the pullout specimen used in this study.

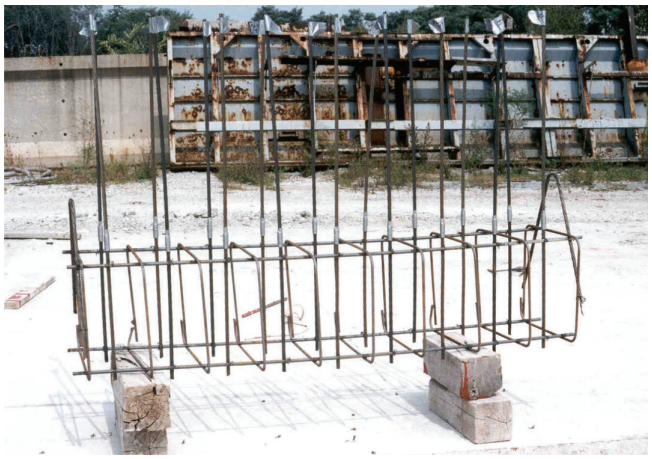

Figure 3.27 Reinforcement cage and strand specimens used in the pullout specimen.

Figure 3.28 Pullout specimen before testing of strands.

numbered and placed in the pullout specimen in a predetermined order. The arrangement of individual strand specimens within the pullout specimen is shown in Figure 3.29. Since the strand used in this study had a nominal diameter of 15.2 mm (0.6 in.) instead of 12.7 mm (0.5 in.) as tested by Logan, the corresponding minimum average pullout capacity (assuming a similar average bond stress at ultimate load) is 192 kN (43.2 kip). The arrangement of individual strand specimens within the pullout specimen is shown in Figure 3.29.

At the time of this study, the local prestressed concrete producer, CSR Hydro-Conduit, Lafayette, Indiana, was using strand manufactured by Insteel. Therefore, it was decided at the outset of this test program that all specimens would contain 15.2 mm (0.6 in.) Insteel strands.

3.2.3 Transfer Length Measurements

Experimental determination of the transfer length was attempted by measuring concrete surface strains at the ends of test specimens. Stainless-steel points were secured to the specimens at 50 mm (2 in.) spacings prior to de-tensioning the strands. The points were mounted using a 5-minute epoxy and were located at the depth of the strand. Distances were measured between points using a Whittemore gage that had a 254 mm (10 in.) gage length and had a differential reading capability of 0.00254 mm (1/1000 in.), with a perceived accuracy of twice this amount. Therefore, the resolution of the gage was about 20 με ($20{\cdot}10^{-6}$).

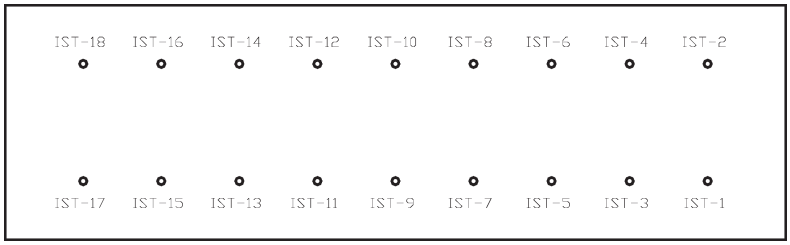

Figure 3.29 Arrangement of individual strand specimens within the pullout specimen.

Surface strain readings were taken prior to de-tensioning, immediately after de-tensioning, and periodically during the first month after stripping. Transfer length measurements were initially taken for the single-strand beam specimens discussed in Section 3.2.6. However, the value of surface strains in these beams from pre-compression (P/A) was relatively small (in the order of 200 με). This factor, coupled with the effects of rapid temperature changes in late Fall and moisture effects on the epoxy used to mount the points, often resulted in unreliable readings during this initial attempt.

Therefore, an additional specimen was fabricated specifically for measuring transfer lengths. This specimen had a cross-section that measured 100×150 mm (4×6 in.) and contained two concentric strands, and was similar in cross-section to specimens cast in another research project that was conducted concurrently with this project but utilized 12.7 mm (0.5 in.) diameter strands. Whittemore readings were taken on both sides and both ends of each specimen, which was approximately 2400 mm (94.5 in.) long. Unfortunately, longitudinal cracks originated in this specimen when the prestressing force was transferred (i.e., when the strands were cut). These cracks served to increase the actual transfer length of the strand (in this test specimen) and were not representative of actual beams designed for use in the field. The formwork and prestressing strands for the transfer length specimen are shown in Figure 3.30 and the Whittemore points mounted on the transfer length specimen are shown in Figure 3.31.

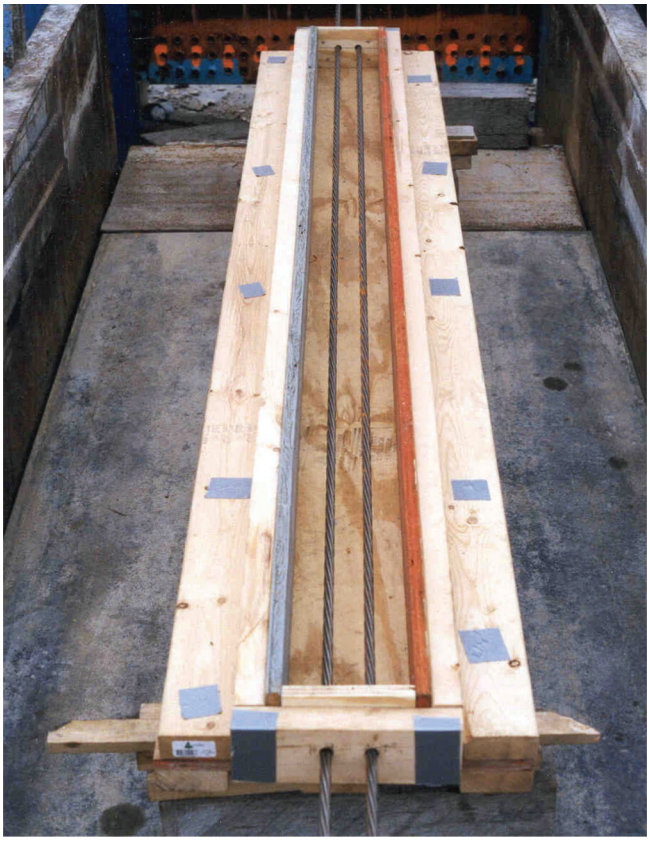

Figure 3.30 Formwork and prestressing strands for transfer length specimen.

Figure 3.31 Whittemore points mounted on a transfer length specimen.

3.2.4 Evaluation of Development Lengths

As indicated by the title of this section, development lengths are evaluated, rather than determined in experimental programs. This is typically done by designing test specimens which are loaded in such a way that the maximum moment occurs at the point in the beam where the provided embedment length L_e is equal to the calculated development length L_d. This point is commonly referred to as the "critical section."

Development length testing in this experimental program consisted of testing six single-strand specimens and two multiple-strand specimens. The test specimens in this study had fully bonded strands and were tested by applying loads from a hydraulic actuator that was located at a distance L_d from the end of the specimen. Loads were applied incrementally until failure of the members occurred. Interpretation of the test results are straight-forward. A flexural failure indicates that the embedment length is adequate to develop the strand, while a bond failure indicates that the embedment length is not sufficient and that the actual development length is larger than the calculated value.

3.2.5 Calculation of Development Lengths for Test Specimens

The ACI development length equation (Equation 2.5) was presented in Section 2.4.3. In this equation, the development length is considered to be a function of the following variables:

f_{se}, the effective stress in the strand after all losses (ksi),

d_b, the nominal diameter of the strand in inches, and f_{ps}, the stress in the strand at nominal strength of the member (ksi).

Thus, the code-prescribed development length is not a single value that can be evaluated for a given strand. Instead, it is a function of both the strand properties and the properties of the member in which it is cast. Interestingly, for a given strand size and member, the development length may be calculated to be different values by different designers, depending on the assumptions which are made in calculating f_{se} and f_{ps}. From Equation 2.5 it can be seen that the calculated development length is largest when f_{ps} is maximized and f_{se} is minimized. In other words, if the designer overestimates f_{ps} while underestimating f_{se} (by overestimating prestress losses), then the calculated development length will be "longest." While there may be other implications on design (i.e., member sizing, stress and camber calculations, etc.), the result of calculating excessively long development lengths (in terms of actual bond performance) is conservative since it will result in longer required embedment lengths.

However, the converse may not be true. If the designer underestimates f_{ps} while at the same time overestimating f_{se} (by underestimating prestress losses), then the calculated development length will be minimized. This calculation will, in turn, lead to shorter required embedment lengths for the strand and bond failure could occur prior to the member reaching nominal capacity.

Since this research was aimed at evaluating the validity of the current code equations for development lengths when normal weight concrete is used, it was determined that, conservatively, the worst-case situations should be tested. With this in mind, the experimental tests in this study were designed so that the "shortest" development lengths that might realistically be calculated by designers would be tested. As discussed above, the "shortest" development lengths are calculated when f_{ps} is minimized and f_{se} is maximized. The stress in the strand at nominal strength of the member, f_{ps}, is typically estimated by either direct calculation from code equations or by a strain compatibility analysis. While the strain compatibility analysis is generally considered to be more accurate, especially when more than one layer of steel is provided, the code equations are typically more conservative and yield a lower estimate of f_{ps}.

Using the ACI Code, the stress in the strand at member nominal capacity may be estimated by the equations in Section 18.7.2 of the code [(*61*), pp. 259–260]. For members with bonded prestressing tendons and no compression reinforcement, the formula for f_{ps} reduces to

$$f_{ps} = f_{pu}\left\{1 - \frac{\gamma_p}{\beta_1}\left[\rho_p \frac{f_{pu}}{f'_c}\right]\right\} \tag{3.1}$$

- where f_{pu} = the specified tensile strength of the prestressed tendons in psi.
- γ_p = a factor for the type of prestressing tendon used (0.28 for low-lax strand).
- β_1 = a factor used to enable ultimate flexural capacity calculations to be made by representing the concrete in compression by an equivalent rectangular stress block.
- ρ_p = the ratio of prestressed reinforcement = A_{ps}/bd_p, where A_{ps} is the area of the prestressed reinforcement in the tension zone, b is the width of the compression face of the member, and d_p is the distance from the extreme compression fiber to the centroid of the prestressed reinforcement.
- f'_c = the specified compressive strength of the concrete in psi.

Thus, in order to test the most severe condition, the stress in the strand at nominal capacity of the test specimens was calculated using Equation 3.1. In addition, the effective prestress after all losses, f_{se}, was calculated by assuming only 8% total losses. This value was also used by Logan (*71*) and is a practical minimum value that might be calculated by design engineers.

3.2.6 Single-Strand Development Length Specimens

Three single-strand development length specimens were fabricated and tested in this study. The purpose of the single-strand specimens was to provide an inexpensive means to conduct multiple development length tests with the same concrete and strand supplier combinations. Design parameters of the single-strand development length specimens are listed in Table 3.3. The single-strand beams were used for two development length tests each–one per end. Shear reinforcement was provided only in the central portion of the beams to ensure that this region would be intact after the first end of the beam was tested. Note, the central portion of the beam was part of the loaded span for the testing of both ends of the single-strand beams.

TABLE 3.3
Design parameters of single-strand development length specimens

Number of beams	Strand producer	Embedment length	Concrete strength	Strand size
3	IST	2170 mm (85.5 in.)	69 MPa (10,000 psi)	15.2 mm (0.6 in.)

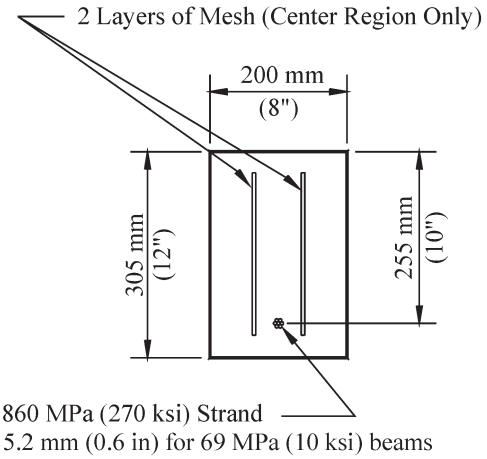

Figure 3.32 Cross-section of single strand development beam.

The shear reinforcement in the center region of the beams was purposefully not centered in the beam. This was to provide the ability to increase the embedment length at one end of the test specimens in the event that initial beam tests based on the calculated development lengths would experience bond failure. However, as will be further discussed in Chapter 5, all single-strand beams were tested at the calculated development lengths of 2170 mm (85.5 in.)

The single-strand specimens had a rectangular cross-section measuring 200×305 mm (8×12 in.), and contained a single prestressing strand located at a depth "*d*" of 255 mm (10 in.). A diagram of the cross-section of a single-strand development length beam is shown in Figure 3.32. The width of 200 mm (8 in.) was slightly larger than the 165 mm (6.5 in.) width used by Logan (*71*) for his single-strand specimens, in order to minimize the depth of concrete in compression and maximize the strain in the prestressed strand at the ultimate flexural capacity of the specimens. The increased specimen width was needed because 15.2 mm (0.6 in.) nominal diameter strands were tested in this study, whereas Logan tested specimens containing only 12.7 mm (½ in.) nominal diameter strands. Using 200 mm (8 in.) wide specimens, the strain in the strands at nominal flexural capacity of the test beams was estimated at 2.7% based on a strain-compatibility analysis. Although this value was lower than the 3.5% value recommended by Buckner (*69*) for minimum strand strains in development length specimens, it was larger than the 2.0% value calculated by Logan for his single-strand beams that failed by strand rupture.

The loading arrangements corresponding to the 69 MPa (10 ksi) rectangular beams are shown in Figure 3.33. As seen in this figure, the calculated development length (and thus the tested embedment length) for these beams was 2170 mm (85.5 in.) Loads

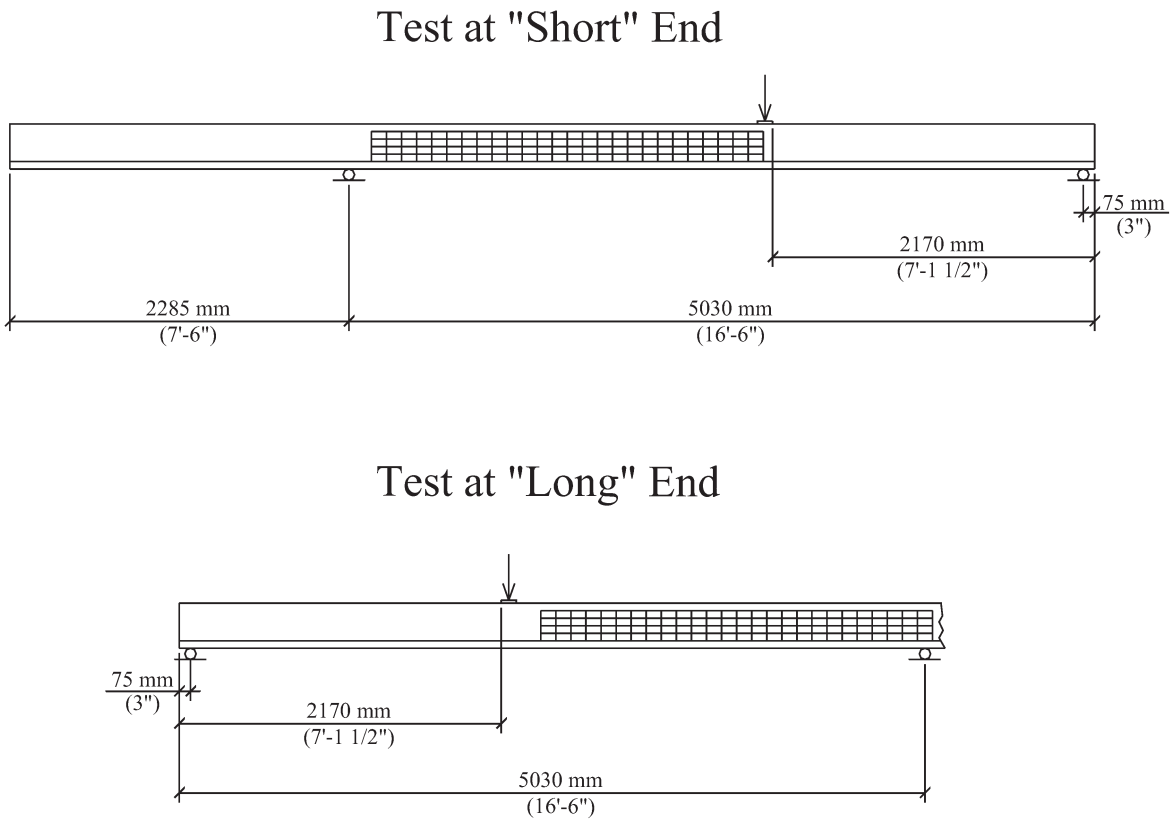

Figure 3.33 Loading arrangements for the 69 MPa (10 ksi) single strand development length beams.

Figure 3.34 Test setup for a single strand development length beam.

were incrementally applied to the beams using a hydraulic ram powered by an electronically controlled power unit supplied by Nachi America. Values of load, and deflection at the applied load, and strand slip at the beam end were recorded throughout the entire loading sequence of all six tests (two tests per beam for three beams). The test setup for a single strand development length beam is shown in Figure 3.34 and the strand slip measuring device used during testing is shown in Figure 3.35.

Figure 3.35 Strand slip measuring device for single-strand development length beams.

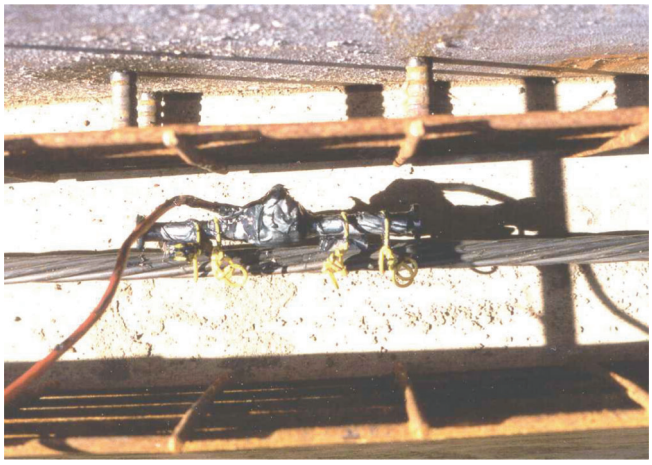

Figure 3.36 Vibrating wire gage attached to a prestressing strand in a single-strand development length beam form.

In order to experimentally determine the amount of prestress losses occurring in the rectangular development length beams, a vibrating wire gage (Geokon Model VCE-4200) was installed at midspan of one of the single-strand development length beams (Beam3). This gage was located at the depth of the single prestressing strand (255 mm (10 in.) below the top surface) as shown in Figure 3.36.

3.2.7 Multiple-Strand Development Length Specimens

As previously mentioned, the purpose of the single-strand specimens in this study was to provide an inexpensive means to conduct numerous development-length tests on beams having the same concrete and strand supplier combination. However, the condition of a beam reinforced with only one strand is never encountered in actual bridge design. Therefore, the possible negative effect of multiple-strands (at close spacing) on development lengths also needed to be addressed. Therefore, at the outset of this experimental program, it was decided that two full-scale specimens containing multiple-strands would be tested in addition to the three single-strand specimens. It was envisioned that these specimens would be designed based on the analysis of test data from the single-strand development length specimens.

As will be discussed in Chapter 5, results from tests on single-strand specimens indicated that the current ACI and AASHTO equations were appropriate for use with 69 MPa (10 ksi) concrete. Therefore, the multiple-strand specimens were designed with an embedment length based on the current code provisions. These specimens each contained 5 strands and had a T-shaped cross-section with a depth of 535 mm (21 in.) and a compression flange of 915 mm (36 in.). In addition, two 9.5 mm (#3) bars were provided at the same depth as the prestressing strands for instrumentation purposes as will be discussed later in this section. A layout of the cross-section of the multiple-strand specimens is shown in Figure 3.37.

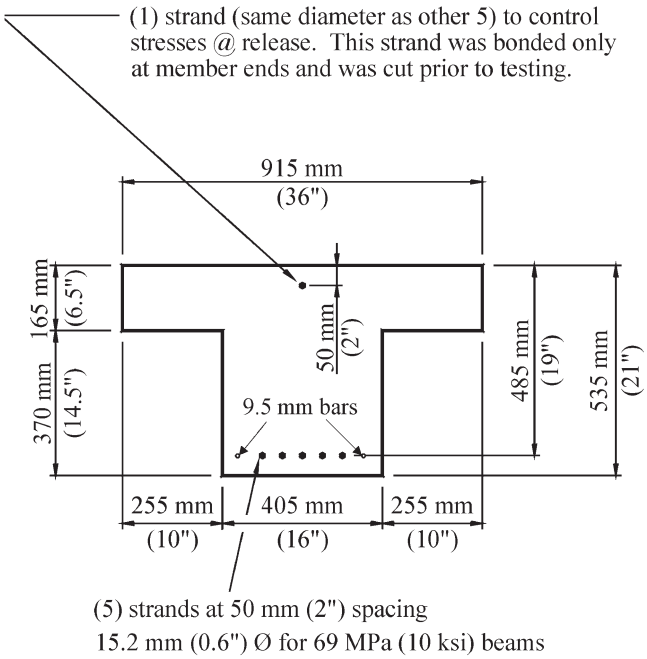

Figure 3.37 Cross-section of multiple-strand development length specimens.

A single top strand was added to control top tensile stresses and allow the specimens to be stripped out of the forms on the day after casting. This strand was bonded only at the member ends and was cut prior to load testing. A plastic de-bonding sleeve was used to prevent bonding of the strand, except at the member ends. To enable cutting of the strand, a Styrofoam blockout was used. The Styrofoam blockout and the plastic de-bonding sleeve are shown in Figure 3.38 and the formwork used to cast the multiple-strand development length specimens is shown in Figure 3.39.

Although it was initially decided that all beams would utilize strands produced by Insteel, the Study Advisory Committee (SAC) decided that each of the two multiple-strand specimens should contain prestressing strands from different manufacturers. This was

Figure 3.38 Styrofoam blockout to enable cutting of the top strand before testing and plastic de-bonding sleeve on the top strand.

Figure 3.39 Formwork for multiple-strand development length specimens.

decided based on findings from Logan's Report [1997], which concluded that there is a significant difference in bond performance in pretensioned concrete beams among strands produced by different strand manufacturers. The use of different strands in the two multiple-strand specimens was enabled by splicing all five strands in the span between the bulkheads of the beams as shown in Figure 3.40. One beam was cast with 15.2 mm (0.6 in.) strands from Insteel, while the other beam used 15.2 mm (0.6 in.) strands from Florida Wire & Cable. Strands supplied by these two companies will be referred to as IST and FWC, respectively. Splicing of the strands ensured that both beams had the same initial tension in the strands. These beams will be referred to in this report as HPC-1 (with IST strands) and HPC-2 (with FWC strands). Table 3.4 contains the design parameters of the multiple-strand development length specimens.

A total of 15 strain gages were used for determining strains in each of the multiple-strand specimens. One

Figure 3.40 Splicing of Insteel and Floride Wire & Cable strands.

TABLE 3.4
Design parameters of multiple strand development length specimens

T-Beam designation	Strand producer	Embedment length	Concrete strength	Strand size
HPC-1	IST	2145 mm (80.5 in.)	69 MPa (10 ksi)	15.2 mm (0.6 in.)
HPC-2	FWC	2145 mm (80.5 in.)	69 MPa (10 ksi)	15.2 mm (0.6 in.)

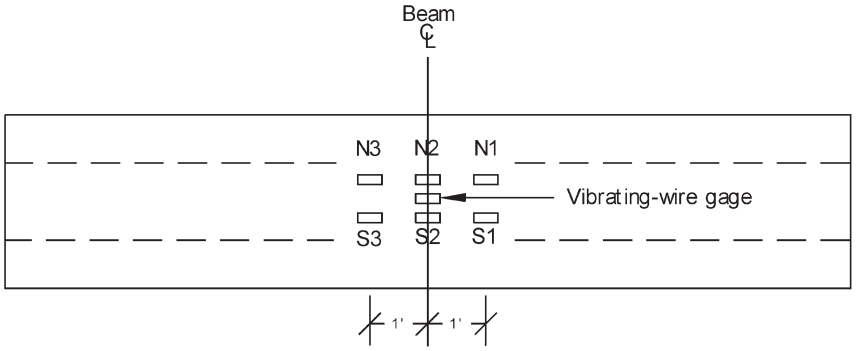

Figure 3.41 Location of internal strain gages at strand level in the multiple-strand development length specimens. Gages N1, N2, N3, S1, S2, and S3 are electrical resistance gages mounted on a 9.5 mm (#3) bars.

Geokon Model VCE-4200 vibrating wire gage was installed at midspan of each of the specimens. This gage was located at the depth of the five prestressing strands (485 mm (19 in.) below the top surface). In addition, strains in the strands were inferred from electrical resistance strain gages that were installed on 9.5 mm (#3) bars placed at the depth of the prestressing steel. The electrical resistance strain gages were used primarily during the load test to failure, since they had a larger strain range capability. The vibrating wire gages were used to measure the change in strain that occurred over a several day period, as they are very stable for long-term measurements. One of the primary reasons for extensive instrumentation in these beams was to gain hands-on experience with the installation and recording of gages in the field. The same gages will be used in the latter part of this study when actual bridge girders for SR 43 are instrumented for in-service monitoring. The locations of the internal strain gages at strand level are shown in Figure 3.41.

Two instrumented 9.5 mm (#3) bars were placed at the level of the strand in each beam. The bars each contained three strain gages–one gage at the center-line of the beam and one gage at 305 mm (12 in.) on each side of the beam center-line. The bars were cast on the outside of the stirrups so that they would not influence the bond of the five strands. The vibrating wire gage and the instrumented bars positioned in the form-work prior to casting the concrete are shown in Figure 3.42.

In addition to the instrumentation inside of the beam, strains at the top surface of the concrete were measured using surface-mounted vibrating wire gages as well as electrical-resistance strain gages. Threaded inserts were cast in the top of the two specimens at mid-span to allow for quick installation of the vibrating wire gages. These gages were installed after the concrete had hardened but prior to de-tensioning the strands. The electrical resistance strain gages were installed after the beams had been shipped to the laboratory but prior to load testing. A total of six electrical resistance surface mounted gages were installed on the top surface of each specimen—two at the center-line of each beam and two on each side of the center-line at a distance of 305 mm (12 in.). The locations of the top surface strain gages are shown in Figure 3.43. A surface-mounted vibrating wire gage positioned over an electrical resistance surface strain gage at mid-span of a multiple-strand development length specimen is shown in Figure 3.44.

Unlike the single-strand specimens, which each were tested at both ends, the multiple-strand specimens were designed with a length that was approximately equal to twice the calculated development length, so that a point load applied at mid-span would effectively test the

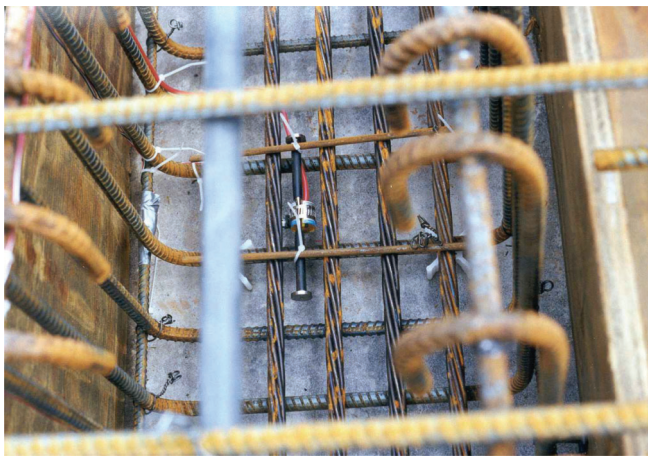

Figure 3.42 Vibrating wire gage and instrumented bars in a T-beam.

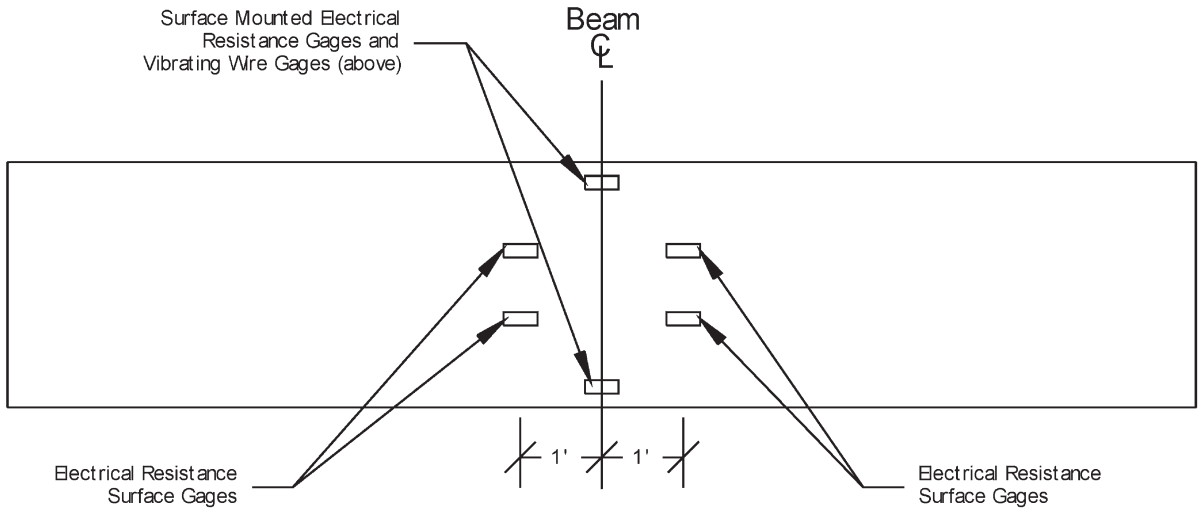

Figure 3.43 Locations of top surface strain gages in multiple-strand development length specimens.

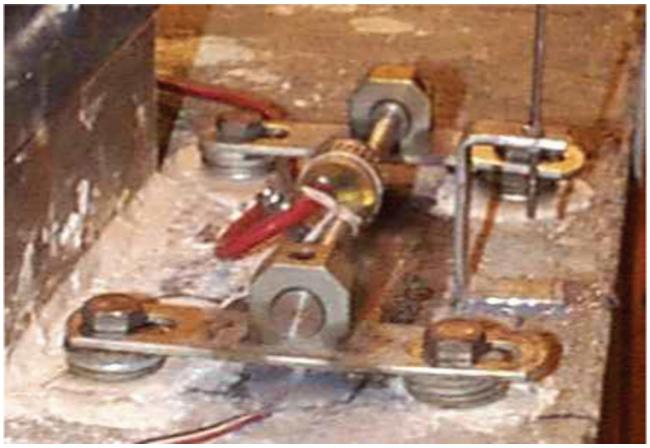

Figure 3.44 A surface mounted vibrating wire gage positioned over an electrical resistance surface gage.

anchorage at both ends simultaneously. The actual length of the beams was 150 mm (6 in.) longer than twice the calculated development length, because the load was applied to the beams through a 150 mm (6 in.) wide steel plate. This ensured that the length of embedment of the strand (from the free end of the beam to the edge of the loading plate) coincided with the development length calculated based on the principles discussed in Section 3.2.5. Dimensions and loading arrangement for the multiple-strand development length specimens are shown in Figure 3.45.

Design of shear steel using the ACI code provisions showed that 13 mm (#4) stirrups at 305 mm (15 in.) spacings would provide sufficient shear reinforcement for the multiple-strand development length specimens in this study. However, transverse reinforcement provided in the specimens was 13 mm (#4) stirrups at 150 mm (6 in.) spacings, or more than twice the code-required amount at the ends of the beams. Shear reinforcement near the point of maximum moment was 13 mm (#4) stirrups at 75 mm (3 in.) spacings, or more than four times the code-required amount. Additional transverse reinforcement was added near the point of maximum moment based on findings in a concurrent study that flexural-shear cracks may affect the development length if sufficient transverse reinforcement is not provided. A two-piece stirrup assembly, shown in Figure 3.46, was used for each of the two multiple-strand development length beams in this study. This

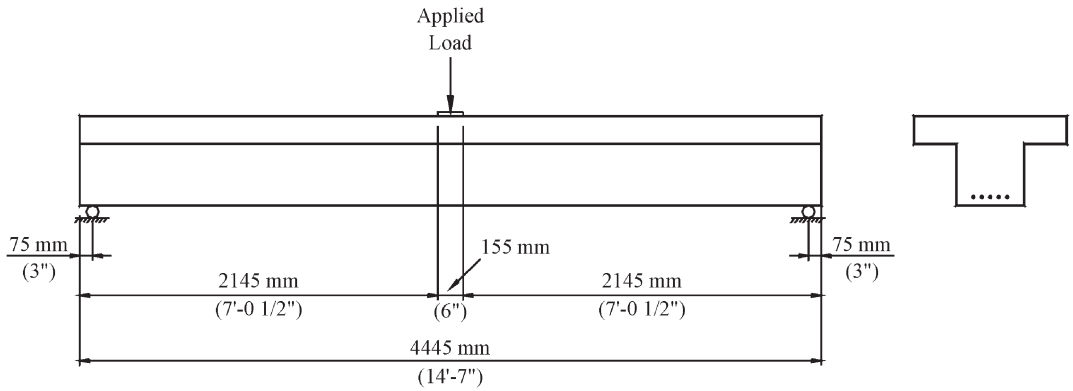

Figure 3.45 Loading arrangement for multiple-strand development length specimens.

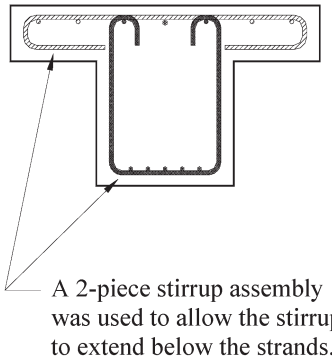

Figure 3.46 Positioning of transverse reinforcement for multiple-strand development length specimens.

Figure 3.47 Stirrup assemblies used below the longitudinal strands in the multiple-strand development length specimens.

allowed for quick form setup times while allowing the vertical stirrups to extend below the bottom strands. Stirrup assemblies used below the longitudinal strands in the development length specimens are shown in Figure 3.47 and the reinforcement used in the flanges is shown Figure 3.48.

Figure 3.48 Reinforcement used in the flanges of the multiple-strand development length specimens.

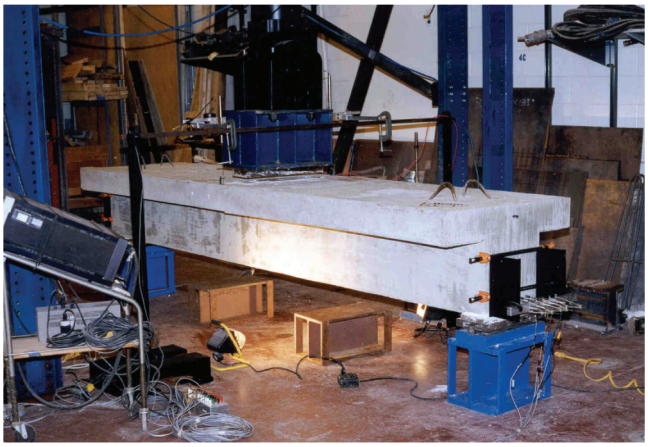

Figure 3.49 Test setup for a multiple-strand development length specimen.

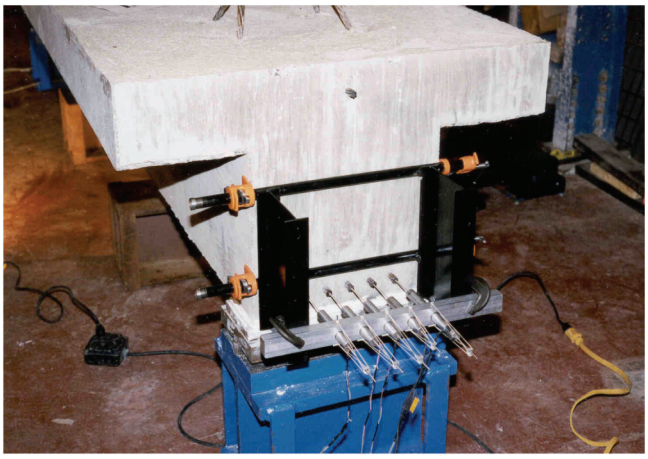

Figure 3.50 Strand slip measuring device for multiple-strand development length specimens.

When testing the specimens, loads were incrementally applied to the beams through a 150 mm wide by 610 mm long (6 × 24 in.) steel plate using a 978 kN (220 kip) capacity MTS hydraulic actuator. Values of load, mid-span deflection, strain, and strand slip for all five strands at both ends of the beam were recorded during the testing of each specimen. The test setup used for the multiple-strand development length specimens is shown in Figure 3.49 and the strand end slip measuring device in Figure 3.50.

4. CONCRETE MIXTURE DEVELOPMENT AND TESTING

During the first meeting of the Study Advisory Committee (SAC) for the portion of this project sponsored by the Indiana Department of Transportation (INDOT) and the Federal Highway Administration (FHWA), some preliminary specifications were set for Indiana's HPC bridge decks and

girders. Water-binder ratios of 0.35 to 0.40 for deck concrete and 0.31 for girder concrete were suggested. The maximum charge passed for both deck and girder concretes was to be limited to 1000 coulombs. In order to attain the low charge passed values, a 5% silica fume replacement was recommended for girder concrete and 5 to 7.5% for deck concrete. Also, replacing 30% of the cement with GGBFS or 20% with fly ash was suggested.

In the United States, fly ash has been the most commonly used supplementary cementitious material and as a result, extensive experience and knowledge related to its use in concrete exists. In the present study, the supplementary cementitious materials considered are GGBFS and silica fume. They are expected to provide potential for durability improvements of concrete that is at least equal to that provided by fly ash.

A preliminary investigation was performed to identify suitable locally available concrete materials. Based on that investigation, it was determined that crushed limestone/dolomite, an INDOT Class AP aggregate, from Delphi, Indiana, would perform better than river gravel as coarse aggregate. The local gravel tends to have higher concentration of chert particles than does the crushed stone. Although chert does not cause structural deficiencies, it causes pop-outs that are unsightly. For fine aggregate, natural river sand was selected over manufactured limestone/dolomite sand. The natural sand was selected because concrete mixtures made with natural sand have lower water requirement than do concrete mixtures made with manufactured sand.

4.1 Girder Concrete

A total of 16 mixtures were produced and tested in order to develop suitable girder concrete. Nine of the mixtures were made in the laboratory and seven were made in the field at the Rinker Materials precast facility in Lafayette, Indiana. The mixture proportions and selected properties of both fresh and hardened concrete made from these mixtures are listed in Sections C.1 and C.2 in Appendix C. The values in Tables C.1 to C.3 are in SI units and the values in Tables C.4 to C.6 are in U.S. customary units. The first letter of the girder mixtures indicates whether they were produced in the laboratory (L) or in the field (F). The second letter (G) stands for girder concrete.

The first field mixture, FG-1, was based on work previously done by Ranagaraju (*76*) at Purdue University. This mixture was used for the single-strand development length specimens and the pullout specimen. The concrete performed satisfactorily and reached a strength of 81 MPa (11.7 ksi) at 28 days. However, the Study Advisory Committee (SAC) for this project later selected to use a mixture design that would result in a charge passed value of less than 1000 coulombs. In order to achieve this goal, nine mixtures (LG-1 to LG-9), incorporating 5% silica fume, were prepared and tested in the lab.

After a mixture with the desired properties (LG-8) had been developed, FG-2 was produced in the field. Despite satisfactory results obtained with the lab mixture, the attempt to duplicate this mixture in the field resulted in concrete with poor workability, even after additional water and HRWR were added. However, the compressive strength values were considerably higher than those measured for the laboratory made concrete, reaching 65 MPa (9.4 ksi) after only one day and 109 MPa (15.6 ksi) after 28 days. An explanation for the rapid strength gain and the high 28-day compressive strength of FG-2 was not readily available. However, the effects of temperature and misinterpretation of the amount of water were considered as possible causes.

The variable that was believed to be most different between FG-2 and the laboratory mixtures preceding the field mixture was believed to be temperature. The temperature of FG-2 was not measured but the temperature of FG-3, produced 24 days later on March 24, 1998, was 14°C (57°F). This value is considerably lower than the measured temperature values of some of the laboratory produced concrete. The temperature of the laboratory deck concrete, believed to be comparable to that of the laboratory girder concrete, generally ranged between 26 and 29°C (79 and 84°F) at the conclusion of mixing.

In an attempt to verify whether the low temperature of FG-2 may have affected the workability, LG-9 was produced after cooling all the materials except the admixtures. This resulted in a concrete temperature of 12°C (54°F). The dosage rate of the HRWR for LG-9 was 1956 mL/100 kg (30.0 oz/100 lb) of cement, or nearly the same as that of FG-2. However, the slump was 178 mm (7 in.) compared with only 51 mm (2 in.) for FG-2. Although the slump of LG-9 was considerably higher than of FG-2, it was comparable to the slump of LG-8 which had a lower water-binder ratio and the dosage rate of the HRWR was only 1310 mL/100 kg (20.1 oz/100 lb) of cement. It should be noted here that a slightly extended mixing time for both FG-2 and LG-9 might have contributed to the need for additional HRWR. A more extensive investigation on the effect of concrete temperature on the effectiveness of chemical admixtures may yield useful information with regard to their recommended dosage.

Based on the rapid strength gain and high 28-day strength of FG-2, the possibility that not all of the specified water had been available was considered. During a field visit to the batch plant to investigate this possibility, a solid explanation was not identified. However, on the day FG-2 was prepared, it was the first batch of the day. It is conceivable that some additional water should be added to the first batch of each day to wet the concrete mixer. As it was not possible to verify this or to quantify how much this may have been, as a precaution, all subsequent trial batches and field trials were done on days which some production had already taken place in the mixer.

After producing FG-2, it was also decided to increase the size of the subsequent trial batches from 0.76 to 1.15 m^3 (1 to 1.5 yd^3) to reduce possible surface effects and increase the uniformity of mixing. Whether this made a

difference is not clear, but the results from mixes FG-3 to FG-5 were generally quite satisfactory. In fact, properties of both fresh and hardened concrete from FG-5, produced on April 15, 1998, were excellent. Further trial testing of mixtures needed for production of the multiple-strand development length specimens was therefore not believed to be necessary.

The multiple-strand development length specimens were fabricated on July 14, 1998. The concrete, mixtures HPC-1 and HPC-2, was proportioned in the same way as FG-5. However, neither fresh nor hardened concrete properties matched those of FG-5. Both the slump and air contents were lower, indicating a possibility of a lower water-binder ratio. However, this may not have been the case as the compressive strengths of the HPC mixtures were also lower than expected. More details regarding the compressive strengths are given in Section 4.1.1.

The reason(s) for the different properties of FG-5 and the HPC mixtures is not known. The same companies supplied all materials and an evaluation of the cement mill certificates did not reveal a change in the cement properties. Again, the temperature of the fresh concrete was considerably different, but it is unclear whether it made a difference. For FG-5, the fresh concrete temperature was 14°C (58°F), compared with 30°C (86°F) for the HPC mixes. In order to reduce the possible effects of temperature and inherent changes in raw materials on field mixtures, it is important to conduct trial pours as close to the construction date as possible.

4.1.1 Compressive Strength

The compressive strength of all girder mixtures was determined at various ages. The results of all the compressive strength tests are listed in Appendix C. The results are listed in SI units in Tables C.1 to C.3 and in U.S. customary units in Tables C.4 to C.6.

As mentioned in Section 4.1, the compressive strength values of the HPC mixtures were lower than expected. The concrete was designed to have a 28-day strength of 69 MPa (10 ksi). The compressive strength of HPC-1 was 70 MPa (10.2 ksi) after 28 days, while that of HPC-2 was only 65 MPa (9.4 ksi). A slight strength reduction was observed for both concretes between 56 and 91 days. However, a gradual strength increase was observed after 91 days. After one year, the compressive strengths had reached 78 and 79 MPa (11.3 and 11.4 ksi) for HPC-1 and HPC-2, respectively.

The effect of different curing conditions on the compressive strength of the specimens was investigated for specimens from mixture HPC-2. One group of specimens was stored outside (unprotected) from the day they were cast and did not receive any special curing. Another group was moist cured for three days before being moved to a 50% relative humidity (RH). The reference specimens were moist cured for the entire testing period.

Storing the specimens outside yielded higher compressive strength values for the first 28 days when compared with moist cured specimens, but not thereafter. The specimens stored outside did not exceed the 69 MPa (10.0 ksi) limit until after one year when they had a compressive strength of 70 MPa (10.2 ksi). Based on the compressive strength results, it appears as if the temperature and/or moisture conditions during the first 28 days were favorable to the specimens stored outdoors. However, subsequent strength gain was minimal, but apparent strength loss, as for the specimens stored at 50% RH, was not observed during the one year testing period.

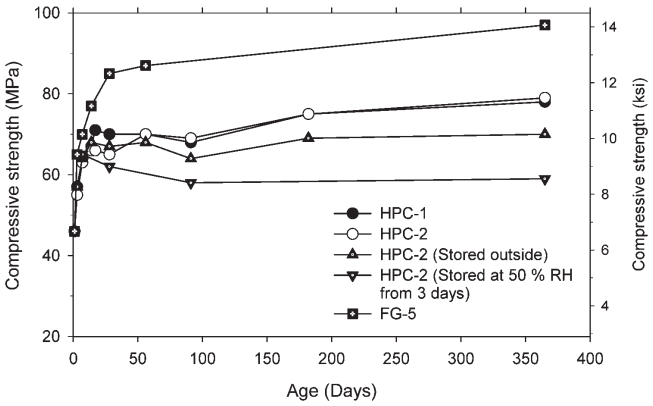

Figure 4.1 Compressive strength development of HPC mixtures used for multiple-strand development length specimens. The strength development of FG-5 is included for reference.

Indoor storage at 50% RH from the age of three days resulted in lower compressive strength than any of the other curing methods for all testing ages except seven days. The initial drying may have increased the compressive strength as the samples were tested without first being saturated. However, the strength reduction after seven days was not expected. After one year, the compressive strength of the cylinders stored at 50% RH had increased by only 7.3% with respect to the 3-day strength. Comparable value for the continuously moist cured cylinders was 43.6%. The compressive strength developments of the HPC mixtures and FG-5 are shown in Figure 4.1.

4.1.2 Static and Dynamic Moduli Developments

The static and dynamic moduli developments were monitored for HPC-2. Two specimens, moist cured for the entire testing period, were monitored for the development of each modulus. The experimental moduli data along with calculated static moduli values based on $E_c = w_c^{1.5} \cdot 33 \cdot f'_c{}^{0.5}$ are shown in Figure 4.2. This equation is recommended by ACI Committee 318 [(*14*), p. 89] for calculating modulus of elasticity of concrete. Use of the equation requires, and yields, values in U.S. customary units where the modulus of elasticity, E_c, and the design strength, f'_c, are in psi, and the concrete density, w_c, is in lb/ft^3. Two values, resulting in upper and lower limits of calculated E_c, were used for f'_c in order to compare calculated values

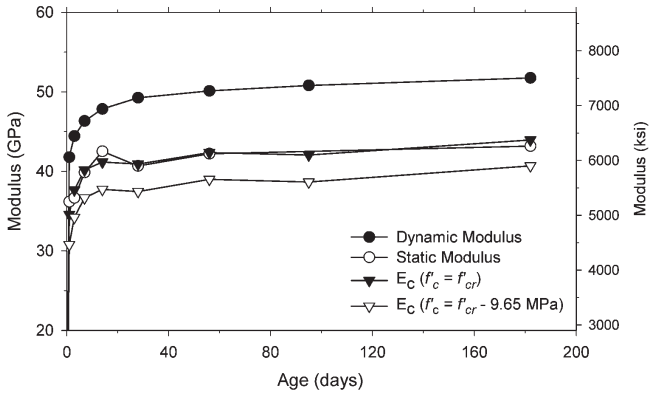

Figure 4.2 Development of static and dynamic moduli for HPC-2. Calculated moduli values based on $E_c = w_c^{1.5} \cdot 33 \cdot f'_c{}^{0.5}$ and two different values of f'_c are included for comparison.

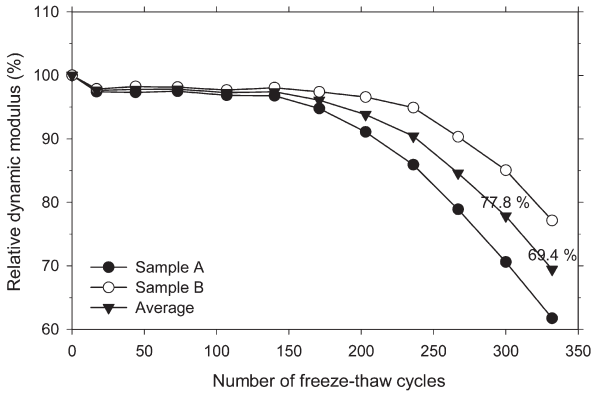

Figure 4.3 Relative dynamic modulus of elasticity of HPC-2 after exposure to rapid freezing and thawing in water.

of E_c with those measured during the experiment. The values of f'_c were f'_{cr} and $f'_{cr} - 9.65$ MPa (1400 psi) where f'_{cr} was the average compressive strength of the test cylinders.

The measured static modulus and the calculated modulus taking f'_c as f'_{cr} resulted in nearly identical values. This indicates that the static modulus of this concrete will not be overestimated using the ACI formula. As would be expected, the dynamic modulus was considerably higher than the static modulus from the beginning. At 180 days, the dynamic modulus had reached a 51.8 MPa (7500 ksi) compared to 43.2 MPa (6260 ksi) for the static modulus.

4.1.3 Resistance to Rapid Freezing and Thawing in Water

Two specimens from HPC-2 were placed in the freeze-thaw machine exposed to rapid freezing and thawing in water after being moist cured for the first 14 days. The test was terminated after 332 freeze-thaw cycles when the average relative dynamic modulus of the two specimens had dropped to 69.4%. After 300 cycles, the relative dynamic modulus was 77.8%, less than 80% as recommended by Goodspeed, Vanikar, and Cook (*77*) for Grade 2 of high performance structural concrete for highway applications. The development of the relative dynamic modulus during the testing period for each specimen and the average of both specimens are shown Figure 4.3.

Based on Figure 4.3, it is apparent that the freeze-thaw durability of the specimens was not sufficient. However, it should be remembered that bridge girders are typically protected from direct exposure to rain and rarely, if ever, fail due to lack of freezing and thawing resistance. A continuous reduction in the relative dynamic modulus of both specimens was observed after only 140 cycles although the extent was larger for Specimen A. The measured air content of the fresh concrete was 5%. Although 5% appears a low value, it falls within the range of 5 to 8% ($6.5\% \pm 1.5\%$) as specified by the Indiana Department of Transportation [(*78*), p. 358].

4.1.4 Electrical Indication of Chloride Ion Penetration Resistance

The electrical indication of chloride ion penetration resistance of mixtures HPC-1 and HPC-2 was tested after 28 and 56 days from casting. Specimens from HPC-2 were also tested after 95 days. All specimens were continuously moist cured until tested. Two specimens from each mixture were tested at each testing date. The charge passed for both mixtures was the same at 28 days, or 1050 coulombs. However, some difference in the average values was observed after 56 days of curing. At that time, the charge passed for HPC-1 was 900 coulombs while it was 720 coulombs for HPC-2. Although there is some difference between the two values, values below 1000 coulombs indicate good quality concrete. The influence of curing time on the charge passed for HPC-1 and HPC-2 is shown in Figure 4.4.

The charge passed results from mixtures HPC-1 and HPC-2 cannot be compared directly to results obtained from comparable mixtures because they were tested at different ages. However, an indirect comparison can be made with results from LG-10 and FG-5, which were

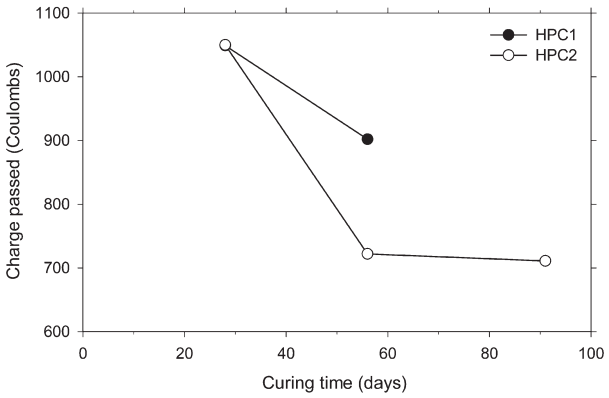

Figure 4.4 Influence of curing time on the charge passed for HPC-1 and HPC-2.

tested at 140 and 155 days, respectively. The average charge passed from two specimens from each of these two mixtures was 550 and 480 coulombs for LG-10 and FG-5, respectively. Based on the 95-day values from HPC-2, those values are lower than would have been expected for HPC-2 at an age of five months although the charge passed is expected to decrease with curing time. Perhaps the charge passed results of the HPC mixtures are in line with the compressive strength results, which were also disappointingly low when compared with results from laboratory and field trials.

4.1.5 Temperature Development at Early Ages

The temperature development in the multiple-strand development length girders, made with the HPC mixtures, was monitored for the first 48 hours after concrete placement. The girders were covered with a black tarp soon after the concrete had been placed. Three companion cylinders were cured next to the girders under the same cover. Temperature variations in the web of girder HPC-2 and the cylinders are shown in Figure 4.5 and temperature variation through the depth of the same girder are shown in Figure 4.6.

Based on the information presented in Figures 4.5 and 4.6, the temperatures of the girders and those of the cylinders were considerably different. The temperature rise in the girders was considerably higher than in the cylinders. Also, the cylinders cooled down faster than the girders. The temperature development in the two girders was very similar.

The concrete mixture design used for the girders was tested at the plant four times before the girders were fabricated in attempt to ensure compatibility with the plant mixer. The field trials were done from February to April 1998, and the cylinders were cured outside at the plant for approximately 20 hours. Specimens from each of the four trial batches had compressive strengths exceeding 83 MPa (12 ksi) after 56 days of moist curing

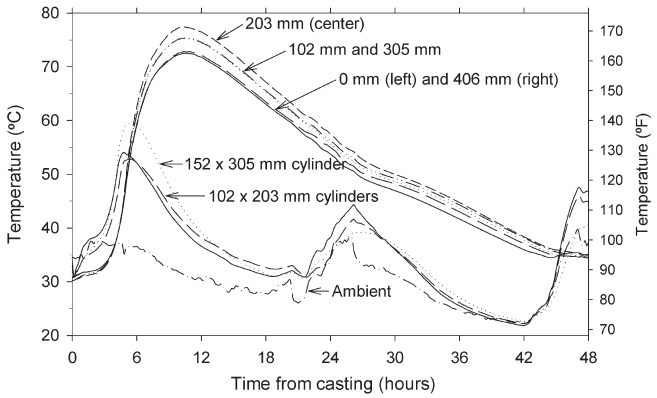

Figure 4.5 Temperature variations in the web of a 406 mm (18 in.) thick multiple-strand development length specimen and companion cylinders during the first 48 hours after casting. The concrete was from mixture HPC-2 and the casting took place around noon.

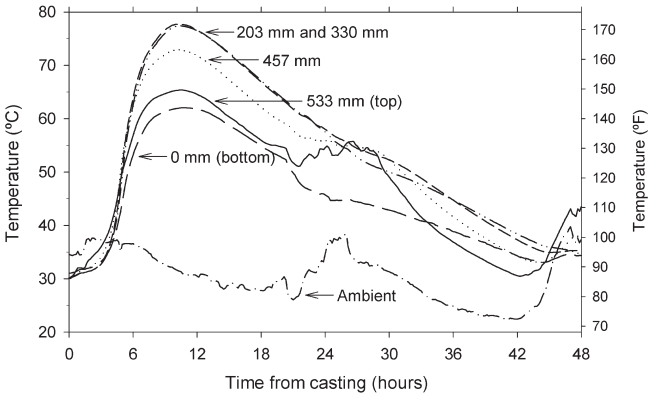

Figure 4.6 Temperature variations through the depth of a 533mm high multiple-strand development length specimen during the first 48 hours after casting. The concrete was HPC-2 and the casting took place around noon.

while specimens fabricated at the same time as the girders (July 14, 1998) had a compressive strengths of 70 MPa (10.1 ksi) after 56 days of moist curing. The reasons for the reduction in compressive strength are unknown. However, strength reduction caused by high early age temperatures remains a possibility that requires further investigation.

4.2 Deck Concrete—Laboratory Trials

Since the beginning of this study, a total of 90 mixtures of 0.042 m^3 (1.5 ft^3) each have been produced and tested in the concrete materials laboratory at Purdue University. Each mixture had slightly different proportions and properties. The mixture proportions and concrete properties of these mixtures are listed in Sections C.3 and C.4 in Appendix. The values in Tables C.1 to C.3 are in SI units and the values in Tables C.4 to C.6 are in U.S. customary units.

4.2.1 Concrete Mixture Development

The first 14 mixtures were used to determine acceptable proportions of cement, sand, and coarse aggregate in terms of workability. After an evaluation of compressive strength data from these mixtures, it became evident that the data were inconsistent at times. A strength difference of up to 23.6% between cylinders from the same batch was observed at 28 days. This inconsistency was first believed to be related to the testing procedure as neoprene pads, as per ASTM C1231 (Standard Practice for Use of Unbonded Caps in Determination of Compressive Strength of Hardened Concrete Cylinders), were used instead of high strength sulfur capping compound and the concrete strength exceeded the 48 MPa (7 ksi) limit specified in the ASTM standard.

The aforementioned laboratory made batches and cylinders were usually made by two workers. The

ASTM C192 (Standard Practice for Making and Curing Concrete Test Specimens in the Laboratory) standard was followed. The cylinders were consolidated by rodding the concrete in three layers as specified in the standard test procedure. Twelve to fourteen cylinders were usually made from each batch and it generally took around 40 minutes to complete measurements of fresh concrete properties and specimen preparation. The specimens were then stored on the laboratory floor for one day before being demolded and moved to the fog room.

A small study, aimed at identifying the source of the compressive strength variations, was done on cylinders from mixes LD-15 to LD-19. Chemical admixtures from two different producers were used when mixing the concrete. Different cylinder capping methods were considered and the effects of using high strength sulfur compound, new neoprene pads, and old neoprene pads were compared. Effects of length of elapsed time from the end of mixing until cylinder fabrication was also considered. Slump, density, and air content of the concrete were measured immediately after the end of mixing and again 30 minutes later. A considerable reduction in air content, and subsequent increase in density, was observed for mixtures LD-15 and LD-17. The other mixtures were also affected by loss of entrained air, but to a much lesser extent.

From each batch, a total of fourteen cylinders were made by the same worker to enhance the reproducibility. The cylinders were made in 15-minute intervals with four cylinders made immediately after mixing was completed, followed by four cylinders 15 minutes later, four cylinders 30 minutes later, and two cylinders 45 minutes after the completion of mixing. Cylinders in each group were made simultaneously. The concrete remaining in the mixer was mixed for 15 seconds after each 15-minute interval. After 28 days of curing in the fog room, the cylinders were tested for compressive strength.

Considerable variations were observed in the compressive strength data. The strength generally increased as the elapsed time from end of mixing until cylinder fabrication increased. For mixture LD-17, the average strength difference for cylinders made 45 minutes apart and tested with new neoprene pads was 23.6%. The fact that this is the same percentage difference as observed earlier should be considered a coincidence. However, based on the data, it can be suggested that the earlier variations in compressive strength depended on factors other than the specimen capping method. The difference in strength for mixture LD-17 was attributed to the loss of entrained air. The air content dropped from 10.0 to 6.9% during the first 30 minutes after mixing. For mixture LD-19, the average strength difference for cylinders made 45 minutes apart and tested with new neoprene pads was 1.9%. The air content dropped from 8.5 to 7.7%. Mixtures LD-17 and LD-19 were made with admixtures from different companies. The use of old neoprene pads did not appear to greatly affect the compressive strength data although greater variations in compressive strength of "identical" cylinders were

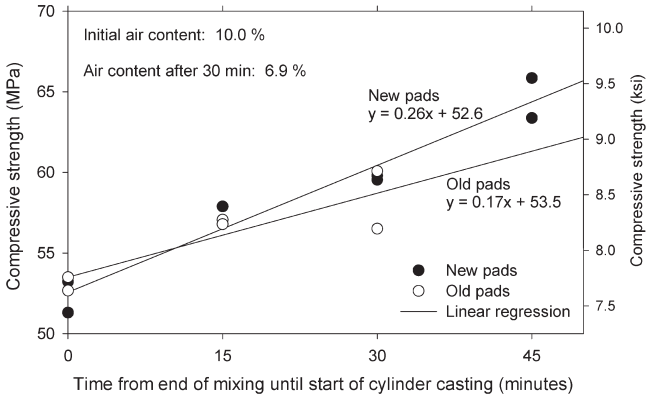

Figure 4.7 Comparison of strength variations for specimens tested using new and old neoprene pads with respect to time from end of mixing for mixture LD-17. Each marker in the figure represents a single cylinder.

observed when using old pads than new pads. However, using high strength sulfur capping compound did not appear to result in consistent data as both high scatter and inconsistency were observed. The compressive strength values were considered inconsistent and they were usually lower than those obtained using neoprene pads. Strength developments for specimens tested using new and old neoprene pads are shown in Figures 4.7 and 4.8 for mixtures LD-17 and LD-19, respectively.

Based on the observations made from the data from mixtures LD-15 to LD-19, the admixtures resulting in greater retention of entrained air were selected for further study. The method of consolidating the cylinders was also changed from rodding to vibrating with a 19 mm (3/4 in.) diameter vibrator to reduce the time needed to fabricate the cylinders. Also, the number of layers of concrete used to fill the cylinders was reduced from three to two at the same time. A comparison study, done on reduced density concrete, resulted in comparable compressive strengths for cylinders consolidated by rodding and vibrating. Compressive strength developments for cylinders made

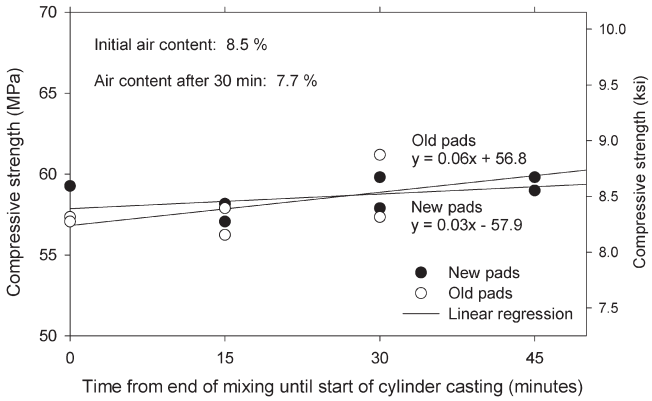

Figure 4.8 Comparison of strength variations for specimens tested using new and old neoprene pads with respect to time from end of mixing for mixture LD-19. Each marker in the figure represents a single cylinder.

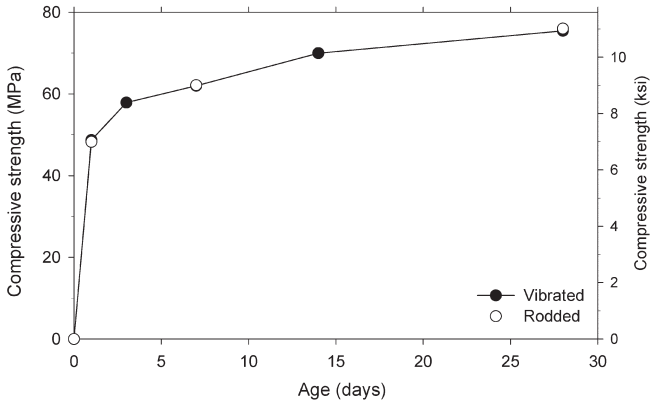

Figure 4.9 Compressive strength development of modified density concrete consolidated by rodding and vibrating. Each marker in the figure represents an average of two cylinders.

from reduced density concrete and consolidated by rodding are shown in Figure 4.9.

Supplementary cementitious materials were evaluated through mixtures LD-20 to LD-35. Only GGBFS and silica fume were considered. In the United States, fly ash has been the most commonly used supplementary cementitious material and as a result, extensive experience and knowledge related to its use in concrete exists. Silica fume and GGBFS are expected to provide potential for durability improvements of concrete that is at least equal to that provided by fly ash.

A wide range of combinations of cement and either or both GGBFS and silica fume were considered. Specimens from most of the deck mixtures were subjected to rapid freezing and thawing in water, freezing and thawing in the presence of deicing chemicals, and electrical tests. Compressive strength was also determined. All the mixtures had a total binder content of 386 kg/m^3 (650 lb/yd^3) and a water-binder ratio of 0.38. The proportion of each of the binders for each mixture is listed in Table 4.1. The results of the tests for deck mixtures are presented in Sections 4.2.2 through 4.2.6.

TABLE 4.1
Proportions of each binder for deck mixes LD-20 to LD-35

Mixture	Cement (%)	Silica fume (%)	GGBFS (%)
LD-20	100	0	0
LD-21	70	0	30
LD-22	95	5	0
LD-23	68	2	30
LD-24	65	5	30
LD-25	60	0	40
LD-26	50	0	50
LD-27	93.5	6.5	0
LD-28	40	0	60
LD-29	92	8	0
LD-30	55	5	40
LD-31	45	5	50
LD-32	30	0	70
LD-33	92	8	0
LD-34	56.5	3.5	40
LD-35	46.5	3.5	50

Mixtures LD-36 to LD-49 were prepared to evaluate the effectiveness of a commercially available shrinkage reducing admixture (SRA). The results of that evaluation are reported in Section 4.2.6. Along with the length change, mass change was monitored as well.

After the initial laboratory phase of this work was completed, final preparations for field trials of selected mixtures were initiated. This work was intended to include only proportioning of air-entraining agent and high range water reducer in order to obtain consistent air content and slump. Mixtures LD-50 to LD-90 were prepared for second phase of the laboratory portion of this work.

Fluctuations in the air content of the fresh concrete had been observed during the initial laboratory phase, but this was generally attributed to changes in the amount of different binders used. The goal of the second laboratory phase was to quickly resolve any issues related to air content and workability and then proceed to the field trials.

Unfortunately, the task of determining the appropriate amount of air-entraining agent required for a given air content took several unexpected turns during which several different combinations of high range water reducers and air-entraining admixtures (AEAs) were tried. The binder content of the mixtures was also increased from 386 to 430 kg/m^3 (650 to 725 lb/yd^3) in hopes of reaching improved consistency in the air content. After preparing mixtures LD-56 to LD-70 with the same combination of chemical admixtures and reaching acceptable levels of air content for the last mixtures, it was particularly unpleasant to see specimens made with concrete containing these same admixtures completely disintegrate in the freeze-thaw machine. The freeze-thaw specimens had been prepared solely for the purpose of using them as dummy specimens as the machine was being fitted for a different size of specimens. However, the effects 99 freeze-thaw cycles had on specimens from mixture LD-57 could not be ignored. The appearance of the specimens after 99 freeze-thaw cycles is shown in Figure 4.10.

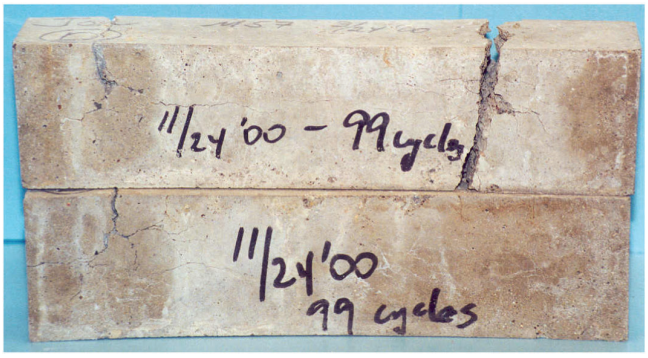

Figure 4.10 Specimens from LD-57 after 99 cycles as dummy specimens in the freeze-thaw machine.

Mixture LD-57 had been found to have an air content of 8% immediately after casting and 7.4% 30 minutes later. Microscopical determination of the air-void parameters of the failed freeze-thaw specimens, performed in accordance with the modified point count method of ASTM C457 (Standard Test Method for Microscopical Determination of Parameters of the Air-Void System in Hardened Concrete), revealed an air content of 6.3%. However, the spacing factor was found to be 0.58 mm (0.023 in.), which is considerably higher than the recommended value of 0.2 mm (0.008 in.). This finding required new trials with a different chemical admixture combination.

After subsequent trials with different chemical admixture combinations did not yield satisfactory results, a decision was made to try different cements. Surprisingly, those trials, listed as mixtures LD-81 and LD-82, immediately yielded acceptable, albeit high, air contents and concrete consistency. Furthermore, the required high range water reducer dosage was reduced by roughly 50%. Once this was discovered, a cement sample was obtained from a local ready-mix plant and tried.

The new cement, manufactured at the same cement plant as the previous cement, yielded results similar to those obtained with the two different cements. Once a sufficient amount of the new cement had been acquired, only eight mixtures, LD-83 to LD-90, were required to determine appropriate dosage rates for the three deck field trial mixtures that had to be pre-proportioned in the laboratory.

4.2.2 Compressive Strength

The compressive strength was determined at various ages for many of the deck mixtures. The results are listed in Sections C.3 and C.4 in Appendix C. The values in Tables C. 1 to C.3 are in SI units and the values in Tables C.4 to C.6 are in U.S. customary units.

The preliminary bridge design calls for deck concrete with a compressive strength of 31 MPa (4.5 ksi). The preliminary mixtures generally had a 28-day compressive strength of at least 55 MPa (8 ksi). Although such high strengths are not required to satisfy the structural design requirements, the high strength can be viewed as a "by-product" of the efforts of enhancing the durability characteristics of the concrete.

4.2.3 Resistance to Rapid Freezing and Thawing in Water

At least one specimen from each mixture was subjected to rapid freezing and thawing in water. The specimens used for freezing and thawing were $76 \times 76 \times 381$ mm ($3 \times 3 \times 15$ in.) beams. All specimens fared well during the test and had a relative dynamic modulus of 95% or more after 300 cycles. Specimens from all of the mixtures, except mixture LD-35, were tested beyond 400 cycles. The additional 100 cycles did not cause a reduction in the relative dynamic modulus below 95% for any of the specimens.

Freeze thaw samples from mixtures LD-28 and LD-32, having 60 and 70% replacement levels of GGBFS, respectively, experienced some exterior deterioration during the latter portion of the test. However, only the specimen from mixture LD-28 had a considerable reduction in the relative dynamic modulus. The relative dynamic modulus of the specimen from mixture LD-28 was at 81% when the test was terminated after 522 cycles. It is of interest to note that the measured air content of mixture LD-28 was the lowest of all the mixtures, or 5.2% at the end of batching. The development of the relative dynamic modulus in specimens made with and without GGBFS is shown in Figure 4.11.

Although specimens made with concretes containing relatively high replacement levels of GGBFS fared well during the freeze thaw test when evaluated based on the relative dynamic modulus, their characteristics were unique. As the test progressed, the sound emitted by the specimens, when tapped, changed and became similar to that emitted by young concretes. At the same time, the stability of the readings, in particular those of the longitudinal frequencies, declined. This instability was particularly evident for mixtures LD-28 and LD-32 which contained 60 and 70% GGBFS, respectively.

The rapid freeze-thaw resistance of specimens made with silica fume was excellent regardless of whether or not they contained GGBFS. None of the specimens exhibited any noticeable reduction in the relative dynamic modulus. The development of the relative dynamic modulus for specimens made with and without silica fume is shown in Figure 4.12 and the development of relative dynamic modulus for specimens made with both silica fume and GGBFS is shown in Figure 4.13. The reduction in relative dynamic modulus for specimen LD-24-A after 220 freeze-thaw cycles can be attributed to an interruption in the test. During the interruption, the specimen was kept frozen, but some loss of moisture may have occurred, resulting in lower frequency values.

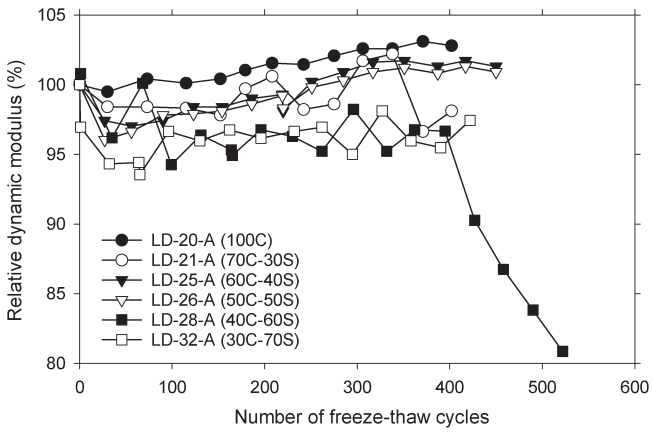

Figure 4.11 Development of relative dynamic modulus during rapid freeze-thaw testing of specimens made with and without GGBFS.

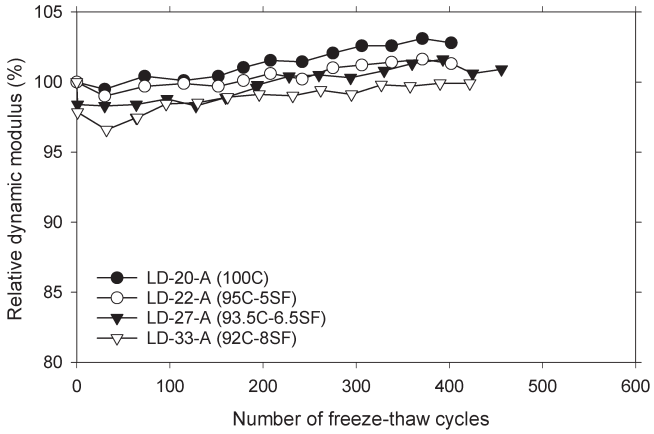

Figure 4.12 Development of relative dynamic modulus during rapid freeze-thaw testing of specimens made with and without silica fume.

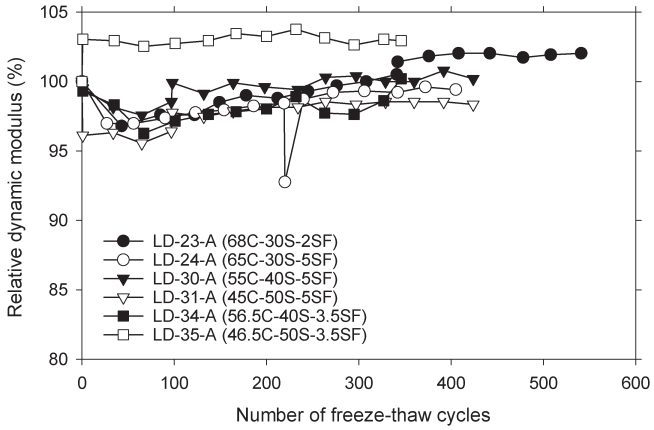

Figure 4.13 Development of relative dynamic modulus during rapid freeze-thaw testing of specimens made with both GGBFS and silica fume.

4.2.4 Resistance to Deicing Salt Scaling

Specimens from mixtures LD-21 to LD-33 were subjected to freezing and thawing in the presence of deicing salts, following the procedure outlined in ASTM C672. Both calcium chloride ($CaCl_2$) and sodium chloride (NaCl) solutions were used. The concentrations were 4% for $CaCl_2$ and 3% for NaCl. One specimen, measuring $188 \times 254 \times 76$ mm ($7.4 \times 10 \times 3$ in.), from each mixture was subjected to each solution. The solutions were confined to the top surface of the specimens by a rubber membrane glued on their sides. Each set of specimens was obtained from one $254 \times 381 \times 76$ mm ($10 \times 15 \times 3$ in.) sample, which was cut into two parts.

The results from the scaling tests varied significantly. Both the combination of the binders used in making the specimens as well as the type of salt used in the ponding solutions clearly affected the results. Specimen made from mixtures incorporating high levels of GGBFS showed noticeably more deterioration than specimens made from mixtures incorporating low levels of GGBFS and specimens containing only silica fume and cement. The total amount of scaling residues collected from each specimen is listed in Table 4.2. For reference, the percentage of each binder is also listed under the heading C-SF-S (Cement-Silica Fume-GGBFS).

Calcium chloride solution is the standard solution for scaling experiments conducted in accordance with ASTM C672. However, INDOT uses NaCl as a deicing salt. It was therefore thought to be beneficial to compare the effects of the two salts. As previously mentioned, the scaling resistance varied with the type of salt solution used. The NaCl solution generally caused more deterioration than the $CaCl_2$ solution. An analysis of the collected scaling residue data, presented in Figure 4.14, indicates that the NaCl solution was more than twice as aggressive as the $CaCl_2$ solution.

Having a combination of both GGBFS and silica fume did not prove to be beneficial with respect to deicing salt scaling resistance. The only ternary system from the laboratory portion of the study to perform relatively well during the scaling test was mixture LD-23 with 2% silica fume and 30% GGBFS. In general, as the replacement levels of the mineral admixtures

TABLE 4.2
Total collected scaling residues after 50 freeze-thaw cycles

		Scaling residue (kg/m^2)		Scaling residue (lb/yd^2)	
Mixture	**C-SF-S (%-%-%)**	**$CaCl_2$**	**NaCl**	**$CaCl_2$**	**NaCl**
LD-21	70-0-30	0.074	0.115	0.136	0.212
LD-22	95-5-0	0.082	0.079	0.151	0.146
LD-23	68-2-30	0.013	0.109	0.024	0.201
LD-24	65-5-30	0.206	1.110	0.380	2.046
LD-25	60-0-40	0.107	0.140	0.197	0.258
LD-26	50-0-50	0.128	0.691	0.236	1.274
LD-27	93.5-6.5-0	0.040	0.076	0.074	0.140
LD-28	40-0-60	1.260	1.971	2.323	3.633
LD-30	55-5-40	0.495	0.672	0.912	1.239
LD-31	45-5-50	0.529	1.585	0.975	2.922
LD-32	30-0-70	0.494	1.212	0.911	2.234
LD-33	92-8-0	0.020	0.180	0.037	0.332

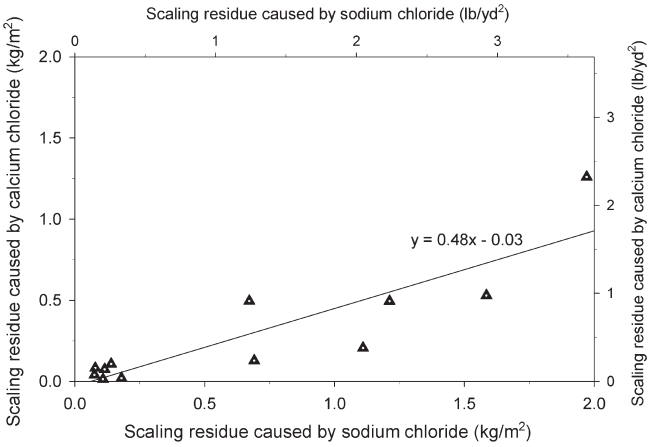

Figure 4.14 Comparison of amount of scaling residues caused by NaCl and $CaCl_2$ salts.

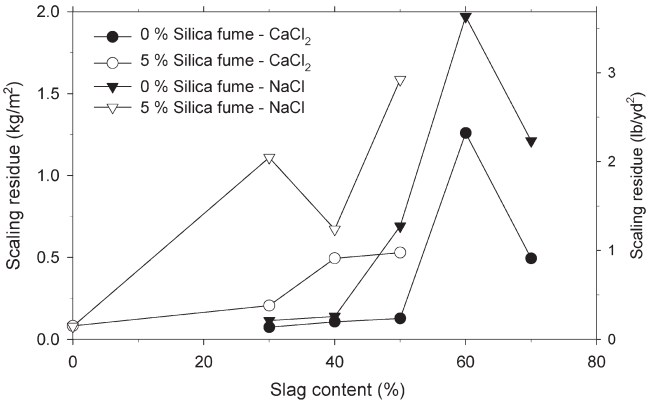

Figure 4.15 Effect of slag content on scaling resistance of concretes with and without 5% silica fume replacement after 50 freeze-thaw cycles.

increased, the scaling resistance generally decreased. Exceptions were the specimens from mixture LD-28 (60% GGBFS) which had a considerably lower scaling resistance than the specimens from mixture LD-32 (70% GGBFS). Coincidentally, the rapid freeze-thaw specimen from LD-28 was the only one to show considerable reduction in the relative dynamic modulus. The deicing scaling resistance is perhaps, in part, not only related to the composition of the binders, but also the air content and internal moisture content of the specimens. The measured air content of mixture LD-28 was the lowest of all the mixtures, or 5.2% at the end of batching. The effect of slag content on scaling resistance of concretes with 0 and 5% silica after 50 freeze-thaw cycles is shown in Figure 4.15.

4.2.5 Indication of Chloride Ion Penetration Resistance

The ability of the concretes to resist chloride ion penetration was evaluated in accordance with the ASTM C1202 test method (Standard Test Method for Electrical Indication of Concrete's Ability to Resist Chloride Ion Penetration). During the test, cylindrical specimens with a diameter of 97 mm (3.8 in.) and a thickness of 51 mm (2 in.) were placed in direct current circuits with a potential of 60 volts. The current in the circuits was monitored and the charge passed, in coulombs, through the sample during six hours was calculated. Two specimens from each mixture were tested after 28 days of moist curing and other two after 91 days of moist curing. The data from each specimen and average value for each mixture for a given testing date are listed in Table 4.3. The percentage of each binder is again listed under the heading C-SF-S (Cement-Silica Fume-GGBFS).

As expected, replacing a portion of the cement with either or both silica fume and GGBFS was an effective

TABLE 4.3
Charge passed during six hours (coulombs) after 28 and 91 days of moist curing

		Charge passed after 28 days of curing (coulombs)			Charge passed after 91 days of curing (coulombs)		
Mixture	**C-SF-S (%-%-%)**	**Spec. 1**	**Spec. 2**	**Avg.**	**Spec. 1**	**Spec. 2**	**Avg.**
LD-20	100-0-0	4019	3506	3763	2722	2666	2694
LD-21	70-0-30	2213	2249	2231	1299	1328	1314
LD-22	95-5-0	1637	1450	1544	839	744	792
LD-23	68-2-30	1882	1525	1704	677	673	675
LD-24	65-5-30	1072	1052	1062	333	330	332
LD-25	60-0-40	2643	2759	2701	1448	1418	1433
LD-26	50-0-50	1817	1861	1839	947	1013	980
LD-27	93.5-6.5-0	1541	1437	1489	727	695	711
LD-28	40-0-60	1111	1078	1095	713	740	727
LD-29	92-8-0	801	754	778	319	309	314
LD-30	55-5-40	753	813	783	274	278	276
LD-31	45-5-50	869	834	852	316	304	310
LD-32	30-0-70	748	711	730	462	486	474
LD-33	92-8-0	944	854	899	343	335	339
LD-34	56.5-3.5-40	1288	1172	1230	420	408	414
LD-35	46.5-3.5-50	985	878	932	377	361	369

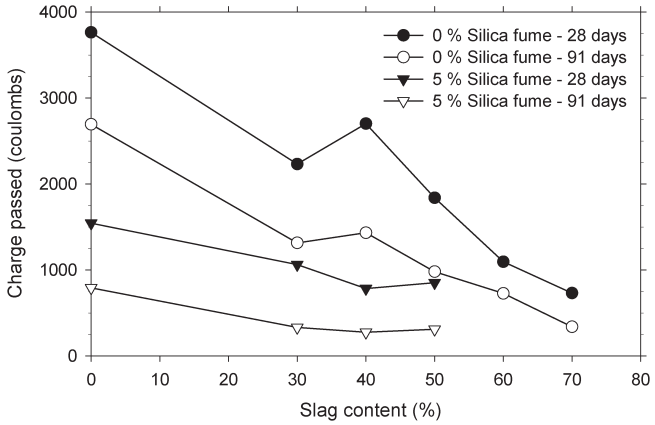

Figure 4.16 Influence of slag content and curing time on the charge passed of deck concrete with and without 5% silica fume.

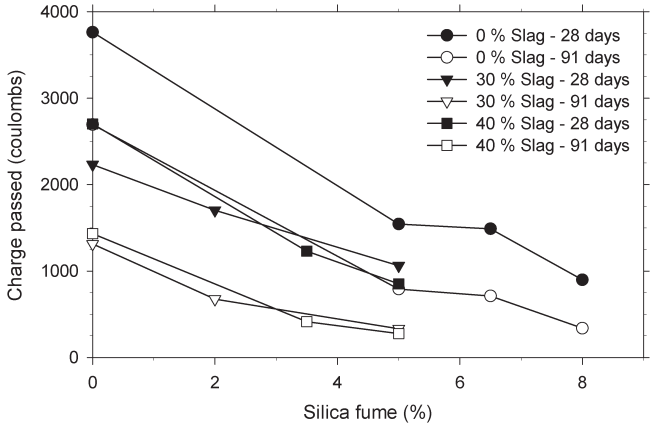

Figure 4.17 Influence of silica fume content and curing time on the charge passed of deck concrete with 0, 30, or 40% slag replacement.

way of reducing the charge passed, in coulombs, during the six-hour test. Extending the curing time from 28 days to 91 days also reduced the charge passed.

In general, using ternary systems with both silica fume and GGBFS appeared to yield the most favorable results. The lowest value, 276 coulombs after 91 days, was obtained for specimens in which a combination of 5% silica fume and 40% GGFFS was used. The effects of increasing the GGBFS content on reducing the charge passed are shown in Figure 4.16. The benefits of 5% silica fume replacement and increased curing time are also illustrated in the figure. Similarly, the effect of increasing the silica fume content on the charge passed is shown in Figure 4.17. Note how effectively the charge passed is reduced when both GGBFS and silica fume are used together. For example, a value of 675 coulombs was achieved after 91 days with a combination of only 2% silica fume and 30% GGBFS (LD-23).

4.2.6 Drying Shrinkage

Drying shrinkage measurements were done on several mixtures following the requirements of ASTM C175. Four specimens, each with a gage length of 254 mm (10 in.), were made from selected mixtures and cured in lime-saturated water for either seven or 28 days before being moved to 50% relative humidity (RH). The drying shrinkage was calculated with respect to two initial lengths, one taken at the age of one day and the other taken at the end of the curing period. The main purpose of the tests was to evaluate the effectiveness of a shrinkage reducing admixture (SRA) to reduce drying shrinkage. The dosage rate of the SRA ranged from 0 to 2% by mass of cement. The water-cement ratio for all of these mixtures, except for two INDOT's Class C mixtures with a water-cement ratio of 0.443, was 0.38. Cement was the only binder used for shrinkage specimens.

Using a SRA admixture presented unique challenges. As the dosage of the SRA was increased, the effectiveness of the AEA decreased. In order to maintain an acceptable level of entrained air, the dosage rate of the AEA was increased. In fact, roughly seven times more AEA was required when the dosage rate of the SRA was increased from 0 to 2% by mass of cement.

Based on the results presented in Figure 4.18 for specimens cured for seven days in lime-saturated water and in Figure 4.19 for specimens cured for 28 days in lime saturated water, the SRA proved to be effective in reducing the drying shrinkage. For specimens cured for seven days, the drying shrinkage at the end of the test (~450 days) ranged from 0.046% to 0.074% for specimens with 2% SRA and Class C concrete (identified with the letter C in the figures), respectively. The total shrinkage was generally reduced when the curing was increased from 7 to 28 days. The shrinkage at the end of the test ranged from 0.043% to 0.061% for specimens cured for 28 days. For minimum requirements of INDOT Class C concrete, see the mixture proportions for mixtures LD-44, LD-45, and LD-49 in Appendix C.

Some length changes were observed during the period, which the specimens were submerged in the lime-saturated water. The length changes during the

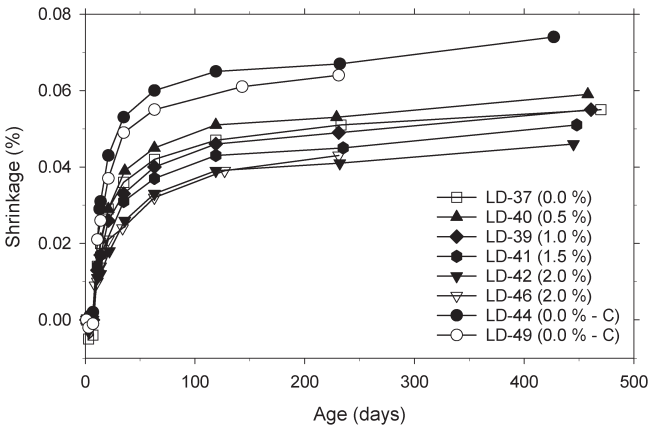

Figure 4.18 Drying shrinkage results for specimens made with and without shrinkage reducing admixture. Specimens were cured in lime-saturated water for seven days. Initial readings were taken at the age of one day.

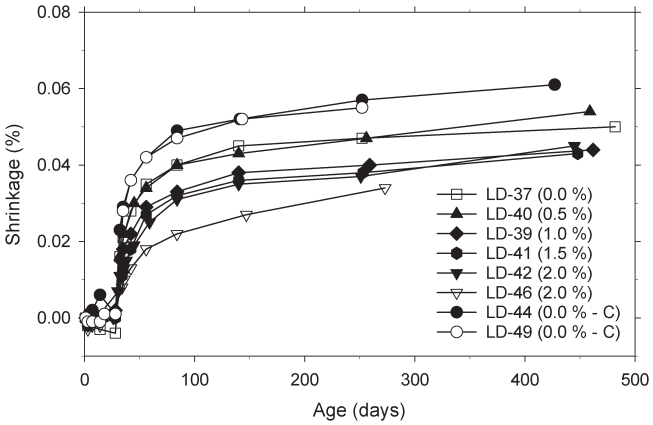

Figure 4.19 Drying shrinkage results for specimens made with and without shrinkage reducing admixture. Specimens were cured in lime-saturated water for 28 days. Initial readings were taken at the age of one day.

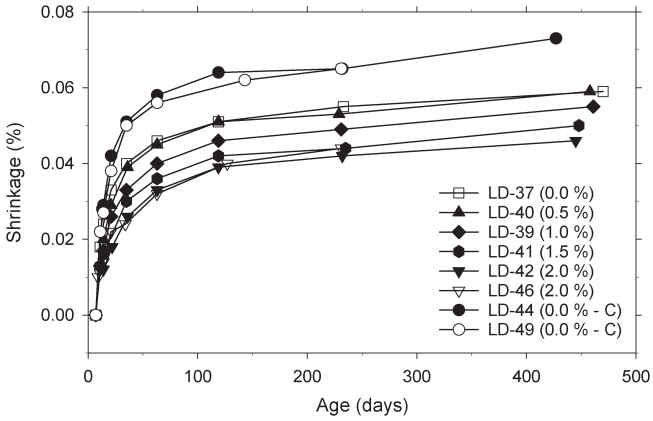

Figure 4.21 Drying shrinkage results for specimens made with and without shrinkage reducing admixture. Specimens were cured in lime-saturated water for seven days. The reference readings were taken at the age of seven days.

curing periods varied from 0.004% expansion to 0.007% length reduction, but were generally within 0.001% expansion and 0.003% length reduction. The reasons behind these variations in length are not known, but in an attempt to verify that they were not due to inconsistent measurements, two sets of two specimens were kept submerged in lime-saturated water for 91 days and their lengths monitored periodically. The results of those measurements are shown in Figure 4.20. During the first 28 days, limited correlation appeared to exist between the two sets of specimens. However, after 28 days, the correlation between the two sets was good, with a difference in length reduction of 0.002% typically observed. The fact that the length difference between the two sets remained nearly constant after 28 days may indicate that variations in length were caused by temperature changes. If the coefficient of thermal expansion for concrete is assumed to be $10{\cdot}10^{-6}$/°C ($5.6{\cdot}10^{-6}$/°F), a length change of 0.001% would be observed for a temperature change of 1°C (1.8°F). The temperature in the laboratory was generally not closely monitored nor controlled and some fluctuations are likely to have occurred. However, that does not explain the inconsistent length changes during the first 28 days, or the gradual length reductions observed during that period.

The general agreement with the amount of SRA and the ultimate shrinkage was satisfactory. However, the benefit of increasing the dosage rate of the SRA to reduce shrinkage was not always clear. In order to eliminate the effects of length changes during the curing period on the ultimate shrinkage, the results were normalized with respect to the specimen lengths at the end of the curing periods. This method appears to give a stronger correlation between the amount of SRA used and the drying shrinkage. Results from specimens cured for 7 days in lime-saturated water are shown in Figure 4.21 and for those cured for 28 days in Figure 4.22.

The mass of each specimen was generally measured each time a shrinkage measurement was done. The mass loss was then calculated with respect to the initial mass and also the mass at the end of the curing period.

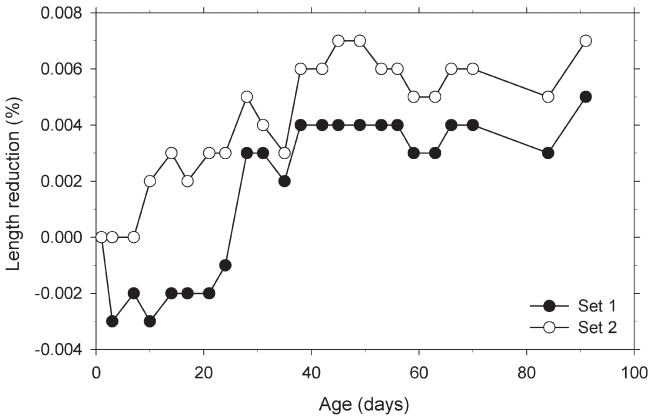

Figure 4.20 Length changes of two sets of specimens from mixture LD-48 during the first 91 days. The specimens were stored in lime-saturated water during the entire test period.

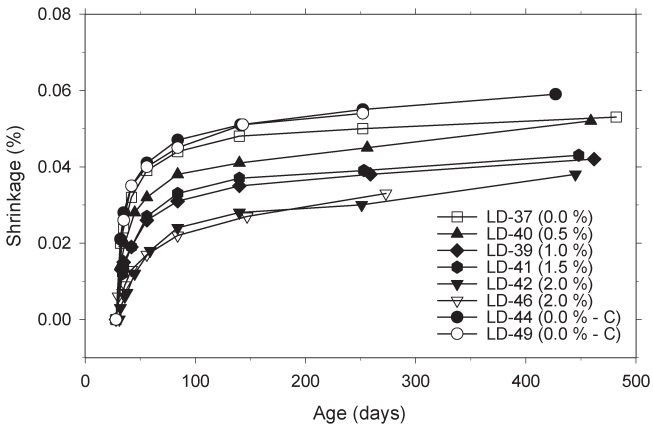

Figure 4.22 Drying shrinkage results for specimens made with and without shrinkage reducing admixture. Specimens were cured in lime-saturated water for seven days. The reference readings were taken at the age of 28 days.

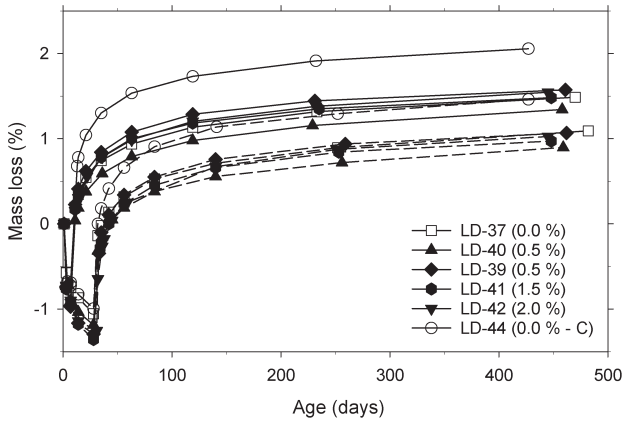

Figure 4.23 Mass loss of specimens made with and without shrinkage reducing admixture. Initial mass (one-day) was used as a reference when calculating the mass loss. Data represented with dashed lines represent specimens, which were cured for 28 days.

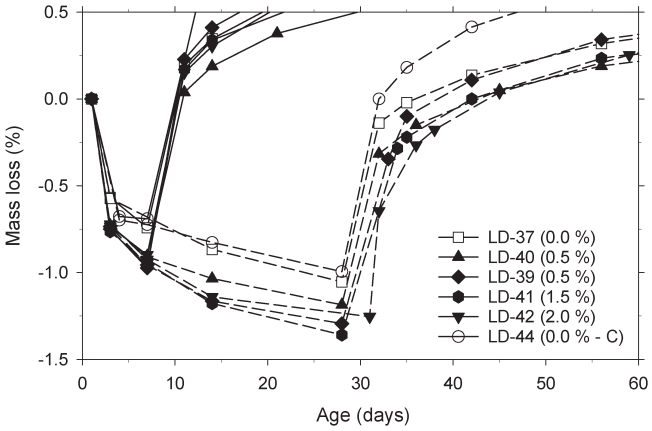

Figure 4.25 Mass loss of specimens made with and without shrinkage reducing admixture during the first 60 days. Data represented with dashed lines represent specimens which were cured for 28 days.

The mass loss of the specimens with respect to initial mass is shown in Figure 4.23 and the mass loss with respect to the weight at the end of the curing period (either seven or 28 days) is shown in Figure 4.24. Data represented with solid lines are for specimens cured for 7 days and data represented with dashed lines are for specimens cured for 28 days. In Figure 4.23, the mass loss is strongly dependent on the length of the curing period. This can be attributed to the greater mass gain of specimens cured for 28 days compared to those cured for only 7 days. When the data are evaluated with respect to the mass at the end of the curing period, the aforementioned trend is no longer clear. However, extending the curing from 7 to 28 days reduced the total mass loss (as well as net mass loss) for specimens from all of the mixtures tested.

The mass changes of the specimens during the first 60 days are perhaps of interest although the significance of this information is uncertain. As shown in Figure 4.25, it appears as if the addition of SRA increased the mass gain of the specimens while submerged in the lime-saturated water. Specimens from LD-37, the reference mixture, and LD-44, the Class C mixture, had similar mass gains, but in both cases the mass gain was smaller than any of the other specimens had. Based on this data, it can be speculated that the additional absorption may have some implications in regard to freezing and thawing resistance of concrete modified with SRA.

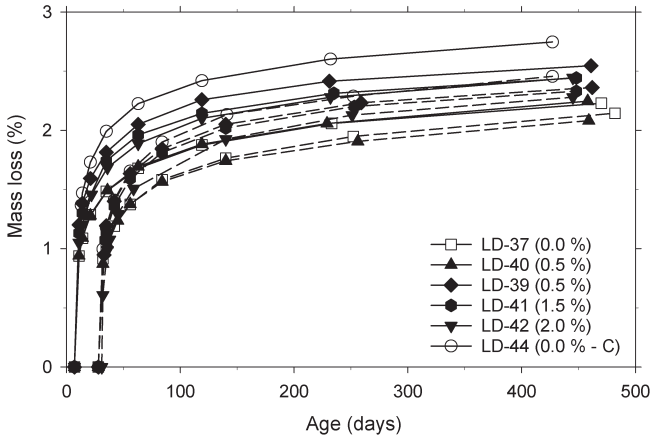

Figure 4.24 Mass loss of specimens made with and without shrinkage reducing admixture. The mass at the end of the curing periods (either seven or 28 days) is used as reference value. Data represented with dashed lines represent specimens, which were cured for 28 days.

4.3 Deck Concrete—Field Trials

Based on results from the laboratory trials with deck concrete, reported in Section 4.2, three mixtures (F-2 to F-4) were selected and tried in the field. In addition, one mixture (F-1), meeting INDOT's requirements for Class C concrete was also tried. The Class C mixture was included to provide a baseline to which the other mixtures could be compared. The mixture proportions and concrete properties of these mixtures are listed in Sections C.5 and C.6 in Appendix C. The values in Table C.5 are in SI units and the values in Table C.6 are in U.S. customary units. The minimum requirements for ClassC concrete include a cement content of 390 kg/m^3 (658 lb/yd^3) and a maximum water-cement ratio of 0.443. Based on the concrete delivery ticket, the actual water-cement ratio of the ClassC concrete used in this study was estimated to be 0.397.

The field trials were conducted in cooperation with Irving Materials, Incorporated. The mixtures were batched at the West Lafayette plant and mixed and delivered to the Civil Engineering Building with front discharge ready mix trucks.

When supplementary materials were used, they were loaded into the truck by hand before the truck was parked under the batch plant. At the batch plant, the rest of the materials, including chemical admixtures and most of the water, were added to the truck. The plant

Figure 4.26 Concrete truck parked outside the Civil Engineering Building during concrete delivery.

was electronically controlled from a separate control room.

Once the materials were in the truck, the truck was used to rapidly mix the concrete for a few minutes. At the conclusion of this mixing, the driver and/or researcher visually evaluated the slump of the concrete. Some of the water withheld earlier was then added to yield the desired slump. The concrete was then gently agitated while in transit to the testing site at the Civil Engineering Building at Purdue University. A concrete truck parked outside the Civil Engineering Building during delivery of concrete is shown in Figure 4.26.

Slump, density, and air content were measured immediately after the trucks arrived on-site. The fresh concrete properties of mixtures F-1 and F-4 were within the specified limits upon arrival, but the air content of mixtures F-2 and F-3 was low. Additional air-entraining agent of the same product as used at the batch plant was then added and the concrete mixed for a few more minutes. This increased the air content of the mixtures to an acceptable level and the concrete was accepted for delivery.

After the fresh concrete properties had been verified to be within the acceptable limits, a group of six to eight workers proceeded to prepare a total of 91 specimens from each of the four mixtures. All specimens were filled and consolidated within about 30 minutes after the preparation of the specimens started. About 30 minutes later, the surfaces of all specimens had been finished and covered with plastic. The mixtures were prepared on four different days from April 16 to 26, 2002.

4.3.1 Compressive Strength Development

The compressive strength of each of the four field trial mixtures was determined after 1, 3, 7, 14, 28, 56, and 91 days of curing. The compressive strength development of the four mixtures is shown in Figure 4.27. Two 102×203 mm (4×8 in.) cylinders were tested for each test. The cylinders were demolded after one day and then stored in the fog room until tested.

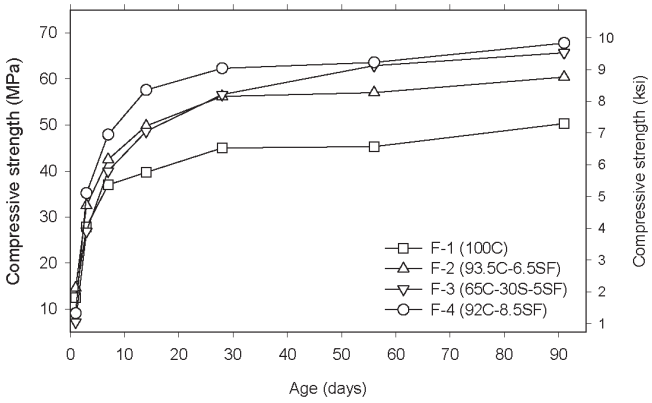

Figure 4.27 Compressive strength development of continuously moist cured specimens from the four field trial mixtures.

The compressive strength development was initially slow and after the first day, the strengths ranged from 7.2 to 14.6 MPa (1.05 to 2.12 ksi). Temperature matched cured specimens, prepared at the same time, had corresponding one-day strengths of 15.5 to 33.5 MPa (2.24 to 4.86 ksi). The strength development of the TMC specimens as well as specimens cured under different humidity conditions is shown and discussed in Section 4.5.

The 28-day strengths ranged from 45.0 to 62.3 MPa (6.53 to 9.03 ksi). Subsequent strength gain was limited except for mixture F-3 (65C-30S-5SF) which seemed to benefit most from additional curing time.

4.3.2 Splitting Tensile Strength Development

Splitting tensile strength of each of the four deck field trial mixtures was tested after 28 and 56 days of curing. Each test result was established from test data from three 152×305 mm (6×12 in.) cylinders tested in accordance with ASTM C496. The results, along with values estimated based on $7.5\sqrt{f'_c}$ (ACI 318-02, p. 103) with f'_c in psi, are presented in Figure 4.28.

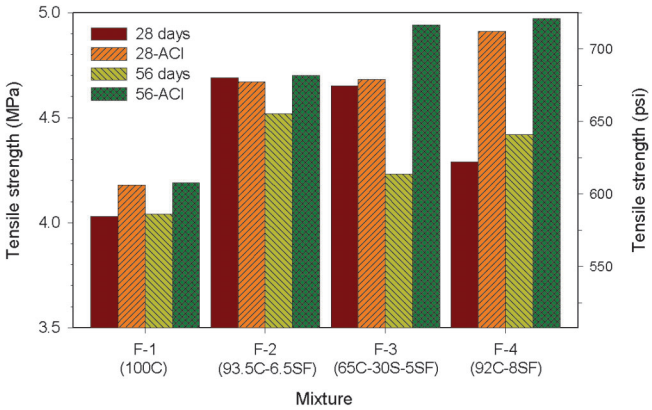

Figure 4.28 Splitting tensile strength for field trial mixtures along with estimated tensile strengths based on $7.5\sqrt{f'_c}$ (ACI 318-02, p. 103).

The 28-day splitting tensile strength ranged from 4.03 to 4.69 MPa (585 to 680 psi) with F-1 having the lowest strength and F-2 the highest strength. The change in splitting tensile strength between 28 and 56 days was minimal with the exception of a 0.42 MPa (60 psi), or roughly 9%, drop for mixture F-3.

Correlation between measured splitting tensile strength and values estimated based on the ACI equation was good for mixtures F-1 and F-2 as well as the 28-day test for F-3 with variations between the two values ranging from −0.4 to 3.9%. However, the correlation for F-4 and the 56-day test for F-3 was not strong with the ACI equation yielding estimates that were between 12.4 and 16.7% higher than the measured values.

4.3.3 Static and Dynamic Moduli Developments

Developments of static and dynamic moduli were monitored for each of the four field trial mixtures. Two specimens, moist cured for the entire testing period, were monitored for the development of each modulus for each mixture. The static modulus development is shown in Figure 4.29 and the dynamic modulus development in Figure 4.30.

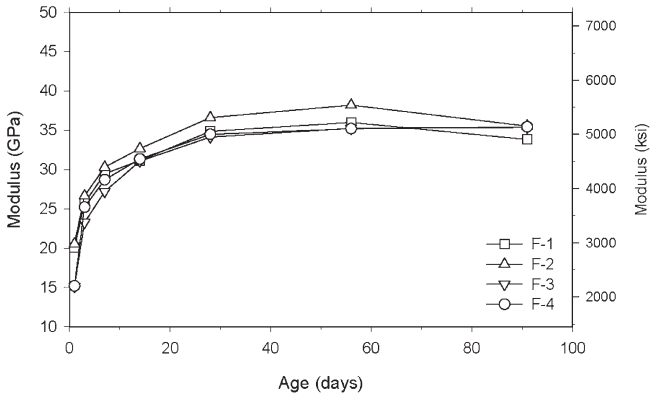

Figure 4.29 Static modulus developments for all field trial deck mixtures.

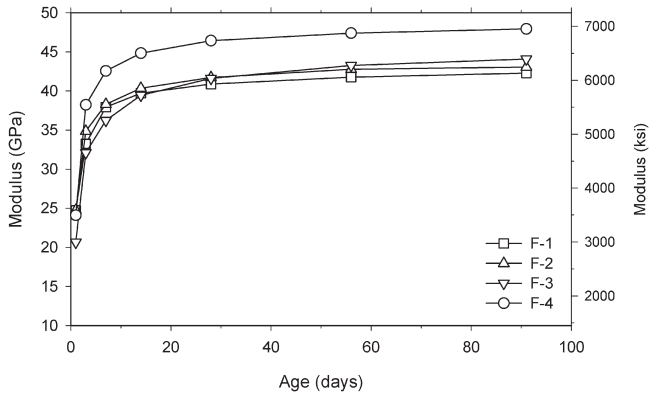

Figure 4.30 Dynamic modulus developments for all field trial deck mixtures.

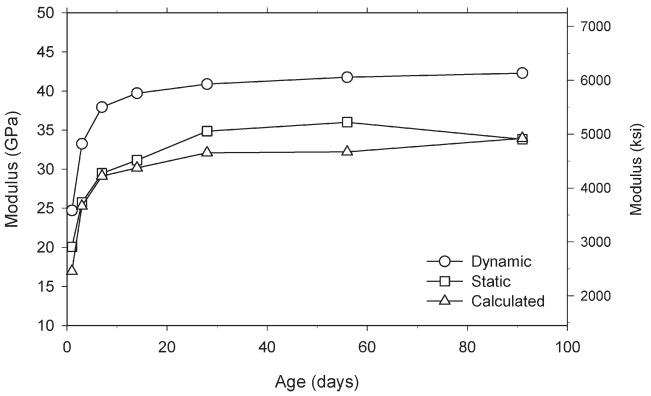

Figure 4.31 Moduli developments for specimens from F-1 (100C). Calculated values based on $E_c = w_c^{1.5} \cdot 33 \cdot f'_c{}^{0.5}$ are included for comparison.

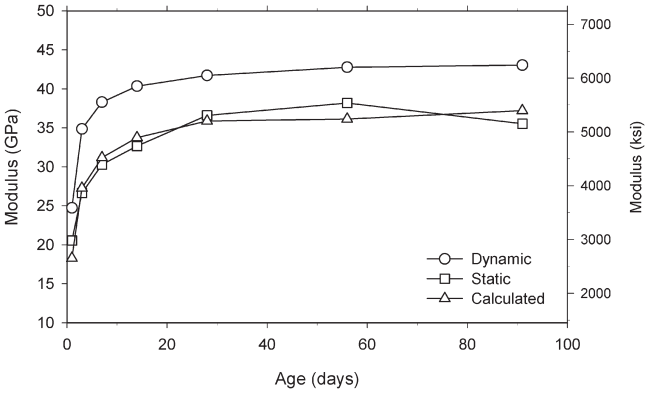

Figure 4.32 Moduli developments for specimens from F-2 (93.5C-6.5SF). Calculated values based on $E_c = w_c^{1.5} \cdot 33 \cdot f'_c{}^{0.5}$ are included for comparison.

After 28 days of curing, the static modulus values ranged from 34.12 to 36.6GPa (4950 to 5310 ksi). Corresponding values for the dynamic modulus were from 40.9 to 46.4GPa (6640 to 5850 ksi). The static modulus values for all four mixtures were quite consistent and similar although a slight abnormality appeared in the 91-day results for two of the mixtures where the modulus was found to decrease from previous measurements. The dynamic modulus values increased rapidly at early ages, but had only slight, but gradual, increase after 28 days.

In addition to measuring and reporting the static and dynamic moduli, the static modulus was estimated using $E_c = w_c^{1.5} \cdot 33 \cdot f'_c{}^{0.5}$ from Section 8.5 in ACI 318-02 [(*14*), p. 89]. The range of the measured values was 83 to 118% of the corresponding calculated values, which is within the typical range of 80 to 120% [(*14*), p. 89]. The development of static, dynamic, and calculated moduli for all four deck field mixtures is shown in Figures 4.31 to 4.34.

4.3.4 Resistance to Rapid Freezing and Thawing in Water

Two specimens from each of the field trial mixtures were tested for freeze-thaw resistance in accordance

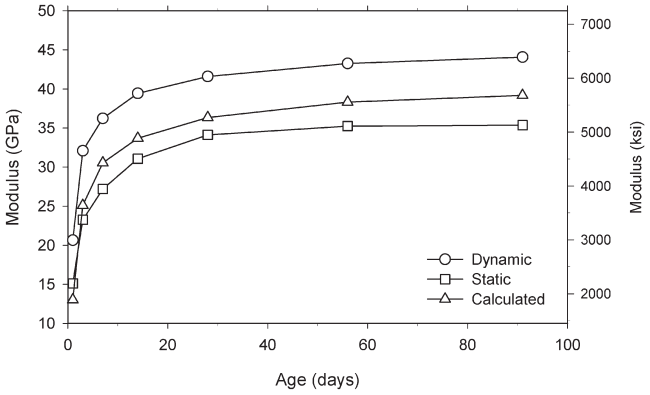

Figure 4.33 Moduli developments for specimens from F-3 (65C-30S-5SF). Calculated values based on $E_c = w_c^{1.5} \cdot 33 \cdot f'_c{}^{0.5}$ are included for comparison.

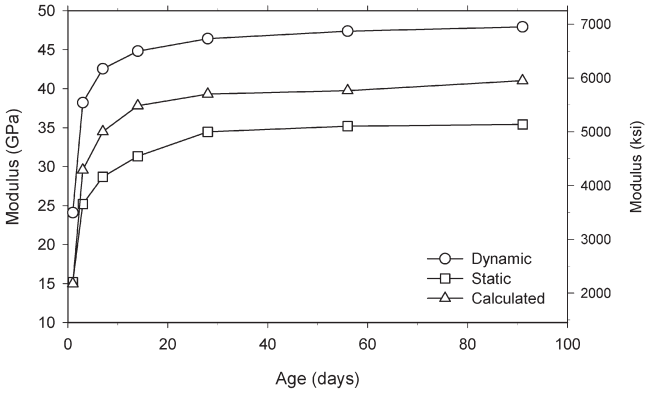

Figure 4.34 Moduli developments for specimens from F-4 (92C-8SF). Calculated values based on $E_c = w_c^{1.5} \cdot 33 \cdot f'_c{}^{0.5}$ are included for comparison.

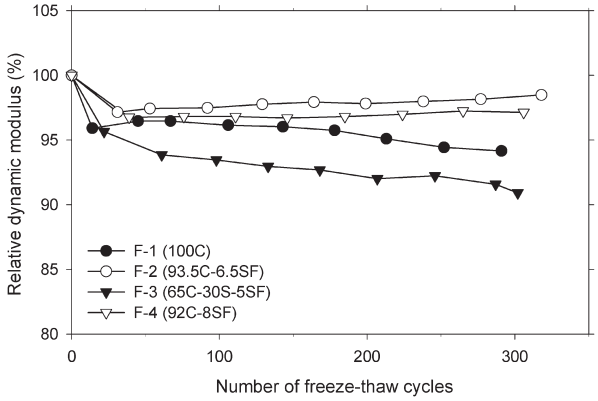

Figure 4.35 Relative dynamic modulus development during freeze-thaw testing of specimens from field trials. Two specimens were tested from each mixture.

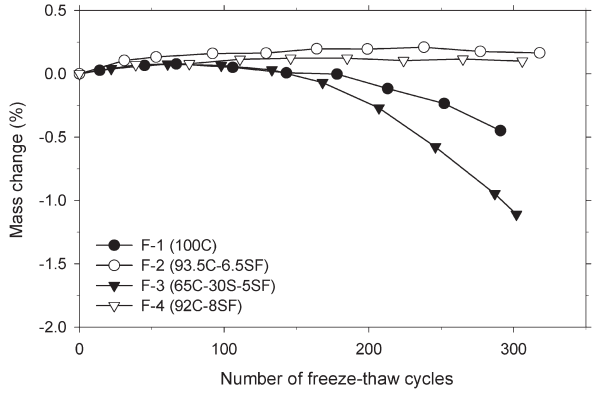

Figure 4.36 Mass change during freeze-thaw testing of specimens from field trials. Two specimens were tested from each mixture.

with ASTM C666, procedure A (freezing and thawing in water). As shown in Figure 4.35, the specimens fared well and the average relative dynamic modulus for all of the mixtures exceeded 90%. In fact, the range was from 90.9% for F-3 to 98.5% for F-2.

In addition to the relative dynamic modulus, mass change of the freeze-thaw specimens was monitored at each testing date. The mass change during the testing period is shown in Figure 4.36. Specimens undergoing freeze-thaw testing in water gain mass due to absorption. They may also loose mass due to deterioration of the surface, or scaling. Without collecting and measuring the mass of the deteriorated material, the effect of each of the two factors on mass change cannot be separated. However, the overall mass change may provide an indication of the scaling potential of the concrete in water.

At the end of the test, specimens from both of the mixtures containing only cement and silica fume (F-2 and F-4) showed a slight increase in their mass. Specimens from F-1 had lost 0.45% of their mass and specimens from F-3 had lost 1.11%. The rate of mass loss for specimens that lost mass increased toward the end of the test. The magnitude of the mass loss for F-1 and F-3 toward the end of the test indicates that absorption has very limited influence on the mass change. Also, most of the absorption is expected to occur during the early part of the test.

4.3.5 Resistance to Deicing Salt Scaling

Four specimens from each of the field mixtures were tested for scaling resistance in the presence of 3% NaCl solution. In general, the ASTM C672 standard was followed. The main adjustment to the standard procedure included the humidity of the freeze-thaw room and the type of salt solution used. In addition, half of the specimens were moist cure for only three days and then cured at 50% RH until testing was initiated at the age of 28 days. The other half of the specimens was moist cured for 14 days and then cured at 50% RH. Also, the scaling resistance of the specimens was evaluated by collecting the scaling residue after each five cycles instead of following the visual rating method outlined in the ASTM standard. Collecting the scaling residue and measuring its dry mass is believed to be more effective in quantifying scaling resistance than the visual rating method.

As the relative humidity in the freeze-thaw room could not be controlled, the specimens were covered with plastic food wrap to provide a constant environment above the salt solution. This in turn minimized the evaporation of solution during each five-day test period and eliminated the need for adding water to the solution to maintain a constant depth of solution. It is believed that covering the specimens with impermeable material may provide more consistent results, as the concentration of the solution is not significantly affected through evaporation and subsequent additions of water.

The average amount of collected scaling residue for each set of specimens is shown in Figure 4.37. The variation in scaling resistance is significant and the difference between the most resistant and the least resistant set is 250 fold. Due to the large variation in the amount of collected scaling residue, the vertical axes in Figure 4.37 are discontinuous with a break between 0.5 and 2.0 kg/m^2 (0.9 and 3.7 lb/yd^2).

Total amount of scaling residue collected from specimens from F-2, moist cured for 14 days, was slightly less than 0.01 kg/m^2 (0.02 lb/yd^2) while the corresponding value for specimens from F-3, also moist cured for 14 days, was 2.38 kg/m^2 (4.39 lb/yd^2). Except for the aforementioned specimens from mixture F-3, which were cured for 14 days, all of the sets yielded less than 0.35 kg/m^2 (0.65 lb/yd^2) of scaling residue, including the specimens from F-3 that were only moist cured for 3 days. For comparison, the maximum allowable amount of scaling residue specified in the special provisions for the SR 43 HPC bridge over Burnett Creek was set at 0.5 kg/m^2 (0.9 lb/yd^2). The complete special provisions are included in Appendix C.

The duration of the scaling test was extended beyond the 50 cycles recommended by ASTM. This was done because the effectiveness of the freeze thaw room was brought into question during the early part of the experiment. It is believed that the room was partly malfunctioning during this part of the experiment and that only some cooling was taking place. After the problem was corrected, each of the specimens underwent 50 cycles. Some of the specimens, particularly those from F-1 and F-2, experienced some freezing and thawing during the days that the room was becoming ineffective. Based on minor amount of collected scaling residue, specimens from F-3 and F-4 may have experienced some mild freezing as well.

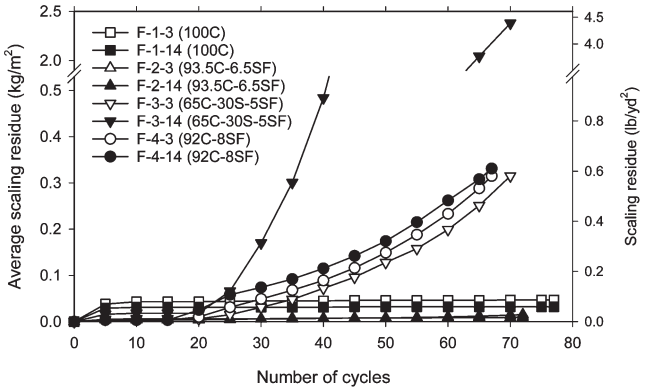

Figure 4.37 Average scaling residue collected during exposure to 3 % sodium chloride solution. The specimens were either moist cured for 3 or 14 days, followed by further curing at 50 % RH until the test was started after a total of 28 days of curing.

Shortening the moist curing period from 14 days to 3 days yielded results different from those anticipated. It was anticipated that shortening the moist curing would adversely affect the scaling resistance. This held true for specimens from F-1 and F-2 where the total amount of scaling was minimal. However, for specimens from F-3 and F-4 where there was noticeable scaling, specimens moist cured for only 3 days fared better than those moist cured for 14 days. The difference in the case of F-4 was minimal, but for F-3 the difference was almost eight fold. Specimens from F-3, moist cured for 14 days, where the only specimens not to meet the criteria set forth in the special provisions for the SR 43 HPC Bridge over Burnett Creek. Based on the standard test procedure that calls for 14 days of moist curing followed with 14 days of air curing, mixture F-3 should therefore not be considered for use in the bridge deck although specimens moist cured for 3 days and then air cured for 25 days met the criteria.

4.3.6 Electrical Indication of Chloride Ion Penetration Resistance

Electrical indication of chloride ion penetration resistance was determined for all four of the field trial mixtures at the ages of 28 and 91 days. At both ages, continuously moist cured (standard), moist cured for 3 days and then air cured, and sealed specimens were tested. In addition, specimens moist cured for seven days and then cured in water bath at 38°C (100°F) for additional 21 days were tested at the age of 28 days. Two specimens, both obtained from the same cylinder were tested for each test. The charge passed for each mixture after 28 days of curing is shown in Figure 4.38 and after 91 days of curing in Figure 4.39. For comparison, the 28-day results from the specimens cured at 38°C (100°F) are also included in Figure 4.40 as this curing regime was developed to estimate the charge passed for fully matured specimens.

As expected, the difference in the charge passed between specimens from mixture F-1 and the other mixtures was considerable as F-1 was the only mixture without supplementary cementitious materials. The charge passed for specimens continuously moist cured for 28 days (standard) ranged from 910 coulombs for F-4 to 7330 coulombs for F-1. Corresponding values after 180 days of curing were 500 and 4900 coulombs. After 91 days of moist curing, the charge passed for specimens from F-3 was 450 coulombs and for specimens from F-2, it was 1210 coulombs.

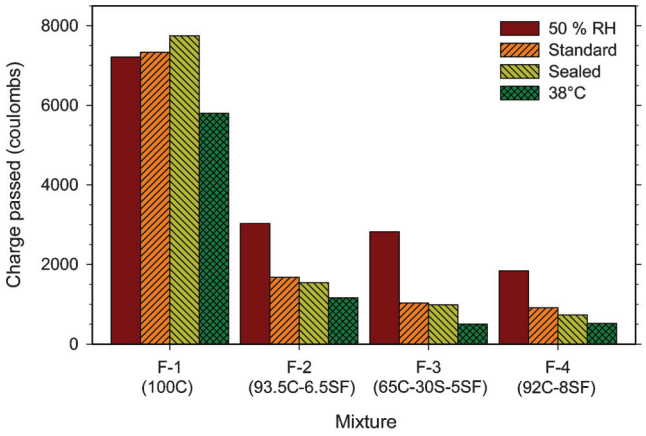

Figure 4.38 Charged passed after 28 days of curing of field trial mixtures.

In the special provisions for the SR 43 HPC bridge over Burnett Creek the maximum allowable charge passed at 56 days was set at 1000 coulombs. It is therefore apparent, even with additional five weeks of moist curing, that mixture F-2 did not meet those specifications. The fact that the results from F-2 did not meet the criteria is further supported by the result from the specimens cured at 38°C (100°F) which had a charge passed of 1160 coulombs. Mixtures F-3 and F-4 had less than 1000 coulombs passed after only 28 days of moist curing and do therefore easily meet the 1000 coulomb after 56 days criteria set forth in the special provisions.

Moist curing the specimens for seven days and then curing them in water at 38°C (100°F) until tested at 28 days appears to be a reasonable method of obtaining estimates of values expected after 180 days of moist curing. For three of the four mixtures, the predicted values were higher than the actual values. The actual values after 180 days of curing were from 4% higher to

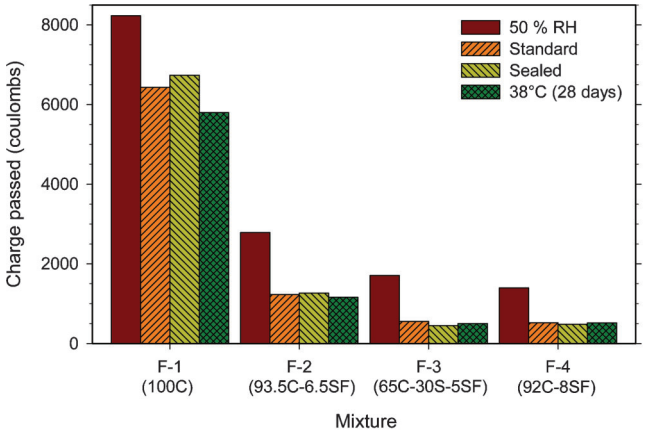

Figure 4.39 Charged passed after 91 days of curing of field trial mixtures. Results from specimens moist cured at room temperature and then in water bath at 38°C (100°F) for 21 days are included for comparison.

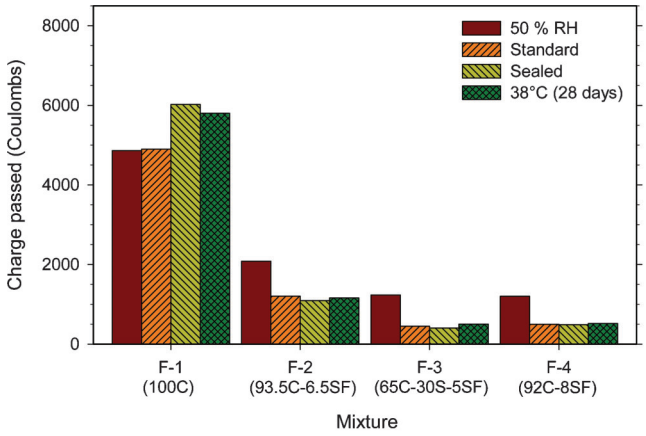

Figure 4.40 Charged passed after 180 days of curing of field trial mixtures. Results from specimens moist cured at room temperature and then in water bath at 38°C (100°F) for 21 days are included for comparison.

18% lower than the predicted values after only 28 days of curing.

Curing the specimens sealed in their plastic molds yielded results similar to those obtained from specimens that were continuously moist cured. In the absence of adequate moist curing facilities, leaving the specimens sealed in their molds appears to be a satisfactory option when the electrical indication of concrete's ability to resist chloride ion penetration is to be determined.

Limiting the moist curing to only three days, followed with curing at 50% RH, generally increased the charge passed significantly when compared with results from all other specimens. The only result that didn't follow this trend was for F-1 at 28 days. In terms of expected resistance to chloride ion penetration, it appears essential to extend the moist curing well beyond three days. The lowest value after 91 days was 1200 coulombs for F-4. The corresponding value for continuously moist cured specimens was 490 coulombs.

4.3.7 Chloride Ion Penetration

Cores were extracted from eight slabs from the field trial mixtures after 90 days of exposure to chloride solutions. Four of the slabs, one from each mixture, were ponded continuously with 3% NaCl for 90 days as per AASHTO T259. The other four slabs were subjected to cycles consisting of four days of ponding with 6% NaCl solution followed by three days of drying under heat lamps. In addition to the chloride profiles, baseline chloride contents were determined along with chloride contents in both fine and coarse aggregates. The testing of the powder samples was carried out at INDOT's Materials and Tests Division in Indianapolis under the supervision of Ms. Youlanda K. Belew.

Baseline chloride contents and chloride contents of both fine and coarse aggregates are listed in Table 4.4. The baseline chloride contents were higher than

TABLE 4.4
Baseline chloride contents and chloride contents of both fine and coarse aggregate

	Chloride concentration	
	(kg/m^3)	(lb/yd^3)
F-1 (100C)	1.02	1.73
F-2 (93.5C-6.5SF)	1.08	1.82
F-3 (65C-30S-5SF)	1.12	1.89
F-4 (92C-8SF)	0.85	1.43
Fine aggregate	0.47	0.79
Coarse aggregate	1.53	2.58

anticipated, as they approximately equal to the typical threshold level for corrosion of 0.9 to 1.2 kg/m^3 (1.5 to 2.0 lb/yd^3) [(*20*), p. 29]. The aggregates, particularly the coarse aggregates, appear to be the source of the baseline chlorides.

Chloride profiles along with curves fitted to the profiles for specimens subjected to the 3% NaCl solution are shown in Figure 4.41. Using Equation 2.2, the curves were fitted to the profiles assuming a constant surface chloride concentration of 18 kg/m^3 (30.3 lb/yd^3) and variable effective chloride ion diffusion coefficients. Mixture F-1 had the highest diffusion coefficient, or $10 \cdot 10^{-12}$ m^2/s. For mixture F-2, the diffusion coefficient was found to be $4 \cdot 10^{-12}$ m^2/s and $2 \cdot 10^{-12}$ m^2/s for mixtures F-3 and F-4. Based on the estimated diffusion coefficients, the time to corrosion of reinforcement in mixtures F-3 and F-4 can be expected to be five times longer than in mixture F-1 and two times longer than in mixture F-2. If the typical time to corrosion in bridge decks is assumed to be 15 years when INDOT Class C concrete (mixture F-1) is used, the time to corrosion of bridge decks utilizing either mixture F-3 or F-4 can be estimated to be 75 years.

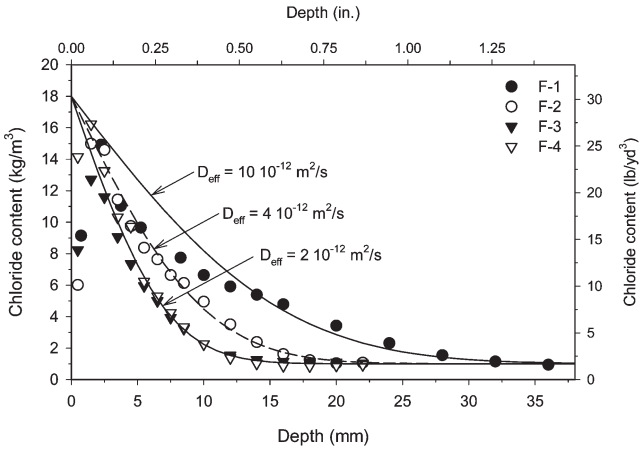

Figure 4.41 Chloride profiles of cores extracted from slabs ponded with 3% NaCl solution for 90 days as described AASHTO T259. The curves were determined by using a fixed surface chloride concentration of 18kg/m^3 (30.3 lb/yd^3) and variable diffusion coefficients as shown.

TABLE 4.5
Comparison of diffusion coefficients obtained from Figure 4.41 and calculated from Equation 2.3

Mixture	Diffusion coefficient from Figure 4.41 (10^{-12} m^2/s)	Diffusion coefficient from Equation 2.3 (10^{-12} m^2/s)
F-1 (100C)	10	16.3
F-2 (93.5C-6.5SF)	4	4.05
F-3 (65C-30S-5SF)	2	2.09
F-4 (92C-8SF)	2	1.98

As the temperature of the ponding slabs was higher than would normally be expected during ponding tests, the effective chloride ion diffusion coefficients for the curves shown in Figure 4.41 can be expected to be higher also. Based on estimates given by Bentur et al. [(*20*), p. 163], diffusion coefficients can be expected to change by roughly a factor of two for each 9°C (16°F). Analysis of the temperature data presented in Figure 3.20 yielded an average weekly temperature of the slabs of 27.2°C (81.0°F). This is 4.2°C (7.6°F) higher than recommended in the standard test procedure of AASHTO T259 and the diffusion coefficients can therefore be expected to be roughly 1.5 times higher than they would have been at the standard temperature. However, using Equation 2.3 to estimate diffusion coefficients based on 91-day charge passed values presented in Figure 4.39, a strong correlation with diffusion coefficients shown in Figure 4.41 can be observed. The two diffusion coefficient values for each field trial mixture are listed and compared in Table 4.5.

Chloride profiles for the four slabs that were subjected to cycles consisting of four days of ponding with 6% NaCl solution followed by three days of drying under heat lamps are shown in Figure 4.42. The results from these specimens are not as consistent as those shown in Figure 4.41 as the chloride ingress was likely caused by a combination of diffusion and absorption. Good fits between the data and curves based on

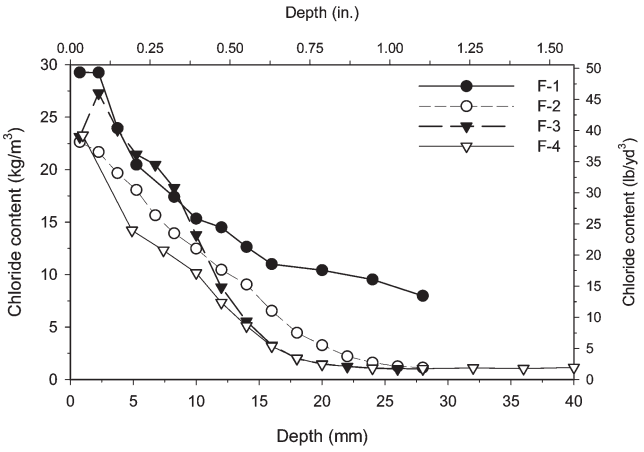

Figure 4.42 Chloride profiles of cores extracted from slabs subjected to weekly cycles of ponding and drying for 90 days. The ponding solution contained 6% NaCl.

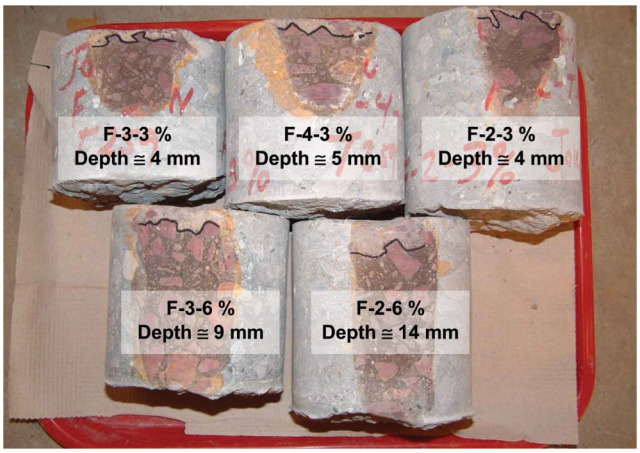

Figure 4.43 Cores from chloride ponding specimens after the chloride fronts were located using a silver-nitrate solution.

diffusion alone were not attained for the results shown in Figure 4.42. However, the relative performance of the mixtures was comparable to that observed for the slabs subjected to constant ponding of 3% NaCl solution with the exception of results from mixture F-3 which had elevated levels of chlorides in the top 12 mm (0.5 in.).

Parts of the surfaces of five of the eight cores were exposed to silver-nitrate solution in an attempt to identify the location of the chloride front. A photograph of the cores after being exposed to the silver-nitrate solution is shown in Figure 4.43. This method appears to result in underestimation of the depth of the chloride front. From comparing the depth measured on the cores with the chloride concentrations at those depths, it appears that a minimum chloride concentration of roughly 8 kg/m^3 (13.5 lb/yd^3) is required for the chlorides to be detectable using the silver-nitrate solution.

4.3.8 Corrosion

As previously discussed in Section 3.1.14, the ability of each of the deck field mixtures to protect reinforcement against corrosion was evaluated by embedding steel rebars in two types of specimens from each mixture. Six individual beams were prepared from each mixture and a series of five sets of bars were placed in the chloride ponding slab. Three of the beams were moist cured for three days while the rest was moist cured for 14 days. Ponding with 6% NaCl solution was started when the specimens were 42 days old. Each weekly cycle consisted of four days of ponding and three days of drying under halogen lamps.

The corrosion measurements included continuous monitoring of current flow and weekly determination of half-cell potentials. The current flow was monitored with a Campbell Scientific CR10X datalogger while half-cell potentials were determined manually with a cupper-sulfate half-cell and a high impedance digital multimeter. The half-cell measurements were done at the end of each ponding period.

After 30 weekly cycles, the results of the corrosion measurements were only partially conclusive. The results of the corrosion measurements for all of the specimens and both test methods are shown in Figures 4.44 through 4.56. Three figures containing corrosion current values for the beams, currents for the series of five sets of bars, and half-cell potentials are included for each mixture. In addition, Figure 4.56, with a narrow vertical scale, is included to show that variations in the current flow exist although not visible in some of the other figures.

Only seven out of the 24 beams have experienced corrosion with six of them being from F-1 (100C). The seventh beam specimen to undergo corrosion was from F-2 (93.5C-6.5SF). That specimen was moist cured for three days. Two additional beams, both from mixture F-2, appeared to undergo some corrosion during the last several weeks although the macrocell current levels remained within acceptable limits. Those specimens were also moist cured for three days.

In ASTM G109, the time to failure is defined as the time required for the average macrocell current to reach 10 μA and at least a half of the specimens having a current in excess of 10 μA. For the beam specimens

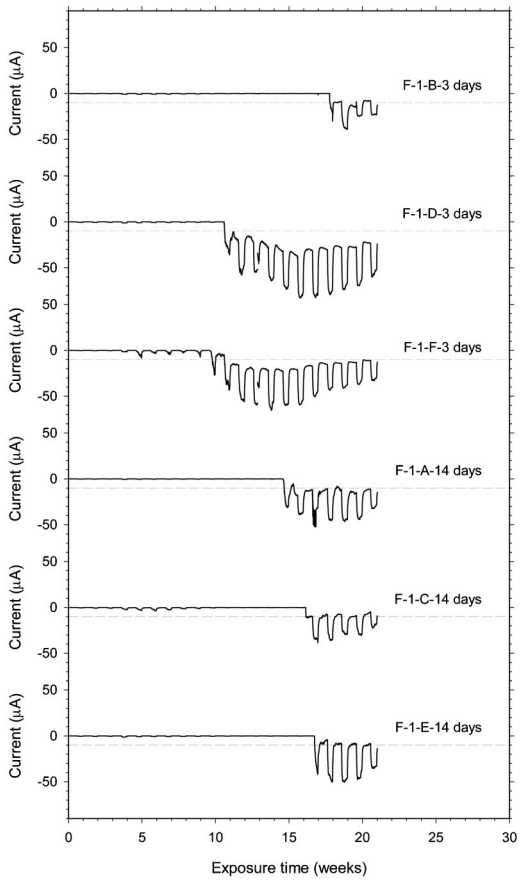

Figure 4.44 Macrocell corrosion currents for ASTM G-109 beams from mixture F-1 (100C). Ponding and measurements of these specimens were discontinued after 21 weeks.

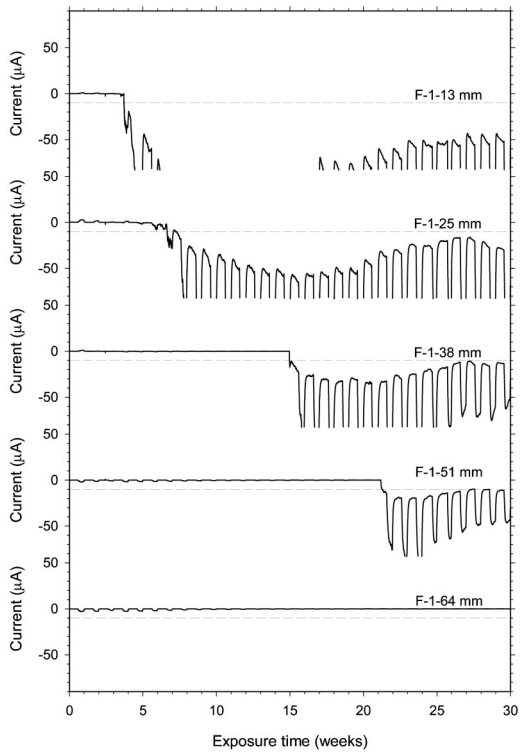

Figure 4.45 Macrocell corrosion currents for series of five sets of steel bars from mixture F-1 (100C).

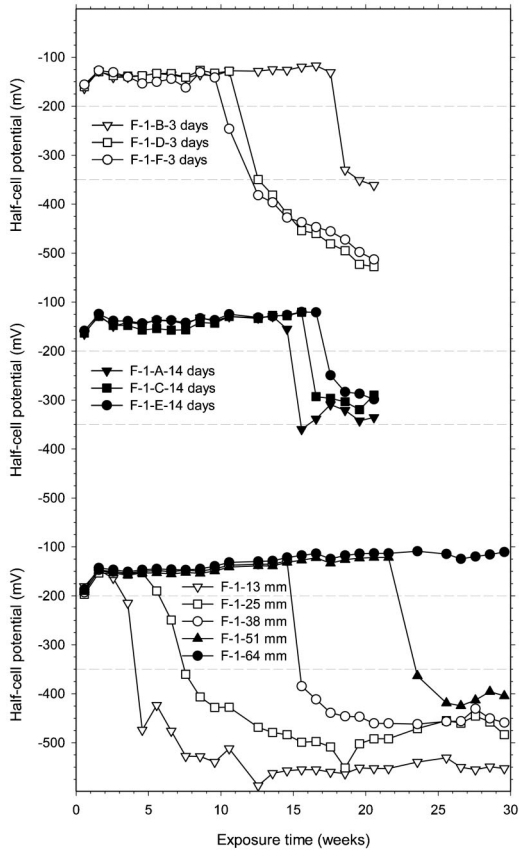

Figure 4.46 Half-cell potentials for all macrocells from mixture F-1 (100C).

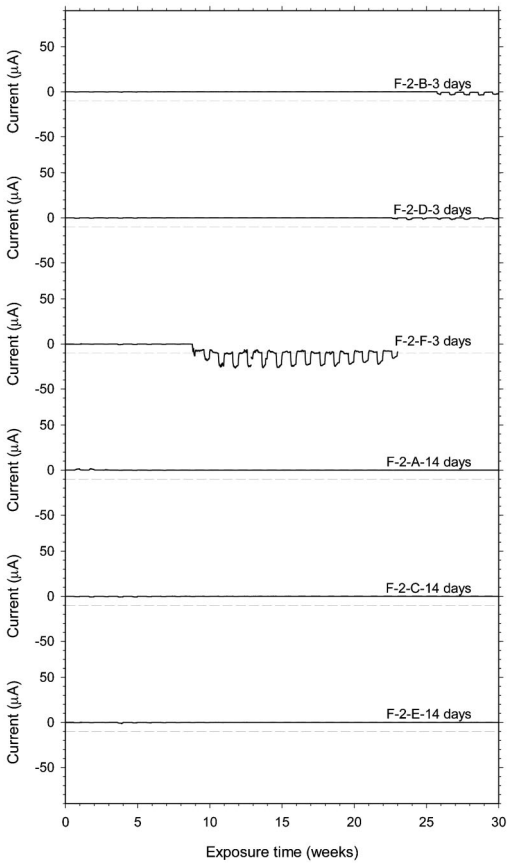

Figure 4.47 Macrocell corrosion currents for ASTM G-109 beams from mixture F-2 (93.5C-6.5SF).

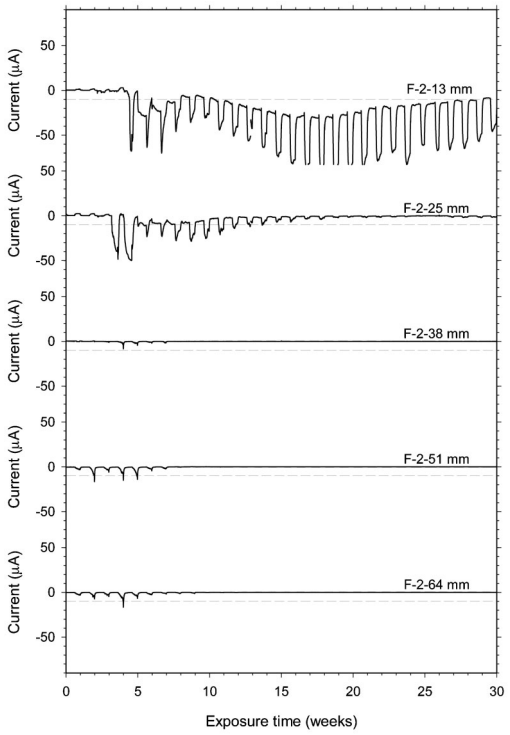

Figure 4.48 Macrocell corrosion currents for a series of five sets of steel bars embedded in large slab from mixture F-2 (93.5C-6.5SF).

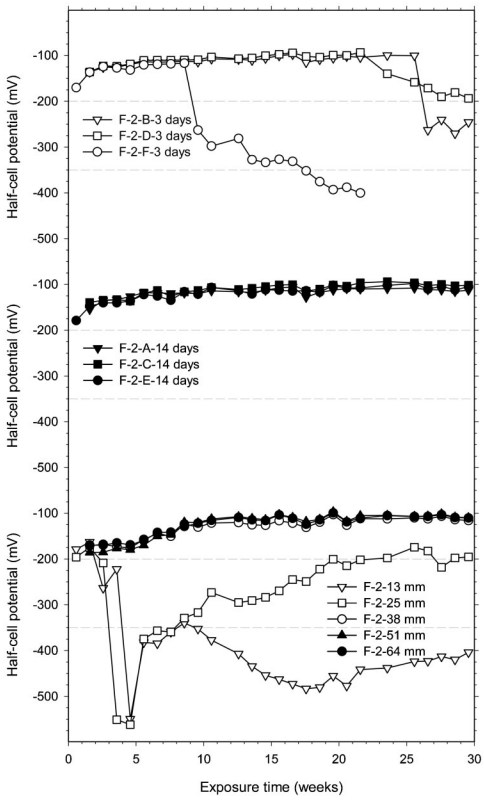

Figure 4.49 Half-cell potentials for all macrocells from mixture F-2 (93.5C-6.5SF).

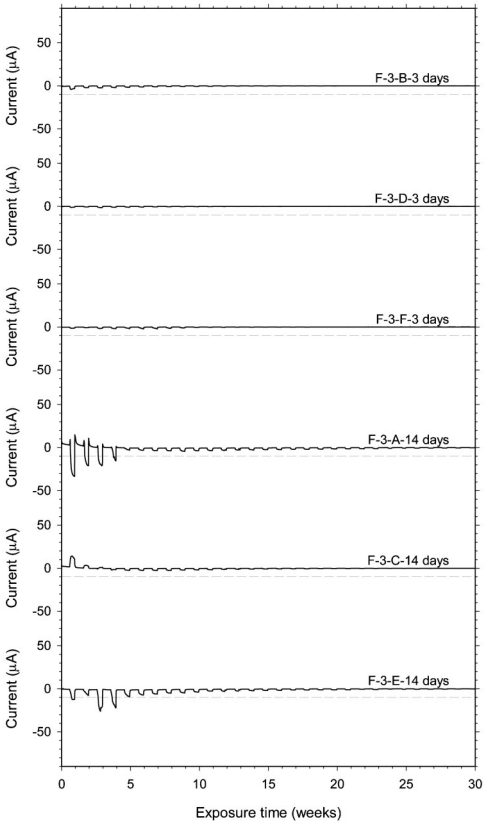

Figure 4.50 Macrocell corrosion currents for ASTM G-109 beams from mixture F-3 (65C-30S-5SF).

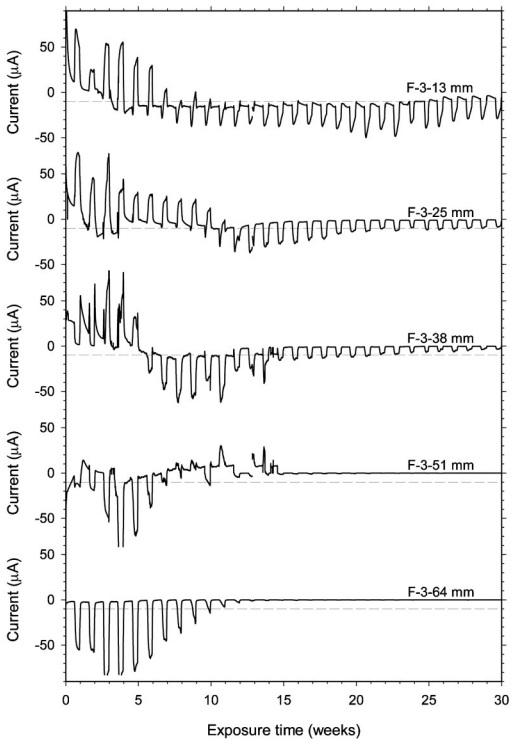

Figure 4.51 Macrocell corrosion currents for a series of five sets of steel bars embedded in large slab from mixture F-3 (65C-30S-5SF).

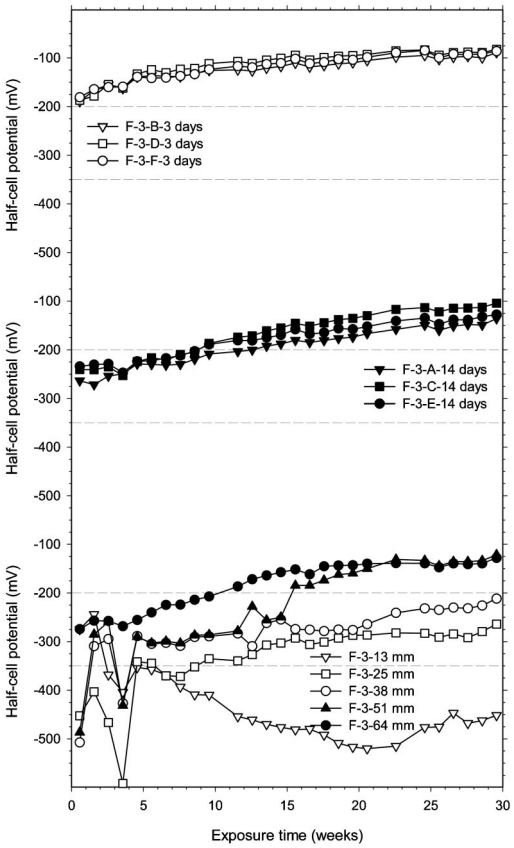

Figure 4.52 Half-cell potentials for all macrocells from mixture F-3 (65C-30S-5SF).

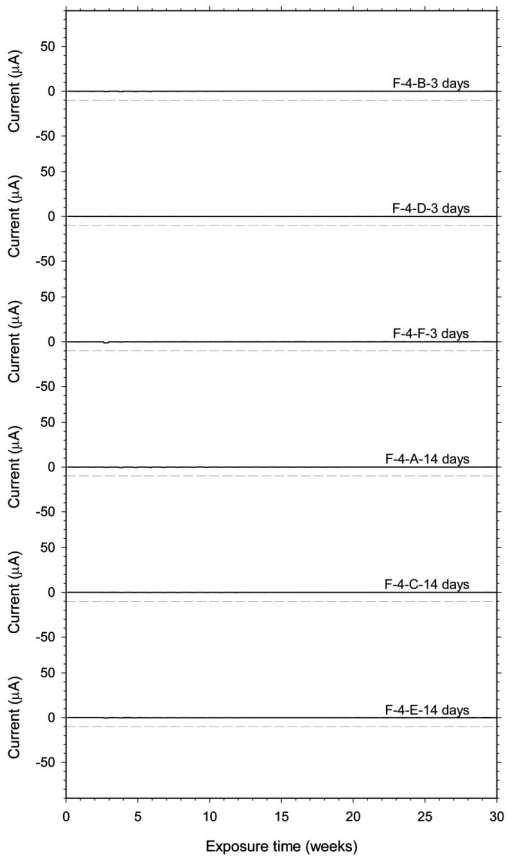

Figure 4.53 Macrocell corrosion currents for ASTM G-109 beams from mixture F-4 (92C-8SF).

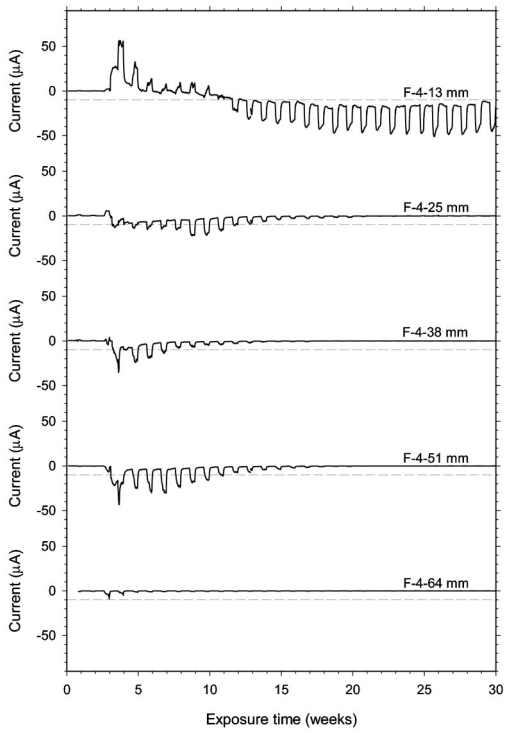

Figure 4.54 Macrocell corrosion currents for a series of five sets of steel bars embedded in large slab from mixture F-4 (92C-8SF).

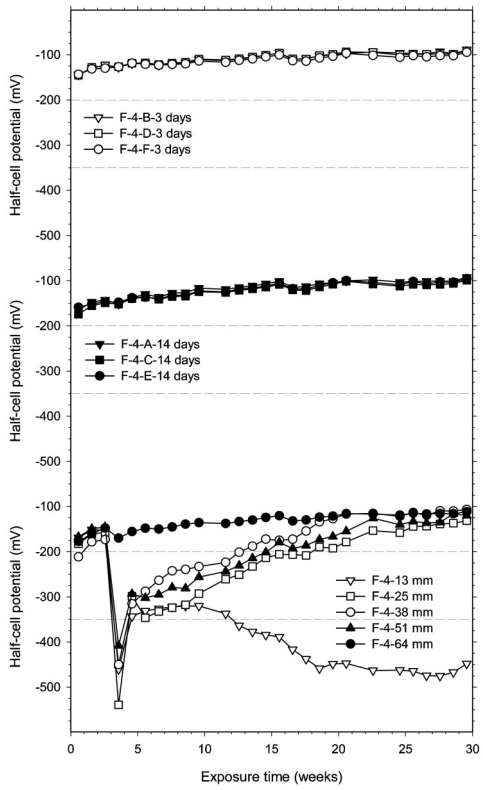

Figure 4.55 Half-cell potentials for all corrosion specimens from mixture F-4 (92C-8SF).

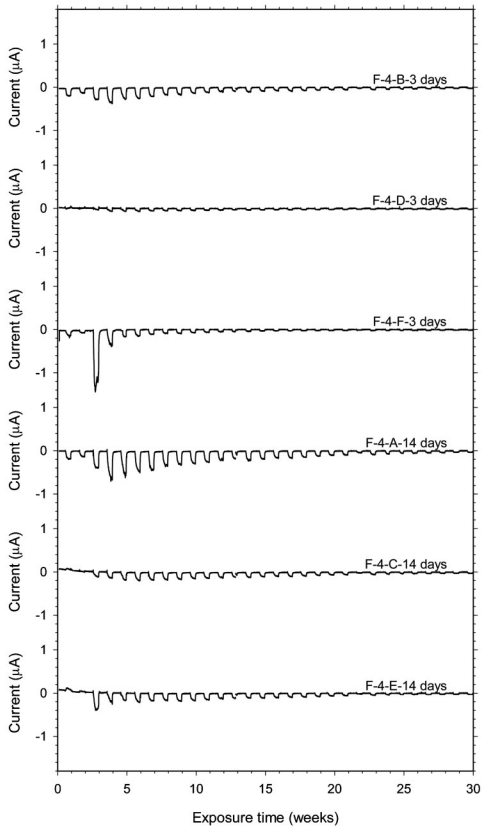

Figure 4.56 Macrocell corrosion currents (narrow vertical scale) for ASTM G-109 beams from mixture F-4 (92C-8SF).

from mixture F-1 that were moist cured for three days, the time to failure was 12 weeks. The series of beams from F-1 that received 14 days of moist curing was approaching failure after 19 weeks of exposure. By extending the moisture curing from 3 to 14 days, the time to failure was increased by at least 67%. Results from half-cell measurement for mixture F-1, shown in Figure 4.46, distinctively point to the time to corrosion with sharp drops in the half-cell potentials.

The analysis of the series of five sets of steel bars in the large slabs were complicated by unanticipated cracking, as shown in Figure 4.57, of the slabs during the initial drying periods. These cracks propagated directly over the Plexiglas supports used for the steel bars. These supports, shown in Figure 3.15, had a thickness of 3.125 mm (0.125 in.). Although the supports were well outside the area of exposed steel, macrocell corrosion current was detected for several of the steel bars sets during the first few weeks.

With internal temperature of the concrete surpassing 60°C (140°F), the expansion of the Plexiglas was apparently large enough to cause the concrete to crack. After some calculations, using approximate values and assuming equal areas of Plexiglas and concrete, the stresses in the concrete would have reached 5.3 MPa (770 psi) if the tensile strength had not been exceeded. Performing those calculations prior to installing the Plexiglas would have disqualified the Plexiglas as a support material.

Once premature corrosion of the series of five sets of steel bars in the large slabs was identified, along with the cause, partitions were installed on the ponding slabs containing the steel bars. These partitions were installed to prevent the salt solution from entering the cracks above the Plexiglas supports. The partitions on one of the ponding slabs can be seen in Figure 4.58.

After the partitions were installed on the ponding slabs, the corrosion activity on bars affected by salt solution entering through the cracks decreased. However, this initial corrosion makes it difficult to clearly identify when corrosion, due to chloride ion diffusion, of the top bars started. Based primarily on half-cell potentials, it appears that the only bars undergoing corrosion are those with a cover of only 13 mm (0.5 in.) if mixture F-1 is excluded where the top four bars were undergoing corrosion after 30 weeks.

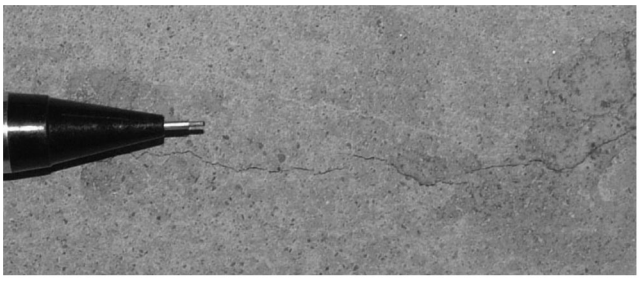

Figure 4.57 Small crack caused by expansion of Plexiglas during heating of ponding slabs. The diameter of the led in the mechanical pencil was 0.5mm (0.02in.).

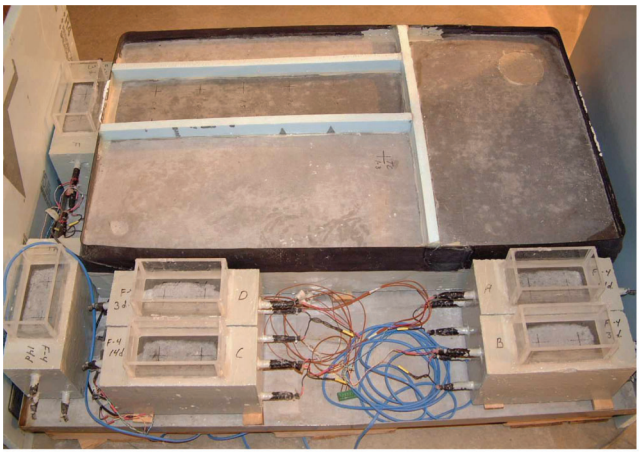

Figure 4.58 Corrosion specimens from mixture F-4. Partitions on ponding slab were used to prevent salt solution from entering cracks above small sheets of Plexiglas used to support ladder macrocells.

Based on ASTM C876, the likelihood of corrosion activity at the time of half-cell measurements is less than 10% if the half-cell potential is higher than –200 mV. If the half-cell potential is lower than –350 mV, the likelihood of corrosion activity is more than 90%. If the readings are between –200 and –350 mV, the corrosion activity is uncertain. Horizontal lines representing the aforementioned guidelines are included on the half-cell plots for reference.

4.3.9 Drying Shrinkage

Length change measurements were done on three specimens from each of the field trial mixtures. The specimens were cured in saturated limewater for the first 28 days before being moved to a 50% relative humidity (RH) room. The reference readings were taken at the end of the curing period. The results of the shrinkage tests are shown in Figure 4.59. Unfortunately, the equipment controlling the humidity and

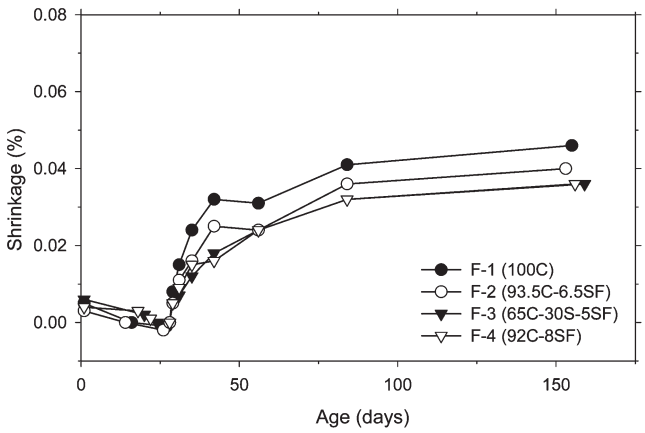

Figure 4.59 Drying shrinkage of specimens from deck field trial mixtures. The reference reading was taken after 28 days of curing in limewater.

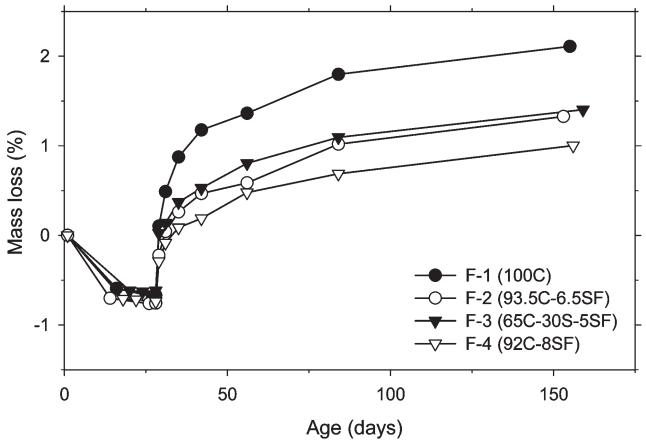

Figure 4.60 Mass loss of specimens from deck field trial mixtures. The reference reading was taken after 28 days of curing in limewater.

temperature in the room experienced some down-time on different occasions during the experiment. This caused both the temperature and humidity to exceed the values listed in ASTM C175. These deviations caused irregularities in the result and slowed the expected rate of shrinkage.

Due to equipment malfunction problems during the shrinkage test, the results should be viewed with caution. Based on the results shown in Figure 4.59, there was not a significant difference between the shrinkage values from different mixture. However, the specimens from mixture F-1 consistently had the highest shrinkage. The initial rate of shrinkage for these specimens is also higher than for the other specimens.

The mass of each specimen was determined along with the length change measurements. The mass loss, shown in Figure 4.60, was then calculated with respect to the mass after 28 days of curing in limewater. The mass loss for mixtures containing supplementary cementitious materials appears comparable, but the mass loss for the plain cement mixture (F-1) is higher. Based on compressive strength and electrical results, it can be estimated that mixture F-1 had a higher water-cement ratio than the other three mixtures. This in turn helps explain the higher mass loss as more water would have been available for evaporation.

4.4 Temperature Matched Curing

Temperature matched curing (TMC) of concrete is a process during which the temperature of small test specimens is controlled (by using a heat source or a cooling unit) to match the temperature of a hydrating larger member and is usually analogous to heat curing as temperature of the large member typically exceeds the temperature of the small test specimens. The matching of the temperatures is accomplished by using the actual temperature of the larger member as an input (reference temperature) for the control unit of the external heat source or cooling unit. This process is important when there is considerable difference in the temperature development of the reference concrete and corresponding test specimens. For example, when compressive strengths during the first three days after casting of the concrete are important, temperature matched curing of test cylinders will typically result in strength values that exceed those of cylinders subjected to standard curing temperatures at 16 to 27°C (60 to 80°F).

In the following section, the temperature developments of insulated concrete from the field trials mixtures are reported. Compressive strength results from TMC specimens are shown in Figures 4.65 through 4.68 in Section 4.5.1. Except during the time the TMC specimens were in the TMC enclosure, every attempt was made to ensure that preparation, curing, and testing of both sets of specimens was identical. The specimens were temperature matched cured for the first 24 hours after casting. Equal number of TMC and control specimens was prepared from every mixture to isolate the effects of TMC.

4.4.1 Temperature Development

In addition to the temperature histories, shown in Figure 4.61, obtained for the four field trial mixtures prepared for this study, the derivatives of the temperature curves are presented in Figure 4.62. The derivatives represent the rate of heat emission. The derivative curves were prepared by taking the average temperature change over a five-minute interval preceding the reported rate change value. In addition to providing the maximum rate of temperature rise, the derivatives highlight the time when the hydration is most active. The temperature histories and respective derivatives are reported for the first 24 hours.

The ambient temperature during the week mixtures F-3 and F-4 was lower than when mixtures F-1 and F-2 were prepared. This resulted in lower temperatures of the fresh concrete for mixtures F-3 and F-4. Lower concrete temperature appears to reduce the maximum temperature as well as the onset of maximum heat rise.

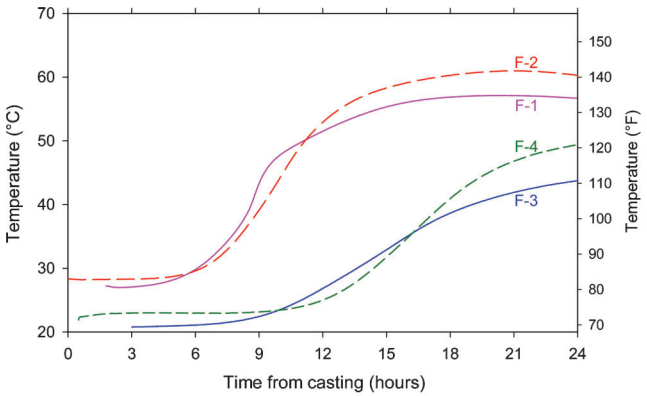

Figure 4.61 Temperature development of the four field trial mixtures during the first 24 hours after casting.

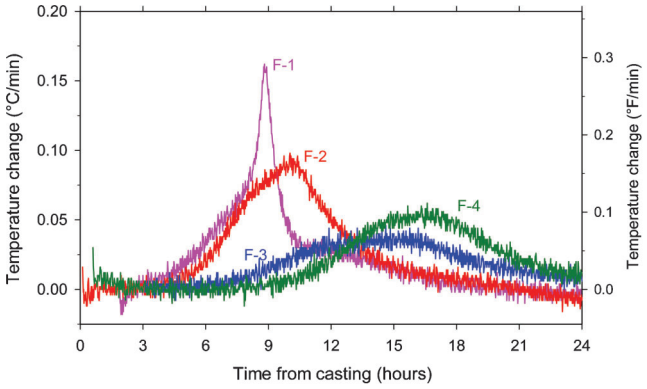

Figure 4.62 Rate of temperature chance of the four field trial mixtures.

4.5 Effects of Moisture Conditions During Curing of Test Specimens

As mentioned in Section 2.3.2, Aïtcin [(*6*), p. 397] suggested that sealing the specimens in plastic, therefore eliminating the need for moist curing, would perhaps best simulate the moisture conditions of structural concrete. During the preparation of the deck field trial specimens, additional cylinders were prepared to evaluate this suggestion. Also, some of the additional cylinders were moist cured for three days and then stored at 50% relative humidity (RH) until being submerged in limewater 24 hours before the scheduled test. The cylinders that were sealed were demolded and placed in limewater 24 hours before being tested. To ensure that no moisture would be lost during storage of the sealed cylinders, electrical tape was wrapped around the lid. Several cylinders with sealed lids are shown in Figure 4.63.

Cylinder stored both sealed in their molds and at 50% RH were either tested in compression or for electrical indication of chloride ion penetration resistance. The results of the electrical indication of chloride ion penetration resistance tests were presented in Section 4.3.6, but the results of the compressive strength tests are presented in the following section.

Figure 4.63 Sealed cylinders stored in the laboratory.

4.5.1 Compressive Strength Development

In Figure 4.64, compressive strengths of cylinders cured at 50% RH from the age of three days and cylinders sealed in their forms are compared with compressive strengths of control cylinders. At the age of 28 days, the agreement between the results of the sealed cylinders and control cylinders was good. The relative strength of the sealed cylinders ranged from 96.1 (F-3) to 101.2% (F-2). However, results from cylinders cured at 50% RH did not compare as well. Corresponding values for those cylinders ranged from 71.2 (F-3) to 83.5% (F-1). Based on these results, it appears acceptable to cure cylinders sealed in their forms for determination of 28-day strengths, but providing only three days of moist curing, followed with curing at 50% RH, results in significant reduction in compressive strengths. Therefore, it is important to adequately moist cure structural concrete in order to achieve desired compressive strengths. This is perhaps particularly important for flexural members as well as thin members where the surface layers are particularly important for structural integrity of the member.

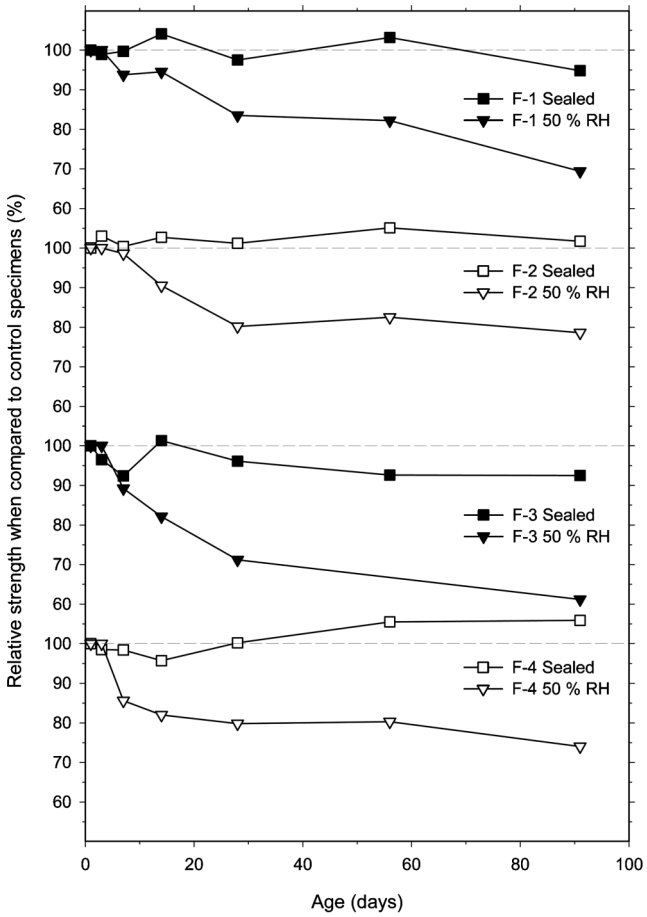

Figure 4.64 Relative compressive strength of different specimens from deck field trial mixtures when compared to control specimens. The specimens were either sealed in their forms or kept at 50% RH until placed in limewater 24 hours before being tested.

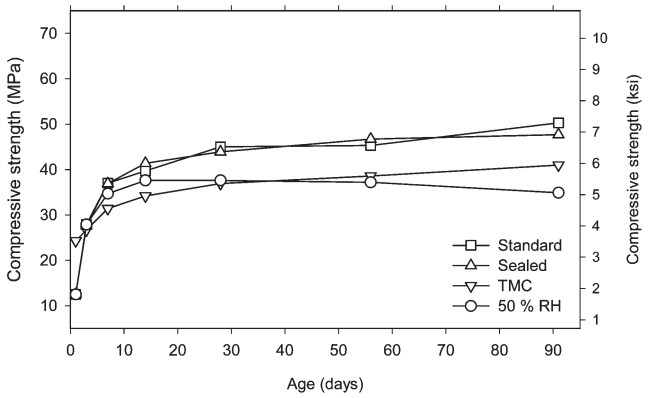

Figure 4.65 Compressive strength development of specimens from F-1 (100C).

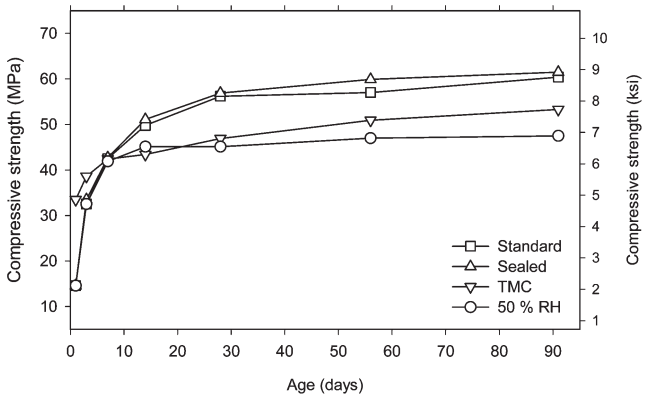

Figure 4.66 Compressive strength development of specimens from F-2 (93.5C-6.5SF).

In addition to the relative strength provided in Figure 4.64, the strength development of all four specimens series from all of the deck field trials are provided in Figures 4.65 through 4.68. As can be seen from these figures, strength increase beyond 14 days for specimens cured at 50% RH is very limited. This corresponds well with the results of the electrical

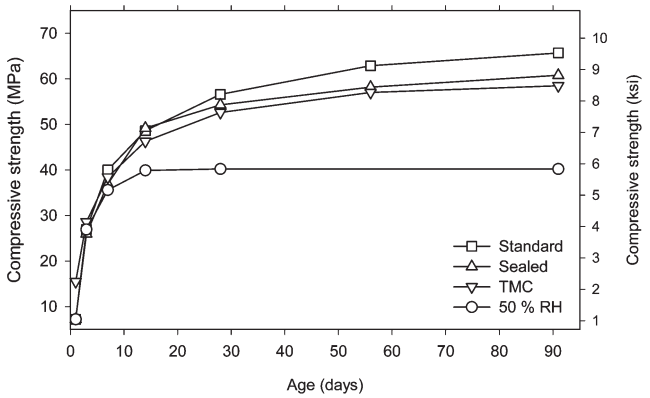

Figure 4.67 Compressive strength development of specimens from F-3 (65C-30S-5SF).

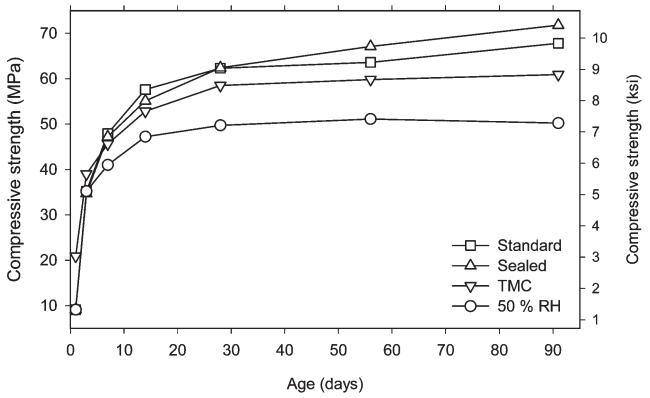

Figure 4.68 Compressive strength development of specimens from F-4 (92C-8SF).

indication of chloride ion penetration resistance tests discussed in Section 4.3.6 where the specimens cured at 50% RH performed poorly. Those results also signify the importance of adequate moist curing to ensure proper hydration and development of optimum strength and durability characteristics of the concrete.

5. STRUCTURAL TESTING

5.1 Pullout Tests

A Moustafa pullout specimen was fabricated and tested as part of this experimental program. The pullout specimen was used to determine the bond quality of the Insteel strand at the beginning of the study (i.e., if the strand met the minimum pullout load of 192 kN (43.2 kip) based on the study by Logan (*71*). The specimen contained a total of eighteen 15.2 mm (0.6 in.) diameter strand specimens.

The pullout specimen was fabricated on 10/28/97 and tested on 10/31/97 (at 3 days) and on 6/18/98 and 6/19/98 (after nearly 8 months had passed). The reason for the long delay is that the load cell that was used to measure the pullout force broke at the end of the first test on 10/31/97. This meant that the rest of the pullout testing could not proceed for several weeks (until a new load cell was acquired) and by then the concrete had essentially reached its full strength.

The strand specimens were pulled out of the block using a hydraulic ram, shown in Figure 5.1, furnished by CSR Hydro Conduit (now Rinker Materials). The load was recorded using a load cell that was placed between two steel plates. The bottom plate had two steel angles welded to the bottom side to allow the same contact area with the concrete block that was specified by Logan (refer to Figure E3 of Appendix E). The maximum load occurring during a given pullout test was stored automatically by the data acquisition system. Also, the load at "first slip" was obtained by placing a small piece of tape near the point where the strand entered the concrete. As soon as a motion was detected, the person monitoring the slip simply pressed a "mouse" button and the computer also recorded this value.

Figure 5.1 Testing of a pullout specimen in the laboratory.

TABLE 5.1
Results of a single pullout test done at 10/31/97. The compressive strength of the concrete was 60 MPa (8.7 ksi)

	Pullout load		Load at first slip	
Specimen	**(kN)**	**(kip)**	**(kN)**	**(kip)**
IST-1	205.3	46.15	—	—

TABLE 5.2
Results of a single pullout test done at 6/19/98. The compressive strength of the concrete was in excess of 80 MPa (11.6 ksi)

	Pullout load		Load at first slip	
Specimen	**(kN)**	**(lb)**	**(kN)**	**(kip)**
IST-2	258.9	58.20	147.0	33.05
IST-3	261.8	58.85	150.6	33.85
IST-4	248.0	55.75	99.0	22.25
IST-5	250.7	56.35	109.0	24.50
IST-6	254.0	57.10	136.1	30.60
IST-7	234.4	52.70	118.5	26.65
IST-8	243.8	54.80	117.9	26.50
IST-9	252.0	56.65	78.7	17.70
IST-10	232.9	52.35	173.0	38.90
IST-11	253.5	57.00	180.8	40.65
IST-12	240.9	54.15	97.9	22.00
IST-13	240.9	54.15	79.2	17.80
IST-14	238.6	53.65	84.5	19.00
IST-15	236.9	53.25	149.5	33.60
IST-16	248.2	55.80	152.6	34.30
IST-17	257.8	57.95	73.2	16.45
IST-18	250.9	56.40	137.4	30.90
Average	**247.3**	**55.59**	**122.6**	**27.57**
Std. dev.	**9**	**1.92**	**30**	**7.40**

The pullout load for one strand specimen is shown in Table 5.1 and the pullout loads and "first slip" values for the remaining 17 strand specimens in Table 5.2. All strands exceeded the minimum recommended pullout capacity of 192 kN (43.2 kip), although only one test was conducted while the concrete was still at an early age. The value of the pullout test conducted on 10/31/97 was 205.3 kN (46.15 kip). The average value of the remainder of the pullout tests, conducted on 6/19/98, was 247.3 kN (55.59 kip). Although not all of the pullout tests were conducted at the specified concrete age, the recorded values seem to indicate the bond quality of the strand used in this study was quite good.

5.2 Measurements of Transfer Length

Values of surface strains were measured on the single-strand development length specimens as well as on the specimen shown in Figure 3.31. The transfer length can then be inferred directly from the recorded values of strain. For a concentrically prestressed member supported along the entire length, such as the transfer length specimen, the member will be under simple axial loading when the prestress force is transferred to the concrete. Thus, the compressive stresses (and hence strains) in the member will vary from zero at the free end to a constant value corresponding to the "P/A" stress. The length it takes for the strand to bond to the concrete and "transfer" the full tension in the cable to the concrete is called the transfer length.

For typical prestressed members, in which the center of gravity of the strand does not pass through the centroid of the cross-section, compressive strains never actually reach a constant value due to the varying moment due to self-weight. However, the change in strain due to the dead-load moment is often small in comparison to the compressive strains induced by prestressing, and the transfer length in these members may still be inferred from measurements of surface strain.

The results of surface strain measurements taken for two of the 69 MPa (10 ksi) single-strand development length specimens are shown in Figure 5.2 and in Figure 5.3 Measurements were taken prior to and immediately after transfer of prestress occurred. The solid vertical lines are drawn at the approximate breaks between the "sloping" portion of the curves where strains are increasing and the "flat" portion corresponding to the region under near-constant stress of P/A. The distance from the end of the transfer specimen to the dashed line is the transfer length.

Observation of these figures reveals that the transfer length for each beam was clearly less than 600 mm (24 in.). A transfer length of 600 mm (24 in.) would correspond to 40 strand diameters for a 15.2 mm (0.6 in.) strand, less than the assumed 50 strand diameters used in the ACI Code for checking shear provisions (ACI Section 11.4.4) [(*61*), p.142]. Thus, the combination of 15.2 mm (0.6 in.) Insteel strand and 69 MPa (10

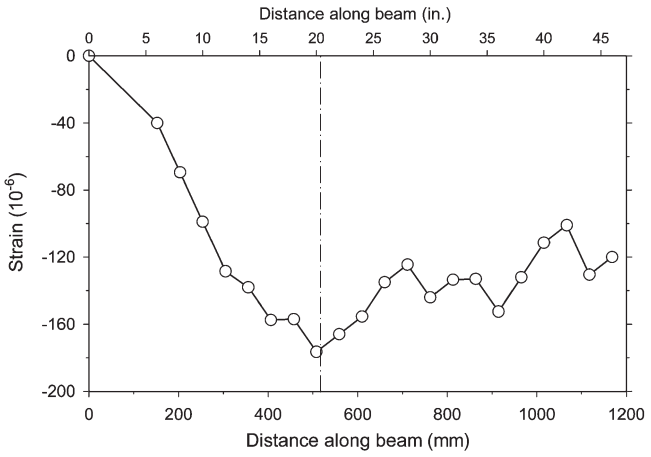

Figure 5.2 Surface strains of single-strand Beam 1 with 15.2 mm (0.6 in.) Insteel strand.

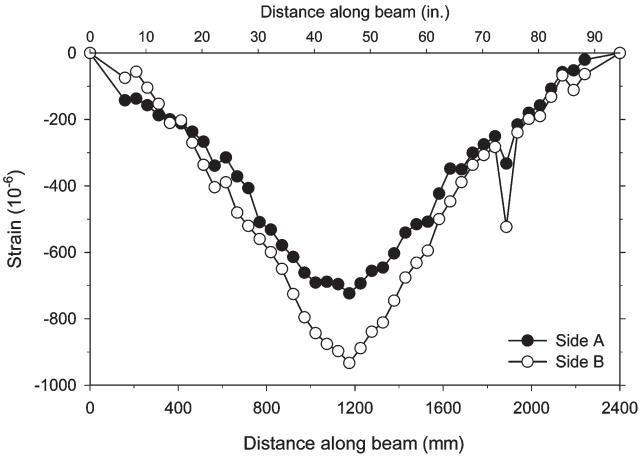

Figure 5.4 Surface strains of transfer length specimen with longitudinal cracking.

ksi) normal weight concrete would meet code requirements for transfer length.

The measured surface strains for the small transfer length specimen (the one shown in Figure 3.31) are shown in Figure 5.4 The transfer length indicated by this specimen is quite long. In fact, the strains never reach a constant value in this specimen, indicating that the strand tension may not have been fully transferred to the concrete at any location along the specimen. The two curves represent values of surface strain on opposite sides of the specimen. The reason for the excessive transfer length in this specimen is that several longitudinal cracks occurred along the length of this specimen upon cutting the prestressed cables and transferring the prestress force. The longitudinal cracks allowed additional slip to occur between the strand and concrete and the transfer length increased.

Longitudinal cracking can sometimes be a problem for prestressed members that have a small cross section, especially when transfer of prestress is done suddenly (by sawing or flame cutting). The purpose for using the small transfer length specimen was to produce higher compressive strains than in the single-strand rectangular beams, so that the measured results would be more reliable. Similar-sized transfer length specimens were successfully used in a concurrent study with 13.3 mm (0.5 in. special) diameter strands. The 15.2 mm (0.6 in.) strands used in this study are apparently too large for the specimen size when transfer of prestress is done suddenly (by flame cutting the strands). The results from this specimen illustrate one of the problems associated with longitudinal cracking at member ends–namely that the length required to transfer the prestress force to the concrete can become excessive, thereby reducing both the amount of shear and moment that the member can carry.

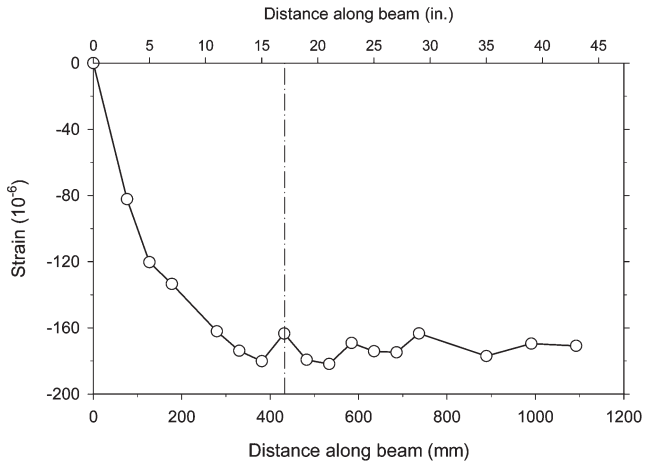

Figure 5.3 Surface strains of single-strand Beam 2 with 15.2 mm (0.6 in.) Insteel strand.

5.3 Development Length Tests on Single-Strand Beams

A total of six single-strand development length tests were conducted in this study (three beams tested at both ends). As discussed in Section 3.2.6, the single-strand beam specimens provided a cost-effective means of conducting many load tests. Appendix E, Section E.1, contains the load-deflection plots recorded for each of the six load tests to failure. Photographs of the specimens during testing, and documentation of the crack patterns occurring in the beams, are contained in Appendix F, Section F.1. The failure loads and deflections corresponding to the maximum sustained load are listed in Table 5.3. Also listed in Table 5.3 is the maximum moment in the beams, which occurred essentially at a distance L_d from the end of the beam. The maximum moment was determined (by Statics) from the measured values of applied load. In every case, the maximum moment withstood by the specimen exceeded the AASHTO nominal moment capacity, M_n, of 61.1 kN·m (45.1 kip·ft) (f_{ps}=1795 MPa (260 ksi)),

TABLE 5.3
Results from flexural tests on single-strand development length specimens

Beam	Maximum load		Maximum moment		Deflection at maximum load		Failure mode
	(kN)	(kip)	(kN-m)	(kip-ft)	(mm)	(in.)	
1S	56.18	12.63	71.0	52.4	57.7	2.3	Shear, then strand rupture
1L	55.07	12.38	71.3	52.6	74.1	2.9	Compression, then strand rupture
2S	57.03	12.82	72.1	53.2	59.9	2.4	Flexure—strand rupture
2L	55.07	12.38	71.3	52.6	57.5	2.3	Flexure—strand rupture
3S	54.31	12.21	68.7	50.7	70.1	2.8	Flexure—strand rupture
3L	54.85	12.33	71.0	52.4	74.3	2.9	Flexure—strand rupture

indicating the beams' strands were adequately developed at a distance from the end of the beam equal to the code-prescribed development length L_d (Using strain compatibility, the nominal moment capacity, M_n, was 64.4 kN·m (47.5 kip·ft) (f_{ps}=1880 MPa (273 ksi)) for f'_c of 83 MPa (12 ksi) and the strand stress-strain relationship represented by Tadros curve). This is consistent with the results from measurements of strand end-slip during testing, which revealed that slip did not occur in any of the specimens prior to failure.

Vibrating wire gage readings from Beam 3 indicated that about an 86 MPa (12.5 ksi) loss of prestress had occurred prior to the beams being tested. Testing of the single-strand beams occurred approximately three months (95 days) after casting. The vibrating wire gage data recorded for single-strand Beam3 is listed in Tables D.1 and D.2 in Appendix D. The 86 MPa (12.5 ksi) loss represents about 6.2% of the original prestress force and seems reasonable based on the AASHTO lumped-sum estimate of total losses (AASHTO Section 5.9.5). Using the AASHTO lumped-sum method, the calculated total loss of prestress would be 165 MPa (24 ksi) for a rectangular beam containing low-relaxation prestressed strands. A loss of prestress of 165 MPa (24 ksi) represents about 11.9% of the original strand stress.

The measured loss of 6.2% means that approximately 52% of the total AASHTO lumped-sum loss occurred during the first three months. Corley and Sozen (*79*) proposed a very simple expression for the time-dependent relationships of both creep and shrinkage. Based on their work, the total proportion "R" of the total time-dependent effect occurring at time t (in days) is obtained from the expression:

$$R = 0.13 \ln(t+1) \qquad (5.1)$$

With t = 95 days, R is calculated as 0.59 from the above expression. Therefore roughly 60% of the losses would be expected to occur during the first three months. The small difference may be explained, in part, by the fact that the AASHTO lumped-sum method typically overestimates the prestress losses in a beam. The designer is given the option by AASHTO to perform a more detailed analysis that would typically result in a lower estimate of total losses.

All of the single-strand development length specimens failed after considerable deflections had occurred. Each of the beams deflected more than 57 mm (2.3 in.) in a 4955 mm (16′–3″) span prior to reaching its ultimate capacity. Five of the six beams tested resulted in flexural failures with rupturing of the prestressing strand. The other beam, 1S, failed in shear.

While the shear failure occurred when the shear stress on the section (V/bd) was less than 0.69 MPa (100 psi), or $1.0 \times \sqrt{f'_c}$ (f'_c in units of psi), it occurred well after yielding of the prestressing steel had occurred and considerable ductility exhibited. The investigators speculate that when the prestressing steel yielded, the effects of dowel action diminished and the lightly-reinforced beams (without stirrups) became susceptible to shear. The initial shear failure in the specimen eventually led to strand rupture, as the large flexure-shear crack produced additional deflection (and rotation). Thus all six tests resulted in rupture of the strand, demonstrating that the AASHTO and ACI development lengths were adequate to develop the 15.2 mm (0.6 in.) strands when used in combination with 69 MPa (10 ksi) concrete.

In summary, test results from the six single-strand development length specimens indicated that the code required development lengths were ample do develop the capacity of a single 15.2 mm (0.6 in.) prestressed strand in a member cast with 69 MPa (10 ksi) normal weight concrete. Therefore, the multiple-strand development length tests were also designed based on the current ACI and AASHTO development lengths. The results of the multiple-strand development length specimens are discussed in Section 5.4.

5.4 Development Length Tests on Multiple-Strand Specimens

Two multiple-strand T-beams were tested in this study to determine the adequacy of applying the current AASHTO and ACI development length equations to members with 69 MPa (10 ksi) normal weight concrete and 15.2 mm (0.6 in.) strands. Results from six development length tests on single-strand beams indicated that the current code required development lengths were conservative for members with a single prestressed strand. Therefore, the sufficiency of these same requirements when applied to members with multiple-strands was also tested.

One of the specimens (HPC-1) contained 15.2 mm (0.6 in.) Insteel strands, while the other T-Beam (HPC-2) contained similar-sized strands produced by Florida

Wire & Cable. The test data, including the failure loads, deflections corresponding to the maximum sustained load, and maximum moments for the specimens are listed in Table 5.4 The load-deflection plots recorded for both load tests are found in Appendix E, Section E.2. Photographs of the specimens during testing, and the corresponding documentation the crack patterns, are contained in Appendix F, Section F.2. The maximum moment resisted by both multiple-strand development specimens exceeded both the AASHTO nominal moment capacity (662 kN·m (489 kip·ft)) (f_{ps}=1830 MPa (265 ksi)) and the moment capacity calculated based on strain compatibility (680 kN·m (502 kip·ft)) (f_{ps}=1930 MPa (280 ksi)), in which the contribution of the two 9.5 mm (#3) instrumented bars stressed to 700 MPa (102 ksi) was accounted for. The stress of 102 ksi was based on actual stress-strain tests of representative bar specimens. The stress-strain relationship for the instrumented bars was previously shown in Figure 3.25. Both multiple-strand specimens failed in flexure by rupturing of all five 15.2 mm (0.6 in.) strands as well as the two 9.5 mm (#3) bars. Both failures were quite ductile, with over 50 mm (2 in.) of deflection prior to reaching the maximum load. Therefore, the full capacities of the strands were realized at a distance from the end of the beams that was equal to the current development length as calculated by the AASHTO and ACI Codes.

Vibrating wire gage readings for HPC-1 indicated that about a 110 MPa (15.9 ksi) loss of prestress had occurred prior to the beams being tested. Similar readings for HPC-2 showed that about a 105 MPa (15.3 ksi) loss of prestress had occurred before the beam was tested. Therefore, losses were essentially equal for both beams. Testing of the beams occurred at 14 and 15 days after casting. The vibrating wire gage data recorded for the beams is listed in Tables D.3 and D.4 for HPC-1 and Tables D.5 and D.6 for HPC-2.

The 110 MPa (15.9 ksi) loss represents about 7.9% of the original prestress force and seems rather high compared for losses after only two weeks. Using the AASHTO lumped-sum method, the calculated total loss of prestress would be 190 MPa (27.7 ksi) for a rectangular beam containing low-relaxation prestressed strands. A loss of prestress of 190 MPa represents about 13.7% of the original strand stress.

Based on the simplified expression from Corley and Sozen (*79*) discussed earlier (Section 5.3), about one third of the total time-dependent losses would be expected to occur during the first two weeks. Based on this principle, the projected total losses would be over 20 percent of the initial prestress force. However, the HPC used in this study may perform differently from the concrete which the simplified expression was developed. In fact, the loss of prestress that occurred during the second week (between 8 and 15 days) after the beam was cast was indeed small (about 0.4% of the total initial stress). Still, the loss of prestress of over 5% of the initial stress due to strand de-tensioning, as indicated by vibrating wire gage data in both multiple-strand beams, is over 2.5 times the amount of losses indicated by similar gage readings in the single-strand beam. Unfortunately, since the beams were tested at the age of two weeks, no data are available about the total loss of prestress that would have occurred in these two beams. All of the vibrating wire gage data have been corrected for thermal effects.

Results from surface-mounted strain gages are shown in Figures 5.5 and 5.6 for HPC-1, and in Figures 5.7 and 5.8 for HPC-2. These figures each show a comparison with surface strains measured with electrical resistance strain gages and a vibrating wire gage mounted directly on top (Figure 2.1). Based on these figures, an excellent correlation existed between the surface-mounted vibrating wire gages and the surface-mounted electrical resistance gages installed at the same location, up to the load at which the strains exceeded the operating range of the vibrating wire gages.

The use of externally mounted vibrating wire gages is beneficial from the standpoint of expense since the gages are re-useable in this condition, as compared to the internally embedded vibrating wire gages. A note of caution, however, is that when externally mounted vibrating wire gages are used in field applications, thermocouples should also be placed in the concrete near the gage location. This is necessary so that proper corrections for thermal effects can be made. The temperature reading for the gage will likely be different than the temperature of the concrete on which the measurement is being made and these effects should be carefully thought through before using externally mounted gages in outdoor applications.

The electrical resistance top surface gages placed at the center-line of the beam indicated that compressive strains reached approximately $3500 \cdot 10^{-6}$ (0.0035) in both T-beams during the failure loading (see Figures 5.6 and 5.7). Flexural calculations in both the AASHTO and ACI codes consider crushing of the concrete to occur at a strain of 0.003. Thus, the higher

TABLE 5.4
Results from flexural tests on multiple strand development length beams

Beam	Maximum load		Maximum moment		Deflection at maximum load		Failure mode
	(kN)	(kip)	(kN-m)	(kip-ft)	(mm)	(in.)	
HPC-1	658	148	723	533	64.7	2.5	Flexure—strand rupture
HPC-2	650	146	713	526	52.0	2.0	Flexure—strand rupture

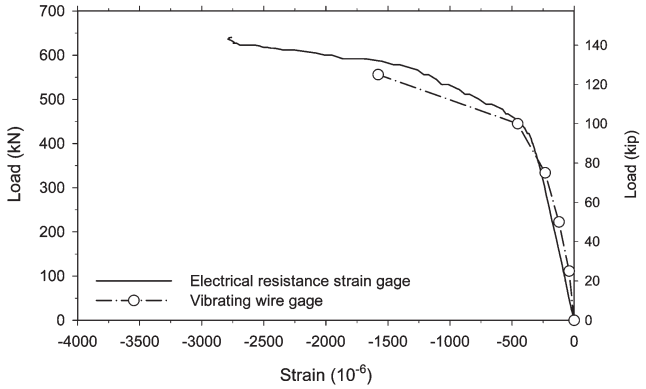

Figure 5.5 Top concrete surface strains measured in HPC-1 (north side of flange).

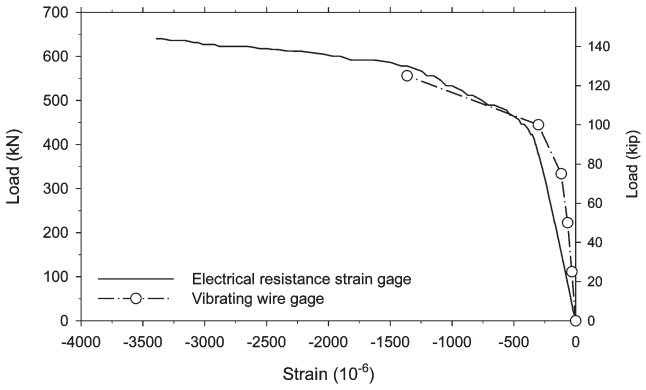

Figure 5.6 Top concrete surface strains measured in HPC-1 (south side of flange).

compressive strains realized in both T-beams help explain why the experimentally determined moments exceeded the calculated moment capacities.

The recorded mid-span strains at the depth of the prestressing steel (480 mm (19 in.) below the top of the beam) are shown in Figures 5.9 and 5.10. These figures are for HPC-1 and HPC-2, respectively. Both figures show an excellent comparison between electrical resistance strain gages N2 and S2 (each installed on a 9.5 mm (#3) reinforcing bar) and the internal vibrating wire gages (Figure 3.36) until the range of the vibrating wire gage was exceeded. The maximum incremental strains recorded during the loading were approximately $25{,}000 \cdot 10^{-6}$ (0.025000) in HPC-1 and $17{,}000 \cdot 10^{-6}$ (0.017000) in HPC-2.

Measured strains in all of the embedded electrical resistance gages for both the multiple-strand beams are shown in Figures 5.11 and 5.12 for both HPC-1 and HPC-2, respectively.

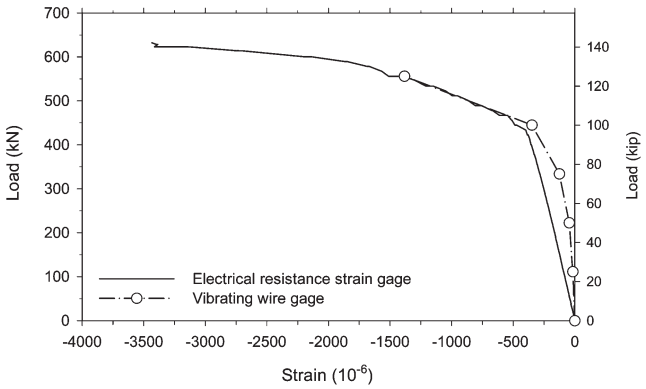

Figure 5.7 Top concrete surface strains measured in HPC-2 (north side of flange).

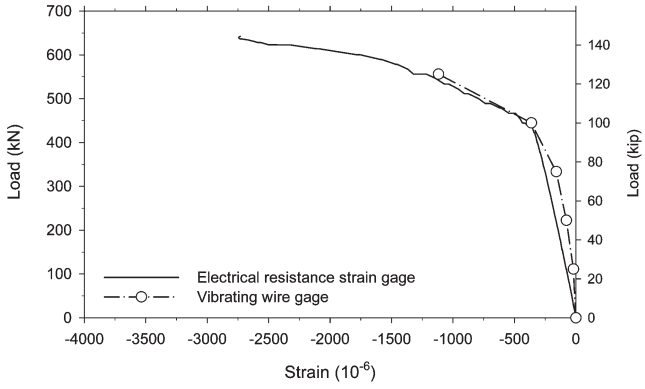

Figure 5.8 Top concrete surface strains measured in HPC-2 (south side of flange).

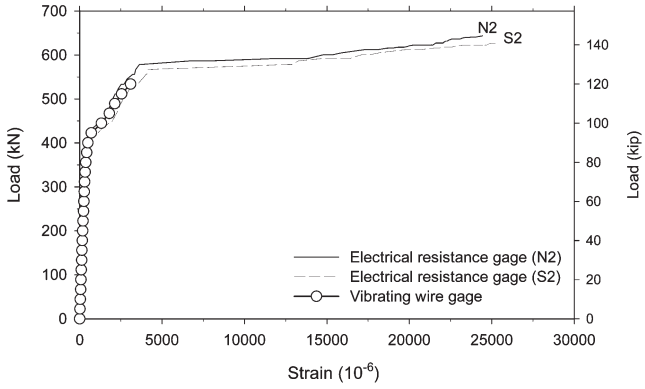

Figure 5.9 Strains measured at centerline of HPC-1 at the strand level.

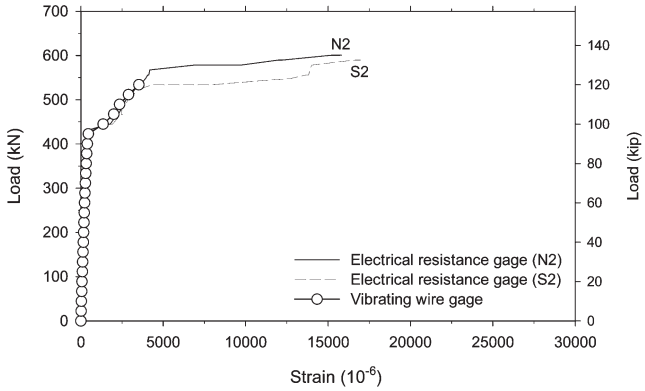

Figure 5.10 Strains measured at centerline of HPC-2 at the strand level.

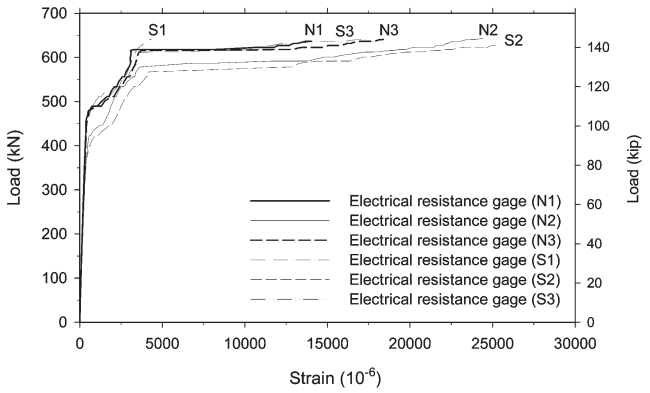

Figure 5.11 Strains from all electrical resistance gages in HPC-1 at strand level.

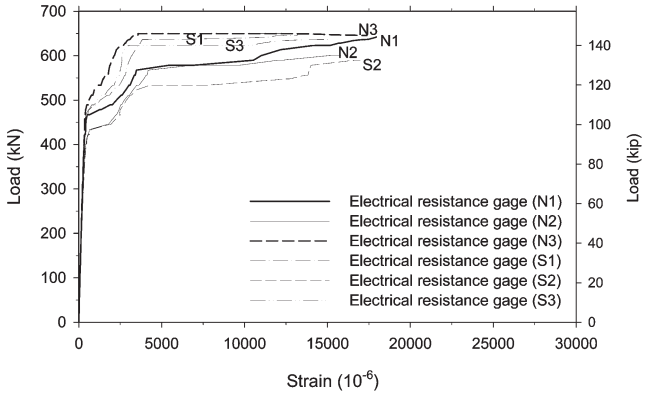

Figure 5.12 Strains from all electrical resistance gages in HPC-2 at strand level.

It is important to note that the above are incremental strains occurring at the level of the strand, and not the strain in the strands. The strands were initially tensioned to 1390 MPa (202 ksi) which corresponds to an initial strain of about 0.007090. At the time of the load tests, the strain in the strands was approximately 0.006500 (due to losses). Therefore, the total strains indicated by the electrical-resistance strain gages were about 0.031000 (3.15%) for HPC-1 and 0.023000 (2.15%) for HPC-2. The actual strand strains in both beams were obviously larger than this at the time of failure (since strand rupture occurred), but were not recorded by the strain gages. The ultimate elongation of the strand used in HPC-1 was reported by the manufacturer (Insteel) to be 6.5%. Information about the ultimate elongation of the (Florida Wire & Cable) strand used in HPC-2 was not available, but was believed to be in excess of 5% based on other strand supplied by that manufacturer.

6. CONCLUSIONS

The conclusions drawn from this study are divided into two sections, one from the materials part of the study (concrete mixture development and testing discussed in Chapter 4) and the other from the structural part of the study (discussed in Chapter5).

6.1 Concrete Mixture Development and Testing

1. In order to reduce possible effects of temperature and account for the change in uniformity of the raw materials used to produce concrete in the field, it is important to conduct trial pours within a few days before the actual pours are to be done.
2. The ACI equation recommended for calculating static modulus of elasticity [(*14*), p. 89] can be used to determine the static modulus of concrete with design strength of 69 MPa (10.0 ksi).
3. The effectiveness of AEAs to entrain and maintain a desired air content in fresh concrete should be carefully evaluated prior to their use in field applications. If changes in the air content of freshly mixed concrete are expected, the timing of specimen preparation is important as the compressive strength of the hardened concrete will vary approximately 5% with each 1% change in the air content.
4. Very good freeze-thaw resistance can be achieved for concrete mixes where up to 70% of the cement has been replaced with GGBFS. Replacing some of the cement with silica fume, or a blend of silica fume and GGBFS, can also result in freeze-thaw durable concrete.
5. Using mineral admixtures, such as a combination silica fume and GGBFS or GGBFS alone, as a replacement for some of the cement may adversely affect the deicing scaling resistance of concrete. The scaling resistance can also be expected to decrease as the proportions of the mineral admixtures increase. Using 3% sodium chloride instead of 4% calcium chloride as a ponding solution will generally accelerate the deterioration. Reducing the period of moist curing and increasing the air curing period was found to improve scaling resistance for the field trial mixture containing both GGBFS and silica fume.
6. Based on the charge passed, in coulombs, during six hours, both silica fume and GGBFS will increase the resistance of concrete to chloride ion penetration. Using a ternary binders system of cement, silica fume, and GGBFS may provide the most favorable results in terms of chloride ion penetration resistance.
7. Shrinkage reducing admixture (SRA) can be used to effectively reduce drying shrinkage. However, before using SRA in concrete intended for freeze-thaw exposure, the compatibility of the SRA and the AEA must be conformed. In this study, the SRA greatly reduced the effectiveness of the AEA.
8. Increasing the moist curing time from 3 to 14 days for regular INDOT Class C concrete, the time to failure of corrosion specimens was increased by at least 67%.
9. Replacing a portion of the cement with GGBFS and/or silica fume and lowering the water/binder ratio resulted in concrete mixtures that greatly reduced chloride ion ingress when compared with the regular INDOT Class C concrete. This in turn substantially extended the time to failure of the corrosion specimens. After 30 weeks of exposure to 6% NaCl solution, only one of 18 specimens made with GGBFS and/or silica fume modified mixture had failed while all six of the specimens made from the regular INDOT Class C concrete had failed after only 19 weeks.

10. Inadequate moist curing of 102 mm (4 in.) diameter concrete cylinders may significantly impair the compressive strength development of the concrete. Based on electrical tests, the ability of inadequately moist cured concrete to resist chloride ion ingress is also compromised.

6.2 Structural Testing

1. Measurements of concrete surface strains in specimens containing 15.2 mm (0.6 in.) strand and 69 MPa (10 ksi) normal density concrete indicated that the transfer length was less than the code assumed 50 strand diameters in the absence of longitudinal splitting cracks at the ends.
2. Six load tests on rectangular single-strand beams and two load tests on multiple-strand beams indicated that in the absence of web shear cracking near the ends, the AASHTO and ACI development length of $L_d = \left(f_{ps} - \frac{2}{3} f_{se}\right) d_b$ provided sufficient embedment to develop the full capacity of a single strand in the 69 MPa (10 ksi) concrete mixes used. Rupture of the prestressing strands occurred in each of the eight load tests.
3. The instrumentation used in the multiple-strand development beams, namely vibrating wire gages, internal electrical resistance strain gages, and surface mounted strain gages gave consistent readings throughout this study. All of the gages survived the casting, de-tensioning, and shipping processes.

7. RECOMMENDATIONS

Based on the findings of this study, the following recommendations are made:

1. Where ingress of chloride ions is likely to cause corrosion of reinforcement, supplementary cementitious materials such as silica fume and/or ground granulated blast furnace slag should be used. The desired proportions of the supplementary materials should depend on exposure conditions and the design life of the structure.
2. The current assumption for transfer lengths equal to 50 strand diameters were conservative for all combinations of strand and concrete mixes tested in the absence of longitudinal splitting cracks. The value of 50 strand-diameters could be used when checking shear provisions for the actual SR 43 bridge girders. If longitudinal splitting is detected, the actual transfer lengths can be as large as 70 strand-diameters.
3. The current AASHTO and ACI development length of $L_d = \left(f_{ps} - \frac{2}{3} f_{se}\right) d_b$ was found adequate for the bridge girders tested in this study. However, development length recommendations from the JTRP Final Report titled "Evaluation of Strand Transfer and Development Lengths in Pretensioned Girders with Semi-Lightweight Concrete" should be followed. The critical section for strand development should be shifted, in the direction of decreasing moment, a distance equal to the effective depth of the girder.
4. Instrumentation to be installed in the SR 43 bridge girders should be similar to the instrumentation used in this study, as all electrical resistance strain gages and vibrating wire gages performed satisfactorily.

REFERENCES

1. Dolan, C. W., C. A. Ballinger, and R. W. LaFraugh. High Strength Prestressed Concrete Bridge Girder Performance. *PCI Journal*, Vol. 38, No. 3, May–June 1993, pp. 88–97.
2. Rostam, S. Design for Durability: The Great Belt Link. In *Concrete Technology: New Trends, Industrial Applications; Proceedings of the International RILEM Workshop on Technology Transfer of the New Trends in Concrete, ConTech '94.* A. Aguado, R. Gettu and S. P. Shah, Eds. E & FN Spon, London, 1995, pp. 127–155.
3. Holley, J. J., M. D. A. Thomas, D. S. Hopkins, K. M. Cail, and M.-C. Lanctôt. Custom HPC Mixtures for Challenging Bridge Design. *Concrete International*, Vol. 21, No. 9, September 1999, pp. 43–48.
4. Bræstrup, M. W., and F. Ennemark. The Øresund Link: 100-Year Service Life. *Concrete International*, Vol. 20, No. 10, October 1998, pp. 62–64.
5. Neville, A. M. *Properties of Concrete*, 4th ed. John Wiley & Sons, New York, 1996.
6. Aïtcin, P.-C. *High-Performance Concrete*. E & FN Spon, London, 1998.
7. AASHTO. *LRFD Bridge Design Specifications*, 1st ed. American Association of State Highway and Transportation Officials, Washington, D.C., 1994
8. Glasser, F. P. Chemical, Mineralogical, and Microstructural Changes Occurring in Hydrated Slag-Cement Blends. In *Materials Science of Concrete II*. The American Ceramic Society, Inc., Westerville, Ohio, 1991, pp. 41–81.
9. ACI Committee 233. Ground Granulated Blast-Furnace Slag as a Cementitious Constituent in Concrete. In *ACI Manual of Concrete Practice*, Part 1. American Concrete InstituteFarmington Hills, Michigan, 1996.
10. Taylor, H. F. W. *Cement Chemistry*, 2nd ed. Thomas Telford Publishing, London, 1997. http://dx.doi.org/10.1680/cc.25929.
11. Moranville-Regourd, M. Cements Made From Blast-furnace Slag. In *Lea's Chemistry of Cement and Concrete*, 4th ed. P. C. Hewlett Ed., Arnold, London, 1998, pp. 633–674.
12. Roy, D. M. The Effect of Blast Furnace Slag and Related Materials on the Hydration and Durability of Concrete. In *Durability of Concrete; G. M. Idorn International Symposium, SP-131*. J. Holm and M. Geiker, Eds. American Concrete Institute Detroit, Michigan, 1992, pp. 195–208.
13. Stark, J., and H.-M. Ludwig. Influence of Water Quality on the Frost Resistance of Concrete. In *Freeze-Thaw Durability of Concrete*. J. Marchand, M. Pigeon and M. Setzer, Eds. E & FN Spon, London, 1997b, pp. 157–164.
14. ACI Committee 318. *Building Code Requirements for Structural Concrete (ACI 318-02) and Commentary (ACI 318R-02)*. American Concrete Institute, Farmington Hills, Michigan, 2002.
15. Khayat, K. H., and P. C. Aïtcin. Silica Fume in Concrete—An Overview. In *Fly Ash, Silica Fume, Slag, and Natural Pozzolans in Concrete, Proceedings: Fourth International Conference, Istanbul, Turkey, May 1992*, SP-132, Vol. II. V. M. Malhotra, Ed. American Concrete InstituteDetroit, Michigan, 1992, pp. 835–872.
16. Ásgeirsson, H. Intermilled Silica Fume in Icelandic Cement. *Concrete International*, Vol. 14, No. 7, July 1992, p. 56

17. Whiting, D., and R. Detwiler. *Silica Fume Concrete for Bridge Decks*. National Cooperative Highway Research Program, Report 410. Transportation Research Board, National Academy Press, Washington, D.C., 1998.
18. Fagerlund, G. Concrete Specifications for the Öresund Link: The Öresund Link—A Short Presentation. In *Durability of Concrete in Saline Environment*, Cementa AB, Danderyd, Sweden, 1996, pp. 187–206.
19. Gjørv, O. E. Effect of Condensed Silica Fume on Steel Corrosion in Concrete. *ACI Materials Journal*, Vol. 92, No. 6, November–December, 1995, pp. 591–598.
20. Bentur, A., S. Diamond, S, and N. S. Berke. *Steel Corrosion of Concrete: Fundamentals and Civil Engineering Practice*. E & FN Spon, London, 1997.
21. Poulsen, E. Estimation of Chloride Ingress into Concrete and Prediction of Service Lifetime with Reference to Marine RC Structures. *Durability of Concrete in Saline Environment*, Cementa AB, Danderyd, Sweden, 1996, pp. 113–126.
22. Leeming, M. B. Durability of Concrete in and Near the Sea. In *Concrete in Coastal Structure*. R. T. L. Allen Ed., Thomas Telford Publishing, London, 1998, pp. 73–98.
23. Al-Amoudi, O. S. B., Rasheeduzzafar, S. N. Abduljauwad, and M. Maslehuddin. Effect of Chloride-Sulfate Ions on Reinforcement Corrosion and Sulfate Deterioration in Blended Cements. In *Fly Ash, Silica Fume, Slag, and Natural Pozzolans in Concrete, Proceedings: Fourth International Conference, Istanbul, Turkey, May 1992*, SP-132, Vol. II. V. M. Malhotra Ed. American Concrete Institute, DetroitMichigan, 1992, pp.1105–1123.
24. Dehghanian, C. Corrosion Behavior of Steel in Concrete Made with Slag-Blended Cement. *Corrosion*, Vol. 55, No. 3, March 1999, pp. 291–296. http://dx.doi.org/10.5006/1.3283990.
25. Sherman, M. R., D. B. McDonald, and D. W. Pfeifer. Durability Aspects of Precast Prestressed Concrete, Part 2: Chloride Permeability Study. *PCI Journal*, Vol. 41, No. 4, July–August, 1996, pp. 75–95.
26. Monfore, G. E. The Electrical Resistivity of Concrete. Research Department Bulletin 224, Research and Development Laboratories of the Portland Cement Association, 1968. Also: *Journal of The PCA Research and Development Laboratories*, Vol. 10, No. 2, May, 1968, pp. 35–48.
27. Shi, C., J. A. Stegemann, and R. J. Caldwell. Effect of Supplementary Cementing Materials on the Specific Conductivity of Pore Solution and its Implications on the Rapid Chloride Permeability Test (AASHTO T277 and ASTM C1202) Results. *ACI Materials Journal*, Vol. 95, No. 4, July–August, 1998, pp. 389–394.
28. Zehetner, K., and W. Lindlbauer. Directly-Trafficable High Performance Concrete Bridge Structures—Practical Utilization Demonstrated by the Example of the Badhausbrücke in Tulln, Austria. In *Utilization of High Strength/High Performance Concrete, Proceedings of Symposium in Sandefjord, Norway*, Vol. 2. I. Holand and E. J. Sellevold Eds. Norwegian Concrete Association, Oslo, 1999, pp. 935–944.
29. Fagerlund, G., and K. Nordström. Studies of the Internal Frost Resistance of HPC. In *Utilization of High Strength/High Performance Concrete, Proceedings of Symposium in Sandefjord, Norway*. I. Holand and E. J. Sellevold Eds. Norwegian Concrete Association, Oslo, 1999, pp. 1092–1103.
30. Petersson, P. E. Scaling Resistance Tests of Concrete—Experience from Practical Use in Sweden. In *Freeze-Thaw Durability of Concrete*. J. Marchand, M. Pigeon and M. Setzer Eds. E & FN Spon, London, 1997, pp. 211–221.
31. Siebel, E., and T. Reschke. Three Different Methods for Testing the Freeze-Thaw Resistance of Concrete with and without De-Icing Salt. In *Freeze-Thaw Durability of Concrete*. J. Marchand, M. Pigeon and M. Setzer Eds. E & FN Spon, London, 1997, pp. 231–246.
32. Stark, J., and H.-M. Ludwig. Freeze-Deicing Salt Resistance of Concretes Containing Blast-Furnace Slag-Cement. In *Freeze-Thaw Durability of Concrete*. J. Marchand, M. Pigeon and M. Setzer Eds. E & FN Spon, London, 1997a, pp. 107–120.
33. Bilodeau, A., and V. M. Malhotra. Deicing Salt Scaling Resistance of Concrete Incorporating Supplementary Cementing Materials: CANMET Research. In *Freeze-Thaw Durability of Concrete*. J. Marchand, M. Pigeon and M. Setzer Eds. E & FN Spon, London, 1997, pp. 121–156.
34. Jacobsen, S., and E. J. Sellevold. Frost/Salt Scaling and Ice Formation of Concrete: Effect of Curing Temperature and Silica Fume on Normal and High Strength Concrete. In *Freeze-Thaw Durability of Concrete*. J. Marchand, M. Pigeon and M. Setzer Eds. E & FN Spon, London, 1997, pp. 93–105.
35. Abrams, D. A. Effect of Curing Condition on the Wear and Strength of Concrete. In *Bulletin 2*, 3rd Printing. Structural Materials Research Laboratory, Lewis Institute, Chicago, 1922.
36. Carette, G. G., and V. M. Malhotra. Long-Term Strength Development of Silica Fume Concrete. In *Fly Ash, Silica Fume, Slag, and Natural Pozzolans in Concrete, Proceedings: Fourth International Conference, Istanbul, Turkey, May 1992*, SP-132, Vol. II. V. M. Malhotra Ed. American Concrete Institute, Detroit, Michigan, 1992, pp. 1017–1044.
37. McDaniel, A. B. Influence of Temperature on the Strength of Concrete. *Engineering Experiment Station, Bulletin No. 81*, University of Illinois, Urbana, Illinois, July, 1915.
38. Sellevold, E. J. High-Performance Concrete: Early Age Cracking, Pore Structure, and Durability. In *International Workshop on High-Performance Concrete*, ACI SP-159. P. Zia, Ed. American Concrete Institute, Farmington Hills, Michigan, 1996, pp. 193–208.
39. Klieger, P. Effect of Mixing and Curing Temperature on Concrete Strength. *Journal of the American Concrete Institute, Proceedings*, Vol. 54, No. 12, June, 1958 pp. 1063–1081. Also: *Research Department Bulletin 103*, Research and Development Laboratories of the Portland Cement Association.
40. Saul, A. G. A. Principles Underlying the Steam Curing of Concrete at Atmospheric Pressure. *Magazine of Concrete Research*, Vol. 2, No. 6, March, 1951, pp. 127–140. http://dx.doi.org/10.1680/macr.1951.2.6.127.
41. Owens, P. L. Effect of Temperature Rise and Fall on the Strength and Permeability of Concrete Made With and Without Fly Ash. In *Temperature Effects on Concrete*, ASTM STP 858. T. R. Naik Ed. American Society for Testing and Materials, Philadelphia, 1985, pp. 134–149. http://dx.doi.org/10.1520/STP34212S.
42. Le Bris, J., P. Redoulez, V. Augustin, J. M. Torrenti, and F. de Larrard. High Performance Concretes in the "Elorn" Bridge. In *High Performance Concrete in Severe Environments*, SP-140. P. Zia Ed. American Concrete Institute, Detroit, Michigan, 1993, pp. 73–93.
43. Burg, R. G., and B. W. Ost. *Engineering Properties of Commercially Available High-Strength Concretes (In-*

cluding Three-Year Data). Research and Development Bulletin RD104T, Portland Cement Association, Skokie, Illinois, 1994.
44. MacGregor, J. G. *Reinforced Concrete: Mechanics and Design*, 3rd ed. Prentice-Hall, Upper Saddle River, New Jersey, 1997.
45. Hognestad, E. *A Study of Combined Bending and Axial Load in Reinforced Concrete Members*. University of Illinois Engineering Experimental Station, Bulletin Series No. 399, University of IllinoisUrbana, Illinois, 1951.
46. Price, W. H. Factors Influencing Concrete Strength. *Journal of the American Concrete Institute*, Vol. 22, No. 6, February 1951, pp. 417–432.
47. Klieger, P. Some Aspects of Durability and Volume Change of Concrete for Prestressing. *Research Department Bulletin 118*, Research and Development Laboratories of the Portland Cement Association, November 1960. Also: *Journal of the PCA Research and Development Laboratories*, Vol. 2, No. 3, September 1960, pp. 2–12.
48. Johnston, C. D. Durability of High Early Strength Silica Fume Concretes Subjected to Accelerated and Normal Curing. In *Fly Ash, Silica Fume, Slag, and Natural Pozzolans in Concrete, Proceedings: Fourth International Conference, Istanbul, Turkey, May 1992*, SP-132, Vol. II. V. M. Malhotra Ed., American Concrete Institute, Detroit, Michigan, 1992, 1167–1187.
49. Khurana, R., and I. Torresan. New Admixturesfor Eliminating Steam Curing and its Negative Effects on Durability. In *Superplasticizers and Other Chemical Admixtures in Concrete*, ACI SP-173. V. M. Malhotra Ed., American Concrete Institute, Farmington Hills, Michigan, 1997, pp. 83–103.
50. Lawrence, C. D. Physiochemical and Mechanical Properties of Portland Cements. In *Lea's Chemistry of Cement and Concrete*, 4th ed. P. C. Hewlett Ed., Arnold, London, 1998, pp. 343–419.
51. Kjellsen, K. O., R. J. Detwiler, and O. E. Gjørv. Pore Structure of Plain Cement Pastes Hydrated at Different Temperatures. *Cement and Concrete Research*, Vol. 20, No. 6, 1990, pp. 927–933. http://dx.doi.org/10.1016/0008-8846(90)90055-3.
52. Blakey, H. Temperature Matching Curing Bath—An Aid to Earlier Formwork Striking. *Concrete*, (London), Vol. 10, No. 4, April 1976, pp. 25–26.
53. Whiting, D., M. Nagi, P. A. Okamoto, T. Yu, D. Peshkin, K. Smith, M. Darter, J. Clifton, and L. Kaetzel. *Optimization of Highway Concrete Technology*. SHRP-C-373. Strategic Highway Research Program, Washington, D.C., 1994.
54. Russell, H. G., R. N. Bruce, and J. J. Roller. Prototype Bridge in High Performance Concrete—A Case Study. In *Utilization of High Strength/High Performance Concrete, Proceedings of Symposium in Sandefjord, Norway*, Vol. 2. I. Holand and E. J. Sellevold Eds. Norwegian Concrete Association, Oslo, 1999, pp. 891–900.
55. Myers, J. J., and R. L. Carrasquillo. Quality Control & Quality Assurance Program for Precast Plant Produced High Performance Concrete U-Beams. In *PCI/FHWA/FIB International Symposium on High Performance Concrete, Proceedings of Symposium in New Orleans, Louisiana*. L. S. Johal Ed., Precast/Prestressed Concrete Institute, Chicago, 1997, pp. 368–382.
56. Sprinkel, M. M., and K. K. McGhee. *Evaluation of Concrete Pavement Patching Techniques*. Publication FHWA/VA-89-22. Virginia Transportation Research Council, Charlottesville, Virginia, 1989.
57. Kaszyńska, M. Hydration Heat and Strength Development in High Performance Concrete. In *PCI/FHWA/FIB International Symposium on High Performance Concrete, Proceedings of Symposium in New Orleans, Louisiana*. L. S.. Johal, Ed. Precast/Prestressed Concrete Institute, Chicago, 1997, pp. 108–117.
58. Abrams, D. A. Effect of Curing Condition on the Wear and Strength of Concrete. *Bulletin 2*, 3rd Printing, Structural Materials Research Laboratory, Lewis Institute, Chicago, 1922.
59. Stocker, M. F., and M. A. Sozen. *Investigation of Prestressed Reinforced Concrete for Highway Bridges, Part VI, Bond Characteristics of Prestressing Strand*. University of Illinois Engineering Experiment Station, College of Engineering, University of Illinois at Urbana-Champaign, 1970.
60. Russell, B., and N. Burns. *Design Guidelines for Transfer, Development and Debonding of Large Diameter Seven Wire Strands in Pretensioned Concrete Girders*. Research Report 1210-5F. Texas Department of Transportation in cooperation with Federal Highway Administration, Austin, Texas, January 1993.
61. ACI Committee 318. *Building Code Requirements for Structural Concrete (ACI 318-95) and Commentary (ACI 318R-95)*. American Concrete Institute, Farmington Hills, Michigan, 1995.
62. Janney, R. J. Nature of Bond in Pretensioned Prestressed Concrete. *Journal of the American Concrete Institute*, Vol. 50, May 1954, pp. 717–736.
63. Hanson, N. W, and P. H. Karr. Flexural Bond Tests of Pretensioned Beams. *ACI Journal, Proceedings*, Vol. 55, January 1959, pp. 783–803.
64. Kaar, P. H, R. W. LaFraugh, and M. A. Mass. Influence of Concrete Strength on Strand Transfer Length. *Journal of the Prestressed Concrete Institute*. Vol. 8, No. 5, Oct. 1963, pp. 47–67.
65. Kaar, P., and D. Magura. Effect of Strand Blanketing on Performance of Pretensioned Girders. *Journal of the Prestressed Concrete Institute,*, Vol. 10, No. 6, Dec. 1965, pp. 20–34.
66. Hanson, N. W. Influence of Surface Roughness of Prestressing Strand on Bond Performance. *PCI Journal*, Vol. 14, No. 1, 1969, pp. 32–45.
67. Anderson, A. R, and R. G. Anderson. An Assurance Criterion for Flexural Bond in Pre-tensioned Hollow Core Units. *ACI Journal*, Vol. 72, No. 8, 1976, pp. 457–464.
68. Brooks, M. D., K. H. Gerstle, and D. R. Logan. Effect of Initial Strand Slip on the Strength of Hollow-Core Slabs. *PCI Journal*, Vol. 33, No. 1 (January–February), 1988, pp. 90–111.
69. Buckner, D. A Review of Strand Development Length for Pretensioned Concrete Members. *PCI Journal*, Vol. 40, No. 2, March–April 1995, pp. 84–105.
70. Logan, D. R. Discussion of "A Review of Strand Development Length for Pretensioned Concrete Members." *PCJ Journal*, Vol. 41, No. 2. March–April 1996, pp. 112–116.
71. Logan, D. Acceptance Criteria for Bond Quality of Strand for Pretensioned Prestressed Concrete Applications. *PCI Journal*, Vol. 42, No. 2, March–April 1997, pp. 52–79.
72. Moustafa, S. Pull-Out Strength of Strand and Lifting Loops. *Concrete Technology Associates*, Technical Bulletin, 74-B5, May 1974.

73. Schiessl, P., and M. Raupach. Monitoring System for the Corrosion Risk of Steel in Concrete Structures. *Concrete International*, Vol. 14, No. 7, 1992, 52–55.
74. Samples, L. M., and J. A. Ramirez. *Methods of Corrosion Protection and Durability of Concrete Bridge Decks Reinforced with Epoxy-Coated Bars—Phase I*. Publication FHWA/IN/JTRP-98/15. Joint Transportation Research Program, Indiana Department of Transportation and Purdue University, West Lafayette, Indiana, 1999. doi: 10.5703/1288284313268.
75. Liu, R. *Development and Evaluation of Cement-based Materials for Repair of Corrosion-damaged Reinforced Concrete Slabs*. Ph.D. Thesis, Purdue University, West Lafayette, Indiana, 2000.
76. Ranagaraju, P., *Mixture Proportioning and Microstructural Aspects of High-Performance Concretes*. Ph.D. Thesis, Purdue University, West Lafayette, Indiana, 1997, 294 pp.
77. Goodspeed, C. H., S. Vanikar, and R. A. Cook. High-Performance Concrete Defined for Highway Structures. *Concrete International*, Vol. 18, No. 2, February 1996, pp. 62–67.
78. Indiana Department of Transportation. *1993 Standard Specifications*, Indiana Department of Transportation, Indianapolis, Indiana, 1993.
79. Corley, W. G., and M. A. Sozen. Time Dependent Deflections of Reinforced Concrete Beams. *Journal of the American Concrete Institute*, Proceedings Vol. 63, No. 3, March 1996, pp. 373–386.

APPENDIX A. PULL-OUT TEST PROCEDURE (MOUSTAFA METHOD)*

OBJECTIVE

Determine the pull-out capacity of as-received strand samples (protected from weathering) and compare that pull-out capacity with the most recent benchmark established in Stresscon Corporation's bond test conducted in May-June 1996 (see Fig. E1). Four strand groups attained transfer and development lengths considerably shorter than the lengths computed by the ACI equations. The average pull-out capacities of each of these four groups ranged from 36.8 to 41.6 kips (164 to 185 kN), respectively.

Based on the excellent transfer/development length performance of all of these top four strand groups, the following benchmark is recommended as the minimum acceptable pull-out capacity:

Average pull-out load = 36 kips (160 kN)
(set of six samples)
Maximum standard deviation = 10 percent

Note that this capacity is only applicable to 0.5 in. (13 mm) diameter, 270 ksi (1862 MPa) strand with an 18 in. (457 mm) embedment, cast in normal weight, well vibrated concrete having a concrete strength at the time of the pull-out test between 3500 and 5900 psi (24.1 and 40.7 MPa).

GENERAL PROCEDURAL COMMENT

To attain results consistent with a long series of tests extending back to 1974, it is of primary importance to closely follow the procedure used in the 1974 and 1992 tests conducted at Concrete Technology Corporation, Tacoma, Washington, and an extensive series of tests subsequently conducted at Stresscon Corporation, Colorado Springs, Colorado, since 1992. This procedure was first developed by Saad Moustafa in 1974 and was modified by Donald Logan, who introduced the 2 in. (51 mm) sleeve at the top concrete surface to eliminate the effects of surface spalling, and es-

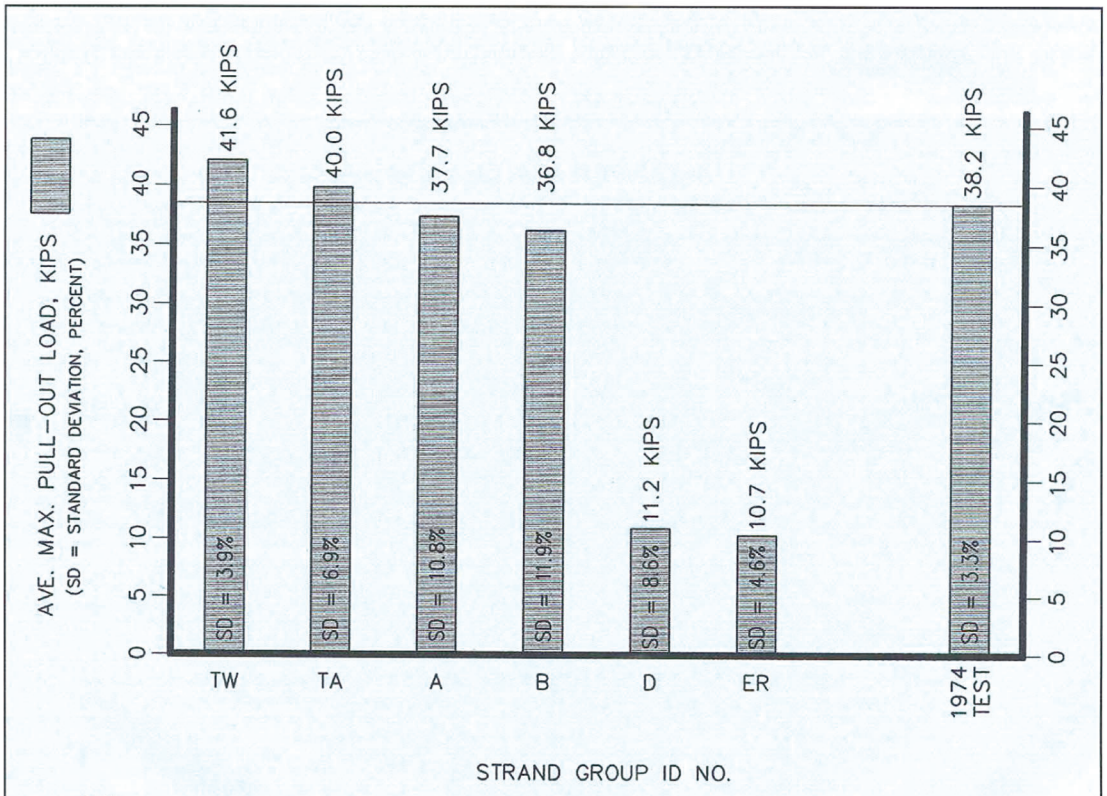

Notes:
(1) The above results are from the strand bond tests conducted at Stresscon Corporation and supervised by Saad Moustafa in May 1996 (six specimens per test).
(2) Strand specimens were embedded 18 in. (457 mm) into well vibrated concrete test blocks. Concrete was Stresscon's standard production mix. All strand was 0.5 in. (13 mm) in diameter.
(3) All strand specimens, except TW, were in their as received condition and were protected from weathering.

*The material in this appendix originally appeared in the March/April 1997 issue of the *Journal of the Precast/Prestressed Concrete Institute* (Vol. 42, No. 2) as part of a special report authored by Donald R. Logan, P.E. titled "Acceptance Criteria for Bond Quality of Strand for Pretensioned Prestressed Concrete Applications." The material herein is reproduced with the permission of the Precast/Prestressed Concrete Institute and Mr. Logan.

tablished the 20 kips per minute (89 kN/minute) load application rate, which is close to the average rate observed in earlier tests.

STRAND PREPARATION PROCEDURE

1. Six strand samples shall be taken from a fresh, unopened pack of unweathered strand (as-received from the manufacturer and not modified in any way by the manufacturer). Samples are to be saw-cut to 34 in. (864 mm) lengths, any projections from the saw-cutting will be removed, and the samples will be straightened by hand if they are bowed more than 3/8 in. (9.5 mm) in their 34 in. (864 mm) length.

2. The strand samples shall be visually examined to verify that they are not rusted. They shall be wiped with a clean paper towel to clean off any loose dirt or incidental rust and to observe the residue on the strand as received from the strand manufacturer. The samples shall *not* be cleaned with acid or any other solvent.

3. If more than one shipment of strand (or more than one manufacturer's strand) is being tested for comparative performance, duct-tape tags shall be attached to the top end of all samples in accordance with an identification system. Each tag shall be marked with indelible ink with its appropriate symbol, and taped securely in a location where they will be visible after casting of the test block.

4. The taped samples shall be tied securely in each test block at the locations indicated in the test block layout drawing. If more than one group is being tested, it is important to have each test block contain an equal number of strand samples from each group distributed alternately throughout that block. This will ensure that each group receives equal concrete quality and equal placement and vibration of the concrete. Refer to Fig. E2 for an example of a test using three different strand groups.

CASTING PROCEDURE

1. Test block forms shall be set up, reinforcing cages installed and securely positioned before any strand samples are tied in place.

2. After the forms and reinforcement have been checked, the tagged strand samples shall be tied securely in place in accordance with the layout shown in the test block layout drawing. The time that the strands are exposed to the weather shall be minimized.

3. Immediately after the strand location and tying procedure is checked and approved, concrete placement shall take place.

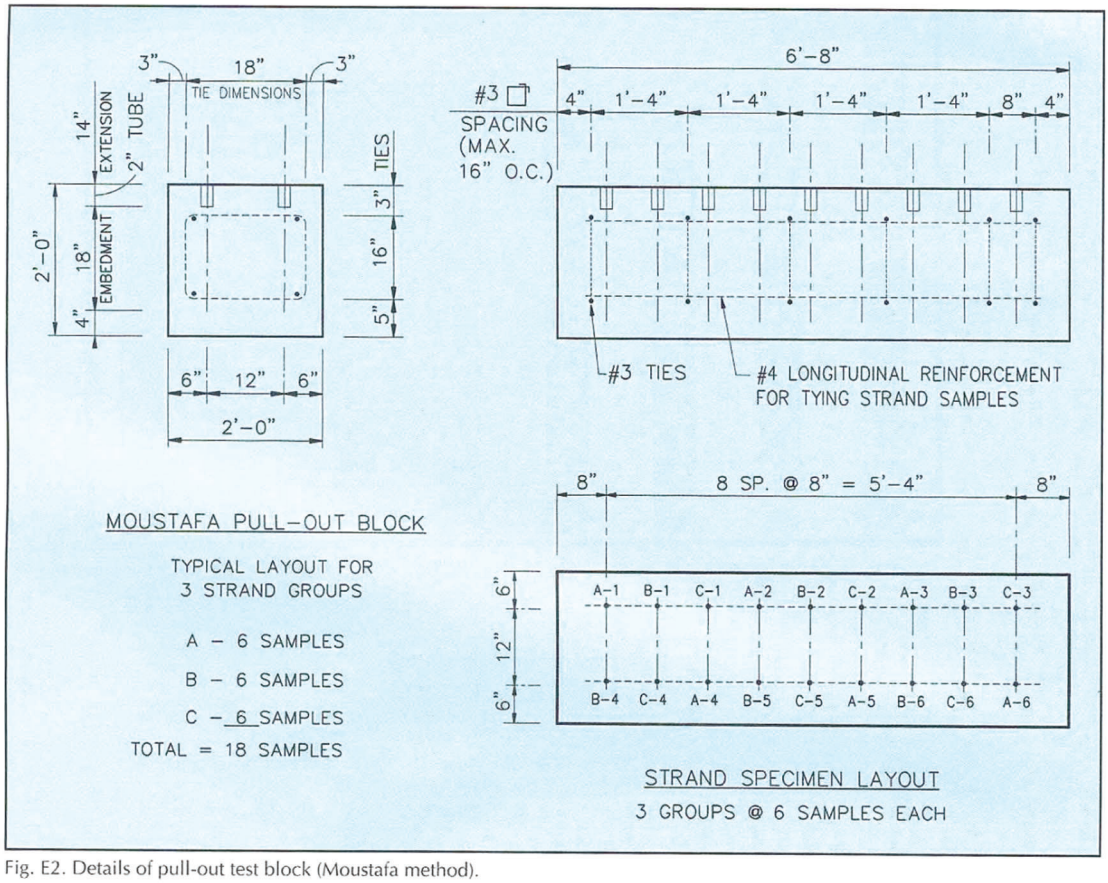

Fig. E2. Details of pull-out test block (Moustafa method).

Table E1. Suggested concrete mix design.

Materials	Quantity per cubic yard*
Cement (Type III)	660 lbs (299 kg)
Concrete sand	1100 lbs (499 kg) (SSD)
Crushed gravel [¾ in. (19 mm)]	1900 lbs (862 kg)
Normal range water reducer	26 oz. (737 g)
Air-entraining agent	0 oz.
High range water reducer	0 oz.
Water	35 gal. (132 l)

* 1 cubic yard = 0.7646 m³.

4. The concrete will be produced from one batch of hard-rock structural concrete mix (without any high range water reducers) that is expected to attain between 3800 and 5000 psi (26.2 and 34.5 MPa) with overnight heat curing (or 2 days of ambient cure). Four cylinders shall be cast from that batch and cured with the test blocks to determine the concrete strength at the time of the test (three cylinders) and one cylinder saved for a 28-day test. A suggested concrete mix design is shown in Table E1.

5. The concrete shall be well-vibrated using internal vibrators, with the concrete at approximately 3 in. (76 mm) slump. The intent of the vibration is to duplicate good, production quality consolidation around the strand samples.

6. The top surface shall be smoothed using a one-pass trowel finish in order to attain flat concrete surfaces adjacent to the strand samples to uniformly support the jack bridging assembly. Special care needs to be taken to avoid moving any strand sample after the vibration is complete. [Do *not* re-adjust the height of any strand sample if it is not exactly at the proper height after vibration. A ¼ to ½ in. (6.3 to 13 mm) extra embedment is not significant.]

7. Support racks shall be placed over the test blocks to keep the curing covers from coming in contact with the tops of the strand samples. Curing compound shall be sprayed on the tops of the blocks to prevent shrinkage cracks from occurring in the top surface.

TESTING PROCEDURE

1. The hydraulic jack shall be a pull-jack with a center hole assembly at the end of the ram (similar to those normally used for single-strand stressing). It shall be tested and calibrated to permit loading to 50 kips (222 kN), and shall have a travel of at least 12 in. (305 mm).

2. The bridging device shall be as shown in Fig. E3.

3. On the day after casting the test blocks (with heat curing), the cylinders shall be tested and the concrete strength recorded. Based on results of past testing, the concrete strength can range from 3500 to 5900 psi (24.1 to 40.7 MPa) without affecting the pull-out strength results.

4. The bridge is slipped over each strand to be tested and placed against the concrete surface. The strand chucks are slipped over the strand to the top of the bridge and light pressure is applied to the jack to seat the jaws of the chuck into the strand.

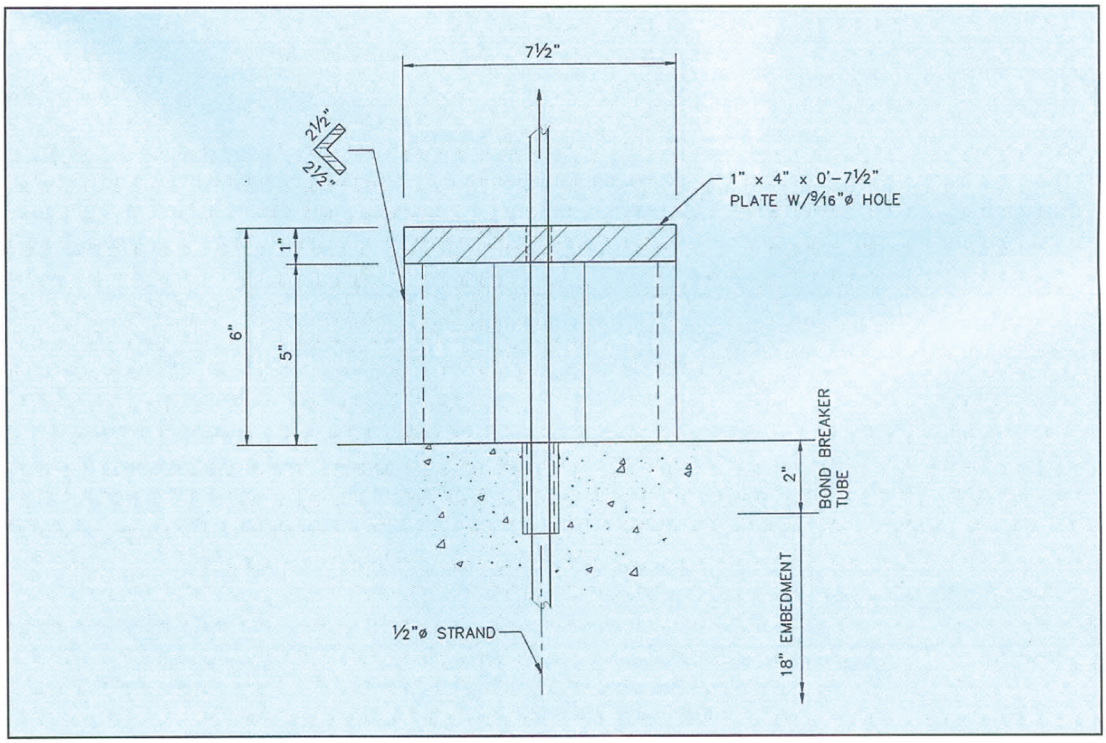

Fig. E3. Bridging device.

5. The jacking load shall be applied in a single increasing application of load at the rate of approximately 20 kips per minute (89 kN per minute) until maximum load is reached and the load gauge indicator can no longer sustain maximum load. Do *not* stop the test at the first sign of movement of the strand sample or for any other reason. The strand samples can pull out as much as 8 to 10 in. (203 to 254 mm) before maximum load is reached with poor bonding strand, and 1 to 2 in. (25.5 to 51 mm) with good bonding strand.

6. The pull-out capacity of the strand sample shall be recorded as the maximum load attained by the strand sample before the load drops off on the gauge and cannot be further increased.

7. The following data shall be recorded for each strand sample:

(a) Maximum capacity (as defined above).

(b) Approximate load at first noticeable movement.

(c) Approximate distance the strand pulls out at maximum load (for general reference, accuracy is not critical).

(d) General description of failure. Typical examples:

(i) Abrupt slip, loud noise. Strand started moving at 35 kips (156 kN). Two wires broke at failure load of 41.2 kips (183 kN).

(ii) Gradual slip, no noise. Strand started moving at approximately 6 kips (26.7 kN).

(iii) Initial movement at approximately 30 kips (133 kN), then abrupt slip at 36.3 kips (161 kN). Loud noise. No broken wires.

(iv) Strand break. All seven wires broke at the chuck.

8. Record data and compute average failure load and standard deviation for each strand group tested. Compare results with minimum requirements for acceptance for pretensioning applications.

APPENDIX B. SAMPLE DATALOGGER PROGRAM

```
;{ CR10}

*Table 1 Program
  01: 60.0     Execution Interval (seconds)

1:   Batt Voltage (P10)
  1: 14    Loc[ Batt_V]

2:   Internal Temperature (P17)
  1: 1     Loc[ Int_Temp]

3:   Temp (107) (P11)
  1: 1     Reps
  2: 6     SE Channel
  3: 3     Excite all reps w/Exchan 3
  4: 2     Loc[ Ref_Temp]
  5: 1.0   Mult
  6: 0.0   Offset

4:   Do (P86)
  1: 44    Set Port 4 High

5:   Beginning of Loop (P87)
  1: 0     Delay
  2: 11    Loop Count

6:   Do (P86)
  1: 76    Pulse Port 6

7:   Excitation with Delay (P22)
  1: 1     Ex Channel
  2: 0     Delay W/Ex (units = 0.01 sec)
  3: 1     Delay After Ex (units = 0.01 sec)
  4: 0     mV Excitation

8:   Thermocouple Temp (DIFF) (P14)
  1: 1     Reps
  2: 21    ñ 2.5 mV 60 Hz Rejection Range
  3: 4     DIFF Channel
  4: 1     Type T (Copper-Constantan)
  5: 2     Ref Temp Loc[ Ref_Temp]
  6: 3 -- Loc[ TCm1_#1]
  7: 1.0   Mult
  8: 0.0   Offset

9:   Thermocouple Temp (DIFF) (P14)
  1: 1     Reps
  2: 21    ñ 2.5 mV 60 Hz Rejection Range
  3: 5     DIFF Channel
  4: 1     Type T (Copper-Constantan)
  5: 2     Ref Temp Loc[ Ref_Temp]
  6: 15-- Loc[ TCm2_#1]
  7: 1.0   Mult
  8: 0.0   Offset

10:  End (P95)

11:  Do (P86)
  1: 54    Set Port 4 Low

12:  If time is (P92)
  1: 0     Minutes (Seconds --) into a
  2: 10    Interval (same units as above)
  3: 10    Set Output Flag High

13:  Real Time (P77)
  1: 0110 Day,Hour/Minute

14:  Average (P71)
  1: 25    Reps
  2: 1     Loc[ Int_Temp]

*Table 2 Program
  02: 1.0 Execution Interval (seconds)

*Table 3 Subroutines

End Program
```

APPENDIX C. CONCRETE MATERIALS RESULTS

MIX PROPORTIONS AND SELECTED PROPERTIES OF GIRDER AND DECK CONCRETES USED IN THIS STUDY

C.1 Results from Girder Mixes (Tables C.1 through C.6)

TABLE C.1
Mix proportions and concrete properties of girder concrete mixes LG-1 to LG-7 (SI units)

Concrete mix	LG-1	LG-2	LG-3	LG-4	LG-5	LG-6	LG-7
Date	2/13/98	2/13/98	2/17/98	2/20/98	2/20/98	2/21/98	2/21/98
Binders:							
Cement (kg/m^3)	464	464	464	464	464	463	463
Silica fume (kg/m^3)	23	23	23	23	23	24	24
Total binder content (kg/m^3)	487	487	487	487	487	487	487
Water:							
Water (L/m^3)	159	158	158	155	162	156	156
Water/binder ratio	0.326	0.324	0.324	0.319	0.333	0.320	0.320
Aggregates:							
Coarse aggregate (kg/m^3)	947	947	947	947	952	949	949
Fine aggregate (kg/m^3)	726	726	726	726	726	726	737
Chemical admixtures:							
HRWR (mL/100 kg)	1434	1219	1043	1363	1121	1630	1487
NRWR (mL/100 kg)	587	587	587	476	567	326	274
AEA (mL/100 kg)	202	137	137	95	65	65	87
Fresh concrete properties:							
Slump (mm)	51	165	133	127	203	76	152
Air content (%)	9.75	7.2	9	8.75	10	4.6	6.5
Unit weight (kg/m^3)	2243	2323	2275	2300	2233	2398	2347
Concrete strength (MPa):							
1 day	44	48	52	63	51		
3 days	50	57	60			70	75
7 days	61	62	63	87	71	79	83
14 days	69	64	71				
28 days	69	73		89	78	90	97
56 days							
91 days							
1 year							
Admixture types:							
HRWR	Darac19	Darac19	Darac19	Darac19	Darac19	Darac19	Darac19
NRWR	Darac55	Darac55	Darac55	Darac55	Darac55	Darac55	Darac55
AEA	Dara1400	Dara1400	Dara1400	Dara1400	Dara1400	Dara1400	Dara1400

TABLE C.2
Mix proportions and concrete properties of girder concrete mixes LG-8, LG-9, and FG-1 to FG-5 (SI units)

Concrete mix	LG-8	LG-9*	FG-1	FG-2	FG-3	FG-4	FG-5
Date	2/26/98	3/3/98	10/28/97	2/28/98	3/19/98	4/3/98	4/15/98
Binders:							
Cement (kg/m^3)	439	439	475	439	439	439	439
Silica fume (kg/m^3)	23	23		23	23	23	23
Total binder content (kg/m^3)	462	462	475	462	462	462	462
Water:							
Water (L/m^3)	147	159	125†	162	157	157	155
Water/binder ratio	0.317	0.345	0.263†	0.350	0.340	0.340	0.336
Aggregates:							
Coarse aggregate (kg/m^3)	949	949	988	949	949	949	949
Fine aggregate (kg/m^3)	780	755	767	848	755	755	755
Chemical admixtures:							
HRWR (mL/100 kg)	1310	1956	1239	2008	1339	1174	1337
NRWR (mL/100 kg)	261	261	261	254	257	254	261
AEA (mL/100 kg)	98	98	81	98	89	95	104
Fresh concrete properties:							
Slump (mm)	133	178	102	51	152	57	165
Air content (%)	7.2	7.8	6.5	5.5	5.2	3.5	6.6
Unit weight (kg/m^3)	2339	2297	2342	2393	2355	2419	2345
Concrete strength (MPa):							
1 day	55	44		65	34	54	46
3 days		54	60	82	59	65	65
7 days (6 days)	78		69	(84)	71	73	70
14 days		73		93	79	77	77
28 days	92	73	81	109	86	74	85
56 days	94	81		101	85	84	87
91 days		80					
1 year	107			111		90	97
Admixture types:							
HRWR	Darac19	Darac19	Darac19	Darac19	Darac19	Darac19	Darac19
NRWR	Darac55	Darac55	Darac55	Darac55	Darac55	Darac55	Darac55
AEA	Dara1400	Dara1400	Dara1400	Dara1400	Dara1400	Dara1400	Dara1400

*Ingredients were cooled prior to mixing.
†Does not include free water on aggregates.

TABLE C.3
Mix proportions and concrete properties of concrete mixes used for multiple-strand development length specimens (SI units)

Concrete mix	HPC-1	HPC-2		
Date	7/14/98	7/14/98		
Binders:				
Cement (kg/m^3)	439	439		
Silica fume (kg/m^3)	23	23		
Total binder content (kg/m^3)	462	462		
Water:				
Water (L/m^3)	155	157		
Water/binder ratio	0.336	0.340		
Aggregates:				
Coarse aggregate (kg/m^3)	949	949		
Fine aggregate (kg/m^3)	755	755		
Chemical admixtures:				
HRWR (mL/100 kg)	1337	1337		
NRWR (mL/100 kg)	261	261		
AEA (mL/100 kg)	103	103		
Fresh concrete properties:				
Slump (mm)	89	127		
Air content (%)	5.4	5.0		
Unit weight (kg/m^3)	2361	2380		
Concrete strength (MPa):				
			HPC-2	
			Outside (from casting)	**50% RH (from 3 days)**
1 day	46	46		
3 days	57	55	57	
7 days	64	63	64	65
14 days	67	66	68	
17 days	71	66		
28 days	70	65	67	62
56 days	70	70	68	
91 days	68	69	64	58
182 days	75	75	69	
1 year	78	79	70	59
Admixture types:				
HRWR	Darac19	Darac19		
NRWR	Darac55	Darac55		
AEA	Dara1400	Dara1400		

TABLE C.4
Mix proportions and concrete properties of girder concrete mixes LG-1 to LG-7 (US customary units)

Concrete mix	LG-1	LG-2	LG-3	LG-4	LG-5	LG-6	LG-7
Date	2/13/98	2/13/98	2/17/98	2/20/98	2/20/98	2/21/98	2/21/98
Binders:							
Cement (lb/yd^3)	782	782	782	782	782	780	780
Silica fume (lb/yd^3)	39	39	39	39	39	41	41
Total binder content (lb/yd^3)	821	821	821	821	821	821	821
Water:							
Water (lb/yd^3)	268	266	266	262	273	263	263
Water/binder ratio	0.326	0.324	0.324	0.319	0.333	0.320	0.320
Aggregates:							
Coarse aggregate (lb/yd^3)	1597	1597	1597	1597	1605	1600	1600
Fine aggregate (lb/yd^3)	1224	1224	1224	1224	1224	1224	1242
Chemical admixtures:							
HRWR (oz/cwt)	22.0	18.7	16.0	20.9	17.2	25.0	22.8
NRWR (oz/cwt)	9.0	9.0	9.0	7.3	8.7	5.0	4.2
AEA (oz/cwt)	3.1	2.1	2.1	1.5	1.0	1.0	1.3
Fresh concrete properties:							
Slump (in.)	2	6.5	5.25	5	8	3	6
Air content (%)	9.75	7.2	9	8.75	10	4.6	6.5
Unit weight (lb/ft^3)	140	145	142	143.6	139.4	149.7	146.5
Concrete strength (ksi):							
1 day	6.31	6.98	7.52	9.13	7.34		
3 days	7.30	8.26	8.77			10.19	10.84
7 days	8.83	9.03	9.17	12.64	10.27	11.44	12.00
14 days	9.97	9.31	10.33				
28 days	10.07	10.60		12.87	11.28	13.03	14.01
56 days							
91 days							
1 year							
Admixture types:							
HRWR	Darac19	Darac19	Darac19	Darac19	Darac19	Darac19	Darac19
NRWR	Darac55	Darac55	Darac55	Darac55	Darac55	Darac55	Darac55
AEA	Dara1400	Dara1400	Dara1400	Dara1400	Dara1400	Dara1400	Dara1400

TABLE C.5
Mix proportions and concrete properties of girder concrete mixes LG-8, LG-9, and FG-1 to FG-5 (US customary units)

Concrete mix	LG-8	LG-9*	FG-1	FG-2	FG-3	FG-4	FG-5
Date	2/26/98	3/3/98	10/28/97	2/28/98	3/19/98	4/3/98	4/15/98
Binders:							
Cement (lb/yd^3)	740	740	800	740	740	740	740
Silica fume (lb/yd^3)	39	39		39	39	39	39
Total binder content (lb/yd^3)	779	779	800	779	779	779	779
Water:							
Water (lb/yd^3)	247	269	210†	273	265	265	262
Water/binder ratio	0.317	0.345	0.263†	0.350	0.340	0.340	0.336
Aggregates:							
Coarse aggregate (lb/yd^3)	1600	1600	1666	1600	1600	1600	1600
Fine aggregate (lb/yd^3)	1314	1272	1293	1430	1272	1272	1272
Chemical admixtures:							
HRWR (oz/cwt)	20.1	30.0	19.0	30.8	20.5	18.0	20.5
NRWR (oz/cwt)	4.0	4.0	4.0	3.9	3.9	3.9	4.0
AEA (oz/cwt)	1.5	1.5	1.3	1.5	1.4	1.5	1.6
Fresh concrete properties:							
Slump (in.)	5.25	7	4	2	6	2.25	6.5
Air content (%)	7.2	7.8	6.5	5.5	5.2	3.5	6.6
Unit weight (lb/ft^3)	146	143.4	146.2	149.4	147.0	151.0	146.4
Concrete strength (ksi):							
1 day	7.92	6.45		9.39	4.99	7.86	6.64
3 days		7.84	8.73	11.87	8.59	9.39	9.48
7 days (6 days)	11.38		9.95	(12.16)	10.29	10.57	10.09
14 days		10.60		13.47	11.39	11.15	11.13
28 days	13.39	10.66	11.69	15.85	12.41	10.80	12.29
56 days	13.57	11.74		14.64	12.28	12.12	12.57
91 days		11.60					
1 year	15.48			16.11		13.05	14.01
Admixture types:							
HRWR	Darac19	Darac19	Darac19	Darac19	Darac19	Darac19	Darac19
NRWR	Darac55	Darac55	Darac55	Darac55	Darac55	Darac55	Darac55
AEA	Dara1400	Dara1400	Dara1400	Dara1400	Dara1400	Dara1400	Dara1400

*Ingredients were cooled prior to mixing.
†Does not include free water on aggregates.

TABLE C.6
Mix proportions and concrete properties of concrete mixes used for multiple-strand development length specimens (US customary units)

Concrete mix	HPC-1	HPC-2		
Date	7/14/98	7/14/98		
Binders:				
Cement (lb/yd^3)	740	740		
Silica fume (lb/yd^3)	39	39		
Total binder content (lb/yd^3)	779	779		
Water:				
Water (lb/yd^3)	262	265		
Water/binder ratio	0.336	0.340		
Aggregates:				
Coarse aggregate (lb/yd^3)	1600	1600		
Fine aggregate (lb/yd^3)	1272	1272		
Chemical admixtures:				
HRWR (oz/cwt)	20.5	20.5		
NRWR (oz/cwt)	4.0	4.0		
AEA (oz/cwt)	1.58	1.58		
Fresh concrete properties:				
Slump (in.)	3.5	5		
Air content (%)	5.4	5.0		
Unit weight (lb/ft^3)	147.4	148.6		
Concrete strength (ksi):				
			HPC-2	
			Outside (from casting)	**50% RH (from 3 days)**
1 day	6.68	6.74		
3 days	8.24	8.00	8.30	
7 days	9.22	9.10	9.24	9.46
14 days	9.71	9.55	9.85	
17 days	10.28	9.51		
28 days	10.15	9.43	9.72	9.06
56 days	10.16	10.11	9.92	
91 days	9.85	9.96	9.35	8.42
182 days	10.86	10.88	9.97	
1 year	11.27	11.42	10.19	8.62
Admixture types:				
HRWR	Darac19	Darac19		
NRWR	Darac55	Darac55		
AEA	Dara1400	Dara1400		

C.2 Results from Deck Mixes (Tables C.7 through C.20)

TABLE C.7
Mix proportions and concrete properties of deck concrete mixes LD-1 to LD-7 (SI units)

Concrete mix	LD-1	LD-2	LD-3	LD-4	LD-5	LD-6	LD-7
Binders:							
Cement (kg/m^3)	384	384	383	383	383	356	356
Silica fume (kg/m^3)							
GGBFS (kg/m^3)							
Total binder content (kg/m^3)	384	384	383	383	383	356	356
Water:							
Water (L/m^3)	150	150	142	142	142	136	135
Water/binder ratio	0.389	0.389	0.370	0.370	0.370	0.382	0.380
Aggregates:							
Coarse aggregate (kg/m^3)	1025	1025	990	990	1000	1009	1009
Fine aggregate (kg/m^3)	777	777	800	800	785	853	853
Chemical admixtures:							
HRWR (mL/100 kg)	619	443	528	613	430	724	737
NRWR (mL/100 kg)		274	563	274	274	254	
AEA (mL/100 kg)	202	138	102	93	93	99	50
Fresh concrete properties:							
Slump (mm)	216	184	216	241	197	222	159
Air content (%)	9.8	9	11.25	7.5	7.7	12	6.4
Unit weight (kg/m^3)	2307	2300	2233	2332	2342	2239	2380
Concrete strength (MPa):							
1 day				17	16	11	20
3 days						38	49
7 days			35	49	45		68
14 days						59	68
28 days (48 days)			43	(61)	58	55	75
56 days						64	75
1 year						74	
Admixture types:							
HRWR	Adva F	Adva F	Adva F	Adva F	Adva F	Adva F	Adva F
NRWR		Darac55	Darac55	Darac55	Darac55	Darac55	
AEA	Darex II	Darex II	Darex II	Darex II	Darex II	Dara1400	Dara1400

TABLE C.8
Mix proportions and concrete properties of deck concrete mixes LD-8 to LD-14 (SI units)

Concrete mix	LD-8	LD-9	LD-10	LD-11	LD-12	LD-13	LD-14
Binders:							
Cement (kg/m^3)	386	326	326	326	326	228	310
Silica fume (kg/m^3)							16
GGBFS (kg/m^3)						98	
Total binder content (kg/m^3)	386	326	326	326	326	326	326
Water:							
Water (L/m^3)	147	124	125	127	124	124	124
Water/binder ratio	0.380	0.380	0.383	0.390	0.380	0.380	0.380
Aggregates:							
Coarse aggregate (kg/m^3)	1009	979	979	979	979	979	979
Fine aggregate (kg/m^3)	798	938	938	938	938	930	931
Chemical admixtures:							
HRWR (mL/100 kg)	848	900	2073	2504	2112	1004	1030
NRWR (mL/100 kg)				196			
AEA (mL/100 kg)	50	49	80	43	54	49	43
Fresh concrete properties:							
Slump (mm)	210	210	152	178	127	171	152
Air content (%)	6.8	8.6	9.1	5.6	7.8	9.8	9.5
Unit weight (kg/m^3)	2368	2339	2313	2398	2348	2291	2287
Concrete strength (MPa):							
1 day	20	17	8	0	9	12	14
3 days	50	41	45	39	41	34	34
7 days	60	54	60	55	53	47	51
14 days	72	64	61	65	61	53	64
28 days	72	65	66	75	65	61	66
56 days	77				66		68
91 days						77	72
1 year		70	79	83			
Admixture types:							
HRWR	Adva F	Adva F	Darac100	Rhe1000	Rhe1000	Adva F	Adva F
NRWR				P100-XR			
AEA	Dara1400	Dara1400	Dara1400	Micro-A	Micro-A	Darex II	Darex II

TABLE C.9
Mix proportions and concrete properties of deck concrete mixes LD-15 to LD-21 (SI units)

Concrete mix	LD-15	LD-16	LD-17	LD-18	LD-19	LD-20	LD-21
Binders:							
Cement (kg/m^3)	386	386	386	386	386	386	270
Silica fume (kg/m^3)							
GGBFS (kg/m^3)							116
Total binder content (kg/m^3)	386	386	386	386	386	386	386
Water:							
Water (L/m^3)	147	142	147	149	147	147	147
Water/binder ratio	0.382	0.369	0.382	0.385	0.380	0.380	0.380
Aggregates:							
Coarse aggregate (kg/m^3)	997	997	997	997	1009	1009	1009
Fine aggregate (kg/m^3)	810	810	810	810	806	806	797
Chemical admixtures:							
HRWR (mL/100 kg)	619	619	769	761	587	704	704
NRWR (mL/100 kg)	587		652	580			
AEA (mL/100 kg)	55	46	46	33	33	33	33
Fresh concrete properties:							
Slump (mm)	178	216	184	152	203	178	165
Air content (%)	9	12.5	10	3.7	8.5	~8.6	6.8
Unit weight (kg/m^3)	2300	2219	2260	2430	2323	2308	2344
Fresh concrete properties (30 minutes):							
Slump (mm)	102	140	121	146	102	~90	114
Air content (%)	6.4	10.5	6.9	3.3	7.7	~7.5	6.4
Unit weight (kg/m^3)	2376	2263	2358	2443	2348	2350	2355
Concrete strength (MPa):							
1 day						19	
3 days						39	36
7 days						49	50
14 days							
28 days						66	72
Admixture types:							
HRWR	Adva F	PS 1140	Adva F	PS 1140	PS 1140	PS 1140	PS 1140
NRWR	Dara 100		Dara 100	Rhe1000			
AEA	Darex II	Micro-A	Darex II	Micro-A	Micro-A	Micro-A	Micro-A

TABLE C.10
Mix proportions and concrete properties of deck concrete mixes LD-22 to LD-28 (SI units)

Concrete mix	LD-22	LD-23	LD-24	LD-25	LD-26	LD-27	LD-28
Binders:							
Cement (kg/m^3)	366	262	250	231	193	361	154
Silica fume (kg/m^3)	19	8	20			25	
GGBFS (kg/m^3)		116	116	154	193		231
Total binder content (kg/m^3)	386	386	386	386	386	386	386
Water:							
Water (L/m^3)	147	147	147	147	147	147	147
Water/binder ratio	0.380	0.380	0.380	0.380	0.380	0.380	0.380
Aggregates:							
Coarse aggregate (kg/m^3)	1009	1009	1009	1009	1009	1009	1009
Fine aggregate (kg/m^3)	799	794	790	794	791	796	788
Chemical admixtures:							
HRWR (mL/100 kg)	838	717	717	535	554	619	567
NRWR (mL/100 kg)							
AEA (mL/100 kg)	33	36	29	29	26	26	26
Fresh concrete properties:							
Slump (mm)	184	197	146	146	184	152	203
Air content (%)	10	10.3	8.8	10	8	9.5	5.2
Unit weight (kg/m^3)	2273	2271	2305	2262	2316	2255	2416
Fresh concrete properties (30 minutes):							
Slump (mm)	114	108	83	76			
Air content (%)	9	9.7	7.7				
Unit weight (kg/m^3)	2292	2284	2323				
Concrete strength (MPa):							
1 day				7	7	17	7
3 days	36	28	32	24	24	35	28
7 days	48	38	48	37	36	43	40
14 days							
28 days	64	60	72	58	57	61	58
Admixture types:							
HRWR	PS 1140	PS 1140	PS 1140	PS 1140	PS 1140	PS 1140	PS 1140
NRWR							
AEA	Micro-A	Micro-A	Micro-A	Micro-A	Micro-A	Micro-A	Micro-A

TABLE C.11
Mix proportions and concrete properties of deck concrete mixes LD-29 to LD-35 (SI units)

Concrete mix	LD-29	LD-30	LD-31	LD-32	LD-33	LD-34	LD-35
Binders:							
Cement (kg/m^3)	355	212	173	116	355	218	179
Silica fume (kg/m^3)	31	20	20		31	14	14
GGBFS (kg/m^3)		154	193	270		154	193
Total binder content (kg/m^3)	386	386	386	386	386	386	386
Water:							
Water (L/m^3)	147	147	147	147	147	147	147
Water/binder ratio	0.380	0.379	0.380	0.380	0.380	0.380	0.380
Aggregates:							
Coarse aggregate (kg/m^3)	1009	1009	1009	1009	1009	1009	1009
Fine aggregate (kg/m^3)	794	787	784	785	794	789	786
Chemical admixtures:							
HRWR (mL/100 kg)	822	691	639	593	737	678	652
NRWR (mL/100 kg)							
AEA (mL/100 kg)	24	26	26	31	18	26	26
Fresh concrete properties:							
Slump (mm)	152	114	184	210	184	191	165
Air content (%)	11	7.8	6.8	7.4	9.2	9.3	8.7
Unit weight (kg/m^3)	2228	2308	2326	2313	2275	2283	2292
Fresh concrete properties (30 minutes):							
Slump (mm)	95	76	121	152		146	114
Air content (%)							
Unit weight (kg/m^3)	2263						
Concrete strength (MPa):							
1 day	20	15	11	4	19	15	12
3 days	34	33	23	19	36	28	27
7 days	44	46	43	35		41	
14 days							
28 days	60	69		47	64	61	54
Admixture types:							
HRWR	PS 1140	PS 1140	PS 1140	PS 1140	PS 1140	PS 1140	PS 1140
NRWR							
AEA	Micro-A	Micro-A	Micro-A	Micro-A	Micro-A	Micro-A	Micro-A

TABLE C.12
Mix proportions and concrete properties of deck concrete mixes LD-36 to LD-42 (SI units)

Concrete mix	LD-36	LD-37	LD-38	LD-39	LD-40	LD-41	LD-42
Binders:							
Cement (kg/m^3)	386	386	386	386	386	386	386
Silica fume (kg/m^3)							
GGBFS (kg/m^3)							
Total binder content (kg/m^3)	386	386	386	386	386	386	386
Water:							
Water (L/m^3)	147	147	147	147	147	147	147
Water/binder ratio	0.380	0.380	0.380	0.380	0.380	0.380	0.380
Aggregates:							
Coarse aggregate (kg/m^3)	1009	1009	1009	1009	1009	1009	1009
Fine aggregate (kg/m^3)	806	806	806	806	806	806	806
Chemical admixtures:							
HRWR (mL/100 kg)	717	698	717	665	645	717	652
NRWR (mL/100 kg)							
AEA (mL/100 kg)	20	20	49	76	39	115	149
SRA (% weight of cem.)			1.0	1.0	0.5	1.5	2.0
Fresh concrete properties (initial):							
Slump (mm)	152		203	210	210	203	197
Air content (%)	8.5	8.8	6.2	8.4	6.1	9.4	6.0
Unit weight (kg/m^3)	2310	2319	2384	2323	2384	2300	2372
Fresh concrete properties (30 minutes):							
Slump (mm)							
Air content (%)			5.5				
Unit weight (kg/m^3)			2422				
Concrete strength (MPa):							
1 day (30 hours)		21		17	18	(17)	11
3 days	39					40	
7 days	52			52	58	53	55
14 days							
28 days (30 days)	62	63		67	(69)	68	(71)
91 days		69		71	77		
Admixture types:							
HRWR	PS 1140	PS 1140	PS 1140	PS 1140	PS 1140	PS 1140	PS 1140
NRWR							
AEA	Micro-A	Micro-A	Micro-A	Micro-A	Micro-A	Micro-A	Micro-A
SRA			Eclipse	Eclipse	Eclipse	Eclipse	Eclipse

TABLE C.13
Mix proportions and concrete properties of deck concrete mixes LD-43 to LD-49 (SI units)

Concrete mix	LD-43	LD-44	LD-45	LD-46	LD-47	LD-48	LD-49
Binders:							
Cement (kg/m^3)	390	390	390	386	386	386	390
Silica fume (kg/m^3)							
GGBFS (kg/m^3)							
Total binder content (kg/m^3)	390	390	390	386	386	386	390
Water:							
Water (L/m^3)	171	173	173	147	147	147	173
Water/binder ratio	0.437	0.443	0.443	0.380	0.380	0.380	0.443
Aggregates:							
Coarse aggregate (kg/m^3)	1038	1038	1038	1009	1009	1009	1038
Fine aggregate (kg/m^3)	702	702	702	966	806	806	702
Chemical admixtures:							
HRWR (mL/100 kg)	326	293	293	782	522	717	326
NRWR (mL/100 kg)							
AEA (mL/100 kg)	33	16	16		150	125	14
SRA (% weight of cem.)				2.0	2.0	2.0	
Fresh concrete properties (initial):							
Slump (mm)	102	89	140	159	184	197	64
Air content (%)	10.5	7.4	8	2.5	11	6.75	5.1
Unit weight (kg/m^3)	2236	2313	2292	2464	2223	2358	2371
Fresh concrete properties (30 minutes):							
Slump (mm)					165		
Air content (%)					10.5		
Unit weight (kg/m^3)					2246		
Concrete strength (MPa):							
1 day		10	12				
3 days				42		35	37
7 days		43		55		47	
14 days							
28 days		52	53	68		59	
91 days							
Admixture types:							
HRWR	PS 1140	PS 1140	PS 1140	PS 1140	PS 1140	PS 1140	PS 1140
NRWR							
AEA	Micro-A	Micro-A	Micro-A		Micro-A	Micro-A	Micro-A
SRA				Eclipse	Eclipse	Eclipse	

TABLE C.14
Mix proportions and concrete properties of deck concrete mixes LD-1 to LD-7 (US customary units)

Concrete mix	LD-1	LD-2	LD-3	LD-4	LD-5	LD-6	LD-7
Binders:							
Cement (lb/yd^3)	648	648	645	645	645	600	600
Silica fume (lb/yd^3)							
GGBFS (lb/yd^3)							
Total binder content (lb/yd^3)	648	648	645	645	645	600	600
Water:							
Water (lb/yd^3)	252	252	239	239	239	229	228
Water/binder ratio	0.389	0.389	0.370	0.370	0.370	0.382	0.380
Aggregates:							
Coarse aggregate (lb/yd^3)	1728	1728	1668	1669	1686	1700	1700
Fine aggregate (lb/yd^3)	1310	1310	1348	1349	1323	1438	1438
Chemical admixtures:							
HRWR (oz/cwt)	9.5	6.8	8.1	9.4	6.6	11.1	11.3
NRWR (oz/cwt)	0.0	4.2	8.6	4.2	4.2	3.9	
AEA (oz/cwt)	3.10	2.11	1.56	1.42	1.42	1.52	0.76
Fresh concrete properties:							
Slump (in.)	8.5	7.25	8.5	9.5	7.75	8.75	6.25
Air content (%)	9.8	9.0	11.3	7.5	7.7	12.0	6.4
Unit weight (lb/ft^3)	144.0	143.6	139.4	145.6	146.2	139.8	148.6
Concrete strength (ksi):							
1 day				2.49	2.29	1.55	2.84
3 days						5.55	7.10
7 days			5.07	7.16	6.49		9.85
14 days						8.57	9.83
28 days (48 days)			6.27	(8.81)	8.42	8.04	10.82
56 days						9.25	10.92
1 year						10.74	
Admixture types:							
HRWR	Adva F	Adva F	Adva F	Adva F	Adva F	Adva F	Adva F
NRWR		Darac55	Darac55	Darac55	Darac55	Darac55	
AEA	Darex II	Darex II	Darex II	Darex II	Darex II	Dara1400	Dara1400

TABLE C.15
Mix proportions and concrete properties of deck concrete mixes LD-8 to LD-14 (US customary units)

Concrete mix	LD-8	LD-9	LD-10	LD-11	LD-12	LD-13	LD-14
Binders:							
Cement (lb/yd^3)	650	550	550	550	550	385	523
Silica fume (lb/yd^3)							28
GGBFS (lb/yd^3)						165	
Total binder content (lb/yd^3)	650	550	550	550	550	550	550
Water:							
Water (lb/yd^3)	247	209	211	215	209	209	209
Water/binder ratio	0.380	0.380	0.383	0.390	0.380	0.380	0.380
Aggregates:							
Coarse aggregate (lb/yd^3)	1700	1650	1650	1650	1650	1650	1650
Fine aggregate (lb/yd^3)	1345	1581	1581	1581	1581	1568	1570
Chemical admixtures:							
HRWR (oz/cwt)	13.0	13.8	31.8	38.4	32.4	15.4	15.8
NRWR (oz/cwt)				3.0			
AEA (oz/cwt)	0.77	0.75	1.22	0.66	0.83	0.75	0.66
Fresh concrete properties:							
Slump (in.)	8.25	8.25	6	7	5	6.75	6
Air content (%)	6.8	8.6	9.1	5.6	7.8	9.8	9.5
Unit weight (lb/ft^3)	147.8	146.0	144.4	149.7	146.6	143.0	142.8
Concrete strength (ksi):							
1 day	2.84	2.43	1.09	0.00	1.31	1.81	2.05
3 days	7.18	5.89	6.47	5.71	5.97	4.88	4.95
7 days	8.67	7.90	8.71	8.00	7.62	6.80	7.34
14 days	10.48	9.23	8.79	9.45	8.83	7.72	9.33
28 days	10.40	9.45	9.51	10.86	9.49	8.81	9.61
56 days	11.16				9.59		9.81
91 days						11.10	10.50
1 year		10.19	11.50	11.98			
Admixture types:							
HRWR	Adva F	Adva F	Darac100	Rhe1000	Rhe1000	Adva F	Adva F
NRWR				P100-XR			
AEA	Dara1400	Dara1400	Dara1400	Micro-A	Micro-A	Darex II	Darex II

TABLE C.16
Mix proportions and concrete properties of deck concrete mixes LD-15 to LD-21 (US customary units)

Concrete mix	LD-15	LD-16	LD-17	LD-18	LD-19	LD-20	LD-21
Binders:							
Cement (lb/yd^3)	650	650	650	650	650	650	455
Silica fume (lb/yd^3)							
GGBFS (lb/yd^3)							195
Total binder content (lb/yd^3)	650	650	650	650	650	650	650
Water:							
Water (lb/yd^3)	249	240	248	250	247	247	247
Water/binder ratio	0.382	0.369	0.382	0.385	0.380	0.380	0.380
Aggregates:							
Coarse aggregate (lb/yd^3)	1680	1680	1680	1680	1700	1700	1700
Fine aggregate (lb/yd^3)	1365	1365	1365	1365	1358	1358	1343
Chemical admixtures:							
HRWR (oz/cwt)	9.5	9.5	11.8	11.7	9.0	10.8	10.8
NRWR (oz/cwt)	9.0		10.0	8.9			
AEA (oz/cwt)	0.84	0.70	0.70	0.51	0.50	0.50	0.50
Fresh concrete properties (initial):							
Slump (in.)	7	8.5	7.25	6	8	7	6.5
Air content (%)	9.0	12.5	10.0	3.7	8.5	~8.6	6.8
Unit weight (lb/ft^3)	143.6	138.5	141.1	151.7	145.0	144.1	146.3
Fresh concrete properties (30 minutes):							
Slump (in.)	4	5.5	4.75	5.75	4	~3.5	4.5
Air content (%)	6.4	10.5	6.9	3.3	7.7	~7.5	6.4
Unit weight (lb/ft^3)	148.3	141.3	147.2	152.5	146.6	146.7	147.0
Concrete strength (ksi):							
1 day						2.79	
3 days						5.71	5.23
7 days						7.12	7.28
14 days							
28 days						9.55	10.38
Admixture types:							
HRWR	Adva F	PS 1140	Adva F	PS 1140	PS 1140	PS 1140	PS 1140
NRWR	Dara 100		Dara 100	Rhe1000			
AEA	Darex II	Micro-A	Darex II	Micro-A	Micro-A	Micro-A	Micro-A

TABLE C.17
Mix proportions and concrete properties of deck concrete mixes LD-22 to LD-28 (US customary units)

Concrete mix	LD-22	LD-23	LD-24	LD-25	LD-26	LD-27	LD-28
Binders:							
Cement (lb/yd^3)	618	442	422	390	325	608	260
Silica fume (lb/yd^3)	33	13	33			42	
GGBFS (lb/yd^3)		195	195	260	325		390
Total binder content (lb/yd^3)	650	650	650	650	650	650	650
Water:							
Water (lb/yd^3)	247	247	247	247	247	247	247
Water/binder ratio	0.380	0.380	0.380	0.380	0.380	0.380	0.380
Aggregates:							
Coarse aggregate (lb/yd^3)	1700	1700	1700	1700	1700	1700	1700
Fine aggregate (lb/yd^3)	1346	1338	1331	1338	1333	1342	1328
Chemical admixtures:							
HRWR (oz/cwt)	12.9	11.0	11.0	8.2	8.5	9.5	8.7
NRWR (oz/cwt)							
AEA (oz/cwt)	0.50	0.55	0.45	0.45	0.40	0.40	0.40
Fresh concrete properties (initial):							
Slump (in.)	7.25	7.75	5.75	5.75	7.25	6	8
Air content (%)	10.0	10.3	8.8	10.0	8.0	9.5	5.2
Unit weight (lb/ft^3)	141.9	141.8	143.9	141.2	144.6	140.8	150.8
Fresh concrete properties (30 minutes):							
Slump (in.)	4.5	4.25	3.25	3			
Air content (%)	9.0	9.7	7.7				
Unit weight (lb/ft^3)	143.1	142.6	145.0				
Concrete strength (ksi):							
1 day				1.03	0.95	2.41	1.05
3 days	5.17	4.00	4.58	3.42	3.50	5.01	4.04
7 days	6.98	5.57	6.98	5.31	5.21	6.25	5.73
14 days							
28 days	9.35	8.63	10.50	8.40	8.32	8.79	8.38
Admixture types:							
HRWR	PS 1140	PS 1140	PS 1140	PS 1140	PS 1140	PS 1140	PS 1140
NRWR							
AEA	Micro-A	Micro-A	Micro-A	Micro-A	Micro-A	Micro-A	Micro-A

TABLE C.18
Mix proportions and concrete properties of deck concrete mixes LD-29 to LD-35 (US customary units)

Concrete mix	LD-29	LD-30	LD-31	LD-32	LD-33	LD-34	LD-35
Binders:							
Cement (lb/yd^3)	598	358	292	195	598	367	302
Silica fume (lb/yd^3)	52	33	33	0	52	23	23
GGBFS (lb/yd^3)	0	260	325	455	0	260	325
Total binder content (lb/yd^3)	650	651	650	650	650	650	650
Water:							
Water (lb/yd^3)	247	247	247	247	247	247	247
Water/binder ratio	0.380	0.379	0.380	0.380	0.380	0.380	0.380
Aggregates:							
Coarse aggregate (lb/yd^3)	1700	1700	1700	1700	1700	1700	1700
Fine aggregate (lb/yd^3)	1339	1326	1321	1323	1339	1330	1325
Chemical admixtures:							
HRWR (oz/cwt)	12.6	10.6	9.8	9.1	11.3	10.4	10.0
NRWR (oz/cwt)	0.0	0.0	0.0	0.0	0.0	0.0	0.0
AEA (oz/cwt)	0.37	0.40	0.40	0.47	0.28	0.40	0.40
Fresh concrete properties (initial):							
Slump (in.)	6	4.5	7.25	8.25	7.25	7.5	6.5
Air content (%)	11.0	7.8	6.8	7.4	9.2	9.3	8.7
Unit weight (lb/ft^3)	139.1	144.1	145.2	144.4	142.0	142.5	143.1
Fresh concrete properties (30 minutes):							
Slump (in.)	3.75	3	4.75	6		5.75	4.5
Air content (%)							
Unit weight (lb/ft^3)	141.3						
Concrete strength (ksi):							
1 day	2.94	2.17	1.59	0.62	2.79	2.21	1.69
3 days	4.87	4.83	3.32	2.83	5.25	4.06	3.86
7 days	6.33	6.66	6.19	5.03		5.95	
14 days							
28 days	8.67	9.97		6.84	9.29	8.87	7.80
Admixture types:							
HRWR	PS 1140	PS 1140	PS 1140	PS 1140	PS 1140	PS 1140	PS 1140
NRWR							
AEA	Micro-A	Micro-A	Micro-A	Micro-A	Micro-A	Micro-A	Micro-A

TABLE C.19
Mix proportions and concrete properties of deck concrete mixes LD-36 to LD-42 (US customary units)

Concrete mix	LD-36	LD-37	LD-38	LD-39	LD-40	LD-41	LD-42
Binders:							
Cement (lb/yd^3)	650	650	650	650	650	650	650
Silica fume (lb/yd^3)							
GGBFS (lb/yd^3)							
Total binder content (lb/yd^3)	650	650	650	650	650	650	650
Water:							
Water (lb/yd^3)	247	247	247	247	247	247	247
Water/binder ratio	0.380	0.380	0.380	0.380	0.380	0.380	0.380
Aggregates:							
Coarse aggregate (lb/yd^3)	1700	1700	1700	1700	1700	1700	1700
Fine aggregate (lb/yd^3)	1358	1358	1358	1358	1358	1358	1358
Chemical admixtures:							
HRWR (oz/cwt)	11.0	10.7	11.0	10.2	9.9	11.0	10.0
NRWR (oz/cwt)							
AEA (oz/cwt)	0.30	0.30	0.75	1.16	0.60	1.77	2.29
SRA (% weight of cem.)			1.00	1.00	0.50	1.50	2.00
Fresh concrete properties (initial):							
Slump (in.)	6		8	8.25	8.25	8	7.75
Air content (%)	8.5	8.8	6.2	8.4	6.1	9.4	6.0
Unit weight (lb/ft^3)	144.2	144.8	148.8	145.0	148.8	143.6	148.1
Fresh concrete properties (30 minutes):							
Slump (in.)							
Air content (%)			5.5				
Unit weight (lb/ft^3)			151.2				
Concrete strength (ksi):							
1 day (30 hours)		3.10		2.51	2.55	(2.47)	1.61
3 days	5.67					5.81	
7 days	7.48			7.48	8.36	7.74	8.04
14 days							
28 days (30 days)	8.93	9.13		9.65	(10.05)	9.83	(10.25)
91 days		9.97		10.23	11.10		
Admixture types:							
HRWR	PS 1140	PS 1140	PS 1140	PS 1140	PS 1140	PS 1140	PS 1140
NRWR							
AEA	Micro-A	Micro-A	Micro-A	Micro-A	Micro-A	Micro-A	Micro-A
SRA			Eclipse	Eclipse	Eclipse	Eclipse	Eclipse

TABLE C.20
Mix proportions and concrete properties of deck concrete mixes LD-43 to LD-49 (US customary units)

Concrete mix	LD-43	LD-44	LD-45	LD-46	LD-47	LD-48	LD-49
Binders:							
Cement (lb/yd^3)	658	658	658	650	650	650	658
Silica fume (lb/yd^3)	0	0	0	0	0	0	0
GGBFS (lb/yd^3)	0	0	0	0	0	0	0
Total binder content (lb/yd^3)	658	658	658	650	650	650	658
Water:							
Water (lb/yd^3)	288	291	291	247	247	247	291
Water/binder ratio	0.437	0.443	0.443	0.380	0.380	0.380	0.443
Aggregates:							
Coarse aggregate (lb/yd^3)	1750	1750	1750	1700	1700	1700	1750
Fine aggregate (lb/yd^3)	1183	1183	1183	1629	1358	1358	1183
Chemical admixtures:							
HRWR (oz/cwt)	5.0	4.5	4.5	12.0	8.0	11.0	5.0
NRWR (oz/cwt)							
AEA (oz/cwt)	0.50	0.25	0.25		2.30	1.92	0.22
SRA (% weight of cem.)				2.00	2.00	2.00	
Fresh concrete properties (initial):							
Slump (in.)	4	3.5	5.5	6.25	7.25	7.75	2.5
Air content (%)	10.5	7.4	8.0	2.5	11.0	6.8	5.1
Unit weight (lb/ft^3)	139.6	144.4	143.1	153.8	138.8	147.2	148.0
Fresh concrete properties (30 minutes):							
Slump (in.)					6.5		
Air content (%)					10.5		
Unit weight (lb/ft^3)					140.2		
Concrete strength (ksi):							
1 day		1.45	1.77				
3 days				6.05		5.13	5.31
7 days		6.25		8.04		6.76	
14 days							
28 days		7.60	7.62	9.89		8.57	
91 days							
Admixture types:							
HRWR	PS 1140	PS 1140	PS 1140	PS 1140	PS 1140	PS 1140	PS 1140
NRWR							
AEA	Micro-A	Micro-A	Micro-A		Micro-A	Micro-A	Micro-A
SRA				Eclipse	Eclipse	Eclipse	

APPENDIX D. VIBRATING WIRE STRAIN GAGE READINGS

D.1 Single-Strand Development Length Specimen (Tables D.1 and D.2)

TABLE D.1
Vibrating wire strain gage data from single-strand development length Beam 3 (metric units)

	Age (days)	Strand stress (MPa)	Strain (10^{-6})	Change in strain (10^{-6})	Change in strand stress (MPa)	Loss (%)
Before cutting strand	0	1392.8	7088	0	0	0.0
After cutting, stripping, and blocking	0.5	1366.7	6955	−132.5	−26.0	−1.9
Before breaking	95	1306.8	6650	−437.6	−86.0	−6.2

TABLE D.2
Vibrating wire strain gage data from single-strand development length Beam 3 (US customary units)

	Age (days)	Strand stress (ksi)	Strain (10^{-6})	Change in strain (10^{-6})	Change in strand stress (ksi)	Loss (%)
Before cutting strand	0	202.0	7088	0	0	0.0
After cutting, stripping, and blocking	0.5	198.2	6955	−132.5	−3.8	−1.9
Before breaking	95	189.5	6650	−437.6	−12.5	−6.2

D.2 Multiple-Strand Development Specimen HPC-1 (Tables D.3 and D.4)

TABLE D.3
Vibrating wire strain gage data from multiple-strand development length specimen HPC-1 (metric units)

	Age (days)	Strand stress (MPa)	Strain (10^{-6})	Change in strain (10^{-6})	Change in strand stress (MPa)	Loss (%)
Before cutting strand	0	1392.8	7088	0	0.0	0.0
After cutting, stripping, and blocking	0	1319.0	6712	−375.6	−73.8	−5.3
	8	1286.9	6549	−539.0	−105.9	−7.6
Before breaking	14	1283.1	6529	−558.4	−109.7	−7.9

TABLE D.4
Vibrating wire strain gage data from multiple-strand development length specimen HPC-1 (US customary units)

	Age (days)	Strand stress (ksi)	Strain (10^{-6})	Change in strain (10^{-6})	Change in strand stress (ksi)	Loss (%)
Before cutting strand	0	202.0	7088	0	0	0.0
After cutting, stripping, and blocking	0	191.3	6712	−375.6	−10.7	−5.3
	8	186.6	6549	−539.0	−15.4	−7.6
Before breaking	14	186.1	6529	−558.4	−15.9	−7.9

D.3 Multiple-Strand Development Specimen HPC-2 (Tables D.5 and D.6)

TABLE D.5
Vibrating wire strain gage data from multiple-strand development length specimen HPC-2 (metric units)

	Age (days)	Strand stress (MPa)	Strain (10^{-6})	Change in strain (10^{-6})	Change in strand stress (MPa)	Loss (%)
Before cutting strand	0	1392.8	7088	0	0.0	0.0
After cutting, stripping, and blocking	0	1321.6	6725	−362.4	−71.2	−5.1
	8	1292.5	6577	−510.2	−100.3	−7.2
Before breaking	15	1287.6	6552	−535.5	−105.2	−7.6

TABLE D.6
Vibrating wire strain gage data from multiple-strand development length specimen HPC-2 (US customary units)

	Age (days)	Strand stress (ksi)	Strain (10^{-6})	Change in strain (10^{-6})	Change in strand stress (ksi)	Loss (%)
Before cutting strand	0	202.0	7088	0	0	0.0
After cutting, stripping, and blocking	0	191.7	6725	−362.4	−10.3	−5.1
	8	187.5	6577	−510.2	−14.5	−7.2
Before breaking	15	186.7	6552	−535.5	−15.3	−7.6

APPENDIX E. LOAD-DEFLECTION CURVES

E.1 Load-Deflection Curves for Single-Strand Specimens (Figures E.1 through E.6)

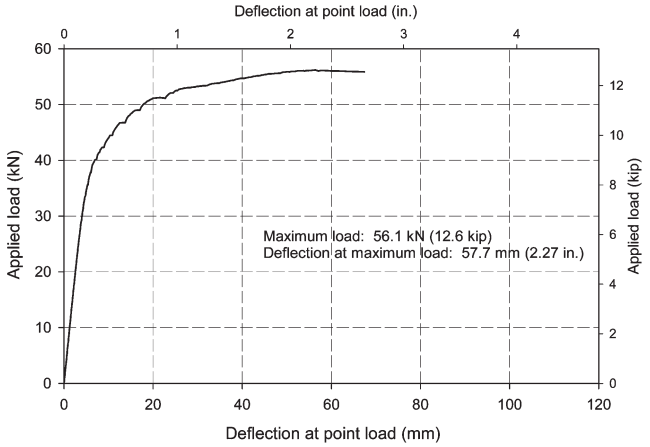

Figure E.1 Load-deflection curve for development length specimen 1S.

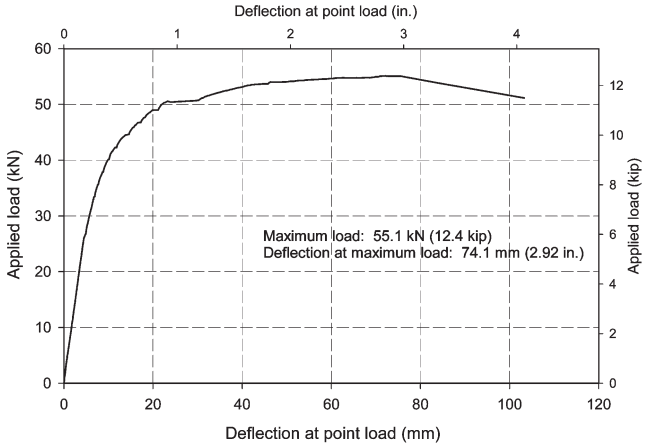

Figure E.2 Load-deflection curve for development length specimen 1L.

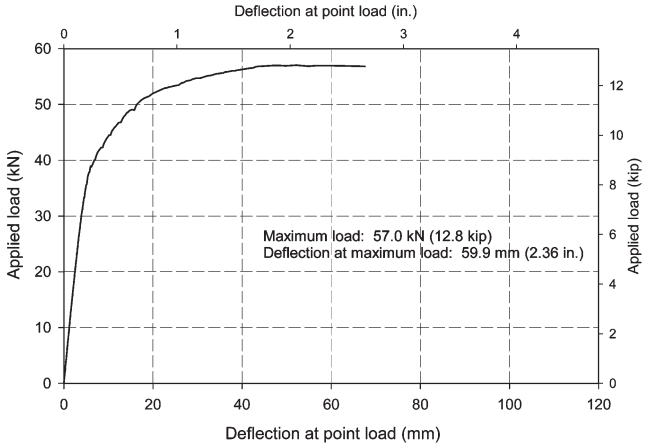

Figure E.3 Load-deflection curve for development length specimen 2S.

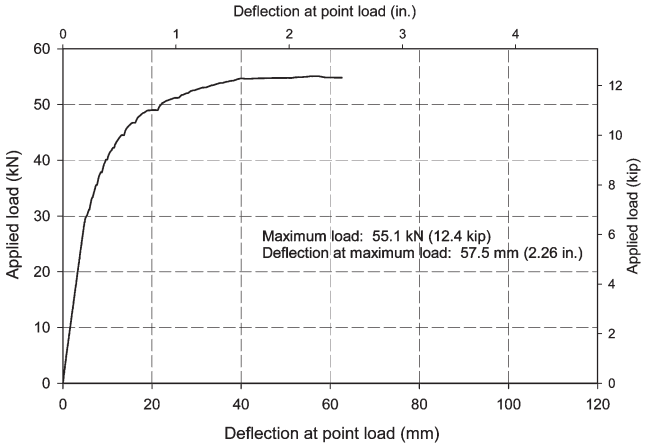

Figure E.4 Load-deflection curve for development length specimen 2L.

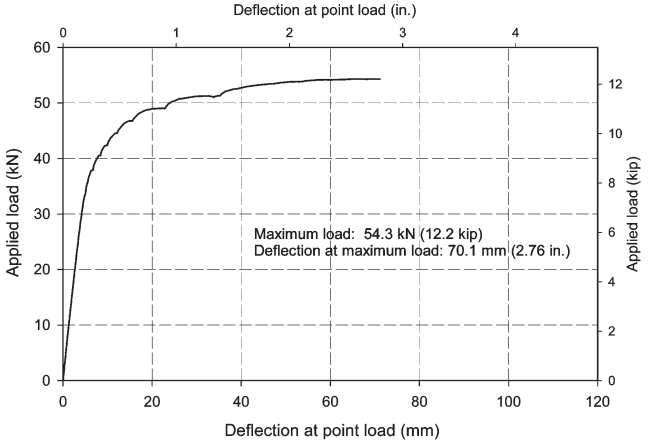

Figure E.5 Load-deflection curve for development length specimen 3S.

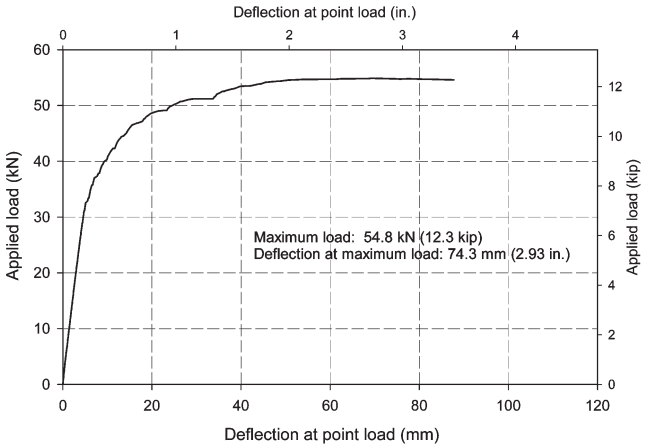

Figure E.6 Load-deflection curve for development length specimen 3L.

E.2 Load-Deflection Curves for Multiple-Strand Specimens (Figures E.7 and E.8)

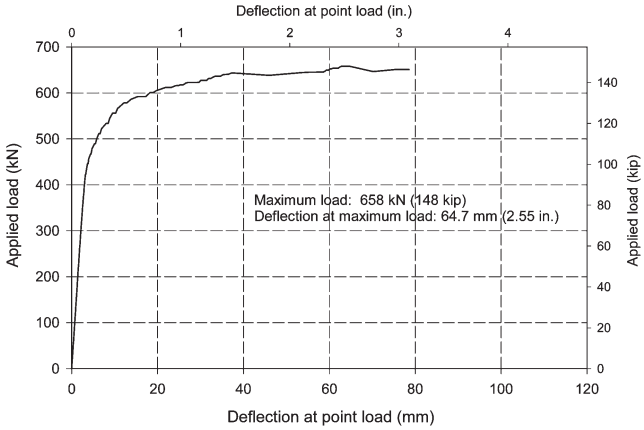

Figure E.7 Load-deflection curve for development length specimen HPC-1.

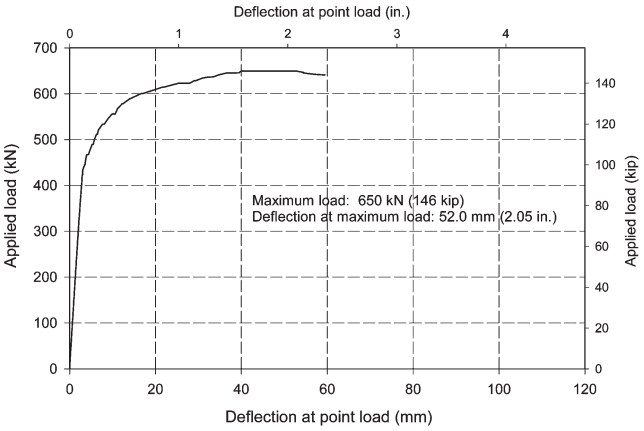

Figure E.8 Load-deflection curve for development length specimen HPC-2.

APPENDIX F. CRACK PATTERNS AND IMAGES

F.1 Crack Patterns and Images of Single-Strand Specimens

F.1.1 Single-Strand Development Length Specimen 1S (Figures F.1 through F.4)

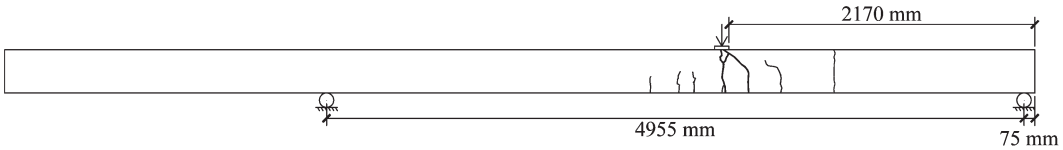

Figure F.1 Test setup and crack patterns for single-strand development length specimen 1S.

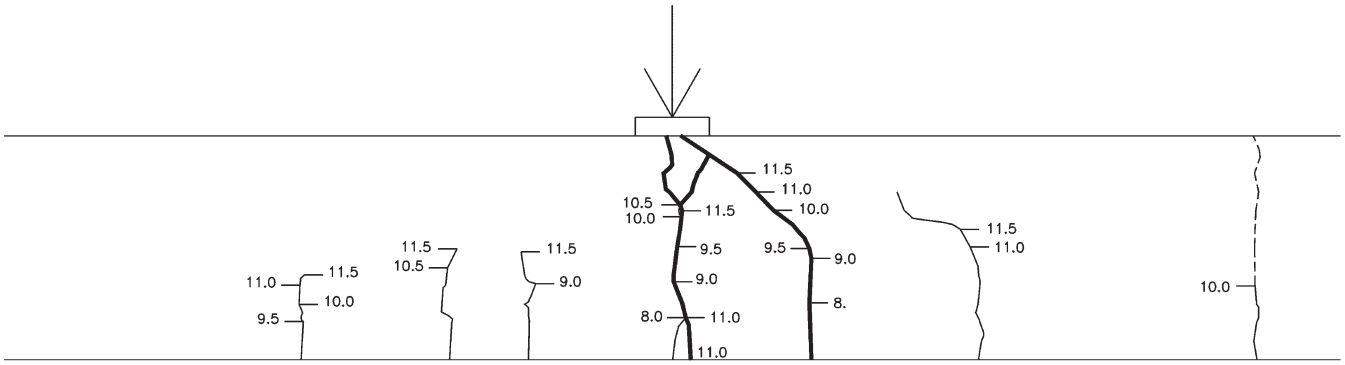

Figure F.2 Crack patterns at failure of single-strand development length specimen 1S.

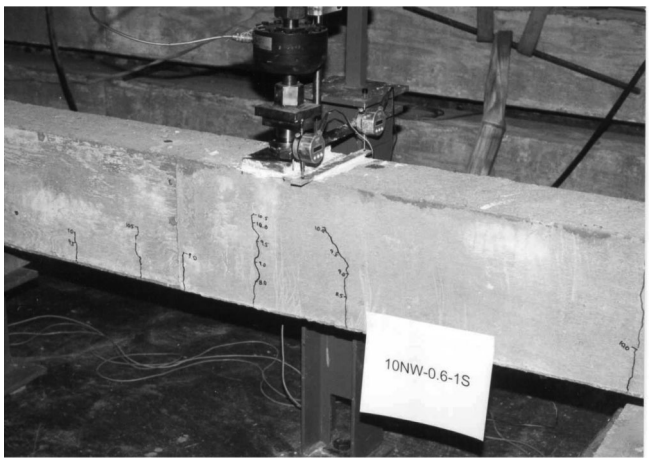

Figure F.3 Single-strand development length specimen 1S before failure.

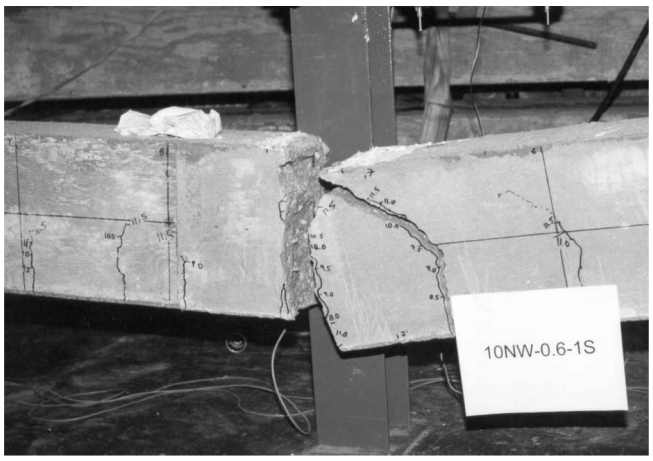

Figure F.4 Single-strand development length specimen 1S after failure.

F.1.2 Single-Strand Development Length Specimen 1L
(Figures F.5 through F.8)

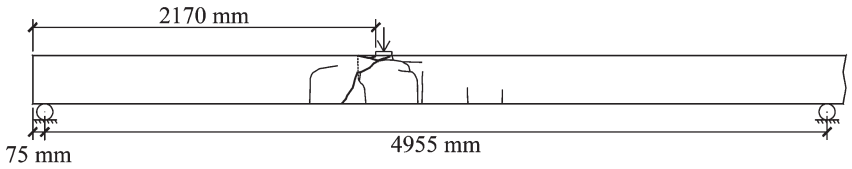

Figure F.5 Test setup and crack patterns for single-strand development length specimen 1L.

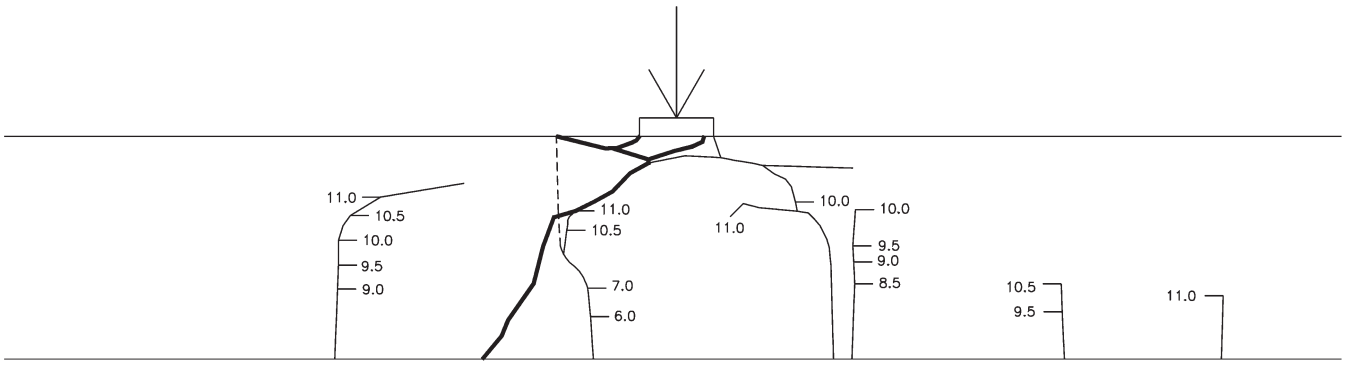

Figure F.6 Crack patterns at failure of single-strand development length specimen 1L.

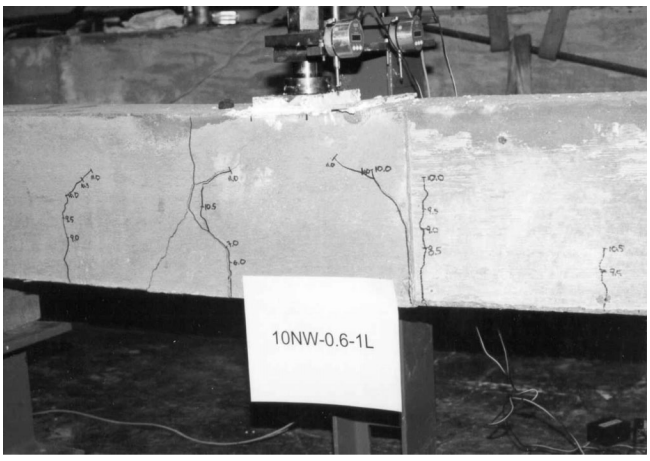

Figure F.7 Single-strand development length specimen 1L before failure.

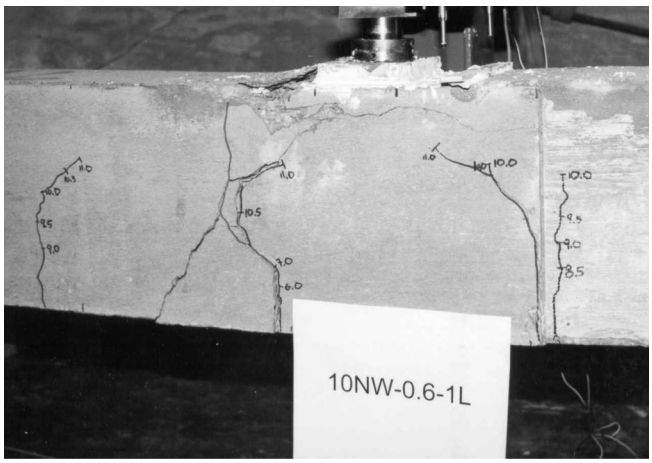

Figure F.8 Single-strand development length specimen 1L after failure.

F.1.3 Single-Strand Development Length Specimen 2S
(Figures F.9 through F.12)

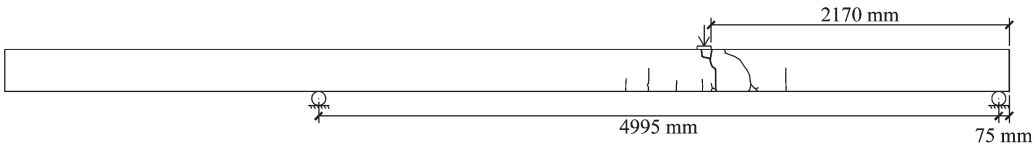

Figure F.9 Test setup and crack patterns for single-strand development length specimen 2S.

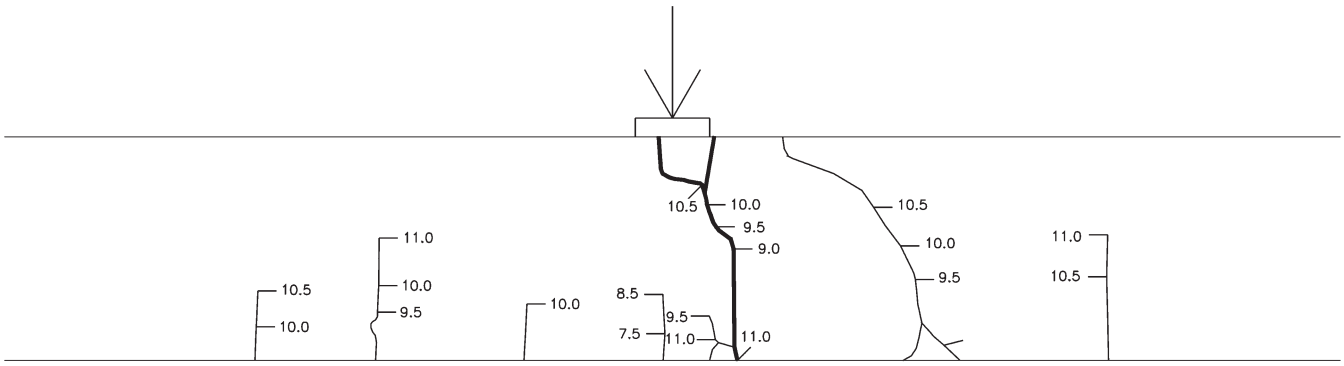

Figure F.10 Crack patterns at failure of single-strand development length specimen 2S.

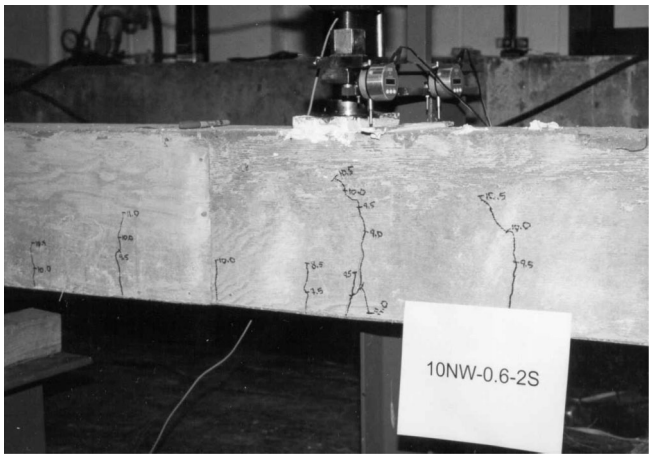

Figure F.11 Single-strand development length specimen 2S before failure.

Figure F.12 Single-strand development length specimen 2S after failure.

F.1.4 Single-Strand Development Length Specimen 2L
(Figures F.13 through F.16)

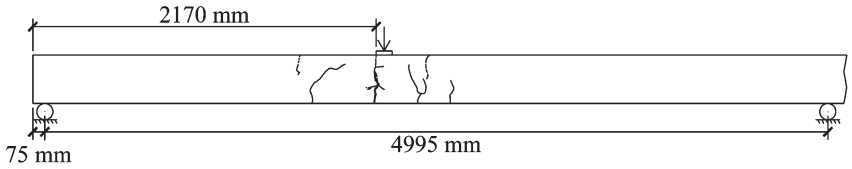

Figure F.13 Test setup and crack patterns for single-strand development length specimen 2L.

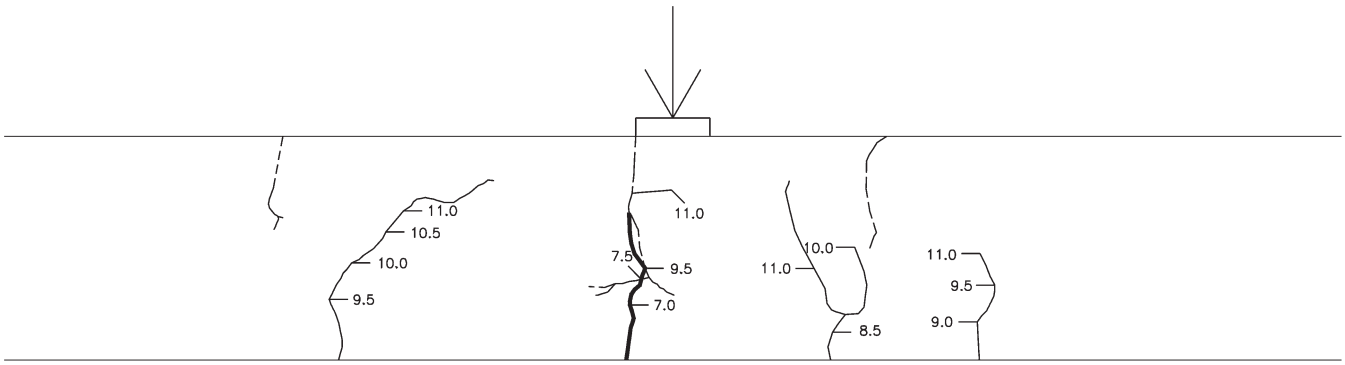

Figure F.14 Crack patterns at failure of single-strand development length specimen 2L.

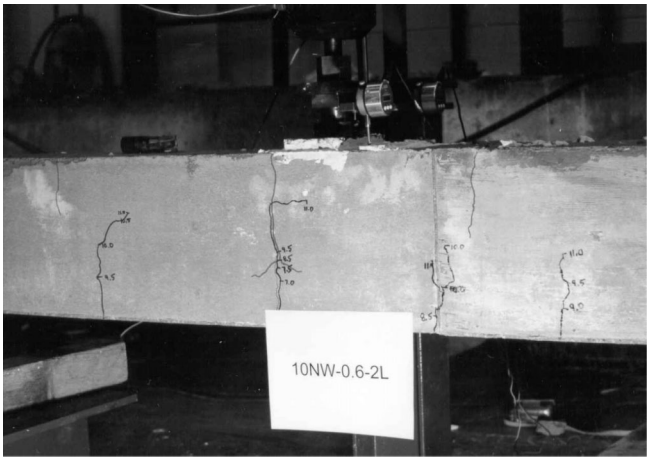

Figure F.15 Single-strand development length specimen 2L before failure.

Figure F.16 Single-strand development length specimen 2L after failure.

F.1.5 Single-Strand Development Length Specimen 3S
(Figures F.17 through F.20)

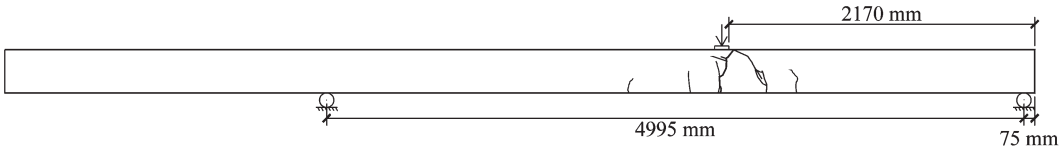

Figure F.17 Test setup and crack patterns for single-strand development length specimen 3S.

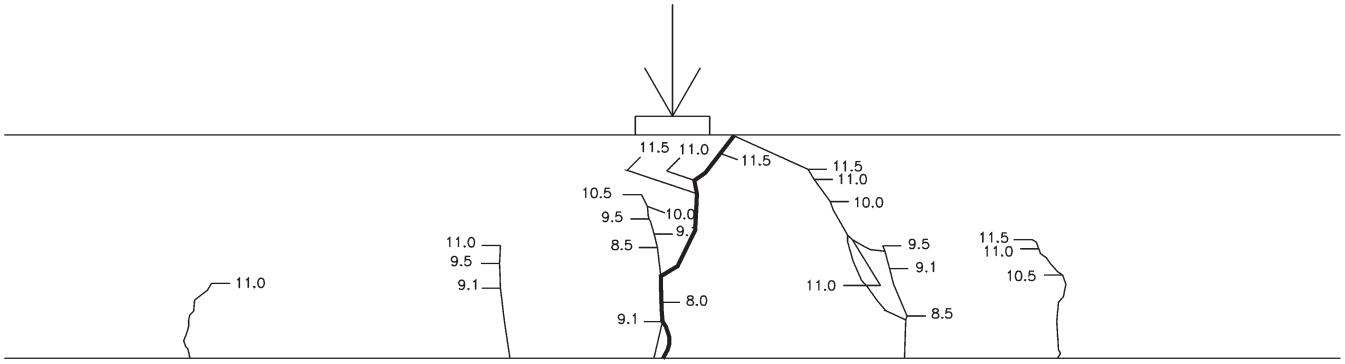

Figure F.18 Crack patterns at failure of single-strand development length specimen 3S.

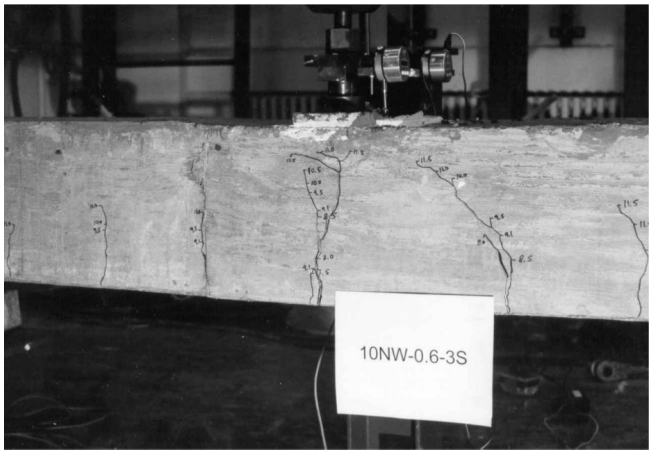

Figure F.19 Single-strand development length specimen 3S before failure.

Figure F.20 Single-strand development length specimen 3S after failure.

F.1.6 Single-Strand Development Length Specimen 3L
(Figures F.21 through F.24)

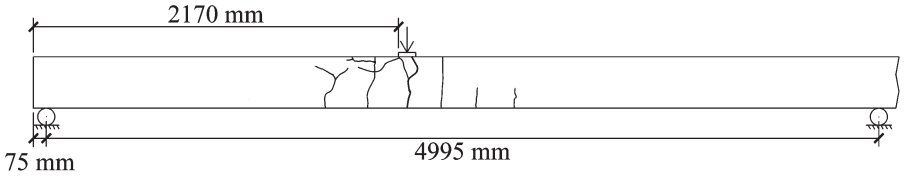

Figure F.21 Test setup and crack patterns for single-strand development length specimen 3L.

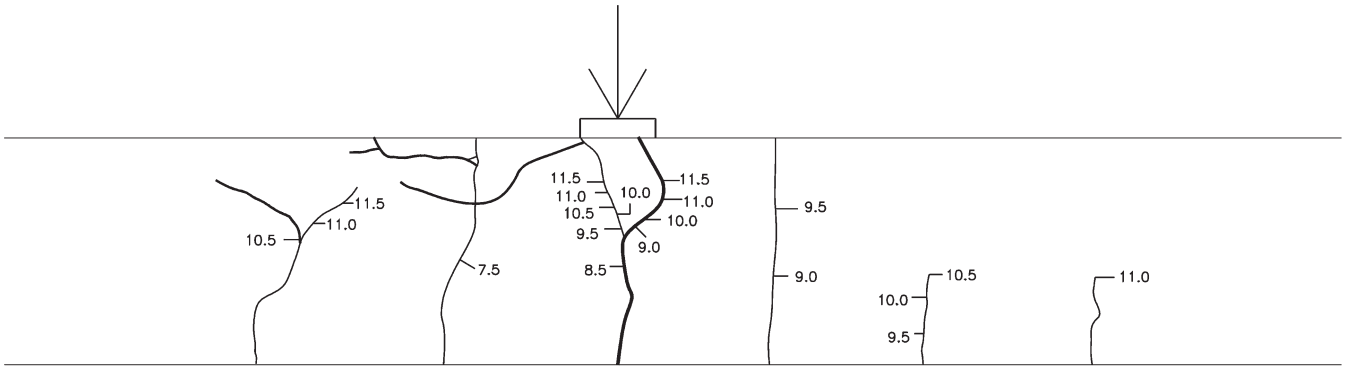

Figure F.22 Crack patterns at failure of single-strand development length specimen 3L.

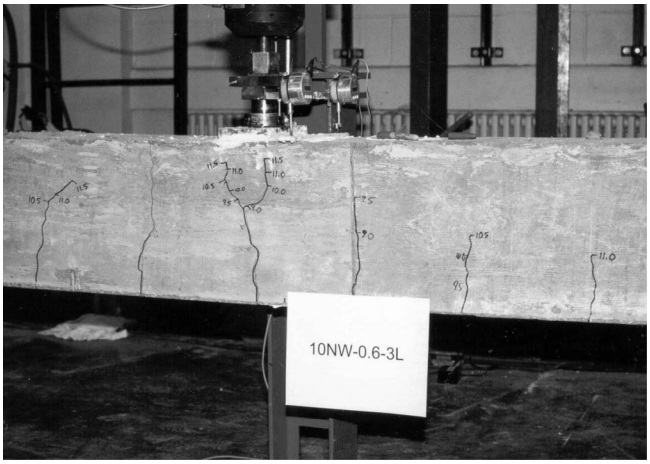

Figure F.23 Single-strand development length specimen 3L before failure.

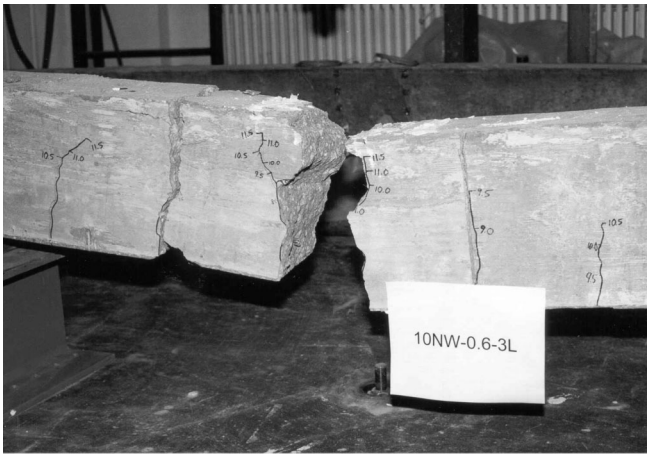

Figure F.24 Single-strand development length specimen 3L after failure.

F.2 Crack Patterns and Images of Multiple-Strand Specimens

F.2.1 Multiple-Strand Development Length Specimen HPC-1 (Figures F.25 through F.32)

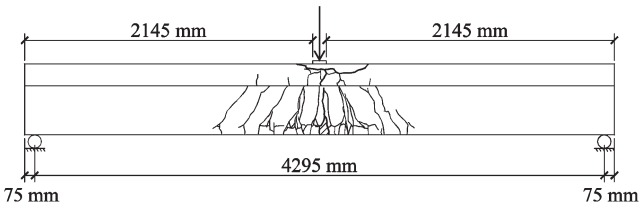

Figure F.25 Test setup and crack patterns for multiple-strand development length specimen HPC-1 (north face).

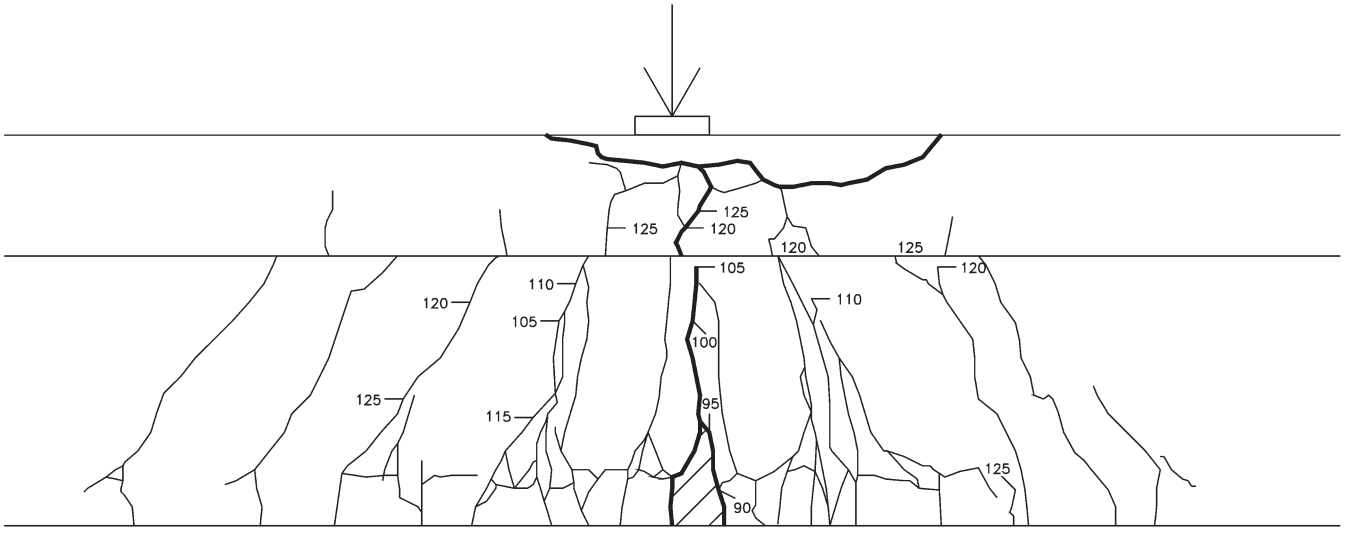

Figure F.26 Crack patterns at failure of multiple-strand development length specimen HPC-1 (north face).

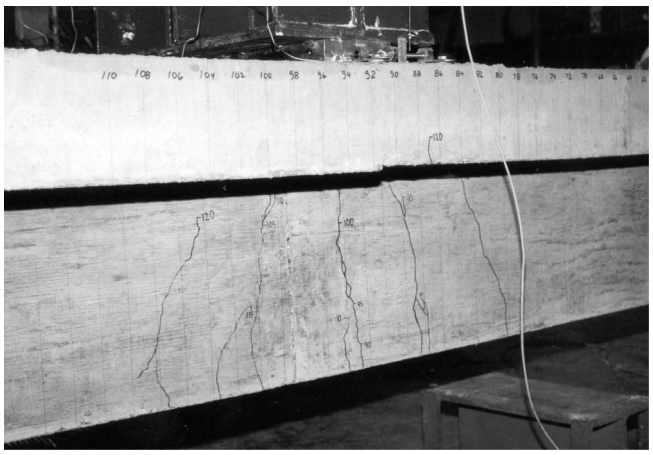

Figure F.27 Multiple-strand development length specimen HPC-1 before failure (north face).

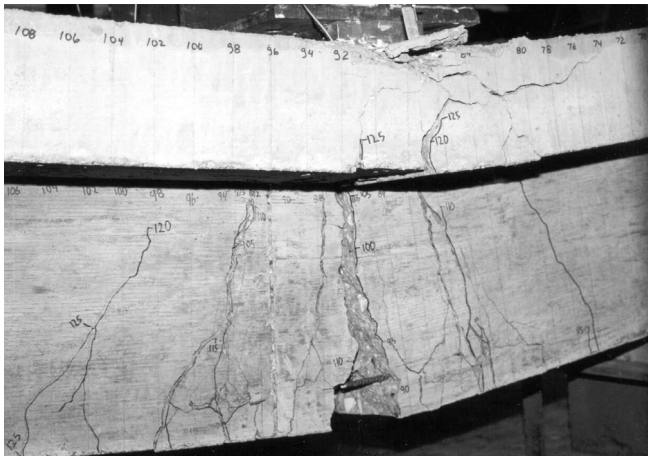

Figure F.28 Multiple-strand development length specimen HPC-1 after failure (north face).

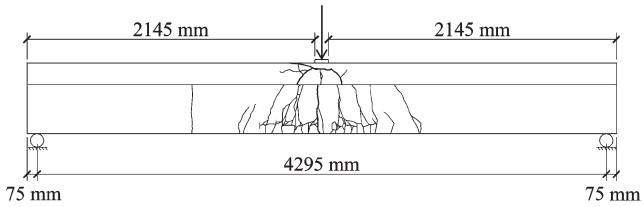

Figure F.29 Test setup and crack patterns for multiple-strand development length specimen HPC-1 (south face).

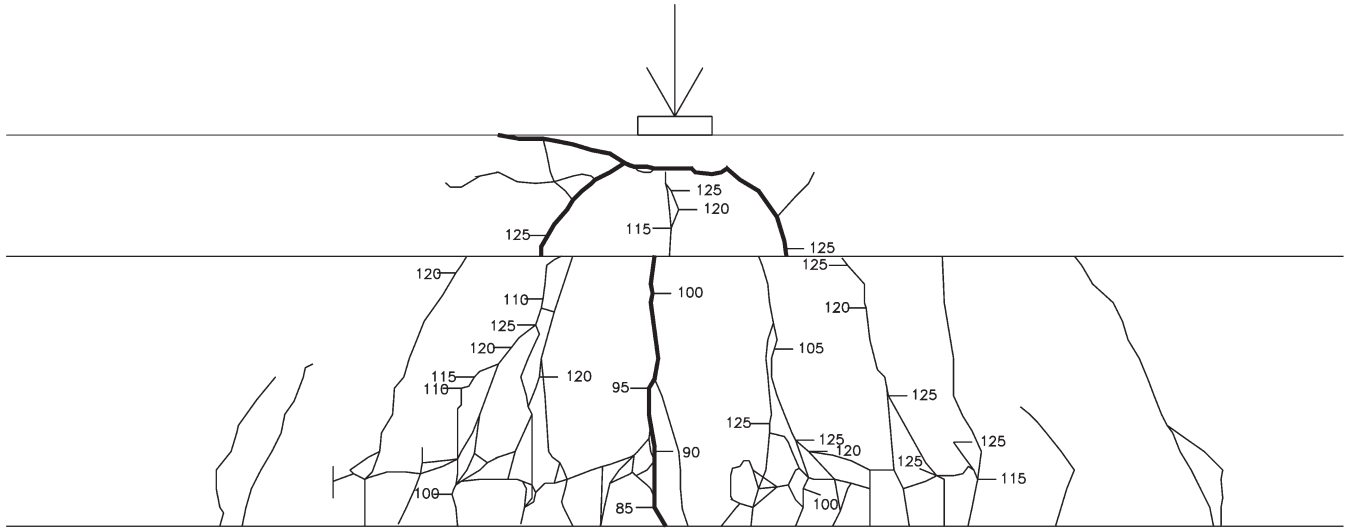

Figure F.30 Crack patterns at failure of multiple-strand development length specimen HPC-1 (south face).

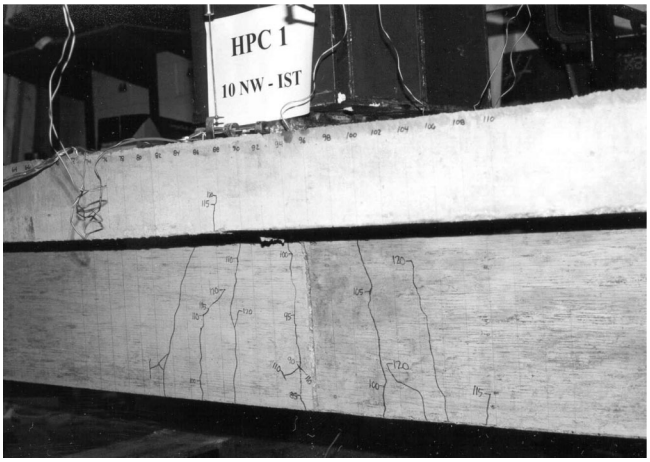

Figure F.31 Multiple-strand development length specimen HPC-1 before failure (south face).

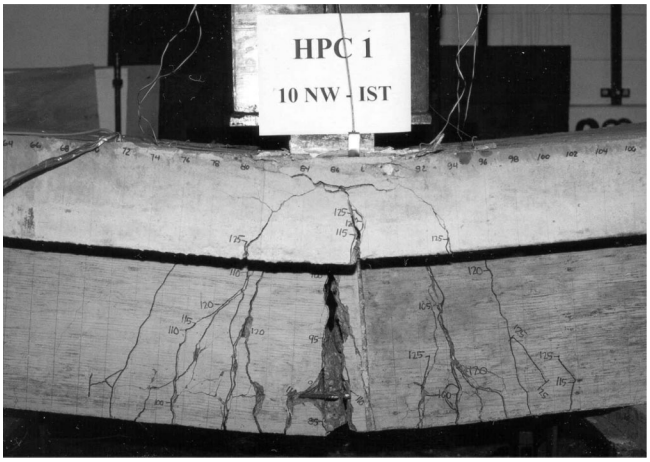

Figure F.32 Multiple-strand development length specimen HPC-1 after failure (south face).

F.2.2 Multiple-Strand Development Length Specimen HPC-2 (Figures F.33 through F.40)

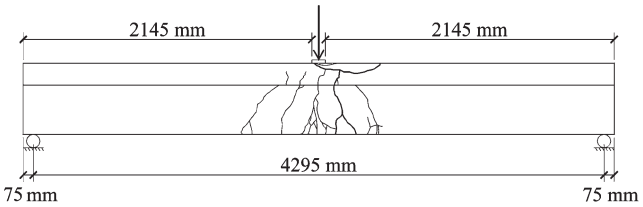

Figure F.33 Test setup and crack patterns for multiple-strand development length specimen HPC-2 (north face).

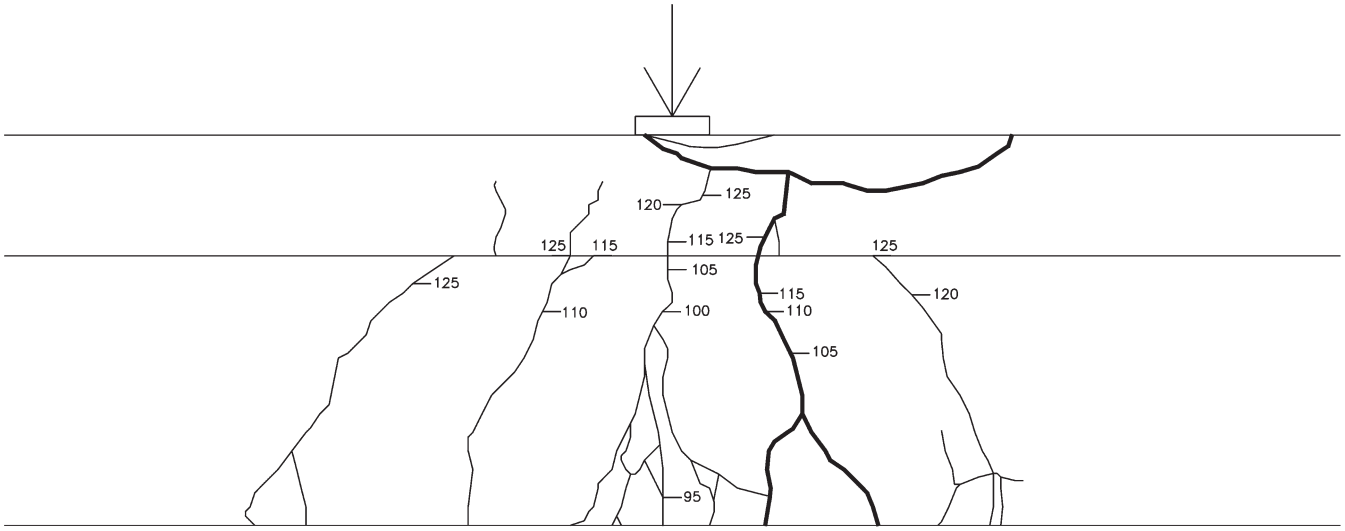

Figure F.34 Crack patterns at failure of multiple-strand development length specimen HPC-2 (north face).

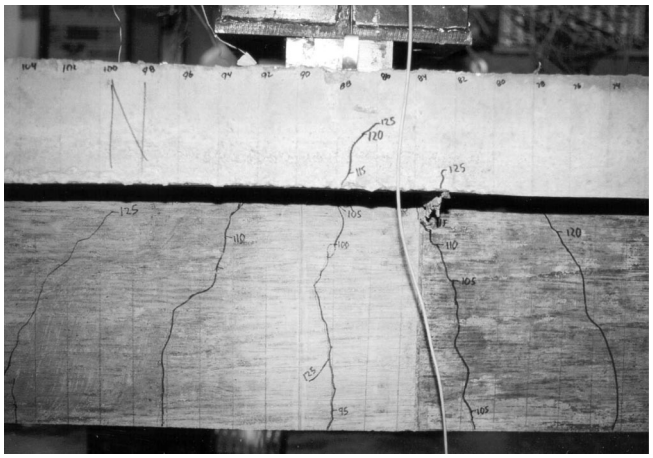

Figure F.35 Multiple-strand development length specimen HPC-2 before failure (north face).

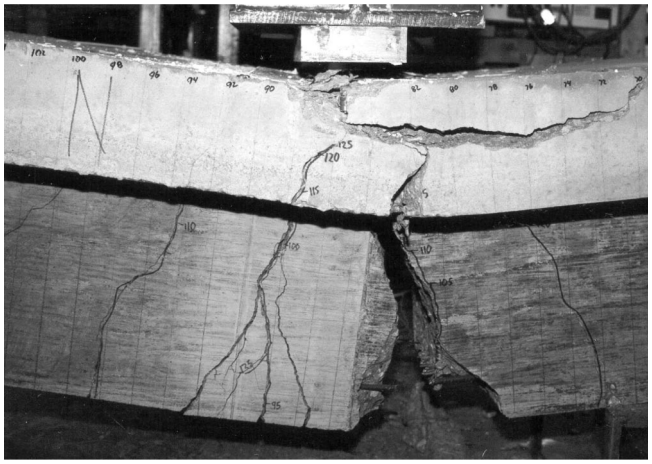

Figure F.36 Multiple-strand development length specimen HPC-2 after failure (north face).

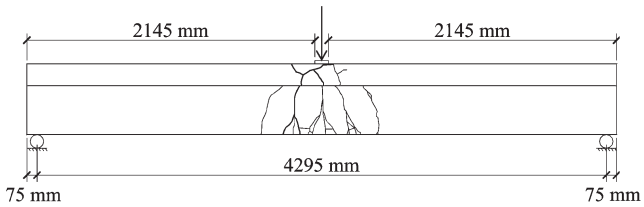

Figure F.37 Test setup and crack patterns for multiple-strand development length specimen HPC-2 (south face).

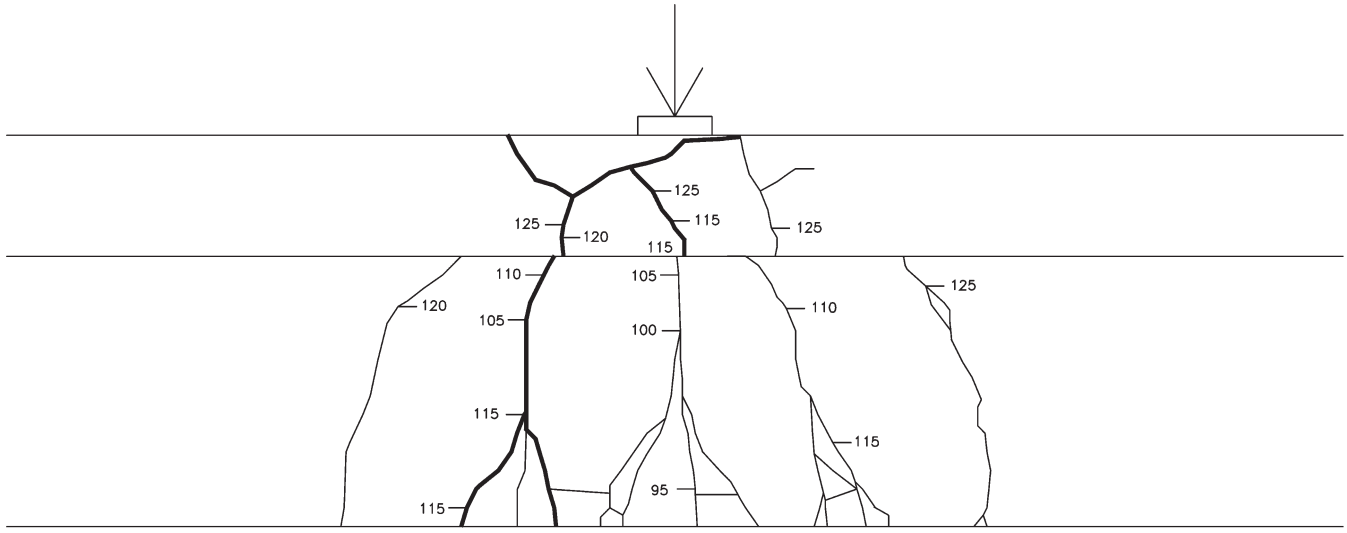

Figure F.38 Crack patterns at failure of multiple-strand development length specimen HPC-2 (south face).

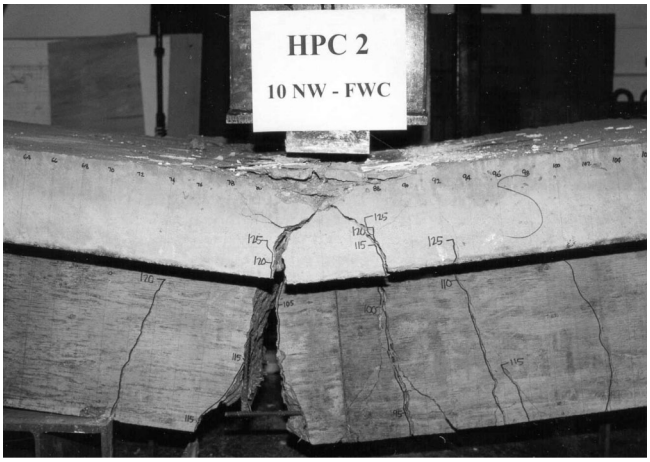

Figure F.39 Multiple-strand development length specimen HPC-2 before failure (south face).

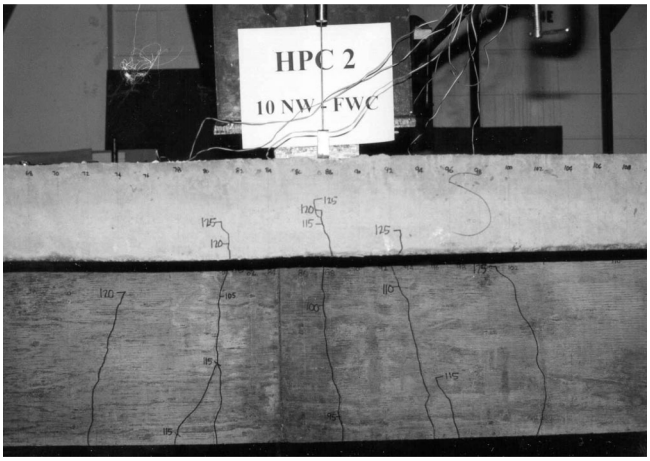

Figure F.40 Multiple-strand development length specimen HPC-2 after failure (south face).

APPENDIX G. SPECIAL PROVISIONS FOR THE INSTRUMENTATION, TESTING, AND CONSTRUCTION OF A HIGH PERFORMANCE CONCRETE (HPC) BRIDGE ON SR 43 OVER BURNETT CREEK, INDIANA

G.1 Introduction

The special provisions outlined in this document are set forth to facilitate the planning and construction of the first high performance concrete (HPC) bridge in the state of Indiana. Guidelines for concrete mixture proportions, requirements for fresh and hardened concrete properties, and details of instrumentation for monitoring of bridge performance are provided. Researchers from Purdue University will assist the contractor in selecting the type of instrumentation that the contractor will purchase for installation and monitoring of the bridge. The researchers will also be present during all critical stages of the construction to install and monitor instrumentation used to obtain performance data on the structure. In addition, the researchers will collect information from the construction process, including materials properties and construction documentation. The information collected by the researchers will be used to prepare a guide for constructing additional HPC bridges in Indiana.

Several types of specialized instrumentation and tests, which will require special considerations during the construction phase, are planned for both the deck and the girders of the bridge. It is the intent of the researchers that these instruments and tests will have minimal effects on the bridge construction although some special considerations will be required.

G.2 General

The overall performance of this HPC bridge will largely depend on the selected proportions for concrete mixtures and on the level of quality control during concrete mixing and placing. It is expected that supplementary cementitious materials will be required for both the deck and the girder mixtures.

In order to evaluate both short and long-term performance of the structure, three of the girders and the deck will be instrumented with strain, temperature, deflection, and corrosion sensors. Researchers from Purdue University will install and monitor the sensors although some instrumentation supports and conduits will need to be installed by the contractor. The researchers will work with the contractor and will oversee the installation process. An initial monitoring program, lasting for six months from the time the bridge is completed, is planned to assess the initial behavior and performance of the bridge.

G.2.1 Meetings

The researchers shall be notified and permitted to attend all meetings between the contractor and INDOT where specifics of the project will be discussed. These meetings shall include both pre-bidding and pre-construction meetings.

G.2.2 Contact Information

Professor Jan Olek, Ph.D., PE
1284 Civil Engineering Building
Purdue University
West Lafayette, IN 47907
Phone: 765 494 5015
Fax: 765 496 1364
E-mail: olek@ecn.purdue.edu

G.3 Girders

This section contains guidelines and special provisions with regard to the construction of the prestressed concrete girders intended for the SR 43 bridge over Burnett Creek. The special provisions contained herein do not cover every aspect of constructing the girders and the contractor is directed to the current INDOT Standard Specifications for items not contained herein. Due to the pioneering nature of this project, the contractor is expected to work closely with both the researchers and INDOT to find solutions to any unusual situations that may occur.

The contractor shall submit a proposed concrete mixture design to the researchers and INDOT at least two months before the construction of the first girder Included with the mixture design shall be a test report containing. The contractor shall also provide a description of how the concrete operation will take place, e.g., how the concrete will be mixed, transported, placed, consolidated, finished, and cured. All materials used for girder concrete shall conform to the applicable INDOT specifications and the special provisions included in this document.

G.3.1 Cementitious Materials

The cement shall be either ASTM Type I, II, or III and be in accordance with 901.01. Silica fume, in accordance with 901.04, shall be incorporated as a supplementary cementitious material.

G.3.2 Chemical Admixtures

All chemical admixtures shall be used within the guidelines given by their manufacturers and as approved by INDOT in accordance with 912.03. Based on experience with trial concrete mixtures as well as field experience, the researchers especially encourage the contractor to pay close attention to the parameters and stability of the air void system in addition to the initial air content.

G.3.3 Aggregates

The fine aggregate shall be natural sand in accordance with 904.01. The coarse aggregate, in accordance with 904.02, shall be class AP or class A crushed limestone/dolomite with a maximum aggregate size of 25.4 mm (1 in.).

G.3.4 Concrete Properties and Proportioning

The amount of cementitious materials shall be limited to a maximum of 463 kg/m^3 (780 lb/yd^3), of which 5 to 6.5% (direct replacement by mass) shall be silica fume. The maximum allowable water/cementitious materials (w/cm) ratio shall be 0.33. When calculating the w/cm ratio, free water from the aggregates as well as admixtures shall be included in the amount of added water. The properties of the fresh girder concrete shall be as follows:

- Slump:152 $\pm$ 51 mm (6 $\pm$ 2 in.)
- Air content: 6.5 $\pm$ 1.5%
- Maximum concrete temperature: 25°C (78°F)

Properties of the hardened girder concrete shall be as follows:

- Minimum compressive strength at release of prestress: 51 MPa (7,400 psi)
- Minimum compressive strength, f'c, at 28 days: 68 MPa (9,900 psi)
- Air content as per ASTM C457: 6.5 $\pm$ 1.5%
- Maximum spacing factor of air voids: 0.25 mm (0.01 in.)
- Minimum relative freeze-thaw durability factor: 90%
- Resistance to chloride ingress at 56 days: $<$1,000 Coulombs

As a reference for the contractor, the following mix proportions have been shown to yield at least the desired strength and resistance to chloride ingress requirements of these special provisions:*

- Cement: 440 kg/m^3 (740 lb/yd^3)
- Densified silica fume:23 kg/m^3 (39 lb/yd^3)
- Free Water: 153 L/m^3 (257 lb/yd^3)
- Coarse aggregate (SSD†): 950 kg/m^3 (1600 lb/yd^3)
- Fine aggregate (SSD): 755 kg/m^3 (1272 lb/yd^3)

G.3.5 Concrete Mixing

To ensure adequate dispersion of the silica fume, it shall be mixed for one minute with at least one-half of the coarse aggregate before any other ingredients are added. Except for this special requirement, normal mixing procedures shall be followed.

G.3.6 Quality Control and Testing Plans

Quality control and testing plans, in accordance with ITM 803, shall be submitted to INDOT and the researchers at least four weeks prior to construction of the first girder. As a part of the quality control and testing plans, the contractor shall name a PCI and/or INDOT certified concrete technician that will be responsible for executing the quality control and testing plans.

G.3.7 Trials Pours

The contractor shall invite representatives from the researchers and INDOT for two separate field trials of the proposed concrete. The first trial, conducted at least four weeks prior to construction of the first girder shall consist of 2.3 m^3 (3 yd^3) (or 75% of the mixer capacity) of concrete and be conducted to verify properties of the proposed mix. The second trial, conducted at least one week and no more than two weeks prior to construction of the first girder, shall consist of constructing a 3 m (10 ft) long section in the actual girder form (or a form of similar size and shape). This trial pour shall be conducted to verify that the proposed, mixing, transporting, placing, and curing procedures will work adequately. The second trial shall be completed with the same equipment and personnel as the girders. The trials will allow potential problems to be identified and corrected before construction of the girders.

During the trials, the contractor's certified concrete technician and the researchers shall conduct materials tests on both the aggregates and the concrete to verify the properties of the proposed mix. In addition, cylinders shall be cast and tested to verify strength development of the concrete. The cylinders from the first trial shall be tested at 1, 3, 7, and 28 days and from the second trial at 1, 3, and 7 days. The cylinders tested for 28-day strength shall be temperature match cured. The reference temperature shall be obtained from a block of concrete that is of size similar to the bottom flange of the actual girders and cast concurrently with the cylinders.

G.3.8 Prestressing Strand Bond Properties

The contractor shall be responsible for ensuring that the proposed concrete and the prestressing strand develop adequate bond. This can be accomplished by conducting pull-out tests using the same materials as proposed for use in the bridge. The contractor shall prepare plans of the pull-out tests and submit to the researchers and INDOT for approval two weeks before constructing the test specimen(s). Representatives from both the researchers and INDOT shall be invited to observe both the construction and testing of the pull-out specimen(s). A minimum of six strand specimens in 'as received' condition shall be tested. The pull-out test specimens shall not be constructed until after the first field trial. A diagram of an acceptable layout of a pull-out specimen is shown in Figure G.1.

G.3.9 Materials Testing

The researchers will conduct comprehensive materials tests of both girder and deck concretes. The contractor shall make available approximately 0.25 m^3 (9 ft^3) of fresh concrete for each of the three instrumented girders and 0.1 m^3 (4 ft^3) for the remaining girders. The contractor shall also make available a level area, next to the girder under construction, that is sufficiently large for specimen preparation and initial (one to two days) storage of field cured specimens. In addition, one 120VAC-15A electrical outlet must be made available within 4 m (10 ft) of the girder under construction during preparation and curing of field cured specimens (up to two days/beam).

G.3.10 Curing

Steam curing of the girders is permitted in case the concrete must be cast during cold weather. If steam curing is not needed to protect the concrete from freezing or to meet construction deadlines, the use of steam curing is discouraged in order to maintain the curing temperature of the concrete as low as possible and reduce potential strength loss caused by elevated curing temperatures. In case steam curing must be used, the temperature of the steam surrounding the girders shall be limited to 30°C (86°F).

Temperature match curing of cylinders used to verify strength at release of the prestress force is permitted with the reference temperature being at the center of the bottom flange. For cylinders used for 28-day strengths, temperature match curing for the first two days is required.

A curing compound shall be applied to the surfaces of the beams within one hour of removal of the forms.

G.3.11 Construction Monitoring

The researchers shall be permitted to be present during the entire construction period of all of the girders as well as during transportation of the girders. During this time, they will monitor the construction process and collect data. The data will include, but not be limited to, strains, material properties, concrete batch proportions, and photographic documentation.

G.3.12 Instrumentation and Monitoring

In order to evaluate both short and long-term performance of the structure, three of the girders will be instrumented with strain, temperature, deflection, and corrosion sensors. Researchers from Purdue University will install and monitor the sensors although some instrumentation supports need to be installed by the contractor. The researchers will work with the contractor and will oversee the installation process.

The monitoring of the instrumentation will, for the most part, need to be performed continuously from the time the sensors are installed. This will be accomplished with battery powered automatic data acquisition systems and should not interfere with the construction. However, manual deflection measurements will be required for the girders, both at the precast plant and later in the completed bridge.

*The contractor still needs to verify that the mix will yield the required properties with his/her materials and equipment.

†Saturated surface dry.

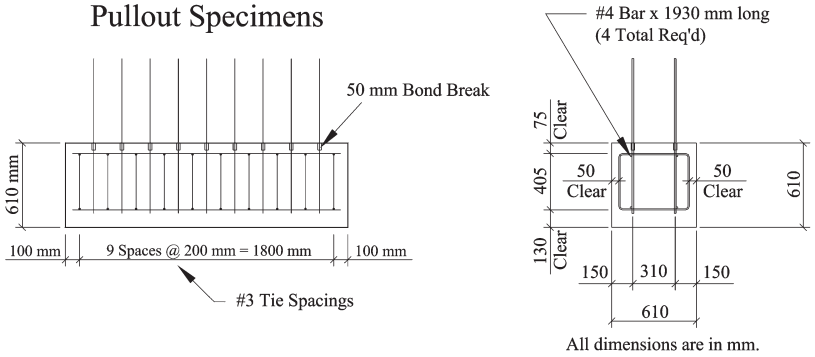

Figure G.1 Details of the pullout specimen used in this study.

G.3.13 Test Methods and Procedures

The following test methods and procedures shall be used:

Water-Cementitious Ratio	ITM 403
Sampling Fresh Concrete	AASHTO T 141
Slump	AASHTO T119
Unit Weight and Relative Yield	AASHTO T 121
Air Content of Fresh Concrete	AASHTO T 152
Air Content of Hardened Concrete	ASTM C 457
Making and Curing Specimens	AASHTO T 23*
Compressive Strength	AASHTO T 22
Freeze-Thaw Durability	AASHTO T 161
Electrical Indication of Concrete's Ability to Resist Chloride Ion Penetration	AASHTO T 277

*Instead of standard curing, all cylinders used for determination of 28-day compressive strength shall be temperature match cured for two days.

G.4 Deck, Approach Slab, Wings, and Railings

This section contains guidelines and special provisions with regard to the construction of the cast in place concrete deck (and concrete deck panels if used by the contractor) intended for the SR 43 bridge over Burnett Creek. The special provisions contained herein do not cover every aspect of constructing the deck and the contractor is directed to the current INDOT Standard Specifications for items not contained herein. Due to the pioneering nature of this project, the contractor is expected to work closely with both the researchers and INDOT to find solutions to any unusual situations that may occur.

The contractor shall submit proposed concrete mixture designs to the researchers and INDOT at least two months before the construction of the bridge. Included with the mixture designs shall be a test report containing measured values of properties listed in Section G.4.4 of this report. These values shall meet or exceed the values listed in Section G.4.4. The contractor shall also provide a description of how the concreting operation will take place, e.g., how the concrete will be mixed, transported, placed, consolidated, finished, and cured. All materials used for deck concrete shall conform to the applicable INDOT specifications.

G.4.1 Cementitious Materials

The cement shall be either AASHTO M85 Type I, II, or III, or AASHTO M240 Type IS or IP and be in accordance with 901.01. Silica fume, in accordance with 901.04, shall be used to replace between 4 and 7% of the cementitious materials. The use of ground granulated blast furnace slag (GGBFS) and/or fly ash is encouraged, but not required. The fly ash and GGBFS shall conform to 901.02 and 901.03, respectively. The maximum replacement of GGBFS is limited to 30% and the maximum replacement level of fly ash is limited to 20%. Both silica fume and GGBFS shall be replace cement at a 1:1 ratio while the ratio for fly ash shall be 1:1.25 by mass.

G.4.2 Chemical Admixtures

All chemical admixtures shall be used within the guidelines given by their manufacturers and as approved by INDOT in accordance with 912.03. Based on experience with trial concrete mixtures as well as field experience, the researchers especially encourage the contractor to pay close attention to the parameters and stability of the air void system in addition to the initial air content.

G.4.3 Aggregates

The fine aggregate shall be natural sand in accordance with 904.01. The coarse aggregate, in accordance with 904.02, shall be class AP crushed limestone/dolomite with a maximum aggregate size of 19 mm (0.75 in.).

G.4.4 Concrete Properties and Proportioning

The amount of cementitious materials shall be limited to a maximum of 430 kg/m^3 (725 lb/yd^3), of which at least 4% and no more than 6% (direct replacement by mass) shall be silica fume. If fly ash is used, no more of than 20% of the cement shall be replaced (using a 1:1.25 by mass replacement ratio) with fly ash. The replacement level of GGBFS shall not exceed 30% (direct replacement by mass) and the combined replacement level of GGBFS, fly ash, and silica fume shall not exceed 35%. The maximum allowable water/cementitious materials (w/cm) ratio shall be 0.38. When calculating the w/cm ratio, free water from the aggregates as well as admixtures shall be included. The properties of the fresh deck concrete shall be as follows:

Slump:	152 ± 51mm (6 ± 2 in.)*
Air content:	6 to 9.5%
Maximum concrete temperature:	25°C (78°F)

*The slump can be lowered for the bridge railings if necessary.

Properties of the hardened deck concrete shall be as follows:

Minimum compressive strength, f'_c, at 28 days:	40MPa (5,800 psi)
Air content as per ASTM C457:	6 to 9.5%
Maximum spacing factor of air voids:	0.20mm (0.008 in.)
Relative freeze-thaw durability factor:	90%
Resistance to chloride ingress at 56 days:	<1,000 Coulombs
Total scaling residue after 50 cycles with NaCl:	0.5kg/m^2 (0.9 lb/yd^2)

G.4.5 Concrete Mixing

To ensure adequate mixing of the silica fume, it shall be mixed for one minute with at least one-half of the coarse aggregate before any other ingredients are added. Except for this special requirement, normal mixing procedures shall be followed.

G.4.6 Placing, Finishing, and Curing

Care shall be taken to minimize damage to the epoxy coated reinforcement. This will include limiting the height the concrete is placed from as well as reminding the workers to use good judgment when working with the exposed reinforcement.

Concrete placing and finishing operations shall not commence if the estimated evaporation will exceed 0.45 kg/m^2/hr (0.1 lb/ft^2/hr). Also, the ambient temperature shall be less than 30°C (86°F) during concreting operations. The contractor shall be responsible for measuring the temperature, wind speed, and relative humidity in order to determine the evaporation rate using the ACI 308 nomograph (found in *ACI Manual of Concrete Practice, Part 2,* published by the American Concrete Institute (*1*)). This nomograph is reproduced here as Figure G.2.

The finishing of the concrete shall be accomplished primarily by mechanical means and hand–finishing shall be avoided except where mechanical finishing cannot be applied.

Curing of the concrete shall start as soon as it has been finished. Initial curing of the concrete that is being placed and finished shall be provided by fine mist (or fog) of water where the application rate is carefully monitored so continuous application can be achieved. Once the concrete has been finished, a moist burlap or cotton mat shall be used to cover the concrete. The fine mist shall be continued to be applied after the concrete has been covered and extreme care shall be taken to prevent any areas from drying. After initial set has taken place or when there is no longer risk of eroding the concrete surface, the concrete shall be continuously sprinkled with fresh water for fourteen days. At the conclusion of the wet curing, two layers of an approved curing compound shall be applied.

G.4.7 Quality Control and Testing Plans

Quality control and testing plans, in accordance with ITM 803, shall be submitted to INDOT and the researchers at least six weeks prior to construction of the deck. As a part of the quality control and testing plans, the contractor shall name a ACI and/or INDOT certified concrete technician that will be responsible for executing the quality control and testing plans.

G.4.8 Trials Pours

The contractor shall invite representatives from the researchers and INDOT for two separate field trials of the proposed concrete. The first trial, conducted at least four weeks prior to construction of the deck shall consist of 3 m^3 (4 yd^3) of concrete and be conducted to verify properties of the proposed mix. The second trial, conducted at least one week and no more than two weeks prior to construction of the deck shall consist of 6 m^3 (8 yd^3) of concrete and be conducted to verify that the proposed, mixing, transporting, placing, and curing procedures will work adequately. The second trial shall be completed with the same equipment and personnel as the bridge deck. The trials will allow potential problems to be identified and corrected before construction of the bridge deck.

G.4.9 Materials Testing

The researchers will conduct comprehensive materials tests on the deck concrete. The contractor shall make available approximately 0.3 m^3 (10 ft^3) of fresh concrete from a single load (truck) of concrete selected by the researchers and approximately 0.1 m^3 (3 ft^3) from each load. The contractor shall also make available a level area, next to the bridge, that is sufficiently large for specimen preparation and initial (one to two days) storage of field cured specimens. In addition, one 120VAC-15A electrical outlet must be made available within 4 m (10 ft) of the specimen preparation area during preparation and curing of field cured specimens (up to two days).

G.4.10 Construction Monitoring

The researchers shall be permitted to be present during the entire construction period of the bridge. During this time, they will monitor the construction process and collect data. The data will include, but not be limited to, strain, material properties, concrete batch proportions, and photographic documentation.

G.4.11 Instrumentation and Monitoring

In order to evaluate both short and long-term performance of the structure, the deck will be instrumented with strain, temperature, deflection, and corrosion sensors. Researchers from Purdue University will install and monitor the sensors although some instrumentation supports need to be installed by the contractor. The researchers will work with the contractor and will oversee the installation process.

The monitoring of the instrumentation will, for the most part, need to be performed continuously from the time the sensors are installed. This will be accomplished with battery powered automatic data acquisition systems and should not interfere with the construction. However, manual deflection measurements will be required for the completed structure.

G.4.12 Test Methods and Procedures

The following test methods and procedures shall be used:

Water-Cementitious Ratio	ITM 403
Sampling Fresh Concrete	AASHTO T 141
Slump	AASHTO T119
Unit Weight and Relative Yield	AASHTO T 121
Air Content of Fresh Concrete	AASHTO T 152
Air Content of Hardened Concrete	ASTM C 457
Making and Curing Specimens	AASHTO T 23
Compressive Strength	AASHTO T 22
Electrical Indication of Concrete's Ability to Resist Chloride Ion Penetration	AASHTO T 277
Freeze-Thaw Durability	AASHTO T 161
Scaling Resistance	ASTM C 672*

*The salt solution shall be 3% NaCl instead of the standard C_aCl_2 solution. The scaling performance shall be evaluated based on the amount of material lost from the specimens. The scaling residue shall be collected, dried, and weighed to the nearest 0.01 g after each five cycles. The total amount of lost material shall be computed after 50 cycles and reported as kg/m^2 (lb/yd^2).

G.5 Concrete Members Not Covered in Sections 5 and 6

Members not covered in Sections 3 and 4 shall be constructed from Class C concrete, as per 702.02, or concrete that exceeds the specifications for Class C concrete.

REFERENCE

1. ACI 308. Standard Practice for Curing Concrete. In *ACI Manual of Concrete Practice, Part 2.* American Concrete Institute, Farmington Hills, Michigan, 1999.

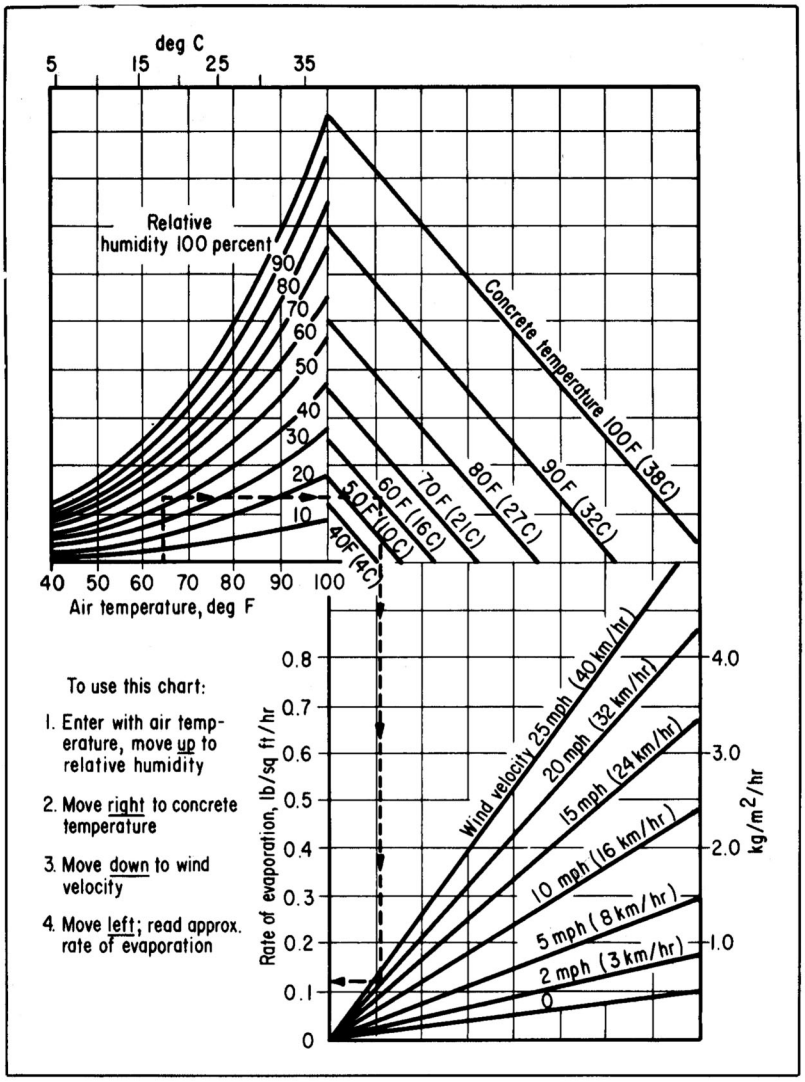

Fig. 1—Effect of concrete and air temperatures, relative humidity, and wind velocity on the rate of evaporation of surface moisture from concrete. This chart provides a graphic method of estimating the loss of surface moisture for various weather conditions. To use the chart, follow the four steps outlined above. When the evaporation rate exceeds 0.2 lb/ft²/hr (1.0 kg/m²/hr), measures shall be taken to prevent excessive moisture loss from the surface of unhardened concrete; when the rate exceeds 0.1 lb/ft²/hr (0.5 kg/m²/hr) such measures may be needed. When excessive moisture loss is not prevented, plastic shrinkage cracking is likely to occur

Figure G.2 Standard practice for curing concrete. (Source: (*1*).)